

**OPTIMAL CONTROL AND COORDINATION OF CONNECTED AND  
AUTOMATED VEHICLES IN A MIXED TRAFFIC ENVIRONMENT**

by

A M Ishtiaque Mahbub

A dissertation submitted to the Faculty of the University of Delaware in partial fulfillment of the requirements for the degree of Doctor of Philosophy in Mechanical Engineering

Spring, 2022

© 2022 A M Ishtiaque Mahbub  
All Rights Reserved

**OPTIMAL CONTROL AND COORDINATION OF CONNECTED AND  
AUTOMATED VEHICLES IN A MIXED TRAFFIC ENVIRONMENT**

by

A M Ishtiaque Mahbub

Approved: \_\_\_\_\_  
Ajay K. Prasad, Ph.D.  
Chair of the Department of Mechanical Engineering

Approved: \_\_\_\_\_  
Levi T. Thompson, Ph.D.  
Dean of the College of Engineering

Approved: \_\_\_\_\_  
Louis F. Rossi, Ph.D.  
Vice Provost for Graduate and Professional Education and  
Dean of the Graduate College

I certify that I have read this dissertation and that in my opinion it meets the academic and professional standard required by the University as a dissertation for the degree of Doctor of Philosophy.

Signed: \_\_\_\_\_  
Andreas A. Malikopoulos, Ph.D.  
Professor in charge of dissertation

I certify that I have read this dissertation and that in my opinion it meets the academic and professional standard required by the University as a dissertation for the degree of Doctor of Philosophy.

Signed: \_\_\_\_\_  
Ajay K. Prasad, Ph.D.  
Member of dissertation committee

I certify that I have read this dissertation and that in my opinion it meets the academic and professional standard required by the University as a dissertation for the degree of Doctor of Philosophy.

Signed: \_\_\_\_\_  
Ioannis Poulakakis, Ph.D.  
Member of dissertation committee

I certify that I have read this dissertation and that in my opinion it meets the academic and professional standard required by the University as a dissertation for the degree of Doctor of Philosophy.

Signed: \_\_\_\_\_  
Huei Peng, Ph.D.  
Member of dissertation committee

*This dissertation is dedicated  
to my mom, who taught me resilience,  
to my dad, who taught me honesty, and  
to my wife, who taught me the meaning of life.*

## ACKNOWLEDGEMENTS

My deepest gratitude goes first to my advisor, Professor Andreas A. Malikopoulos, who expertly guided me through all the stages of my Ph.D. program. His insight launched the greater part of this dissertation. His kind mentoring, guidance, patience, and enthusiasm have inspired and encouraged me to a great extent to accomplish this work.

I express my humble gratitude to Professor Huei Peng, whose guidance throughout my Ph.D. program has been invaluable. I would also like to acknowledge and express my sincerest gratitude to the rest of my committee members, Professor Ioannis Poulakakis and Professor Ajay K. Prasad, for their insightful comments and suggestions. My appreciation is also extended to my peers at the Information and Decision Science Lab, and to the faculty and staff at the University of Delaware, who have made my experience in Delaware a cherishable one.

The undertaking of such a long-term commitment would not be possible without the support and sacrifice of my wife, Zannatul Mawa, to whom I am forever indebted. I am also extremely grateful to my family and friends for their continuous help, support, and love that carried me through the challenging times.

## TABLE OF CONTENTS

<b>LIST OF TABLES</b> . . . . .	<b>xi</b>
<b>LIST OF FIGURES</b> . . . . .	<b>xiii</b>
<b>ABSTRACT</b> . . . . .	<b>xviii</b>
 <b>Chapter</b>	
<b>1 INTRODUCTION</b> . . . . .	<b>1</b>
1.1 Motivation . . . . .	1
1.2 Literature Review . . . . .	3
1.2.1 Coordination using Connectivity and Automation . . . . .	3
1.2.2 Decentralized Optimal Control Framework . . . . .	5
1.2.3 Coordination in a Mixed Traffic Environment . . . . .	8
1.2.4 Vehicle Platooning and Stability . . . . .	9
1.2.5 Vehicle Platooning in a Mixed Traffic Environment . . . . .	11
1.3 Identification of the Research Gaps . . . . .	13
1.4 Research Contributions . . . . .	21
1.5 Dissertation Overview . . . . .	26
 <b>2 OPTIMAL COORDINATION AT A TRAFFIC CORRIDOR</b> . . . . .	 <b>29</b>
2.1 Energy-Optimal Coordination at Multiple Adjacent Intersections . . . . .	30
2.1.1 Problem Formulation . . . . .	30
2.1.2 Modeling Framework and Constraints . . . . .	32
2.1.3 Upper-Level Vehicle Coordination Problem . . . . .	35
2.1.4 Low-Level Energy Minimization Problem . . . . .	37
2.1.5 Closed-Form Analytical Solution . . . . .	38
2.1.5.1 Analytical Solution without Interior Constraints . . . . .	39

2.1.5.2	Analytical Solution with Interior Constraints . . . . .	39
2.1.6	Simulation Results and Discussion . . . . .	41
2.2	Isolated and Coordinated Control at a Traffic Corridor . . . . .	45
2.2.1	Isolated Conflict Zone Control . . . . .	46
2.2.2	Coordinated Corridor Control . . . . .	47
2.2.3	Performance Evaluation and Comparison . . . . .	48
2.3	Concurrent Optimization of Vehicle Dynamics and Powertrain . . . . .	52
2.3.1	Supervisory Controller Architecture . . . . .	52
2.3.2	Optimization of the Powertrain Controller . . . . .	54
2.3.3	Powertrain Calibration with VESIM . . . . .	57
2.3.4	Integration of Powertrain Controller in VESIM . . . . .	58
2.3.5	Vehicle Dynamics and Powertrain Controller Performance . . . . .	59
2.4	Experimental Validation of Optimal Controllers: From Simulation to Field Test . . . . .	67
2.4.1	A Sequential Test Strategy for Connected Automated Vehicles . . . . .	67
2.4.2	Simulation Framework . . . . .	68
2.4.3	Hardware-in-the-Loop (HIL) Test . . . . .	71
2.4.4	Bench Test of Integrated System . . . . .	73
2.4.5	Virtual Reality Based Field Test . . . . .	74
2.4.5.1	Audi A3 System Architecture . . . . .	76
2.4.5.2	MQTT and Socket Based Connectivity Protocols . . . . .	77
2.4.5.3	Optimal Vehicle Dynamics Controller Integration . . . . .	78
<b>3</b>	<b>MOTION PRIMITIVES WITH CONSTRAINED OPTIMAL CONTROL . . . . .</b>	<b>82</b>
3.1	A Condition-Based Framework for Constrained Optimal Control . . . . .	83
3.1.1	Comparison With Related Work . . . . .	83
3.1.2	Constrained Optimal Control Problem . . . . .	85
3.1.3	Low-level Optimal Control Problem . . . . .	86
3.1.4	Unconstrained Solution . . . . .	88
3.1.5	Analysis of the Constrained Optimal Control Problem . . . . .	89
3.1.5.1	Condition of Constraint Exclusion . . . . .	90

3.1.5.2	Conditions of Constraint Activation . . . . .	95
3.1.5.3	Interdependence of Constraint Activation Cases . . . . .	97
3.1.6	Analytical Solution of the Constrained Optimal Control Problem . . . . .	100
3.1.7	Simulation Results and Summary . . . . .	112
3.2	Decentralized Optimal Coordination with Safety Constraints . . . . .	115
3.2.1	Modeling Framework: Decentralized Coordination . . . . .	116
3.2.2	Throughput Maximization with Dynamic Resequencing . . . . .	118
3.2.3	Energy-Optimal Motion Primitives with Safety Constraints . . . . .	121
3.2.4	Simulation Results and Summary . . . . .	126
<b>4</b>	<b>OPTIMAL CONTROL IN A MIXED TRAFFIC ENVIRONMENT . . . . .</b>	<b>131</b>
4.1	Safety-Aware Control at a Mixed Traffic Signalized Junction . . . . .	131
4.1.1	Optimal Control at a Signalized Intersection . . . . .	133
4.1.1.1	Communication Structure . . . . .	133
4.1.1.2	Vehicle Dynamics and Constraints at Mixed Traffic . . . . .	134
4.1.2	Data-Driven Predictive Control Framework . . . . .	136
4.1.2.1	Online Car-following Model Parameter Estimation . . . . .	137
4.1.2.2	Predictive Control Problem . . . . .	139
4.1.3	Numerical Validation . . . . .	140
4.1.4	Results and Discussions . . . . .	141
4.2	Coordination at a Mixed Traffic Corridor . . . . .	143
4.2.1	Hierarchical Control Framework . . . . .	146
4.2.2	Analysis of the Penetration Impact . . . . .	147
<b>5</b>	<b>PLATOON FORMATION IN A MIXED TRAFFIC ENVIRONMENT . . . . .</b>	<b>152</b>
5.1	A Condition-based Control Framework for Platoon Formation . . . . .	153
5.1.1	Problem Formulation . . . . .	154

5.1.2	Control Framework for Platoon Formation . . . . .	159
5.1.2.1	Feasibility of Platoon Formation . . . . .	161
5.1.2.2	Scalability of the Control Framework . . . . .	163
5.1.3	Numerical Validation: Highway Platooning . . . . .	165
5.2	A Model-Agnostic Optimal Platoon Formation Framework . . . . .	167
5.2.1	Receding Horizon Control Framework . . . . .	170
5.2.1.1	Augmented CAV dynamics . . . . .	171
5.2.1.2	Prediction Model . . . . .	172
5.2.1.3	Formulation of the Optimal Control Problem . . . . .	173
5.2.2	Sensitivity, Scalability and Robustness Analysis . . . . .	175
5.3	A Safety-Prioritized Predictive Framework for Platoon Formation . . . . .	180
5.3.1	Comparison with Related Work . . . . .	181
5.3.2	Problem Formulation . . . . .	182
5.3.2.1	Vehicle Control Model . . . . .	185
5.3.2.2	Communication Structure . . . . .	187
5.3.2.3	Platoon Formation Problem: Mixed Environment . . . . .	188
5.3.3	Feasibility of Platoon Formation . . . . .	191
5.3.4	Model-Independent Control Framework . . . . .	194
5.3.4.1	Augmented CAV Dynamics for Multi-successor Safety . . . . .	195
5.3.4.2	Linear Receding Horizon Formulation . . . . .	197
5.3.4.3	Optimal Control Problem . . . . .	199
5.3.5	Model-dependent Control Framework . . . . .	200
5.3.5.1	Nonlinear Receding Horizon Control . . . . .	201
5.3.5.2	Data-Driven Receding Horizon Control . . . . .	202
5.3.5.3	Online Car-following Model Parameter Estimation . . . . .	204
5.3.6	Simulation Results and Discussion . . . . .	205
5.3.6.1	Simulation Setup . . . . .	206
5.3.6.2	Platoon Formation and Safety . . . . .	207

5.3.6.3	Online Parameter Estimation . . . . .	208
5.3.6.4	Scalability . . . . .	210
5.3.6.5	Robustness . . . . .	211
5.3.6.6	Computational Efficiency . . . . .	211
5.3.6.7	Prediction Accuracy . . . . .	211
5.3.6.8	Sensitivity Analysis . . . . .	214
<b>6</b>	<b>OPTIMAL PLATOON COORDINATION IN A MIXED TRAFFIC ENVIRONMENT . . . . .</b>	<b>217</b>
6.1	Cooperative Merging of Platoons with Delayed Communication . . . . .	217
6.1.1	Modeling Framework: Platoon Coordination . . . . .	218
6.1.1.1	Network Topology and Communication . . . . .	219
6.1.1.2	Dynamics and Constraints . . . . .	221
6.1.1.3	Information Structure . . . . .	224
6.1.2	Optimal Control of Platoon Leaders . . . . .	225
6.1.3	Optimal Control of Followers Within Each Platoon . . . . .	228
6.1.4	Delay in Platoon Communication . . . . .	230
6.1.5	Implementation of the Optimal Coordination Framework . . . . .	231
6.1.6	Simulation Example . . . . .	232
6.2	Coordination of Mixed Platoons at On-Ramp Merging . . . . .	237
6.2.1	Modeling Framework: Mixed Platoon . . . . .	238
6.2.1.1	Vehicle Dynamics . . . . .	241
6.2.1.2	System Constraints . . . . .	243
6.2.1.3	Information Structure . . . . .	247
6.2.2	Coordination Framework for Mixed Platoons . . . . .	248
6.2.2.1	Optimal Control of Problem for Platoon Leaders . . . . .	248
6.2.2.2	Feasibility and Existence . . . . .	249
6.2.2.3	Safety Guaranteed Control Bound Within Each Platoon . . . . .	251
<b>7</b>	<b>CONCLUSION . . . . .</b>	<b>254</b>
7.1	Summary . . . . .	254
7.2	Future Direction . . . . .	256

Appendix

A ..... 287

## LIST OF TABLES

2.1	Percentage improvement in fuel economy over the baseline scenario under different traffic conditions. . . . .	50
2.2	PT controller validation for standardized drive cycles. . . . .	62
2.3	Fuel Efficiency Improvement for VD and PT controller. . . . .	66
2.4	Mean and standard deviation of the MPG <sub>e</sub> distribution for different traffic flow scenarios. . . . .	66
2.5	Summary of fuel consumption [MPG <sub>e</sub> ] comparison in simulation. . . . .	70
2.6	Summary of travel time comparison in simulation. . . . .	70
2.7	Summary of energy improvement in HIL Test. . . . .	73
2.8	Summary of MPG <sub>e</sub> Improvement in Field Test. . . . .	81
2.9	Summary of travel time comparison of field test. . . . .	81
4.1	Parameters of the controller . . . . .	141
4.2	Fuel economy improvement for HDVs. . . . .	149
5.1	Simulation parameters considered. . . . .	176
5.2	Receding horizon controller parameters . . . . .	176
5.3	Nominal values of the car-following model . . . . .	206
5.4	Parameters of the receding horizon control framework . . . . .	207
5.5	Platoon formation time and solving time for L-RHC, N-RHC and DD-RHC in simulations with different number of following HDVs. . . . .	212

6.1	Summary of performance metrics . . . . .	237
A.1	Traffic volume at different routes within Mcity network. . . . .	287
A.2	Simulation Parameters . . . . .	287
A.3	VESIM parameters calibrated with Audi A3 specification. . . . .	288

## LIST OF FIGURES

2.1	Corridor with connected and automated vehicles. . . . .	31
2.2	Illustration of the corridor in Mcity. . . . .	42
2.3	Optimal vehicle trajectory traveling through two adjacent intersections. . . . .	42
2.4	Collision-free optimal trajectory of 10 CAVs approaching towards intersection-1 (left) and cumulative fuel consumption of the optimized and baseline scenarios (right). . . . .	43
2.5	Stoppage time (left) and average coefficient of power demanded (right) of the optimized and baseline scenarios. . . . .	44
2.6	Fleet travel time of the optimized and baseline scenarios. . . . .	44
2.7	The corridor in Mcity with the conflict zones. . . . .	46
2.8	Vehicle speed profiles under different VD control approaches. . . . .	49
2.9	Speed profiles for all CAVs under different VD control approaches and demand levels. . . . .	51
2.10	Travel time distribution under different VD control approaches and traffic demand levels. . . . .	52
2.11	Supervisory control architecture. . . . .	53
2.12	The test vehicle, Audi A3 e-tron, in Mcity. . . . .	54
2.13	VESIM Model for modelling the powertrain of the plug-in hybrid electric vehicle. . . . .	57
2.14	VESIM calibration model for hold battery mode. . . . .	59

2.15	Pareto efficiency set of the powertrain controller. . . . .	60
2.16	The UDDS drive cycle traced by the baseline (Audi A3) powertrain and the optimal controlled Pareto efficient powertrain. . . . .	62
2.17	Engine operating points without and with the PT controller. . . . .	63
2.18	Average vehicle speed trajectories for high traffic volume. . . . .	63
2.20	Medium traffic volume. . . . .	72
2.21	High traffic volume. . . . .	72
2.22	Bench test model emulating the virtual reality based field test. . . . .	73
2.23	Workflow of virtual reality based V2X enabled field test in Mcity. . . . .	74
2.24	Communication protocol for the Audi A3 etron. . . . .	78
2.25	Workflow of VD Controller implementation within the head unit of Audi A3. . . . .	79
2.26	Speed profile of the Audi A3 etron considering the baseline and optimal VD controlled case at the field test in Mcity. . . . .	80
3.1	A traffic network of connected automated vehicles approaching a four-way signal-free intersection. . . . .	86
3.2	Optimal control trajectory for the unconstrained (blue), state constraint $v_i(t) - v_{max} \leq 0$ only (red) and both state-control constraint (green) case. . . . .	113
3.3	Optimal speed trajectory for the unconstrained (blue), control constraint $u_i(t) - u_{max} \leq 0$ only (red) and both state-control constraint (green) case. . . . .	114
3.4	Corridor with connected and automated vehicles. . . . .	116
3.5	Unconstrained (left) and rear-end safety constrained state trajectory (right) of CAV i with respect to its immediately preceding vehicle k. . . . .	127
3.6	The corridor in Mcity. . . . .	128

3.7	Vehicle trajectories inside the corridor for (a) baseline and (b) optimal controlled case. The control zone for each of the conflict zones are shown for comparison. . . . .	129
3.8	Accumulated fuel consumption over time for the baseline and optimal controlled vehicles. . . . .	130
4.1	A connected and automated vehicle (CAV) and human-driven vehicles (HDV) approaching a signalized intersection at red-light signal phase.	132
4.2	The structure of the proposed control framework to address Problem 4.1.1. . . . .	137
4.3	Speed and headway of the three vehicles considered in the simulation.	142
4.4	Longitudinal trajectories in the simulations with different numbers of vehicles approaching the intersection. . . . .	142
4.5	Estimates for the car-following parameters of the HDV-2 . . . . .	143
4.6	Impact of CAV penetration rate on the fuel economy under low, medium, and high traffic volumes. . . . .	150
4.7	Effect of different penetration rates of CAVs on average speed and travel time. . . . .	150
4.8	High traffic volume speed profile at the baseline, 50% penetration rate and 100% scenario. Stop-and-go driving behavior decreases for 50% and is avoided at 100% penetration case. . . . .	151
5.1	A CAV (red) traveling with two trailing HDVs (yellow), where the HDVs' state information is estimated (top scenario) by the coordinator within the buffer zone, and the platoon is formed (bottom scenario) by controlling the CAV inside the control zone. . . . .	155
5.2	Predecessor-follower coupled car-following dynamic. . . . .	156
5.3	Platoon formation for $N = 3$ , where the position (top) and headway (bottom) of the vehicles are illustrated. . . . .	166

5.4	Percentage deviation of actual platoon formation time vs. desired platoon formation time for $N = 2, 3$ and 4 under the consideration of different platoon transition duration $\tau^t$ (subfigure (a)), perception delay $\eta_i$ (subfigure (b)), and car-following model parameters $\rho_i$ and $\alpha$ (subfigure (c)-(d)), respectively. . . . .	167
5.5	Platoon formation with OVM car-following model (5.38) for $N = 4$ , where the (a) position trajectory, (b) vehicle headway, (c) speed trajectory and (d) the CAV control trajectory are shown. . . . .	177
5.6	Platoon formation with IDM car-following model (5.39) for $N = 4$ , where the (a) position trajectory and (b) vehicle headway, (c) speed trajectory and (d) the CAV control trajectory are shown. . . . .	178
5.7	Platoon formation with IDM car-following model (5.39) for $N = 4$ , where the sensitivity of the platoon formation time under varying (a) prediction horizon $T_p$ , (b) control horizon $T_c$ , (c) sample time $\tau$ and (d) desired time headway $\rho$ are illustrated. . . . .	179
5.8	Safe platoon formation with IDM car-following model (5.39) for 6, 7, 8 and 9 vehicles. . . . .	179
5.9	The target CAV (green) is traveling with $N$ trailing HDVs (blue) and a PV (orange). The communication structure is shown according to Section 5.3.2.2. . . . .	184
5.10	The structure of the proposed control framework to address Problem 5.3.1. . . . .	203
5.11	Longitudinal trajectories, speed, headways and speed gaps of the vehicles for DD-RHC in the simulation without a preceding vehicle. . . . .	209
5.12	Longitudinal trajectories, speed, headways and speed gaps of the vehicles for DD-RHC in the simulation with a preceding vehicle (PV). . . . .	210
5.13	Estimates of the car-following parameters for all HDVs. . . . .	212
5.14	Longitudinal trajectories of the vehicles in the simulations with different number of following HDVs. . . . .	213
5.15	Comparison on prediction accuracy of three internal prediction models using root mean square errors (RMSEs). . . . .	213

5.16	Platoon formation time under varying parameters of the OVM car-following models. . . . .	215
6.1	On-ramp merging with a single merging point for platoons of CAVs. The control zone is highlighted in light blue color, the entry time and exit time to the control zone are depicted with circles, and example sets of platoon leaders and followers are shown. . . . .	219
6.2	Network topology for information flow: (i) bidirectional inter-platoon communication (dashed double-headed arrow) between the platoon leaders via the coordinator, and (ii) unidirectional intra-platoon communication (solid single-headed arrow) from platoon leader to the platoon followers. . . . .	220
6.3	The position trajectories of the optimally coordinated CAV platoons at the (a) main road and (b) ramp road are shown. . . . .	234
6.4	Speed profiles of 400 vehicles traveling through the on-ramp merging scenario for three cases: (a) baseline without platooning, (b) baseline with platooning and (c) optimal platoon coordination. . . . .	235
6.5	Comparison of performance metrics: (a) cumulative fuel consumption of optimal coordination (black) vs. baseline with platooning (red), and (b) total travel time distribution of optimal coordination (blue) vs. baseline with coordination (maroon). . . . .	236
6.6	(a) On-ramp merging scenario for platoons of mixed vehicles, where the leader of each platoon is the CAV (red vehicles) and the rest of the platoon members are HDVs (gray vehicles). The control zone is highlighted in green color, the entry time $t_{i,0}^0$ and exit time $t_{i,0}^f$ to the control zone for each platoon $i$ are depicted with circles, and example of sets $\mathcal{L}(t)$ and $\mathcal{N}_i$ according to the Definitions 6.2.1 and 6.2.2 are shown. (b) Communication structure for information flow: (i) V2V-enabled bidirectional flow of information between the CAVs (double-headed dashed red arrow), (ii) V2V-enabled unidirectional flow of information from the HDVs to the CAVs (single-headed dashed red arrow), and (iii) unidirectional driver perception from preceding vehicle to the following HDVs (single-headed solid black arrow). . . . .	238

## ABSTRACT

The emergence of connected and automated vehicles (CAVs) introduces a novel dimension to the mobility paradigm that enables efficient communication and real-time computation of control actions to optimize vehicle performance, traffic efficiency, and other associated benefits. While several studies have shown the benefits of CAVs to improve vehicle- and network-level performance by alleviating congestion at specific traffic scenarios, most of these efforts have focused on 100% CAV penetration rate without considering the interaction with human-driven vehicles (HDVs). The consideration of such utopian scenarios may have facilitated the initial development of CAV technologies, but cannot be realized in current transportation conditions. It is expected that CAVs will gradually penetrate the market and interact with HDVs over the next several years. Therefore, for the CAVs to be deployed en masse, technological advancements are needed to be made considering a mixed traffic environment, where CAVs can safely co-exist with the HDVs in the traffic network. In general, a mixed traffic environment poses significant modeling and control challenges due to the stochastic nature of human-driving behavior and lack of communication. Therefore, the question that still remains unanswered is, “how can CAVs safely interact and co-exist with HDVs?” In this dissertation, I address this question through the development of an optimal control and coordination approach.

In the first part of my dissertation, I explore one extreme of the mixed traffic environment spectrum, which is the 100% CAV penetration case, and address the research gaps in the literature related to CAV coordination at traffic corridors consisting of different traffic scenarios. I propose a vehicle dynamics (VD) controller that yields a closed-form analytical solution to the optimal control problem and minimizes transient

engine operation and travel time of the CAVs. The effectiveness of the VD controller is validated through a sequential experimentation methodology that shows real-world improvement in fuel economy and traffic throughput. Furthermore, I investigate the problem of trajectory optimization in the presence of system constraints, which is difficult to solve in real time due to its iterative solution methodology according to the standard Hamiltonian analysis. To this end, I develop a condition-based control framework that can identify the activation of system constraints a priori. The proposed framework can explicitly incorporate the state, control, and safety constraints in its formulation, and derive constrained motion primitives for the CAVs with an efficient, real-time implementable algorithm.

In the second part of my dissertation, I address a mixed traffic environment consisting of CAVs and HDVs, and investigate the implication of vehicle- and network-level control of CAVs. First, I consider the problem of deriving safe trajectories for the CAVs in the presence of HDVs with unknown driving behavior, and propose a predictive control approach that considers the future trajectories of the HDVs to ensure collision safety. Then, I investigate the impact of partial penetration of CAVs from a network-level perspective, which indicates that the higher penetration rates of CAVs improve transportation safety and performance metrics, while lower penetration cases result in traffic congestion.

In an effort to address CAV coordination in a mixed traffic environment to alleviate traffic congestion, I propose a novel control paradigm that leverages the concept of vehicle platooning. I transform the problem of mixed traffic coordination into two hierarchical optimal control problems: (i) a platoon formation problem to indirectly control the motions of the HDVs within the network, and once the mixed platoons are formed, (ii) a platoon coordination problem to lead the platoons through a traffic scenario. To address the former problem, I investigate the feasibility of platoon formation by controlling the CAVs, and propose a comprehensive model-agnostic optimal controller which ensures platoon formation without having explicit knowledge

of the human driver behavior. Then, I develop a safety-aware, multi-objective receding horizon controller that considers linear, non-linear, and data-driven prediction models, and enables the formation of vehicle platoon satisfying the system constraints that include enhanced safety. The proposed controller is able to form platoons at low penetration rates while it is robust against a wide range of human driving behavior. Subsequently, to coordinate the platoons formed in (i), I develop a robust, single-level, multi-objective optimal platoon coordination framework that accounts for the effect of delayed communication and system constraints. The closed-form analytical solution of the proposed framework can be implemented in real time with the enforcement of lateral and rear-end collision avoidance constraints in the presence of bounded delays.

The research efforts pursued in this dissertation bridge the gap between the two extremes of the mixed traffic environment spectrum, and thus, have a significant impact on the future of mobility. By adopting the computationally efficient and real-time implementable control framework proposed in this dissertation, CAVs can derive optimal motion primitives that can ensure safe and improved mobility in a mixed traffic environment.

*“A journey of a thousand miles begins with a single step.”*

—Chinese proverb

## Chapter 1

### INTRODUCTION

#### 1.1 Motivation

The demand for intelligent transportation systems and mobility solutions worldwide is rapidly growing due to several reasons. About 55% of the world’s population currently live in urban areas, which is expected to rise to 68% by 2050 [1]. Conventional mobility technologies and traffic management systems cannot cope with this growing demand as the capacity of the current transportation network is being overwhelmed. Based on the 2019 Urban Mobility Report, Schrank et al. [2] reported that in 2019 congestion in the United States caused urban commuters to spend 8.7 billion additional hours on the road at an additional cost of 3.5 billion gallons of fuel, resulting in a total cost estimated at \$190 billion. A report by INRIX projects the combined annual cost of traffic congestion in the United States, UK, France, and Germany to reach \$293B by 2030, which is a 50% increase from 2013 [3]. According to a recent report from World Economic Forum , traffic congestion has cost the U.S. economy nearly \$87 billion in 2018 [4]. The transportation sector is one of the major contributors to greenhouse gas emissions as well. According to the Inventory of U.S. Greenhouse Gas Emissions and Sinks [5], transportation accounted for the largest portion (29%) of total U.S. greenhouse gas emissions in 2017. In addition to having an adverse effect on economic and environmental aspects, inefficient and overwhelmed transportation systems also have a profound impact on human lives, since traffic congestion leads to risky driving maneuver that has serious safety implication. Congestion at traffic junctions such as ramp merging, roundabouts and intersections also consists of a high degree of safety-risks leading to increased traffic accidents. Apart from the inherent complexity arising from

a complicated driving maneuver in these scenarios, additional safety risks result from driver anxiety, fatigue, distraction, and discomfort of the manually driven vehicles [6]. The U.S. National Highway Traffic Safety Administration (NHTSA) reports that 75% of accidents in the United States are caused at the traffic junctions [7]. In 2018, 36,560 people lost their lives in road crashes, where 2,841 lives were claimed due to distracted driving along with 9,378 speeding-related deaths [8].

The emergence of connected and automated vehicles (CAVs) introduces a novel dimension to the mobility paradigm that enables efficient communication and real-time computation of control actions. CAVs have attracted considerable attention for the potential of improving mobility and safety along with energy and emission reduction [9, 10]. CAVs can share endogenous and exogenous information with the neighboring agents by subscribing to vehicle-to-vehicle (V2V), vehicle-to-infrastructure (V2I), and vehicle-to-everything (V2X) communication protocols, and derive their control policies to achieve the desired objectives. To explore the full extension of this emerging technology, several aspects in the domain of the CAV-enabled mobility such as real-time control, motion planning, powertrain control, etc., have drawn considerable attention [11]. It is important to note that, the combination of real-time vehicle dynamics control and motion planning of CAVs gives birth to the concept of the automated highway system and signal-free intersections (see [12–14]) that can eliminate congestion at major traffic arteries. Tachet et al. [15] and Lioris et al. [16] indicated that transitioning from intersections with traffic lights to autonomous ones has the potential of doubling capacity and reducing delays. Indeed, the deployment of CAVs are demonstrated to alleviate congestion at the major transportation segments such as urban intersections [17–19], merging roadways [20–22], roundabouts [23, 24], speed reduction zones (SRZ) [25] and traffic corridors [26]. The impact of the CAV technology on the future of mobility and safety has become evident by the rapid development of the real-time implementable computational framework and efficient control algorithm [20, 27–30], and therefore has been a great interest of research in recent years [11, 31].

While several studies have shown the benefits of CAVs to improve vehicle- and network-level performance, and alleviate traffic congestion at specific traffic scenarios, most of these efforts have focused on 100% CAV penetration rate without considering the interaction with human-driven vehicles (HDVs). The consideration of such utopian scenarios may have facilitated the initial development of CAV technologies, but cannot be realized in current transportation conditions. It is expected that CAVs will gradually penetrate the market and interact with human-driven vehicles over the next several years [32]. Therefore, to be able to deploy the CAVs en masse, technological advancements are needed to be made considering a mixed traffic environment, where CAVs need to safely co-exist with the HDVs in the traffic network. In general, a mixed traffic environment poses significant modeling and control challenges due to the stochastic nature of human driving behavior and the lack of common information flow. Considering near-future CAV deployment, recent studies have already started exploring the traffic and energy impact of partial CAV penetration under different transportation scenarios [33–36]. However, the question that still remains unanswered is, “how can CAVs safely interact and co-exist with HDVs?” In this dissertation, I address this question through optimal control and coordination approach.

In what follows, I attempt to summarize the work reported in the literature to date on CAV control, coordination, and platooning. Any such effort has obvious limitations due to the vastness of the rich literature in this area. Thus, the focus is limited to reference only the research efforts that are important for understanding the fundamental concepts introduced in this dissertation, and for explaining any significant departures of the proposed research from the existing literature.

## **1.2 Literature Review**

### **1.2.1 Coordination using Connectivity and Automation**

Several research efforts have been reported in the literature proposing optimization and control approaches for coordinating CAVs at different traffic scenarios

that include merging at roadways and roundabouts, crossing intersections, cruising in congested traffic, passing through speed reduction zones, and lane-merging or passing maneuvers. In terms of energy impact, many studies have shown that significant fuel consumption and travel time benefits could be achieved through eco-driving and vehicle coordination without sacrificing driver safety [28, 37–41].

One of the early efforts in the direction of CAV coordination was proposed by Athans [42] for safe and efficient coordination of merging maneuvers to avoid congestion. Earlier efforts on coordinating CAVs to improve traffic flow also include approaches such as fuzzy logic [43], genetic algorithms [44], rule-based cooperation [36] and swarm optimization algorithms [45]. Since then, a significant number of research efforts reported in the literature tried to achieve safe and efficient coordination of CAVs at various traffic scenarios, where potential vehicle collisions may occur [46–55].

In recent years, the adoption of optimal control approach to control and coordinate the CAVs to improve urban mobility and traffic safety has gained traction. Both the *centralized* and *decentralized* framework are reported in the literature for optimal coordination of CAVs. In centralized approaches, there is at least one task in the system that is globally decided for all vehicles by a single central controller, whereas in a decentralized approach, the vehicles are treated as autonomous agents that collect traffic information to optimize their specific performance criteria while satisfying physical constraints. One of the main objectives of centralized and decentralized optimal coordination is to smooth the traffic flow by reducing spatial and temporal speed variations, and minimizing braking events. A significant number of approaches explored several domains of the optimal CAV coordination such as automated intersection crossing [28, 56–58], cooperative merging [27, 40, 41], roundabout [24, 59, 60], and speed harmonization through optimal vehicle control [61].

In 2004, Dresner et al. [46] presented one of the earliest directions in optimal coordination by introducing a reservation scheme to control a single intersection consisting of two roads. Similar approaches have been reported in the literature for safe

and efficient coordination of CAVs at urban intersections [47–49, 62]. Colombo et al. [62] constructed the invariant set for the control inputs that ensure lateral collision avoidance. Some approaches have focused on coordinating vehicles at intersections to improve the traffic flow [50, 51, 55]. The optimal control problem of coordinating the CAV in intersection with the cost function involving travel time has also been proposed [52–54, 63, 64]. In [65], an energy optimal scheme has been proposed for CAVs by probabilistic prediction of traffic lights in an intersection. Kim et al. [55] proposed a model predictive control (MPC) based approach which allows each vehicle to optimize its movement locally with a given cost function. Makarem et al. [66] formulated the optimal control problem as a linear quadratic regulator (LQR), and solved it using MPC. Qian et al. proposed a hierarchical control framework, where a high-level CAV coordination and a low-level multi-objective optimization scheme have been introduced. Several papers have also focused on multi-objective optimization problems using a receding horizon control (RHC) framework either in a centralized or decentralized setup [30, 67, 68]. Additional details of the research efforts in optimal coordination of CAVs can be found in the survey papers [6, 11, 31].

### 1.2.2 Decentralized Optimal Control Framework

In a decentralized optimal control framework, the vehicles are treated as autonomous agents that collect traffic information to optimize their specific performance criteria while satisfying physical constraints. A decentralized optimal framework to minimize travel time has been proposed in [69], where an optimization problem is solved to find the minimum time once the merging sequence is determined. Kamal et al. [70] proposed Pontryagin minimum principle (PMP) based numerical algorithms for CAV coordination in a signal-free intersection. Dynamic programming (DP) has been used in [65, 71] to compute the optimal control input, which is inherently not feasible for real-time application due to high computational effort. Sciarretta et al. [72] developed an eco-driving controller for CAVs for adaptive cruise control maneuver,

where the optimal problem minimizes the energy consumption with speed constraint. A speed advisory system has been proposed in [73], where the longitudinal dynamics of each CAV is optimized to minimize fuel consumption without considering the state and control constraints. In [71], the authors provided a PMP-based speed profile optimization framework for minimizing fuel consumption, where the CAV dynamics is not subject to any safety or acceleration/deceleration constraint. Detailed discussions of the research efforts reported in the literature on the coordination of CAVs can be found in [11, 74, 75].

In recent years, the decentralized optimal control framework has been researched extensively for real-time coordination of CAVs in different transportation segments. For example, the decentralized control framework was adopted in [20, 27, 40, 76, 77] for coordinating CAVs at highway on-ramps, in [64, 78, 79] at intersections, in [23, 59, 60] at roundabouts and [80] at traffic corridors. These efforts considered a control zone inside of which the CAVs can communicate with each other.

In decentralized optimal control approaches, the performance metrics that are generally considered for formulating the optimal control problem are travel time, energy consumption, and passenger safety. Several decentralized control approaches can be found in recent literature [20, 61, 78], where the control problem to maximize throughput and energy efficiency has been addressed. Consideration of more than one objective function leads to the formulation of the multi-objective optimal control problem that can be solved in different manners. For example, a hierarchical framework has been proposed in [27, 28, 40] that first solves an upper-level travel time minimization problem to generate optimal merging time, and then uses this result in a low-level energy minimization problem to generate the optimal motion primitive. On the other hand, a joint optimization framework has been proposed in [35, 76] that solves the multi-objective optimal control problem by considering the convex combination of cost functions consisting of energy consumption, travel time, passenger comfort, and safety. The trade-offs among the considered optimization objectives have been studied extensively

in these efforts.

Enforcement of system constraints is an important aspect while formulating and solving a decentralized optimal control problem to ensure passenger and component safety. The solution methodology of the unconstrained coordination problem has been extensively explored in [6, 20, 81], and validated experimentally at the University of Delaware scaled smart city using robotic CAVs [82–84] in a merging roadway scenario. However, the solution methodology of the constrained optimal control problem is challenging according to the standard Hamiltonian analysis [85]. Therefore, many research efforts have addressed only the partial constrained cases, i.e., either the state or the control constraints, in their optimal control problem [71, 73, 86]. For example, Wang et al. [87] formulated the multi-objective optimization problem for the CAVs approaching an intersection, and derived the solution without considering the safety constraint. A PMP-based approach was employed in [71] for optimizing the speed profile for fuel consumption minimization without considering the acceleration or safety constraint. Han et al. [86] proposed a safety-based eco-driving control for CAVs by considering the state constraints. The solution of the optimal control problem considering state and control constraints was presented in [28] at an urban intersection without considering rear-end collision avoidance constraint, and the conditions under which the latter does not become active were presented in [61]. More recently, a single-level multi-objective framework has been proposed for CAV coordination, where the state, control, and safety constraints are enforced a priori while solving the optimal control problem [88] using the feasibility zone approach. This approach has demonstrated remarkable results in different applications such as the enforcement of control barrier certificates [89], coordination based on Q-learning [90], traffic corridor coordination [64], etc. Another direction which the researchers have explored in the domain of decentralized coordination is the consideration of system uncertainty. Several such approaches have employed dynamic resequencing [91, 92], reinforcement learning [90, 93] and control barrier functions [89, 94] to handle system uncertainties in a decentralized optimal

control problem.

### 1.2.3 Coordination in a Mixed Traffic Environment

Despite all the potential CAV functionalities explored in the literature, the realization of an automated traffic scenario is restricted to a 100% CAV penetration rate, where all the vehicles on the road are assumed to have connectivity and automation. With the current market and manufacturer trend, the existence of a 100% CAV penetration rate is not expected before 2060 [95]. As a result, any control framework developed for CAV coordination considering 100% penetration rate is not tractable for real-world implementation and needs to be improved by considering a mixed traffic environment.

The impact of partial CAV penetration in terms of fuel consumption and traffic throughput has been studied through microscopic [14, 36, 96, 97] or meso/macroscopic simulation [98, 99] environments. Rios-Torres and Malikopoulos [96] concluded that the fuel improvement is significant only in the case of 100% CAV penetration rate near low traffic volume. Similar rule-based studies have been also reported in the literature that characterized the impact of CAV penetration in a mixed traffic environment [35, 100]. In these approaches, each CAV dynamics is optimized for energy consumption which does not account for the uncertainties ensuing from the random driving pattern of HDVs modeled with a conventional car-following model [101]. These penetration studies provide valuable insight into the macroscopic impact of a mixed traffic environment, but they do not address the vehicle-level control problem. Thus, researchers have also explored the possibility of vehicle-level control for CAV coordination in a mixed traffic environment. For example, the longitudinal dynamics of each CAV is optimized for fuel consumption minimization in [73] considering a mixed traffic environment at a signalized intersection. Jian [102] investigated the effect on fuel consumption and traffic throughput in a signalized intersection considering partial CAV penetration. The optimization problem was solved using an iterative method whereas

the HDV dynamics was modeled using intelligent driver model car-following dynamics. Ntousakis et al. [40] formulated an LQR-based automated on-ramp merging framework to be solved by MPC, which takes into account possible disturbances inside the control zone. They extended the problem to include manually driven vehicles following simple car-following dynamics. A distributed MPC framework is proposed by Qian et al. [68] for smooth trajectories of CAVs in an automated intersection by selecting a quadratic running cost for penalizing the input variable. The modeling of successive vehicle dynamics through MPC is computationally exhaustive due to the limited computational capability of the vehicle onboard. A common shortcoming of the reported approaches [20, 35, 40, 100, 103, 104] considering the mixed traffic environment is that the dynamics of the human-driven vehicles are always modeled with simplified car-following models to numerically simulate the actual human-driven vehicles on the road. However, the stochastic driving pattern and other uncertainties related to the HDVs have not been considered in the mathematical formulation, leaving the framework intractable for practical implementation. Complex coupled vehicle dynamics between the CAVs and HDVs, and trajectory uncertainties under different CAV penetration rates have not been addressed in these papers as well. Some efforts have developed a learning-based algorithm to mitigate the uncertainties of HDV trajectories, but are not real-time implementable due to high computational complexity [105, 106]. Therefore, although the above approaches [40, 96, 102, 104] deal with the problem of CAV and HDV interaction in a mixed traffic environment, a mathematically rigorous optimal control framework is yet to be addressed in the literature for a stable traffic interaction of CAVs and HDVs in the context of automated traffic coordination.

#### 1.2.4 Vehicle Platooning and Stability

An important direction toward the development and implementation of CAV technology is the platoon-based operation that has the potential of yielding additional improvement in vehicle and network performance. Significant research efforts have

been reported in the literature in terms of vehicle platoon formation and stability. The concept of forming platoons of vehicles traveling at a high speed has been a popular system-level approach to address traffic congestion. Some of the earliest research efforts to adopt vehicle platooning to address network congestion have been done in the 1980s and 1990s [107–109]. Since then, research interest in vehicle platooning has gained an ever-increasing momentum. The Energy ITS project in Japan [110], the Safe Road Trains for the Environment program [111], and the California Partner for Advanced Transportation Technology [112] are among the mostly-reported efforts in this area. Maiti et al. [113] developed a formal model for vehicle platooning using an ontology, and maintained that the different derived operations such as merge and split can be expressed as an aggregate of primitive operations. Lioris et al. [16] analyzed the potential mobility benefit from a platoon of CAVs under three different queuing models. The authors concluded that at a signalized intersection, the formation of platoons by the CAVs can increase the traffic throughput by double in contrast to the conventional passing of the vehicles. The literature on vehicle platooning can be broadly classified into two major categories: (a) platoon formation, where individual vehicles aim at creating a previously non-existent platoon or join an already existing platoon [114–117], and (b) platoon control, where vehicles within an established platoon are controlled to achieve some objectives, such as string stability, safe following gap control, coordination, etc [118–122]. A detailed overview of the literature on vehicle platooning can be found in the survey papers [123, 124].

Stability is a fundamental concept that is often associated with the research on vehicle platooning. In a locally stable platoon, each vehicle adjusts its motion to return to the equilibrium position after a perturbation is introduced in the system, and in a string stable platoon, the introduced perturbation is not amplified in the along the platoon. Both centralized and decentralized control approaches have been addressed in the literature regarding the stability of vehicle platoons. Kaku et al. [125] developed a centralized controller for a platoon of three CAVs using the LQR

approach for minimizing the overall fuel consumption of the platoon and compared its performance to the decentralized one. Dunbar et al. [126] proposed a distributed receding horizon control for a platoon of CAVs having non-linear decoupled double integrator dynamics and addressed the string stability of such platoon. A receding horizon control framework is applied to different vehicle connectivity topologies, namely leader-follower and predecessor-follower communication. Details of this formulation can be found in the literature [127, 128]. Morbidi et al. [129] synthesized an LQR control policy with measurable disturbances for a two-vehicle platoon where the string stability is established through feedback and feed-forward controller gain. In addition, the  $H_2$  and  $H_\infty$  performance criteria, denoting the group behavior and string stability of the platoon, are simultaneously achieved using a compensator-blending method. Some approaches have focused on the string stability only in the case of deceleration or “brake control” of the leading CAV. In this area, Li et al. [130] and Guo et al. [131] proposed a hierarchical framework for cooperative braking of a CAV inside a homogeneous vehicle platoon. The upper layer consists of a leading CAV with a linear controller designed to ensure the asymptotic convergence of the vehicle’s target set point after a braking event. On the other hand, the lower-level controller for the follower vehicles is designed based on the integrated sliding mode formulation considering the constant spacing and constant time headway policy.

The literature addressing platoon control and string stability mentioned so far only considered distributed control of the vehicles inside the platoon with decoupled dynamics, and an assumption of 100% penetration.

### 1.2.5 Vehicle Platooning in a Mixed Traffic Environment

The problem of platoon formation, in general, has been widely studied considering 100% CAV penetration. For example, some approaches based on MPC have been widely studied that guarantee string stability and safety [123, 132–134].

On the other hand, the literature on platoon formation is sparse in the context

of a mixed traffic environment. One of the most prevalent research directions towards developing a control framework for mixed traffic environment has been the development of cruise controller and adaptive cruise controller (ACC), [132, 135], where a CAV preceded by a single or a group of HDVs employs control algorithm to optimize a given objective, e.g., improvement of fuel economy [136], minimization of backward propagating wave [137], etc. A variation of the ACC framework has been developed to control CAVs in a mixed traffic environment [103, 138, 139] to tackle the HDV behavior and to ensure rear-end collision avoidance. Recently, some efforts have combined the concept of ACC with V2V communication protocol and proposed cooperative ACC [137, 140] for the CAVs traveling within a mixed traffic environment. Other approaches have employed robust or data-driven MPC models to ensure the safety of the CAV in mixed vehicle platoon [136, 141, 142]. The complexities in modeling the coupled dynamics and string stability during the interaction among CAVs and HDVs inside a platoon are yet to be fully understood. On this note, the research from Gong et al. [143] has been the most significant in addressing the coupled dynamics of a platoon of vehicles while considering the distributed control based on constrained optimization. The error states are used to formulate a primal-dual problem and solved using the dual-based optimization scheme to ensure platoon transient traffic smoothness with proven convergence. For an asymptotic dynamic performance, a closed-loop unconstrained linear system has also been established. Liu et al. [104] designed a provably safe vehicle trajectory policy and coordination rules for a longitudinal roadway under mixed traffic conditions. The HDVs are modeled with a car-following model while the CAVs follow the MPC protocol with the capability of platoon formation. Li et al. [144] proposed a dedicated short-range communication based vehicle platoon control considering vehicle-to-everything communication. With the leader-follower communication topology, stable platoon formation and merging were achieved in field experiments validating the proposed framework. Ntousakis et al. [145] reviewed the controller modeling efforts for the adaptive cruise control (ACC) systems based on different car-following models, which gives an insight into the potential coupled dynamics in a string of HDVs.

Accurate estimation and prediction of the HDV motion are essential to developing any feedback controller for the CAVs. For example, the performance of MPC-based controllers is greatly affected by the accuracy of prediction of the HDV trajectories within a look-ahead horizon. Several research efforts reported in the literature have considered different methodologies to estimate and predict the driving behavior of HDVs and incorporated them into their control framework. A variation of the car-following model to design an eco-ACC controller has been considered in [146]. A cooperative adaptive cruise controller has been proposed in [147] where the control parameters are derived using system identification on real-world experimental data. Naus et al. [148] proposed an explicit MPC-based ACC controller with constant speed prediction, whereas Dollar et al. [149] utilized an IDM model to identify offline the human driving styles in a car-following scenario. Jin et al. [150] proposed an optimal cruise control design in which feedback gains and driver reaction time of HDVs were estimated in real time by a sweeping least squares method. Gong and Du [151] developed a cooperative MPC framework and combined Newell car-following model with an online curve matching algorithm to anticipate the response delay of the HDVs.

### 1.3 Identification of the Research Gaps

Based on the literature discussed in the previous section, I have identified several open-ended questions and research gaps that are needed to be addressed to develop a tractable pathway for CAV deployment in a mixed traffic environment. In what follows, I present a detailed exposition of the research gaps in the literature related to the optimal control and coordination of CAVs.

**1. Traffic corridor problem:** The coordination framework for CAVs reported in the literature only considered single and isolated traffic scenarios in the formulation, e.g., on-ramp merging roadways, intersections, roundabouts, etc. For example, research efforts reported in the literature have primarily focused an individual transportation segment for CAV coordination [30, 67, 68, 152–154].

In general, the problem of CAV coordination in a traffic corridor has been addressed using a centralized control framework [47–49, 62]. Among these efforts, [56] investigate coordination in intersections using a phase conflict map to remove stop-and-go traffic signals. This work was extended later on and considered a corridor with multiple intersections [155]. Centralized controllers are by design computationally inefficient due to the high volume of information usually being processed at the central mainframe structure. Therefore, CAV coordination using the centralized control framework is not a tractable solution.

In contrast, several decentralized optimal control approaches have been reported in the literature for real-time coordination of CAVs at different transportation scenarios, e.g., at highway on-ramp merging [27, 40], signal-free intersection [28], roundabout [23], and speed reduction zone [61]. These approaches consider single and isolated traffic scenarios in their formulation. Therefore, the fundamental structure considered in these approaches fails if the traffic scenarios are closely spaced, or the roadways leading to the traffic segment are asymmetric. Furthermore, optimization of only an individual or isolated traffic segment in a traffic corridor may also result in traffic inefficiency, transient engine operation upstream or downstream of the traffic segment, or safety implications [83]. A complete decentralized optimal control framework for CAV coordination in a traffic corridor consisting of multiple adjacent traffic scenarios has not been investigated in detail.

**2. Constrained optimal control problem:** The computational complexity to solve a combined state, control and safety constrained decentralized optimal control framework has not been addressed in the literature. Several decentralized optimal control approaches can be found in recent literature [20, 40, 156], where the control problem to maximize throughput and energy efficiency has been addressed without considering the system constraints. The solution to the state and control unconstrained control problem presented in [61] and [40] shows acceleration spikes (jerk) at the boundaries of the optimization horizon, possibly exceeding the vehicle’s physical limitation

and giving rise to an undesired driving experience. To mitigate the aforementioned terminal acceleration jerk, Ntousakis et al. [40] reformulated the optimal control problem with vehicle acceleration as an additional state and using jerk as the control input. This approach provides safe state/control values at the terminal points, but can not guarantee that the state and control constraints will not become active within the optimization horizon. Therefore, the unconstrained solution can only guarantee that none of the constraints are violated at the boundaries of the optimization horizon, hence may not be admissible in a real-world application.

In general, it is difficult to solve the constrained optimal control problems in real time due to its iterative solution structure according to the standard Hamiltonian analysis that results in a complex arc-stitching methodology. Some approaches reported in the literature have addressed partial constrained cases, i.e., either the state or the control constraints, in their optimal control problem [71, 73, 86]. For example, the longitudinal dynamics of a CAV are optimized for fuel consumption minimization in [73], but the authors did not consider the speed and acceleration constraints while formulating the Hamiltonian. A similar approach was employed in [71] for optimizing the speed profile for fuel consumption minimization without including the acceleration constraint. Han et al. [86] proposed a safety-based eco-driving control for CAVs. The constrained optimal solution, in this case, only considers the state constraints and does not include the control constraints in the formulation. Another way of approaching the constrained optimal control problem has been explored using the feasibility zone analysis [29, 87], which results in weaker enforcement of the constraints compared to the explicit incorporation of the system constraints in the Hamiltonian formulation. Some approaches have also addressed the constrained optimal control problem by relaxing the terminal boundary conditions [35, 87]. However, none of these efforts address the problem of explicit incorporation of all the state, control, and safety constraints in their optimal control formulation given the terminal boundary conditions.

The standard methodology to solve the constrained optimal control problem using the Hamiltonian analysis requires piecing the unconstrained and constrained arcs together resulting in recursive numerical computations until all of the constraint activation cases are resolved. Such methodology has been explored in some efforts found in the literature [28, 29, 35, 157]. However, this iterative way of piecing the constrained and unconstrained arcs together until all the constraints activation cases are accounted for is computationally expensive and might prevent real-time implementation. Moreover, the solution framework of the constrained optimization problem using Hamiltonian analysis adopted in these efforts only addresses individual constraint activation cases without addressing the explicit interdependence between multiple constraint activation cases. The notion of the interdependence of the constraint activation cases has not been fully explored in the literature.

**3. Mixed traffic scenario:** The inherent problem of dealing with a mixed traffic environment is the fact that the dynamics of HDVs, with the uncertainties in their driving behavior, are assumed to be controlled only by human drivers. Thus the presence of HDVs seriously inhibits any potential formulation of a distributed control strategy to achieve vehicle cooperation at different traffic scenarios. Few papers in the literature only analyzed the impact of a mixed traffic environment without addressing the stochastic nature of the coupled HDV dynamics. To date, no rigorous mathematical framework has been presented in the literature to address the problem of optimally coordinating CAVs through traffic different scenarios in a mixed traffic environment with partial CAV penetration. Coordinating CAVs and HDVs so that they can safely co-exist, remains a challenging problem.

Recent efforts have reported several optimal control approaches for coordination of CAVs at different traffic scenarios such as on-ramp merging roadways [40], roundabouts [23, 59], speed reduction zones [61], signal-free intersections [55, 62, 158, 159], and traffic corridors [83, 155]. These approaches have focused on 100% CAV penetration rates without considering human-driven vehicles (HDVs). However, the existence

of having a transportation network with a 100% CAVs is not expected before 2060 [95]. Therefore, the need for a mathematically robust and tractable control framework considering a *mixed traffic environment* consisting of both CAVs and HDVs is essential.

One of the most important research directions toward a rigorous control framework for mixed traffic environment has been the development of CAV cruise controller and adaptive cruise controller [132, 135], where a CAV preceded by a single or a group of HDVs employs control algorithm to optimize a given objective, e.g., improvement of fuel economy [136], minimization of backward propagating wave [137, 140], etc. These approaches, however, cannot be adopted for coordinating CAVs at automated traffic scenarios such as signal-free intersections, automated on-ramp merging, etc.

To establish an automated traffic scenario, the presence of HDVs poses significant modeling and control challenges to the CAVs due to the stochastic nature of the human-driving behavior. Some approaches reported in the literature [73] have included car-following models (e.g.,[101, 160, 161]) while others have been based on reinforcement learning [105, 106]. These approaches, however, do not provide a complete coordination framework to impart any control framework on the HDVs in the network, rather enable the CAVs to derive their trajectory based only on the estimation of the HDV states assuming well-known car-following models (e.g.,[101, 160, 161]). Such framework may result in traffic gridlock, i.e., HDVs on the arterial roadway yielding or stopping to the vehicles on a priority roadway, defeating the purpose of an automated traffic coordination framework [28].

The impact of partial CAV penetration in terms of fuel consumption and traffic throughput has been studied by Rios-Torres and Malikopoulos[96], where the authors concluded that the fuel improvement is significant only in the case of 100% CAV penetration rate near low traffic volume. Here, each CAV dynamics is optimized for energy consumption which does not account for the uncertainties ensuing from the random driving pattern of HDVs modeled with a conventional car-following model [101]. The longitudinal dynamics of each CAV are optimized for fuel consumption minimization

in [73] for a mixed traffic environment in a signalized intersection, but the speed and acceleration constraints were not considered while formulating the Hamiltonian. Jian [102] investigated the effect on fuel consumption and traffic throughput in a signalized intersection considering partial CAV penetration. The optimization problem was solved using an iterative method whereas the HDV dynamics were modeled using intelligent driver model car-following dynamics. Ntousakis et al.[40] formulated an LQR-based automated on-ramp merging framework to be solved by MPC, which takes into account possible disturbances inside the control zone. They extended the problem to include manually driven vehicles following simple car-following dynamics. A distributed MPC framework is proposed by Qian et al. [68] for smooth traversal of CAVs in an automated intersection by selecting a quadratic running cost for penalizing the input variable. The modeling of successive vehicle dynamics through MPC is computationally exacting due to the limited computational capability of the vehicle onboard. A common shortcoming of the reported approaches [20, 40, 103, 104, 162] considering the mixed traffic environment is that the dynamics of the human-driven vehicles are always modeled with simplified car-following models to numerically simulate the actual human-driven vehicles on the road. However, the stochastic driving pattern, coupled car-following dynamics, and other uncertainties related to the HDVs have not been taken into consideration in the mathematical formulation, leaving the framework vulnerable during practical implementation. Complex vehicle dynamics for CAVs and HDVs and trajectory uncertainties under different CAV penetration rates have not been addressed in these papers as well. Therefore, although these approaches [40, 96, 102, 104, 130] deal with the problem of CAV-HDV interaction, a mathematically rigorous optimal control framework is yet to be addressed in the literature to date for a stable traffic interaction of CAVs and HDVs in the context of automated traffic coordination.

**4. Formation and impact of mixed platoons:** Although cooperative adaptive cruise control and CAV platoon dynamics in a 100% CAV penetration setting have

been explored in the literature, formation and stability analysis of mixed platoons consisting of CAVs and HDVs has not been reported in the literature.

The problem of platoon formation has been widely studied considering 100% CAV penetration. For example, some approaches based on MPC (or distributed MPC) have been studied that guarantee string stability and safety [123, 132–134]. Such approaches, however, cannot be directly applied to a mixed traffic environment with partial CAV penetration due to the presence of uncontrollable HDVs. On the other hand, the literature on platoon formation is sparse in the context of a mixed traffic environment. One of the most important research directions towards developing a control framework for mixed traffic environment has been the development of cruise controller and adaptive cruise controller (ACC), [132, 135], where a CAV preceded by a single or a group of HDVs employs control algorithm to optimize a given objective, e.g., improvement of fuel economy [136], minimization of backward propagating wave [137], etc. A variation of the ACC framework has been developed to control CAVs in a mixed traffic environment [103, 138, 139] to tackle the HDV behavior and to ensure rear-end collision avoidance. Recently, some efforts have combined the concept of ACC with a V2V communication protocol and proposed a connected cruise controller or cooperative ACC [137, 140] for the CAVs traveling within a mixed traffic environment. These approaches consider nonlinear dynamics and communication delays in a mixed connected platoon, where the CAV controller can only maintain a desired gap from the preceding vehicle. Other approaches have employed robust or data-driven MPC methods to ensure the safety of the CAV in mixed vehicle platoon [141, 142]. These approaches are limited to the cases where the objective is to control the target CAV to join and/or to maintain the stability and safety of an already formed platoon.

### **5. System uncertainty in a mixed traffic environment:**

The effect of system uncertainty and imperfect communication has been widely studied in the literature in terms of the 100% CAV penetration rate. Several approaches have employed dynamic resequencing [91, 92], reinforcement learning [90, 93],

control barrier functions [89, 94] and robust controller design [137] to handle system uncertainties. These approaches have been demonstrated to handle uncertainties in system dynamics and communication considering the CAVs. However, they do not explicitly consider a mixed traffic environment, where additional system uncertainties originating from the HDV behavior must be taken into account while deriving safe motion primitives for the CAVs.

The most relevant research efforts regarding the uncertainty of HDV dynamics have been done in the context of developing, calibrating, and validating the car-following model to emulate the human driving behavior [161, 163]. However, the interaction of CAVs and HDVs in a mixed traffic environment results in state estimation and dynamics prediction problems. Predicting HDV dynamics modeled with arbitrary car-following dynamics introduces additional complexity in the system that has not been addressed in the literature.

Accurate estimation and prediction of the HDV motion are essential to developing any feedback controller for the CAVs. For example, the performance of the MPC-based controllers is greatly affected by the accuracy of prediction of the HDV trajectories within a look-ahead horizon. Several research efforts reported in the literature have considered different methodologies to estimate and predict the driving behavior of HDVs and incorporated them into their control framework [146, 147, 164]. However, ACC controllers using car-following models such as the intelligent driver model (IDM) [161] do not always perform well while they exhibit string stability implications that can lead to rear-end collision[164]. A cooperative adaptive cruise controller has been proposed in [147] where the control parameters are derived using system identification on real-world experimental data. The issue with such an approach is, that the control parameters cannot capture the instantaneous changes in HDV behavior. Naus et al. [148] proposed an explicit MPC-based ACC controller that employs a prediction model considering the time-invariant speed of the preceding vehicle within the prediction horizon, and does not incorporate the complex car-following dynamics of the

human drivers.

In this dissertation, I will address the research gaps discussed above and advance the state of the art with the contributions outlined in the following section.

## 1.4 Research Contributions

The overarching goal of the proposed dissertation research is to develop an optimal control framework for coordinating CAVs through automated traffic scenarios in a mixed traffic environment consisting of conventional human-driven vehicles. The traffic scenarios considered here can be the roadways with the possibility of traffic congestion, e.g., highway on-ramp merging roads, roundabouts, speed reduction zones, urban intersections, etc.

The key contributions of this dissertation are summarized as follows:

*Contribution 1:* Development of a condition-based optimal CAV control framework that can handle the state, control, and safety constraints while deriving optimal motion primitives. The proposed framework yields a closed-form analytical solution to the constrained optimal control problem using an efficient, real-time implementable control algorithm.

*Contribution 2:* Development of a safety-aware multi-objective receding horizon control framework for mixed platoon formation that considers linear, non-linear, and data-driven prediction models for HDVs' trajectory estimation, and satisfies the system constraints with enhanced rear-end collision safety.

*Contribution 3:* Development of a robust, single-level, multi-objective optimal platoon coordination framework that can account for the effect of bounded communication delays and system constraints.

The first contribution addresses the major gaps in the literature related to the development of an optimal controller that can explicitly handle the system constraint

activation, as detailed in the previous section. In general, it is difficult to solve a constrained optimal control problem in real time due to its iterative nature. For example, the standard methodology to solve the constrained optimal control problem (see [28]) is to employ Hamiltonian analysis with interior point state and/or control constraints. To derive the optimal solution in this manner, one needs to iteratively piece the constrained and unconstrained arcs together until all the constraints activation cases are accounted for, which can be computationally expensive and might prevent real-time implementation. To address this issue, I develop a condition-based control framework that can identify the activation of system constraints a priori. The salient features of this contribution that advances the state of the art are: (1) an in-depth exposition of the properties of the different combinations of the state and control constraint activation cases and a set of a priori conditions to identify the constrained solution without any recursive steps, (2) elimination of the recursive solution structure for the state and control constrained optimal control problems for CAV coordination by considering the constraint activation conditions, and (3) an explicit expression of the junction point between the constrained and unconstrained arcs leading to a closed-form analytical solution of the constrained optimal control problem that can be used to derive constrained motion primitives for the CAVs with an efficient, real-time implementable algorithm. The aforementioned contributions are included in the following publications [165–168].

- A M Ishtiaque Mahbub and Andreas A Malikopoulos. Conditions to Provable System-Wide Optimal Coordination of Connected and Automated Vehicles. *Automatica*, 131(109751), 2021.
- A M Ishtiaque Mahbub and Andreas A Malikopoulos. Conditions for state and control constraint activation in the coordination of connected and automated vehicles. *Proceedings of 2020 American Control Conference*, pages 436–441, 2020.
- AM Ishtiaque Mahbub, Andreas A Malikopoulos, and Liuhui Zhao. Decentralized optimal coordination of connected and automated vehicles for multiple traffic scenarios. *Automatica*, 117(108958), 2020.

- A M Ishtiaque Mahbub, Andreas A Malikopoulos, and L. Zhao. Impact of connected and automated vehicles in a corridor. *In Proceedings of 2020 American Control Conference*, 2020, pages 1185–1190. IEEE, 2020.

The second contribution addresses the problem of deriving the optimal trajectory of a CAV in a mixed traffic environment that considers the interaction of HDVs. Since HDVs cannot be controlled directly, and any prediction of their future trajectories suffers from stochastic human driving behavior, it is challenging to establish any cooperation between the CAVs and HDVs. The proposed hypothesis is that the motion trajectory of the CAV can be controlled directly to restrict the motion of its trailing HDVs, thus imparting indirect control on the HDVs. One natural solution to validate the above hypothesis is to leverage the concept of vehicle platooning, where a CAV within the network can be controlled to force the trailing HDVs to form a platoon. As our second contribution, I propose a constrained multi-objective receding horizon control framework that considers linear, non-linear, and data-driven prediction models, and enables mixed platoon formation by directly controlling the CAVs with enhanced rear-end collision safety. The optimization objectives of the CAV are (a) to form a platoon with the trailing HDVs, and (b) to minimize its control effort. Our proposed platoon formation framework employs a receding horizon controller that uses a *multi-successor safety constraint* to enforce rear-end collision avoidance constraint for multiple trailing HDVs while deriving and implementing the optimal control input of the CAV. I propose two variants of the receding horizon control, namely, a model-dependent and a model-independent framework that employs different prediction models for estimating the HDV trajectories: (a) a naive linear constant speed model, (b) a nonlinear car-following model with nominal parameters and (c) a data-driven model that estimates the driving behavior of the HDVs in real time using recursive least squares algorithm to better predict the futures trajectories. In short, the approach proposed in this contribution will guarantee the indirect control of the HDVs by forming mixed platoons. These contributions are included in the following publications [169–172].

- A M Ishtiaque Mahbub and Andreas A Malikopoulos. A Platoon Formation Framework in a Mixed Traffic Environment. *IEEE Control Systems Letters (L-CSS)*, 6:1370–1375, 2021.
- A M Ishtiaque Mahbub and Andreas A. Malikopoulos. Platoon Formation in a Mixed Traffic Environment: A Model-Agnostic Optimal Control Approach. *Proceedings of 2022 American Control Conference*, 4746–4751, 2022.
- A M Ishtiaque Mahbub, Viet-Anh Le, and Andreas A. Malikopoulos. A Safety-Prioritized Receding Horizon Control Framework for Platoon Formation in a Mixed Traffic Environment. *in review*, 2022.
- A M Ishtiaque Mahbub, Viet-Anh Le, and Andreas A. Malikopoulos. Safety-Aware and Data-Driven Predictive Control for Connected Automated Vehicles at a Mixed Traffic Signalized Intersection. *10th IFAC Symposium on Advances in Automotive Control (to appear)*, 2022.

The third contribution addresses the problem of vehicle coordination in a mixed traffic environment. Generally, the HDVs in a mixed traffic network do not communicate and cooperate with other vehicles, which poses major difficulty in establishing a coordination framework at traffic scenarios such as signal-free intersections, automated on-ramp merging, etc. This contribution enables optimal coordination of CAVs and HDVs at automated traffic scenarios using vehicle platooning. To this end, I develop a robust, single-level, multi-objective optimal platoon coordination framework that can coordinate the mixed platoons through an automated highway on-ramp merging scenario. The proposed framework jointly maximizes the energy efficiency and throughput of the network and is robust enough to mitigate the worst-case scenario attributed to communication delay. The improvement of vehicle performance metrics such as energy efficiency and travel time in the context of a mixed platoon are also explored through this contribution. The following papers contain these contributions [173, 174].

- A M Ishtiaque Mahbub, Behdad Chalaki, and Andreas A Malikopoulos. A constrained optimal control framework for vehicle platoons with delayed communication. *Special Issue of Network and Heterogeneous Media: Traffic and Autonomy (accepted)*, 2022.
- A M Ishtiaque Mahbub, Hao Wang, Gabor Orosz, and Andreas A. Malikopoulos. Coordination of Mixed Platoons at On-Ramp Merging: A Constrained Optimal Control Framework. *in review*, 2022.

The key contributions of this dissertation as described above are the result of the gradual evolution of my research efforts in the domain of optimal control for CAVs. Several other efforts are aimed at addressing the research gaps related to the decentralized optimal coordination of CAVs in a traffic corridor consisting of multiple congestion scenarios. These efforts were reported in the following list of publications:

- A M Ishtiaque Mahbub, Liuhui Zhao, Dimitris Assanis, and Andreas A Malikopoulos. Energy-Optimal Coordination of Connected and Automated Vehicles at Multiple Intersections. In *Proceedings of 2019 American Control Conference*, pages 2664–2669, 2019.
- A M Ishtiaque Mahbub, V. Karri, Darshil Parikh, S. Jade, and Andreas A Malikopoulos. A decentralized time- and energy-optimal control framework for connected automated vehicles: From simulation to field test. In *SAE Technical Paper 2020-01-0579*. SAE International, 2020.
- A M Ishtiaque Mahbub and Andreas A Malikopoulos. Concurrent optimization of vehicle dynamics and powertrain operation using connectivity and automation. In *SAE Technical Paper 2020-01-0580*. SAE International, 2020.
- Liuhui Zhao, A M Ishtiaque Mahbub, and Andreas A Malikopoulos. Optimal vehicle dynamics and powertrain control for connected and automated vehicles. *Proceedings of 2019 IEEE Conference on Control Technology and Applications (CCTA)*, pages 33–38, 2019.

There are several other contributions as a result of the collaboration with my peers in the Information and Decision Science Lab. These contributions are not included in this dissertation but have been reported in the following publications:

- Logan E Beaver, Behdad Chalaki, A M Mahbub, Liuhui Zhao, Ray Zayas, and Andreas A Malikopoulos. Demonstration of a Time-Efficient Mobility System Using a Scaled Smart City. *Vehicle System Dynamics*, 58(5):787–804, 2020.
- Behdad Chalaki, Logan E. Beaver, A M Ishtiaque Mahbub, Heeseung Bang, and Andreas A. Malikopoulos. A research and educational robotic testbed for real-time control of emerging mobility systems: From theory to scaled experiments. *IEEE Control Systems Magazine*, 2022 (in press).

In summary, the key contributions discussed in this section will provide a rigorous mathematical solution to the problem of optimal control and coordination of

CAVs in a mixed traffic environment. The outcome of the proposed research direction not only provides a vehicle-level performance improvement but also realizes the automated coordination and merging concept, which increases the traffic performance from a macroscopic viewpoint. Compared to the utopian scenario with 100% CAV penetration, the developed control framework will be implementable online in real-world mixed traffic network with a variety of scenarios.

## 1.5 Dissertation Overview

The remainder of this dissertation follows the following structure.

**Chapter 2** provides some of our preliminary research efforts related to the decentralized time- and energy-optimal coordination of CAVs traveling through a traffic corridor consisting of major traffic congestion scenarios. In Section 2.1, I present an energy-optimal VD controller for coordinating CAVs at multiple adjacent intersections using interior-point constraints. In Section 2.2, I provide a detailed comparative analysis between the conventional isolated control approach and the coordinated control approach developed in Section 2.1. I then extend the control paradigm in Section 2.3 and show that the VD controller can be combined with a powertrain control architecture to harness additional energy consumption benefits. To validate the effectiveness of the VD controller, I present a sequential experimentation methodology in Section 2.4 that shows significant improvement in terms of fuel economy and traffic throughput. The content presented in this chapter is acquired from the following papers [175–178].

- A M Ishtiaque Mahbub, Liuhui Zhao, Dimitris Assanis, and Andreas A Malikopoulos. Energy-Optimal Coordination of Connected and Automated Vehicles at Multiple Intersections. In *Proceedings of 2019 American Control Conference*, pages 2664–2669, 2019.
- A M Ishtiaque Mahbub, V. Karri, Darshil Parikh, S. Jade, and Andreas A Malikopoulos. A decentralized time- and energy-optimal control framework for connected automated vehicles: From simulation to field test. In *SAE Technical Paper 2020-01-0579*. SAE International, 2020.
- A M Ishtiaque Mahbub and Andreas A Malikopoulos. Concurrent optimization of vehicle dynamics and powertrain operation using connectivity and automation. In *SAE Technical Paper 2020-01-0580*. SAE International, 2020.
- Liuhui Zhao, A M Ishtiaque Mahbub, and Andreas A Malikopoulos. Optimal vehicle dynamics and powertrain control for connected and automated vehicles. *Proceedings of 2019 IEEE Conference on Control Technology and Applications (CCTA)*, pages 33–38, 2019.

**Chapter 3** presents a rigorous mathematical framework to efficiently handle the constrained optimal control problems. In Section 3.1, I provide a condition-based control framework that can derive constrained motion primitives in real time by identifying the constraint activation cases a priori. An extension of this methodology is discussed in Section 3.2, where the CAV control framework explicitly incorporates the safety constraints while deriving the optimal trajectory for traversing a traffic corridor. The content presented in this chapter is acquired from the following papers [165–168].

- A M Ishtiaque Mahbub and Andreas A Malikopoulos. Conditions to Provable System-Wide Optimal Coordination of Connected and Automated Vehicles. *Automatica*, 131(109751), 2021.
- A M Ishtiaque Mahbub and Andreas A Malikopoulos. Conditions for state and control constraint activation in the coordination of connected and automated vehicles. *Proceedings of 2020 American Control Conference*, pages 436–441, 2020.
- AM Ishtiaque Mahbub, Andreas A Malikopoulos, and Liuhui Zhao. Decentralized optimal coordination of connected and automated vehicles for multiple traffic scenarios. *Automatica*, 117(108958), 2020.
- A M Ishtiaque Mahbub, Andreas A Malikopoulos, and L. Zhao. Impact of connected and automated vehicles in a corridor. *In Proceedings of 2020 American Control Conference*, 2020, pages 1185–1190. IEEE, 2020.

**Chapter 4** explores the domain of mixed traffic environment. In Section 4.1, I consider the problem of deriving a safe trajectory for the CAV approaching a signalized intersection in the presence of HDVs with unknown driving behavior. Subsequently, I investigate the impact of partial penetration of CAVs in a traffic corridor to quantify the network-level performance in Section 4.2. The content presented in this chapter is acquired from the following papers [172, 179].

- A M Ishtiaque Mahbub, Viet-Anh Le, and Andreas A. Malikopoulos. Safety-Aware and Data-Driven Predictive Control for Connected Automated Vehicles at a Mixed Traffic Signalized Intersection. *10th IFAC Symposium on Advances in Automotive Control (to appear)*, 2022.
- A. Valencia, A M Mahbub, and Andreas A Malikopoulos. Performance analysis of optimally coordinated connected automated vehicles in a mixed traffic environment. *In 30th Mediterranean Conference on Control and Automation*, 2022 (accepted).

**Chapter 5** addresses the problem of platoon formation in a mixed traffic environment. First, I explore the feasibility of mixed platoon formation in Section 5.1. Then, I present a model-agnostic optimal platoon formation framework in Section 5.2. Continuing further, in Section 5.3 I develop a safety-prioritized framework for creating a mixed platoon of vehicles by proposing a constrained multi-objective receding horizon control approach that considers linear, non-linear, and data-driven prediction models with enhanced safety guarantee. The content presented in this chapter is acquired from the following papers [169–171].

- A M Ishtiaque Mahbub and Andreas A Malikopoulos. A Platoon Formation Framework in a Mixed Traffic Environment. *IEEE Control Systems Letters (LCCS)*, 6:1370–1375, 2021.
- A M Ishtiaque Mahbub and Andreas A. Malikopoulos. Platoon Formation in a Mixed Traffic Environment: A Model-Agnostic Optimal Control Approach. *Proceedings of 2022 American Control Conference*, 4746–4751, 2022.
- A M Ishtiaque Mahbub, Viet-Anh Le, and Andreas A. Malikopoulos. A Safety-Prioritized Receding Horizon Control Framework for Platoon Formation in a Mixed Traffic Environment. *in review*, 2022.

**Chapter 6** presents a single-level optimal control framework for platoon coordination. I first develop the platoon coordination framework for 100% CAV penetration case in Section 6.1, and then extend the methodology to incorporate mixed traffic environment in Section 6.2 for an on-ramp merging scenario. The content presented in this chapter is acquired from the following papers [173, 174].

- A M Ishtiaque Mahbub, Behdad Chalaki, and Andreas A Malikopoulos. A constrained optimal control framework for vehicle platoons with delayed communication. *Special Issue of Network and Heterogeneous Media: Traffic and Autonomy (accepted)*, 2022 (arXiv:2111.08080).
- A M Ishtiaque Mahbub, Hao Wang, Gabor Orosz, and Andreas A. Malikopoulos. Coordination of Mixed Platoons at On-Ramp Merging: A Constrained Optimal Control Framework. *in review*, 2022.

Finally, **Chapter 7** summarizes the contributions of this dissertation and provides concluding remarks with a note on future research directions.

## Chapter 2

### OPTIMAL COORDINATION AT A TRAFFIC CORRIDOR

Urban intersections, merging roadways, roundabouts, and speed reduction zones along with the driver responses to various disturbances are the primary sources of bottlenecks in corridors that contribute to traffic congestion. As a potential solution to eliminate traffic congestion at these major traffic scenarios, researchers have proposed different optimal coordination frameworks using CAVs. More recently, a decentralized optimal control framework has been established for coordinating CAVs in different transportation scenarios. A closed-form, analytical solution without considering state and control constraints was presented in [20], [27], and [40] for coordinating online CAVs at highway on-ramps, in [28, 78] at intersections, and in [23] at roundabouts. These efforts only considered CAV coordination at an isolated traffic scenario. However, these approaches fail to consider the following aspects.

1. The control framework for isolated traffic scenarios might fail in the presence of closely-spaced adjacent traffic scenarios.
2. A traffic corridor including multiple traffic scenarios can have inefficient vehicle trajectories in the uncontrolled regions.

In this chapter, I present a decentralized energy-optimal VD controller that employs a coordinated control strategy for CAVs traveling through a traffic corridor considering a 100% CAV penetration rate. Subsequently, I provide a comparative analysis of the coordinated and isolated control strategy. Additionally, I show that the developed VD controller can be combined with a powertrain control architecture to harness additional energy consumption benefits. To validate the effectiveness of

the VD controller, I present a sequential experimentation methodology that shows significant improvement in terms of fuel economy and traffic throughput.

## 2.1 Energy-Optimal Coordination at Multiple Adjacent Intersections

In this section, I address the problem of optimally coordinating CAVs at multiple adjacent intersections through the development of a coordinated coordination strategy. Specifically, I address the gaps in the state of the art with the following contributions: (1) development of a decentralized CAV coordination policy for throughput maximization in a traffic corridor with multiple signal-free adjacent intersections, (2) formulation of an energy-optimal control framework considering interior boundary constraints, and (3) derivation of a closed-form analytical solution that yields optimal control policy for CAV coordination. We evaluate the effectiveness of the solution through simulation. Fuel consumption and travel time are significantly reduced compared to the baseline scenario designed with conventional fixed time signalized intersections.

### 2.1.1 Problem Formulation

Let us consider a traffic corridor (Fig. 2.1) consisting of two adjacent urban intersections separated by a length  $D$ . Each intersection includes an area of potential lateral collision defined as the *merging zone*, shown by the red squares of length  $S_z$  for merging zone  $z$ ,  $z = 1, 2$ , in Fig. 2.1. The length and geometry of the merging zones are not restrictive. Both intersections are located within a *control zone* illustrated in Fig. 2.1, inside of which the CAVs can communicate with each other and with a coordinator. The distance between the entry of the control zone and the entry of the merging zone  $z$  is denoted by  $L_z$ . Thus, the distance from the entry of the control zone to the nearest and farthest entry of the merging zone is  $L_z = L$  and  $L_z = L + S_z + D$ , respectively (Fig. 2.1). When a CAV enters the control zone, it exchanges information with other CAVs as well as the coordinator to derive its optimal control input (acceleration/deceleration) to cross the intersections without any rear-end or lateral collision. Note that, the

coordinator only facilitates the communication among the CAVs and is not involved in any decision-making process. In the remainder of this dissertation, I use a similar structure for formulating the problems that includes the reference of control zone and coordinator without repetition of the definition.

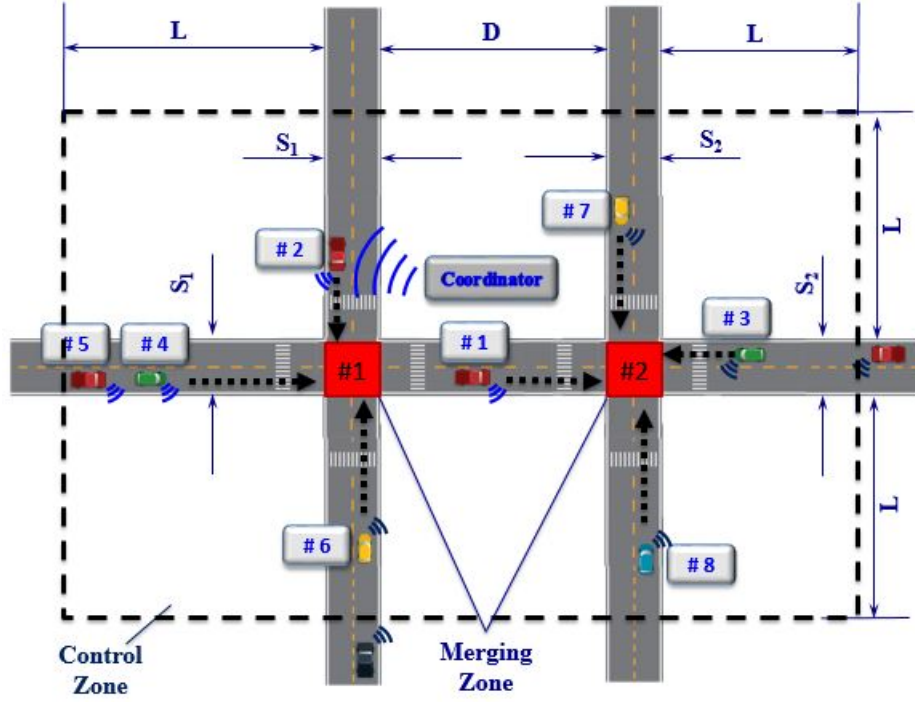


Figure 2.1: Corridor with connected and automated vehicles.

Let  $N(t) \in \mathbb{N}$  be the number of CAVs inside the control zone of the corridor at time  $t \in \mathbb{R}^+$  and  $z = 1, 2$  be the number of merging zones of the intersections. When a CAV enters the control zone of the corridor, the coordinator receives its route information and assigns a unique identification number  $i \in \mathbb{N}$ . Let  $\mathcal{N}(t) = \{1, \dots, N(t)\}$  be the merging sequence that the vehicles enter the control zone. Let  $t_i^0$  be the initial time that vehicle  $i$  enters the control zone of the corridor, and  $t_i^{mz}$  and  $t_i^{fz}$  be the time that CAV  $i$  enters and exits each merging zone  $z, z = 1, 2$  along its route, respectively. Let  $t_i^f$  be the time that the CAV  $i$  exits the last conflict zone on its route. Therefore,  $t_i^f = t_i^{m2}$  if the last conflict zone ID is  $z = 2$ .

**Definition 2.1.1.**  $\mathcal{Q}^z(t)$  is a local merging sequence such that  $\mathcal{Q}^z(t) \subset \mathcal{N}(t)$  and includes all CAVs  $M^z(t) \in \mathbb{N}$  at time  $t \in \mathbb{R}^+$  that will be entering the merging zone  $z$ ,  $z = 1, 2$ .

For example, CAV #2, 3, 4, 5, 6  $\in \mathcal{Q}^1(t)$  but CAV #1, 7, 8  $\notin \mathcal{Q}^1(t)$  (Fig. 2.1). Similarly, CAV #1, 3, 4, 5, 7, 8  $\in \mathcal{Q}^2(t)$  but CAV #2, 6  $\notin \mathcal{Q}^2(t)$  (Fig. 2.1). If a CAV  $i$  enters the control zone at time  $t_i^0$  with a route designating to cross the merging zone  $z$ , i.e.,  $i \in \mathcal{Q}^z(t)$ , it needs to compute the optimal time  $t_i^{m_z^*}$  to enter the merging zone  $z$ ,  $z = 1, 2$ , to avoid collision. The order of CAV  $i \in \mathcal{Q}^z(t)$  satisfies the following condition,

$$t_i^{m_z^*} \geq t_{i-1}^{m_z^*}, \quad \forall i \in \mathcal{Q}^z(t), \quad i > 1. \quad (2.1)$$

When a CAV  $i \in \mathcal{Q}^z(t)$  enters the control zone at time  $t_i^0$ , the merging time  $t_i^{m_z} = t_i^0 + \frac{L_z}{v_i(t_i^0)}$  corresponding to its initial constant speed is compared to the optimal merging time  $t_{i-1}^{m_z^*}$  of the previous CAV in the queue. If the following condition holds

$$t_i^{m_z} \geq t_{i-1}^{m_z^*}, \quad i \in \mathcal{Q}^z(t), \quad i > 1, \quad (2.2)$$

then the merging sequence  $\mathcal{Q}^z(t)$  is remained unchanged. However, if (2.2) does not hold,  $\mathcal{Q}^z(t)$  can be updated to change the order of the CAVs entering the merging zone so that (2.1) is not violated. The policy through which the merging sequence  $\mathcal{Q}^z(t)$  is updated can be obtained as the result of an upper level vehicle coordination problem, as described in the following section. Once the optimal merging time  $t_i^{m_z^*}$  is fixed, each vehicle solves a lower-level energy minimization problem that yields an analytical, closed-form optimal solution.

### 2.1.2 Modeling Framework and Constraints

Each CAV is modeled as a double integrator,

$$\dot{p}_i = v_i(t), \quad \dot{v}_i = u_i(t), \quad (2.3)$$

where  $p_i(t) \in \mathcal{P}_i$ ,  $v_i(t) \in \mathcal{V}_i$ , and  $u_i(t) \in \mathcal{U}_i$  denote the position, speed and acceleration of each vehicle  $i$  in the control zone of the corridor. The sets  $\mathcal{P}_i$ ,  $\mathcal{V}_i$ , and  $\mathcal{U}_i$ ,  $i \in \mathcal{N}(t)$ , are complete and totally bounded subsets of  $\mathbb{R}$ . Let  $x_i(t) = [p_i(t) \ v_i(t)]^T$  denote the state of each vehicle  $i$ , with initial value  $x_i^0 = x_i(t_i^0) = [p_i^0 \ v_i^0]^T$ , where  $p_i^0 = p_i(t_i^0) = 0$  at the entry of the corridor, taking values in  $\mathcal{X}_i = \mathcal{P}_i \times \mathcal{V}_i$ . The state space  $\mathcal{X}_i$  for each vehicle  $i$  is closed with respect to the induced topology on  $\mathcal{P}_i \times \mathcal{V}_i$  and thus, it is compact.

We need to ensure that for any initial state  $(t_i^0, x_i^0)$  and every admissible control  $u_i(t)$ , the system (2.3) has a unique solution  $x_i(t)$  on some interval  $[t_i^0, t_i^f]$ . The following observations from (2.3) satisfy some regularity conditions required both on the model and admissible controls  $u_i(t)$  to guarantee local existence and uniqueness of solutions for (2.3): a) The model is continuous in  $u$  and continuously differentiable in the state  $x$ , b) The first derivative of the model in  $x$  is continuous in  $u$ , and c) The admissible control  $u_i(t)$  is continuous with respect to  $t$ .

To ensure that the control input and vehicle speed are within a given admissible range, the following constraints are imposed,

$$\begin{aligned} u_{min} \leq u_i(t) \leq u_{max}, \quad \text{and} \\ 0 \leq v_{min} \leq v_i(t) \leq v_{max}, \quad \forall t \in [t_i^0, t_i^f], \end{aligned} \tag{2.4}$$

where  $u_{min}$ ,  $u_{max}$  are the minimum and maximum acceleration for each vehicle  $i \in \mathcal{N}(t)$ , and  $v_{min}$ ,  $v_{max}$  are the minimum and maximum speed limits respectively.

To characterize the physical location of the CAV  $i-1 \in \mathcal{Q}^z(t)$  inside the control zone, three subsets  $\mathcal{L}_i^z(t)$ ,  $\mathcal{O}_i^z(t)$  and  $\mathcal{C}_i^z(t)$  of  $\mathcal{Q}^z(t)$  with respect to CAV  $i$  are defined as follows.

**Definition 2.1.2.** 1) The set  $\mathcal{L}_i^z(t)$  contains all vehicles traveling in the same direction and same lane as vehicle  $i$  with a potential of rear-end collision, e.g.,  $\mathcal{L}_5^1(t)$  contains CAV #4 (Fig. 2.1), 2)  $\mathcal{O}_i^z(t)$  contains all vehicles that travel in the opposite direction as vehicle  $i$ , and thus no rear-end or lateral collision is possible, e.g.,  $\mathcal{O}_1^2(t)$  contains

CAV #3 (Fig. 2.1), and 3)  $\mathcal{C}_i^z(t)$  contains all vehicles from different entry points with the possibility of lateral collision with vehicle  $i$ , e.g.,  $\mathcal{C}_8^z(t)$  contains CAV #1 (Fig. 2.1).

To ensure the absence of rear-end collision of two consecutive vehicles traveling in the same lane, the position of the physically immediately preceding CAV  $k \in \mathcal{L}_i^z(t)$  should be greater than or equal to the position of the following vehicle plus a predefined safe distance headway  $\delta_i(t)$ , which is a function of speed  $v_i(t)$ . Thus we impose the rear-end safety constraint,

$$p_k(t) - p_i(t) \geq \delta_i(t), \quad \forall t \in [t_i^0, t_i^f]. \quad (2.5)$$

For each CAV  $i \in \mathcal{Q}^z(t)$ , the lateral collision is possible within the set  $\Gamma_i$ ,

$$\Gamma_i \triangleq \{t \mid t \in [t_i^{mz}, t_i^{fz}]\}. \quad (2.6)$$

Lateral collision between any two CAVs  $i, j \in \mathcal{Q}^z(t)$  can be avoided if the following constraint hold

$$\Gamma_i \cap \Gamma_j = \emptyset, \quad \forall t \in [t_i^{mz}, t_i^{fz}], \quad i, j \in \mathcal{Q}^z(t). \quad (2.7)$$

**Assumption 2.1.1.** Left/right turns or lane changes inside the control zone are not allowed.

**Assumption 2.1.2.** Communication among CAVs occurs without any delays and errors. Each CAV  $i$  is equipped with sensors to measure and share their local information.

**Assumption 2.1.3.** None of the state and control constraints are active at time  $t_i^0$  when each CAV  $i \in \mathcal{N}(t)$  enters the control zone.

Assumption 2.1.1 is imposed to simplify the problem and focus on the implications of the analytical solution without adding more degrees of complexity and can be relaxed to allow left/right turns and lane changes without loss of generality. Assumption 2.1.2 may be strong, but it is relatively straightforward to relax it as long as the noise in the measurements and/or delays is bounded. For example, we can determine

upper bounds on the state uncertainties as a result of sensing or communication errors and delays, and incorporate these into more conservative safety constraints. Finally, Assumption 2.1.3 ensures that, for each CAV  $i \in \mathcal{N}(t)$ , the initial state and control input at the entry of the control zone is feasible. This implies that the initial condition for the optimal control problem will be feasible.

### 2.1.3 Upper-Level Vehicle Coordination Problem

The upper level vehicle coordination problem provides the time  $t_i^{m_z^*}$  that each CAV  $i \in \mathcal{Q}^z(t)$  uses to enter the merging zone  $z, z = 1, 2$ . For  $i = 1$ , due to the absence of any prior CAV inside the control zone, the safety constraints (2.5) and (2.7) are not active. This leads to the trivial solution  $v_1^*(t) = v_i^0, \forall t \in [t_i^0, t_i^{m_z^*}]$  and  $t_i^{m_z^*} = t_i^0 + \frac{L_z}{v_i(t_i^0)}$ . For the rest of the CAVs  $i \in \mathcal{Q}^z(t)$ , we seek to maximize the traffic throughput by minimizing the inter-vehicle gaps according the following optimization scheme,

$$\min_{t(2:M^z(t))} \sum_{z=1}^2 \sum_{i=2}^{M^z(t)} (t_i^{m_z} - t_{i-1}^{m_z}) = \min_{t(M^z(t))} \sum_{z=1}^2 (t_{M^z(t)}^{m_z} - t_1^{m_z}) \quad (2.8)$$

subject to : (2.1), (2.4), (2.5), (2.7).

The solution of the optimal control problem (2.8) recursively yields a feasible merging time  $t_i^{m_z^*}$  for each vehicle  $i$  to cross the merging zone  $z$  satisfying condition (2.1)

**Theorem 2.1.3.** *If the state and control constraints in (2.4) are inactive, the solution  $\mathcal{T}^* = \{t_2^{m_z^*}, \dots, t_{M^z(t)}^{m_z^*}\}$  of (2.8) can be obtained through the following recursive structure over  $i = 2, \dots, M^z(t)$  for each  $z, z = 1, 2$ ,*

$$t_i^{m_z^*} = \begin{cases} t_k^{m_z^*} + \frac{\delta_i(t)}{v_k(t_k^{m_z^*})}, \text{ if } i-1 \in \mathcal{L}_i^z(t), \\ \max \left\{ t_{i-1}^{m_z^*}, t_k^{m_z^*} + \frac{\delta_i(t)}{v_k(t_k^{m_z^*})} \right\}, \\ \text{ if } i-1 \in \mathcal{O}_i^z(t) \\ \max \left\{ t_{i-1}^{m_z^*} + \frac{S_z}{v_{i-1}(t_{i-1}^{m_z^*})}, \right. \\ \left. t_k^{m_z^*} + \frac{\delta_i(t)}{v_k(t_k^{m_z^*})} \right\}, \text{ if } i-1 \in \mathcal{C}_i^z(t) \end{cases} \quad (2.9)$$

*Proof.* We need to consider three cases based on the interdependency between CAV  $i$  and  $i - 1$ .

Case 1: If  $i - 1 \in \mathcal{L}_i^z(t)$ , then (2.5) becomes active whereas (2.7) becomes inactive. As CAV  $i - 1$  also represent the CAV  $k$ , which is physically located in front of  $i$ , we can denote  $i - 1$  as  $k$  in this particular case. From (2.5) we get,  $(p_k(t_i^{m_z}) - p_i(t_i^{m_z})) = L_z + v_k(t_i^{m_z} - t_k^{m_z}) - L_z \geq \delta_i(t)$ , yielding  $t_i^{m_z^*} = t_k^{m_z^*} + \frac{\delta_i(t)}{v_k(t_k^{m_z^*})}$ . According to (2.1),  $t_i^{m_z^*} \geq t_{i-1}^{m_z^*}$ . Therefore,  $t_i^{m_z^*} = \max\left\{t_k^{m_z^*} + \frac{\delta_i(t)}{v_k(t_k^{m_z^*})}, \frac{L_z}{v_{max}} + t_i^0\right\}$ .

Case 2: If CAV  $i - 1 \in \mathcal{O}_i^z(t)$ , then constraint (2.7) and (2.5) are not active for CAV  $i$ . In this case, the inter-vehicle time gap  $(t_i^{m_z} - t_{i-1}^{m_z^*})$  can be minimized by setting the optimal solution  $t_i^{m_z^*}$  such that  $t_i^{m_z^*} = t_{i-1}^{m_z^*}$ . However, constraint (2.5) becomes active if there exists at least one CAV  $k, k \in \mathcal{L}_i^z(t)$ . Following the reasoning from case (1), we get,  $\max\left\{t_{i-1}^{m_z^*}, t_k^{m_z^*} + \frac{\delta_i(t)}{v_k(t_k^{m_z^*})}\right\}$ , if  $i - 1 \in \mathcal{O}_i^z(t)$ .

Case 3: If  $i - 1 \in \mathcal{C}_i^z(t)$ , (2.7) becomes active. In this case,  $(t_i^{m_z} - t_{i-1}^{m_z^*})$  can be minimized by taking  $t_i^{m_z} = t_{i-1}^f = t_{i-1}^{m_z^*} + \frac{S_z}{v_{i-1}(t_{i-1}^{m_z^*})}$ . Again, if there exists a vehicle  $k \in \mathcal{L}_i^z(t)$ , (2.5) becomes active. To satisfy (2.1), we have  $t_i^{m_z^*} = \max\left\{t_{i-1}^{m_z^*} + \frac{S_z}{v_{i-1}(t_{i-1}^{m_z^*})}, t_k^{m_z^*} + \frac{\delta_i(t)}{v_k(t_k^{m_z^*})}\right\}$   $\square$

If the condition (2.2) is violated, two special cases arise. Based on the following proposition, CAV  $i$  can either follow  $i - 1$  or reach the merging zone before  $i - 1$ .

**Proposition 2.1.1.** *If there exists a CAV  $j \in \mathcal{C}_i^z(t) : |t_i^{m_z} - t_j^{m_z^*}| < \rho_i$  or  $k \in \mathcal{L}_i^z(t)$ , the order of the CAVs in  $\mathcal{Q}^z(t)$  is conserved and  $t_i^{m_z^*}$  is calculated by (2.9). If there is no CAV  $k \in \mathcal{L}_i^z(t)$  and  $|t_i^{m_z} - t_j^{m_z^*}| \geq \rho_i, \forall j \in \mathcal{C}_i^z(t)$ , then the order of the CAVs in  $\mathcal{Q}_i^z(t)$  is updated and  $t_i^{m_z^*} = t_i^0 + \frac{L_z}{v_i(t_i^0)}$ . Here,  $\rho_i$  is a predefined safe time headway.*

*Proof.* Part 1: If there exists a CAV  $k \in \mathcal{L}_i^z(t)$ , or  $j \in \mathcal{C}_i^z(t) : |t_i^{m_z} - t_j^{m_z^*}| < \rho_i$ , CAV  $i$  cannot have a collision free trajectory. This implies  $i$  cannot travel with its initially

calculated merging time  $t_i^{mz}$  and has to merge after CAV  $i - 1$ . To satisfy (2.1), the merging sequence is conserved, and  $t_i^{mz^*}$  is calculated by (2.9) which minimizes (2.8).

Part 2: With the absence of  $k \in \mathcal{L}_i^z(t)$ , if  $|t_i^{mz} - t_j^{mz^*}| \geq \rho_i, \forall j \in \mathcal{C}_i^z(t)$ , vehicle  $i$  can have a collision-free trajectory and maintain its initial velocity such that  $t_i^{mz^*} = t_i^{mz} = t_i^0 + \frac{L_z}{v_i(t_i^0)}$ . In this case, the merging sequence is updated so that (2.1) is not violated.  $\square$

#### 2.1.4 Low-Level Energy Minimization Problem

For each vehicle  $i \in \mathcal{N}(t)$ , we formulate the decentralized optimal control problem that minimizes the cost function  $J_i(u(t))$  in  $[t_i^0, t_i^f]$ ,

$$\min_{u_i \in U_i} J_i(u(t)) = \int_{t_i^0}^{t_i^f} C_i(u_i(t)) dt, \quad (2.10)$$

subject to : (2.3), (2.4),  $p_i(t_i^0) = 0, p_i(t_i^{mz}) = L_z,$

and given  $t_i^0, v_i^0, t_i^{mz}$ .

Here,  $C_i(u_i(t))$  is monotonically increasing function of the control input  $u_i(t)$  and can be viewed as a measure of energy. When  $C_i(u_i(t))$  is considered as the  $L^2$ -norm of the control input, i.e.  $C_i(u_i(t)) = \frac{1}{2}u_i^2(t)$ , the transient engine operation can be minimized, which eventually represents the minimization of fuel consumption [180]. Note that, the safety constraints are not included in (2.10). The lateral collision constraint (2.7) is implicitly included by solving the upper-level vehicle coordination problem. The rear-end collision constraint (2.5) can be avoided under proper initial conditions  $[t_i^0, v_i^0(t)]$  as described in [28].

In what follows, we provide the closed-form solution of the optimal control problem formulated in (2.10) for each vehicle  $i \in \mathcal{N}(t)$ .

### 2.1.5 Closed-Form Analytical Solution

The solution of the constrained problem has been addressed in [28], and it requires the constrained and unconstrained arcs of the state and control input to be pieced together to satisfy the Euler-Lagrange equations and necessary condition of optimality. Due to the page limitations, we provide the general formulation and include only the solution of the unconstrained case here. From (2.10), the state equations (2.3) and the constraints (2.4), for each vehicle  $i \in \mathcal{N}(t)$  the Hamiltonian function with the state and control adjoined is

$$H_i(t, x(t), u(t)) = \frac{1}{2}u_i^2 + \lambda_i^p \cdot v_i + \lambda_i^v \cdot u_i + \mu_i^a \cdot (u_i - u_{max}) + \mu_i^b \cdot (u_{min} - u_i) + \mu_i^c \cdot (v_i - v_{max}) + \mu_i^d \cdot (v_{min} - v_i), \quad \forall i \in \mathcal{N}(t), \quad (2.11)$$

where  $\lambda_i^p$  and  $\lambda_i^v$  are the co-state components, and  $\mu_i^a, \mu_i^b, \mu_i^c$  and  $\mu_i^d$  are the Lagrange multipliers.

$$\mu_i^a = \begin{cases} > 0, & u_i(t) - u_{max} = 0, \\ = 0, & u_i(t) - u_{max} < 0, \end{cases} \quad (2.12)$$

$$\mu_i^b = \begin{cases} > 0, & u_{min} - u_i(t) = 0, \\ = 0, & u_{min} - u_i(t) < 0, \end{cases} \quad (2.13)$$

$$\mu_i^c = \begin{cases} > 0, & v_i(t) - v_{max} = 0, \\ = 0, & v_i(t) - v_{max} < 0, \end{cases} \quad (2.14)$$

$$\mu_i^d = \begin{cases} > 0, & v_{min} - v_i(t) = 0, \\ = 0, & v_{min} - v_i(t) < 0. \end{cases} \quad (2.15)$$

The Euler-Lagrange equations can be written as,

$$\dot{\lambda}_i^p(t) = -\frac{\partial H_i}{\partial p_i} = 0, \quad (2.16)$$

and

$$\dot{\lambda}_i^v = -\frac{\partial H_i}{\partial v_i} = \begin{cases} -\lambda_i^p, & v_i(t) - v_{max} < 0 \text{ and} \\ & v_{min} - v_i(t) > 0, \\ -\lambda_i^p + \mu_i^c, & v_i(t) - v_{max} = 0, \\ -\lambda_i^p - \mu_i^d, & v_{min} - v_i(t) = 0. \end{cases} \quad (2.17)$$

The necessary condition for optimality is

$$\frac{\partial H_i}{\partial u_i} = u_i + \lambda_i^v + \mu_i^a - \mu_i^b = 0. \quad (2.18)$$

### 2.1.5.1 Analytical Solution without Interior Constraints

If the inequality state and control constraints (2.4) are not active, we have  $\mu_i^a = \mu_i^b = \mu_i^c = \mu_i^d = 0$ . Applying the necessary condition, the optimal control can be given

$$u_i(t) + \lambda_i^v = 0, \quad i \in \mathcal{N}(t). \quad (2.19)$$

From Euler-Lagrange equations, we have  $\lambda_i^p(t) = a_i$ , and  $\lambda_i^v(t) = -(a_i \cdot t + b_i)$ . The coefficients  $a_i$  and  $b_i$  are constants of integration corresponding to each vehicle  $i$ . From (2.19), the optimal control input (acceleration/deceleration) as a function of time, and the corresponding state trajectories are given by

$$u_i^*(t) = a_i \cdot t + b_i, \quad \forall t \geq t_i^0. \quad (2.20a)$$

$$v_i^*(t) = \frac{1}{2}a_i \cdot t^2 + b_i \cdot t + c_i, \quad \forall t \geq t_i^0 \quad (2.20b)$$

$$p_i^*(t) = \frac{1}{6}a_i \cdot t^3 + \frac{1}{2}b_i \cdot t^2 + c_i \cdot t + d_i, \quad \forall t \geq t_i^0, \quad (2.20c)$$

where  $c_i$  and  $d_i$  are constants of integration. The constants of integration  $a_i$ ,  $b_i$ ,  $c_i$ , and  $d_i$  can be computed once at time  $t_i^0$  using the initial and final conditions, and the values of the one of terminal transversality condition, i.e.,  $\lambda_i^v(t_i^{mz}) = 0$ .

### 2.1.5.2 Analytical Solution with Interior Constraints

In the case that the path of vehicle  $i$  consists of more than one merging zone, for example, the eastbound CAV  $i$  enters from the left and travels through merging zones #1 and #2 in Fig. 2.1 between the time  $t_i^0$  that the vehicle enters the control zone and the time  $t_i^f$  that the vehicle exits the merging zone #2, vehicle  $i$  has to travel

across the intermediate merging zone #1 at the designated time  $t_i^{m_1}$ . Therefore, we need to impose an additional interior boundary condition [33]

$$p_i(t_i^{m_1}) = L_1. \quad (2.21)$$

If a speed constraint  $v_1$  is imposed as an interior boundary condition, then

$$v_i(t_i^{m_1}) = v_1. \quad (2.22)$$

Let  $t_i^{m_1^-}$  and  $t_i^{m_1^+}$  represents the time just before and after the jump conditions. Then

$$\lambda_i^p(t_i^{m_1^-}) = \lambda_i^p(t_i^{m_1^+}) + \pi_0, \quad (2.23)$$

$$\lambda_i^v(t_i^{m_1^-}) = \lambda_i^v(t_i^{m_1^+}) + \pi_1, \quad (2.24)$$

$$H^- = H^+ - \pi_0 \cdot v_i(t_i^{m_1}) - \pi_1 \cdot u_i(t_i^{m_1}), \quad (2.25)$$

where  $\pi_0$  and  $\pi_1$  are constant Lagrange multipliers, determined so that (2.23) and (2.24) are satisfied. Equations (2.23)- (2.25) imply discontinuities in the position and speed co-states and the Hamiltonian at  $t_i^{m_1}$ . The two arcs, i.e., equations before and after  $t_i^{m_1}$ , are pieced together to solve the problem with 9 or 10 unknowns [if (2.22) is also imposed] including the constants of integration,  $\pi_0$  and/or  $\pi_1$ , and the corresponding equations: the initial conditions, i.e.,  $v_i(t_i^0)$  and  $p_i(t_i^0)$ , the interior conditions as defined in (2.21), [and/or (2.22)] the final conditions, i.e.,  $\lambda_i(t_i^{m_z}), p_i(t_i^{m_z})$ , and the junction point defined in (2.23) [and/or (2.24)].

To derive online the optimal control for each vehicle  $i$ , we need to calculate the constants of integration at time  $t_i^0$ , so that the controller yields the optimal control

online for each vehicle  $i$ . We form the following system of nine equations, namely

$$\begin{pmatrix} \frac{(t_i^0)^2}{2} & (t_i^0) & 1 & 0 & 0 & 0 & 0 & 0 & 0 \\ \frac{(t_i^0)^3}{6} & \frac{(t_i^0)^2}{2} & t_i^0 & 1 & 0 & 0 & 0 & 0 & 0 \\ \frac{(t_i^{m_1})^3}{6} & \frac{(t_i^{m_1})^2}{2} & t_i^{m_1} & 1 & 0 & 0 & 0 & 0 & 0 \\ \frac{(t_i^{m_1})^2}{2} & t_i^{m_1} & 1 & 0 & -\frac{(t_i^{m_1})^2}{2} & -t_i^{m_1} & -1 & 0 & 0 \\ 0 & 0 & 0 & 0 & \frac{(t_i^{m_2})^3}{6} & \frac{(t_i^{m_2})^2}{2} & (t_i^{m_2}) & 1 & 0 \\ 0 & 0 & 0 & 0 & -t_i^{m_2} & -1 & 0 & 0 & 0 \\ 0 & 0 & 0 & 0 & \frac{(t_i^{m_1})^3}{6} & \frac{(t_i^{m_1})^2}{2} & t_i^{m_1} & 1 & 0 \\ t_i^{m_1} & 1 & 0 & 0 & -t_i^{m_1} & -1 & 0 & 0 & 0 \\ 1 & 0 & 0 & 0 & -1 & 0 & 0 & 0 & -1 \end{pmatrix} \cdot \begin{pmatrix} a_i \\ b_i \\ c_i \\ d_i \\ g_i \\ h_i \\ q_i \\ w_i \\ \pi_0 \end{pmatrix} = \begin{pmatrix} v_i(t_i^0) \\ p_i(t_i^0) \\ p_i(t_i^{m_1}) \\ 0 \\ p_i(t_i^{m_2}) \\ \lambda_i^v(t_i^{m_2}) \\ p_i(t_i^{m_1}) \\ 0 \\ 0 \end{pmatrix}, \forall t \geq t_i^0. \quad (2.26)$$

where  $a_i, b_i, c_i, d_i$  are the constants of integration for the first arc, and  $g_i, h_i, q_i, w_i$  are the constants of integration for the second arc.

### 2.1.6 Simulation Results and Discussion

To evaluate and validate the effectiveness of the proposed approach, I conducted computational studies using the commercial software platforms of TASS International PreScan in conjunction with Mathworks MATLAB and Simulink. A corridor with two adjacent intersections (intersection-1 and intersection-2) is considered in Mcity (Fig. 2.2), a 32 acre vehicle testing facility. The dimensions of the conflict zones are 18 m  $\times$  12 m for intersection-1 and 34 m  $\times$  28 m for intersection-2. The length of the control zone to be 100 m is measured from the entry of each intersection. Six different routes have been designed for the scenario in Fig. 2.2 with 14 CAVs: 1) two eastbound routes with 5 CAVs, 2) two westbound routes with 4 CAVs, 3) one southbound route with 2 CAVs, and finally, 4) one northbound route with 3 CAVs. Note that, east and westbound vehicles travel through only one intersection in their path. The routes and CAV positions were designed in such a way that the trajectories of the CAVs present a worst-case collision scenario. To analyze the individual performance of the simulated

CAVs, we considered a northbound vehicle (ego-CAV) as the test vehicle (see Fig. 2.2).

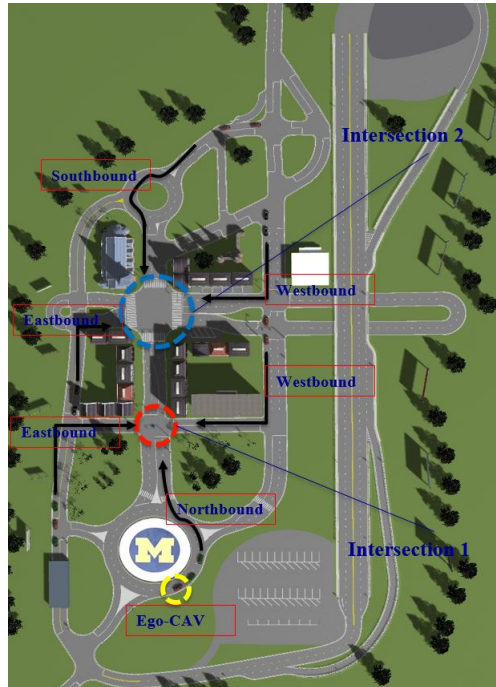


Figure 2.2: Illustration of the corridor in Mcity.

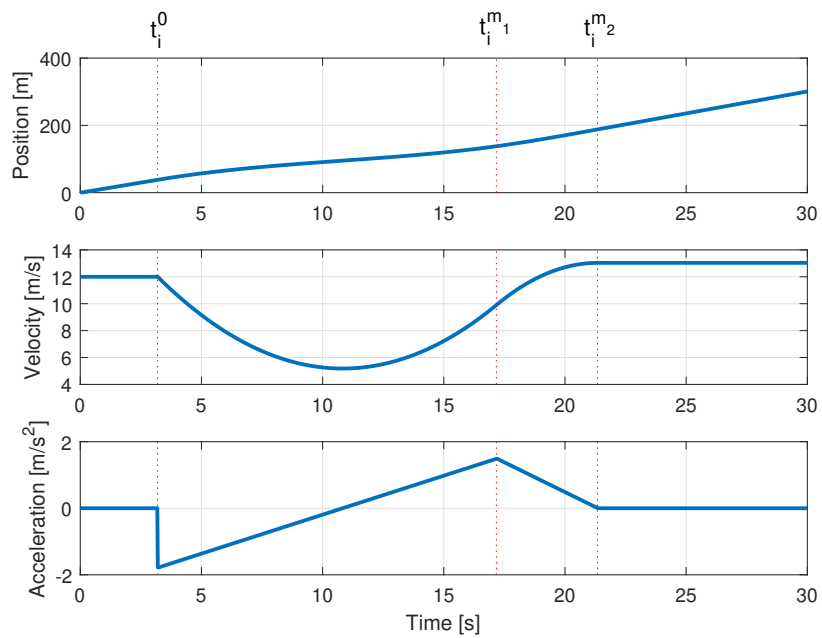


Figure 2.3: Optimal vehicle trajectory traveling through two adjacent intersections.

The merging scenario at intersection-1 with 10 incoming CAVs is depicted in Fig. 2.4 (left). Note that, CAV#4 heading westbound and CAV#7 heading eastbound are allowed to enter the conflict zone at the same time since their routes have opposite directions and thus are non-conflicting. The simulation results for the decentralized optimization problem for the ego-CAV are depicted in Fig. 2.3. It is observed that the optimal control takes hold of the ego-CAV at the entry of the control zone denoted at time  $t_i^0$  and leads it optimally through intermediate collision points of intersection-1 at time  $t_i^{m1}$  and  $t_i^{m2}$ . Also note that, within the time horizon  $t_i^{m2} - t_i^{m1}$ , we have linear control input profile, quadratic speed profile, and cubic path trajectory according to (2.20). To compare the performance of the proposed optimal solution, we construct

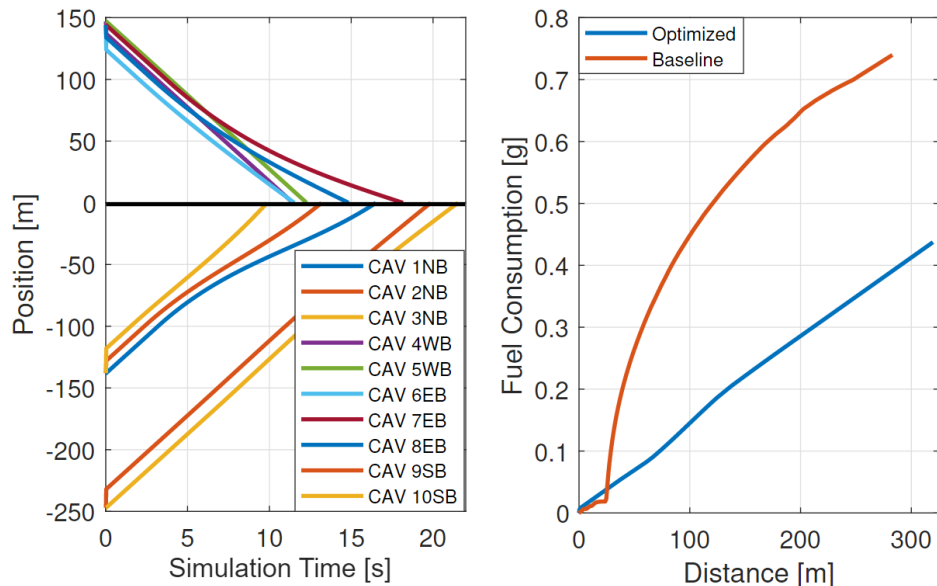


Figure 2.4: Collision-free optimal trajectory of 10 CAVs approaching towards intersection-1 (left) and cumulative fuel consumption of the optimized and baseline scenarios (right).

a baseline scenario with fixed time signaled intersections with a switching time of 10 seconds. The vehicles were governed by the *Gipps* car-following model [101]. To quantify the effect of optimal vehicle coordination on fuel consumption, a polynomial meta-model proposed in [67] was used. A comparison of fuel consumption for the ego-CAV between the baseline and optimized scenarios is shown in Fig. 2.4 (right). We

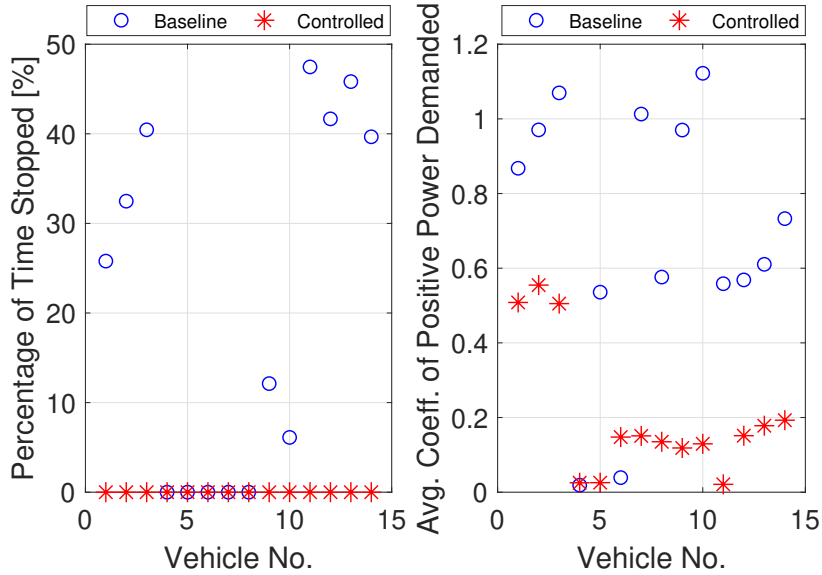


Figure 2.5: Stoppage time (left) and average coefficient of power demanded (right) of the optimized and baseline scenarios.

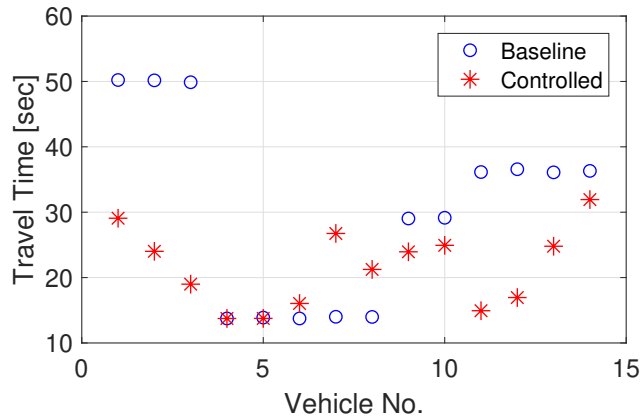


Figure 2.6: Fleet travel time of the optimized and baseline scenarios.

observe 40.9% improvement in fuel efficiency for the ego-CAV under the constructed baseline scenario.

The proposed framework alleviates stop-and-go driving, and thus, minimizes associated transient engine operation in this corridor, yielding improvements in fuel consumption. To quantitatively investigate this observation, the individual drive cycles of the vehicles in the baseline and optimized scenarios are analyzed using three metrics: (1) total travel time, (2) stop factor, and (3) average coefficient of power demanded.

The stop factor provides a convenient indication of idle engine operation over a driving cycle. The coefficient of power demanded provides an indication of the transient engine operation since it is proportional to the power demanded by the driver. Total stoppage time in the drive cycle, shown in Fig. 2.5 (left), was eliminated for every vehicle in the fleet. The coefficient of power demand, shown in Fig. 2.5 (right), only considers vehicle power demanded under both positive acceleration and velocity events and was able to be reduced by 40.8% across the fleet of 14 vehicles. The total travel time (Fig. 2.6) for all 14 vehicles was improved by 13.2% with the proposed framework compared to the baseline scenario.

In this section, I addressed the problem of coordinating CAVs at two signal-free adjacent intersections by formulating a decentralized optimal control problem. A closed-form analytical solution is presented that considers interior boundary conditions and provides optimal fuel-efficient and collision-free trajectories to the CAVs for their predetermined routes. The proposed decentralized framework exhibits significant improvement in terms of fuel efficiency, average power demand, and average travel time when compared to the baseline scenario.

## 2.2 Isolated and Coordinated Control at a Traffic Corridor

Implementation of different coordination strategies can impact the performance of CAVs traveling through a traffic corridor consisting of multiple congestion scenarios. In this section, I consider two coordination strategies: (1) an isolated control approach, where no information is shared among the coordinators, and (2) a coordinated control approach, where all the coordinators share common information. The objective of each CAV is to optimize its trajectories in terms of energy consumption and travel time while implementing one of the above control strategies. We evaluate the effectiveness of the proposed architecture through a simulation environment and provide a comparison of the performance of the two different control approaches.

In the following section, the two approaches for the vehicle dynamics (VD)



Figure 2.7: The corridor in Mcity with the conflict zones.

controller, namely, isolated control and coordinated corridor control, are introduced.

### 2.2.1 Isolated Conflict Zone Control

Let us consider a corridor that contains three conflict zones (Fig. 2.7), e.g., a merging roadway (conflict zone 1), a speed reduction zone (conflict zone 2), and a roundabout (conflict zone 3), as shown in Fig. 2.7. Upstream of each conflict zone, we have a control zone where CAVs coordinate with each other. For each control zone, there is a coordinator that communicates with the CAVs traveling within that specific control zone. In the isolated control approach: (1) none of the CAVs can communicate outside of the current control zone, and (2) none of the coordinators share their information with each other.

Let  $z \in \mathcal{Z}$  be the index of a conflict zone in the corridor. When a CAV enters the control zone, the coordinator receives its information and assigns a unique identity  $i$  to the CAV. Let  $t_i^{0z}$  be the time when CAV  $i$  enters the control zone towards conflict

zone  $z$ , and  $t_i^{fz}$  be the time when CAV  $i$  exits the corresponding control zone. In each control zone, we denote the sequence of the CAVs to be entering a conflict zone as  $\mathcal{N}_z(t) = \{1, \dots, N(t)\}$ . Thus, the following optimization problem is formulated for each CAV in the queue  $\mathcal{N}_z(t)$

$$\min_{u_i} \frac{1}{2} \int_{t_i^{0z}}^{t_i^{fz}} u_i^2(t) dt, \quad \forall i \in \mathcal{N}_z(t), \quad \forall z \in \mathcal{Z} \quad (2.27)$$

Subject to : (2.3), (2.4), (2.7), (2.5),

$$p_i(t_i^{0z}) = p_i^{0z}, \quad v_i(t_i^{0z}) = v_i^{0z}, \quad p_i(t_i^{fz}) = p_z,$$

and given  $t_i^{0z}, t_i^{fz}$ .

where  $p_z$  is the location (i.e., entry position) of conflict zone  $z$ ,  $p_i^{0z}, v_i^{0z}$  are the initial position and speed of CAV  $i$  when it enters the control zone of conflict zone  $z$ . The analytical solution of the above optimal control problem has been presented for the unconstrained case in [27, 61, 78], and for the constrained case in Chapter 3, and thus omitted here.

## 2.2.2 Coordinated Corridor Control

In this control approach, we consider a single coordinator that monitors all CAVs traveling along the corridor. Note that the coordinator serves as an information center that can collect vehicular data through V2I and/or V2V communication, and is not involved in any decision on the CAV operation. Roadside units could be placed in each conflict zone and used to transmit data between CAVs and the coordinator. Thus, the coverage of the coordinator is flexible and the length of the corridor could be extended in the presence of connected infrastructure.

Let  $\mathcal{N}(t) \in \mathbb{N}$  be the number of CAVs in the corridor at time  $t \in \mathbb{R}^+$ . When a CAV enters the boundary of the corridor, it broadcasts its route information to the coordinator. Then, the coordinator assigns a unique integer  $i$  that serves the identification purpose inside the corridor. Let  $t_i^0$  be the initial time that CAV  $i$  enters the corridor,  $t_i^z$  be the time for CAV  $i$  to enter the conflict zone  $z$ ,  $z \in \mathcal{Z}$ , and  $t_i^f$  be

the time for CAV  $i$  to enter the final conflict zone. To avoid any possible collision, the merging time  $t_i^z$  for each CAV  $i$  can be computed using the upper level coordination policy presented in Section 2.1.3. The upper-level scheduling procedure yields the sequence that the CAVs will be traversing through the corridor. Each CAV  $i$  determines the time  $t_i^z$  that will be entering the conflict zone  $z \in \mathcal{Z}$  upon arrival at the entry of the corridor. Thus, the next CAV  $i + 1$ , upon its arrival at the entry of the corridor, will search for feasible times to cross the conflict zones based on available time slots. The recursion is initialized when the first CAV enters the control zone, i.e., it is assigned  $i = 1$ . For each CAV, the following optimal control problem is formulated, the solution of which yields the optimal control input (acceleration/deceleration) to achieve the assigned time  $t_i^z$  (upon arrival of CAV  $i$ ) without collision

$$\min_{u_i} \frac{1}{2} \int_{t_i^0}^{t_i^f} u_i^2(t) dt, \quad \forall i \in \mathcal{N}(t) \quad (2.28)$$

Subject to : (2.3), (2.4), (2.7), (2.5),

$$p_i(t_i^0) = p_i^0, v_i(t_i^0) = v_i^0, p_i(t_i^z) = p_z,$$

$$\text{and given } t_i^0, t_i^z, t_i^f, \quad \forall z \in \mathcal{Z},$$

where  $p_i^0, v_i^0$  are the initial position and speed of CAV  $i$  when it enters the corridor, and  $t_i^z$  is the time when CAV  $i$  enters the conflict zone  $z$ . The details of deriving the closed-form analytical solution of the lower-level optimal control problem using interior point constraints is presented in Section 2.1.3, and thus omitted here.

### 2.2.3 Performance Evaluation and Comparison

We primarily focus on two aspects of the analysis: 1) evaluation of the network performance under the two different control approaches, and 2) evaluation of the efficiency under three different traffic levels (i.e., light, medium, and heavy traffic conditions). To this end, we develop the following three scenarios.

**Scenario 1: (Baseline)** All vehicles in the network are non-connected and non-automated vehicles. In this scenario, the Wiedemann car following model [160] built-in VISSIM is applied. The intersection is controlled by a fixed-time signal controller, whose signal timing is optimized for the traffic condition set in the study.

**Scenario 2: (Isolated conflict zone control)** We consider 100% market penetration of CAVs in this scenario. The vehicles optimize their trajectory based on the isolated conflict zone control approach presented in Section 2.2.1.

**Scenario 3: (Coordinated corridor control)** We consider 100% market penetration of CAVs in this scenario. The vehicles optimize their trajectory based on the coordinated corridor control approach presented in Section 2.2.2.

The corridor has a length of 1.3 km in MCity (Fig. 2.7). The desired speeds for the highway, urban and SRZ are set as 17 m/s, 11 m/s, and 8 m/s respectively. The length of the speed reduction zone is 125 m. For Scenario 2, the length of the control zone for the on-ramp, the SRZ, and the roundabout were selected to be 150 m.

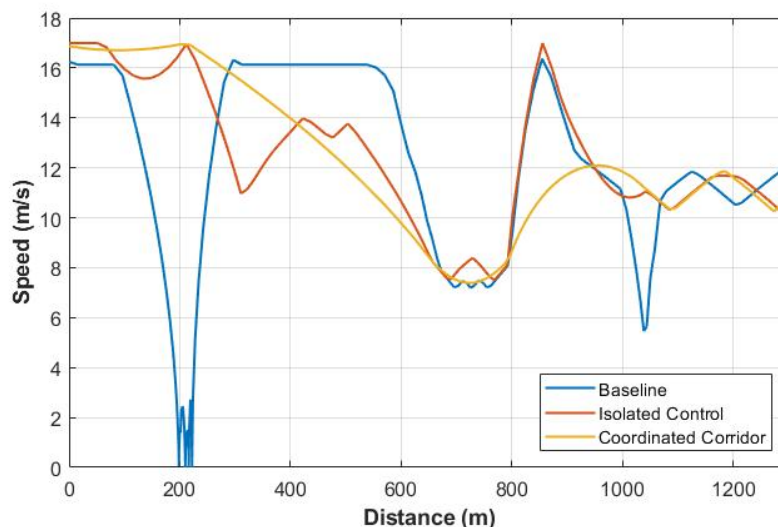


Figure 2.8: Vehicle speed profiles under different VD control approaches.

We plot vehicle trajectories in Fig. 2.9 to investigate the network-level performance of the controllers. Under Scenario 1, the vehicles need to slow down or stop before merging into the highway or roundabout. Therefore, we can see in the top panel

of Fig. 2.9 that there are a significant number of stop-and-go events in vehicle speed profiles under the baseline scenario. Under scenario 2 (shown in the middle panel of Fig. 2.9), with an isolated control scheme, we observe smooth speed profiles inside each control zone. At the downstream of each conflict zone, vehicles exit from the VD control zone, thus we see similar speed patterns as under scenario 1 outside the control zones. We also note that while the isolated control approach is able to eliminate stop-and-go driving, the resulting increased traffic flow into the downstream speed reduction zone leads to speed reduction downstream of the highway on-ramp segment. This implies that a lack of coordination among the vehicles of different control zones results in inefficient transient driving behavior. On the contrary, with the coordinated control scheme under scenario 3, traffic information of the entire corridor is shared among all vehicles. Therefore, all the CAVs travel through the corridor are able to optimize their trajectories both at the upstream and downstream of the conflict zones, and drive smoothly throughout the corridor, even with high traffic demand levels (as shown in the bottom panel of Fig. 2.9). The elimination of transient engine operation between the uncontrolled zone of the traffic scenarios has significant implications in terms of fuel economy. In Table 2.1, it can be observed that the coordinated corridor control approach leads to significantly higher fuel economy improvement in comparison with the isolated control approach under low, medium, and high traffic volumes. This improvement can be attributed to the fact that, since the coordinated corridor control approach eliminates all the uncontrolled patches between the control zones of different traffic scenarios as opposed to the isolated control approach, and optimizes the complete route inside the corridor, it leads to improved fuel efficiency.

Table 2.1: Percentage improvement in fuel economy over the baseline scenario under different traffic conditions.

	<b>High [%]</b>	<b>Medium [%]</b>	<b>Low [%]</b>
<b>Isolated Control</b>	14.9	10.3	8.2
<b>Coordinated Control</b>	29.9	24.4	22.4

Under three different traffic conditions, we calculate vehicle travel times through

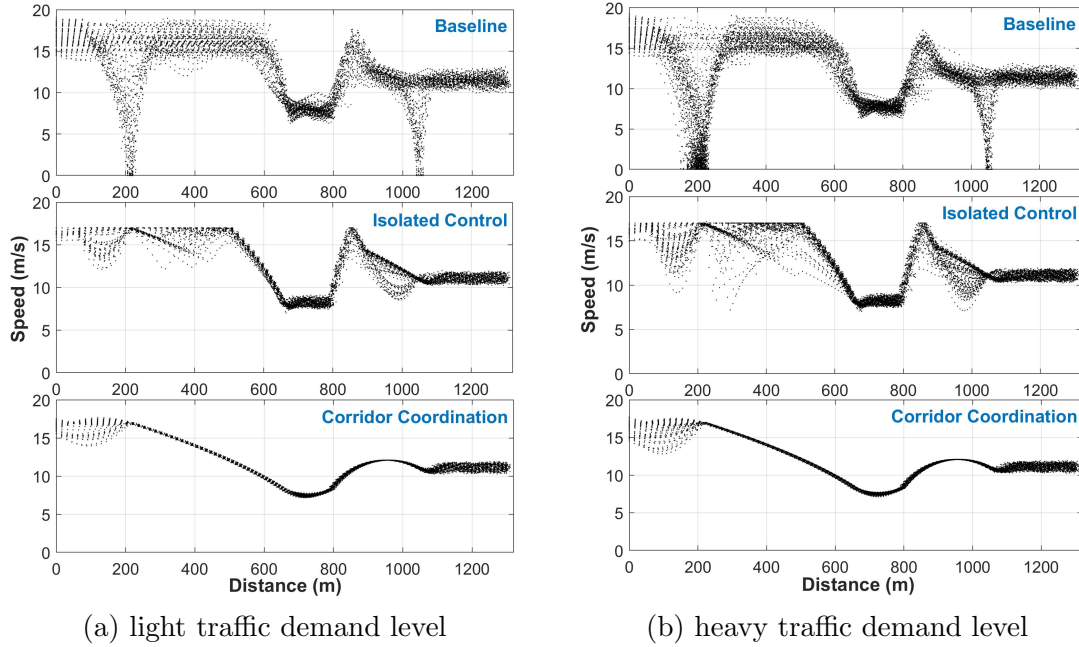


Figure 2.9: Speed profiles for all CAVs under different VD control approaches and demand levels.

the corridor under different VD control approaches and plot travel time distribution in Fig. 2.10. We observe that with a coordinated corridor control approach, due to longer preparation for downstream roadway segments, the average travel time under light traffic conditions is longer than the baseline scenario. However, the results reveal that through the corridor coordination, the traffic flow is further smoothed (much lower variation in vehicle travel times as shown in Fig. 2.10) compared to the isolated conflict zone control approach.

In this section, we compared the efficiency of different VD control approaches and showed that the coordinated corridor approach improves significantly fuel efficiency compared to the isolated conflict zone control approach.

Note that, each CAV has different subsystems that can leverage the developed VD controller to generate improved performance. For example, if we consider that the CAVs are plug-in-hybrid-electric vehicles (PHEVs), then the VD controllers developed in the previous sections can be combined with a powertrain (PT) control architecture

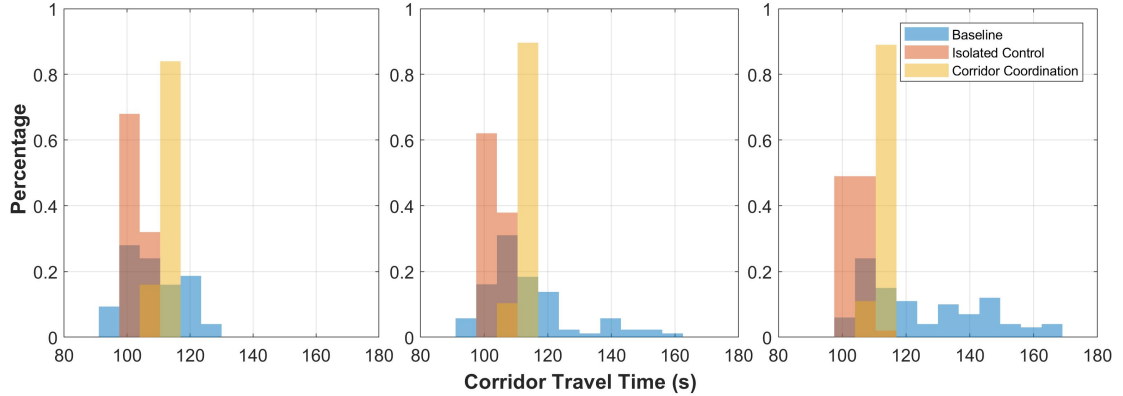


Figure 2.10: Travel time distribution under different VD control approaches and traffic demand levels.

to harness additional energy consumption benefits. In the following section, I explored the concept of coupling the VD and PT controllers of the CAV, and show that the combination can improve fuel economy.

### 2.3 Concurrent Optimization of Vehicle Dynamics and Powertrain

In this section, I explore the possibility of concurrent optimization of the CAV’s vehicle dynamics and powertrain. Specifically, I propose a supervisory control architecture for CAVs that optimizes (1) the vehicle’s speed profile, aimed at minimizing stop-and-go driving, and (2) the powertrain efficiency of the vehicle for the optimal speed profile derived in (1). The complexity of the problem dimensionality can be managed by establishing two parallel and appropriately interacting computational levels: (1) a cloud-based, and (2) a vehicle-based level. Thus, the proposed control framework can be implemented onboard the vehicle in real time with minimal computational effort.

#### 2.3.1 Supervisory Controller Architecture

We consider a network of connected and automated PHEVs (CA-PHEVs) driving through a corridor in Mcity that consists of several conflict zones, e.g., a merging at roadways on-ramp, a speed reduction zone, and a roundabout, as shown in Fig. 2.2. The CA-PHEVs are retrofitted with necessary communication devices to interact with

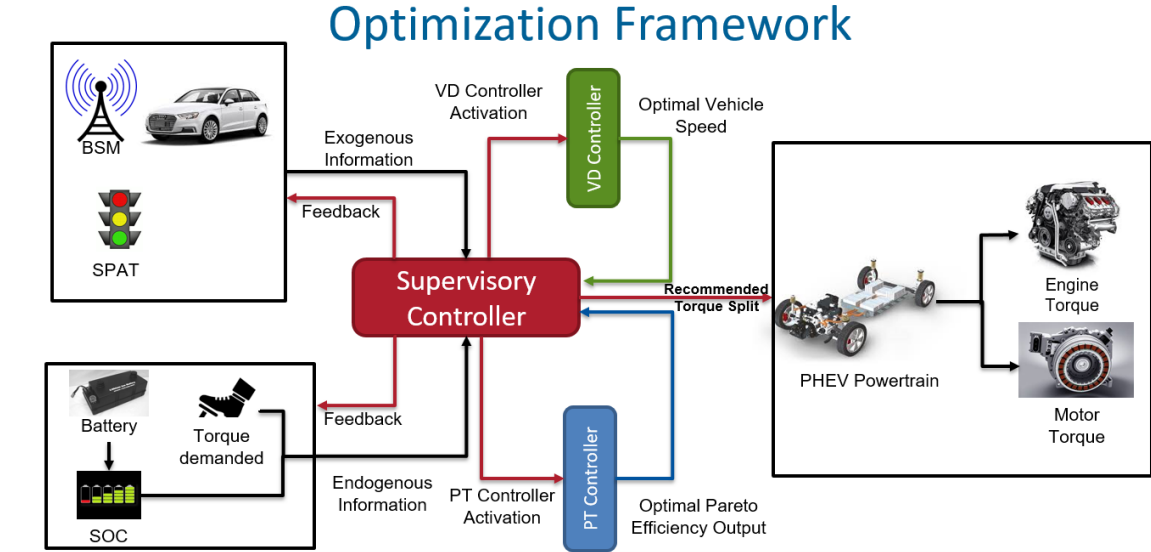


Figure 2.11: Supervisory control architecture.

other CA-PHEVs and structures within their communication range through V2V and V2I communication. In this work, the CA-PHEV under consideration is an Audi A3 e-tron plug-in hybrid electric vehicle (Fig. 2.12).

The supervisory controller oversees the VD and PT controllers, and communicates the endogenous and exogenous information appropriately, as shown in Fig. 2.11. The VD controller optimizes online the acceleration/deceleration and speed profile of the vehicle in situations where there is a potential conflict with other vehicles, e.g., in traffic lights, stop signs, roundabouts, etc, to avoid stop-and-go driving. The PT then controller computes the optimal nominal operation (set-points) for the engine and motor corresponding to the optimal solution of the VD controller. The supervisory controller coordinates the VD and PT controllers to ensure the optimal solution yielded by the VD controller is feasible for the PT controller and eventually results in maximization of the vehicle’s energy efficiency.

Similar to Section 2.2, we consider a corridor that contains three conflict zones  $z = 1, 2, 3$  representing a merging roadway, a speed reduction zone, and a roundabout respectively. The corridor containing the CA-PHEV’s main route is illustrated by the

black trajectory in Fig. 2.7. The details of the setup are the same as in Section 2.2. The objective of each CA-PHEV is to derive its optimal control input (acceleration) to cross each of the conflict zones without any rear-end or lateral collision with other vehicles, and simultaneously optimize its powertrain to achieve better energy efficiency. The VD control framework for CAVs traveling through traffic corridors has been presented in the previous sections (see Sections 2.1 and 2.2). Therefore, the focus of the following section is only on developing the powertrain control architecture.



Figure 2.12: The test vehicle, Audi A3 e-tron, in Mcity.

### 2.3.2 Optimization of the Powertrain Controller

The CA-PHEV considered here has a parallel configuration, where the gasoline engine and the electric motor can provide the necessary power to the wheel either independently or in combination. The engine, which can be fully decoupled in electric motor-only operation, is connected to the integrated motor-generator (IMG) unit through a singular clutch, which is in turn connected to a dual-clutch transmission. The electric motor is coupled with the engine and gearbox and can act as a generator for charging the battery.

The vehicle is operated on the battery-hold mode, and thus, the state-of-charge (SOC) of the battery is constrained within a 1% SOC bandwidth around the target

$SOC_{target}$  with lower bound  $SOC_{lb}$  and upper bound  $SOC_{ub}$ . Based on the current SOC of the battery, the controller decides whether to charge or discharge the battery.

Following the modeling framework in [181], the evolution of the CA-PHEV state is modeled as a controlled Markov chain with a finite state space,  $\mathcal{S} \subset \mathbb{R}^n$ , and finite control space,  $\mathcal{U} \subset \mathbb{R}^m$ ,  $n, m \in \mathbb{N}$ , from which the power management controller selects control actions. In our formulation, the state space is the entire range of the engine and motor speed,  $\mathcal{S} \subset \mathbb{R}^2$ , where the engine and motor speed progress in a compact subset of  $\mathbb{R}$ . The control space  $\mathcal{U}$  is the vector of the engine and motor torque,  $\mathcal{U} \subset \mathbb{R}^2$ .

The evolution of the state occurs at each of a sequence of stages  $t = 0, 1, \dots$ , and it is portrayed by the sequence of the random variables  $X_{t(1:2)} = (X_{t(1)}, X_{t(2)})^T = (N_{eng}, N_{mot})^T \in \mathcal{S}$  and  $U_{t(1:2)} = (U_{t(1)}, U_{t(2)})^T = (T_{eng}, T_{mot})^T \in \mathcal{U}$ , corresponding to the HEV state (engine and motor speed) and control action (engine torque and motor torque) respectively. For each state  $X_{t(1:2)} = i \in \mathcal{S}$  a nonempty set  $\mathcal{C}(i) \subset \mathcal{U}$  of admissible control actions (engine and motor torque) is given which implies that at each state  $i \in \mathcal{S}$ , the control action set  $\mathcal{C}(i) \subset \mathcal{U}$  should include only the control actions that satisfy the physical constraints of the engine and the motor. At each stage  $t$ , the controller observes the engine and motor speed,  $X_{t(1:2)} = i \in \mathcal{S}$ , which is a function of the vehicle speed, and executes an action,  $U_{t(1:2)} = \mu(X_{t(1:2)})$  (engine and motor torque), from the feasible set of actions,  $U_{t(1:2)} \in \mathcal{C}(i)$ , at that state. At the same stage  $t$ , an uncertainty,  $W_{t(1:2)}$ , is incorporated in the system consisting of the torque demanded by the driver as designated by the pedal position, e.g., accelerator or brake. At the next stage,  $t + 1$ , the system transits to the state  $X_{t+1(1:2)} = j \in \mathcal{S}$  and a one-stage expected cost,  $k(X_{t(1:2)}, U_{t(1:2)})$ , is incurred corresponding to the engine's and motor's efficiency. After the transition to the next state, a new action is selected and the process is repeated. The state transition from one state to another is imposed by a discrete-time equation that describes the dynamics of the CA-PHEV.

The objective of the PT controller is to derive a control policy that minimizes the long-run expected average cost of the CA-PHEV to split the torque demanded

by the driver between the engine and the motor for the optimal speed profile derived by the VD controller as a solution of Eq. (2.10). For the power management control problem here, we select the average cost criterion as we wish to optimize the efficiency of each CA-PHEV on average, hence

$$J^\pi = \lim_{T \rightarrow \infty} \frac{1}{T+1} \mathbb{E}^\pi \left[ \sum_{t=0}^T k(X_{t(1:2)}, U_{t(1:2)}) \right], \quad (2.29)$$

where  $k(X_{t(1:2)}, U_{t(1:2)})$  is the one-stage cost of CA-PHEV. However, the computational burden associated with deriving the optimal control policy in Eq. (2.20) prohibits online derivation onboard a vehicle. It has been shown [182] that the optimal control policy in Eq. (2.29) is equivalent to the Pareto control policy that can be derived by formulating a multiobjective problem. The latter consists of the engine's efficiency,  $\eta_{eng}$ , and the motor's efficiency,  $\eta_{mot}$ . Given the engine and motor speed  $X_{t(1:2)}$ , the objective is to find the optimal control action  $U_{t(1:2)}$  (engine and motor torque) that optimizes a multiobjective function reflecting both the engine's and the motor's efficiency. Hence, one of the objectives is the engine's efficiency

$$f_1(N_{eng}, T_{eng}) = \eta_{eng}, \quad (2.30)$$

and the other one is the motor's efficiency,

$$f_2(N_{mot}, T_{mot}) = \eta_{mot}. \quad (2.31)$$

The multiobjective optimization problem is formulated as

$$\begin{aligned} & \min_{U_t} k(X_{t(1:2)}, U_{t(1:2)}) = \\ & \max_{U_t} (\alpha \cdot f_1(X_{t(1)}, U_{t(1)}) + (1 - \alpha) \cdot f_2(X_{t(2)}, U_{t(2)})), \quad (2.32) \\ & \text{s.t. } \sum_{i=1}^2 U_{t(i)} = T_{driver}, \end{aligned}$$

where  $\alpha$  is a scalar that takes values in  $[0,1]$ ,  $X_{t(1:2)} = (X_{t(1)}, X_{t(2)})^T = (N_{eng}, N_{mot})^T \in \mathcal{S}$ ,  $U_{t(1:2)} = (U_{t(1)}, U_{t(2)})^T = (T_{eng}, T_{mot})^T \in \mathcal{U}$  is the vector of engine and motor torque. The multiobjective optimization problem in Eq. (2.32) yields the Pareto efficiency set

between the engine and the motor by varying  $\alpha$  from 0 to 1 at any given state of the HEV. For each state of the CA-PHEV and torque demand, we derive the Pareto efficiency set of Eq. (2.32) offline and store it in a table. If there are multiple solutions, then one of these solutions is selected randomly since all of them will yield the same one-stage expected cost. The Pareto control policy is then implemented online using this table.

### 2.3.3 Powertrain Calibration with VESIM

To model the powertrain of Audi A3 etron, we adopt a hybrid electric vehicle simulation tool VESIM [183], and create separate powertrain models for the baseline scenario and the optimized scenario. The purpose of this model is to represent the hybrid PT controller architecture of an HEV. The general architecture of the VESIM model is illustrated in Fig. 2.13. We modify the VESIM to generate two different vehicle powertrain models as follows. The baseline VESIM model has been calibrated

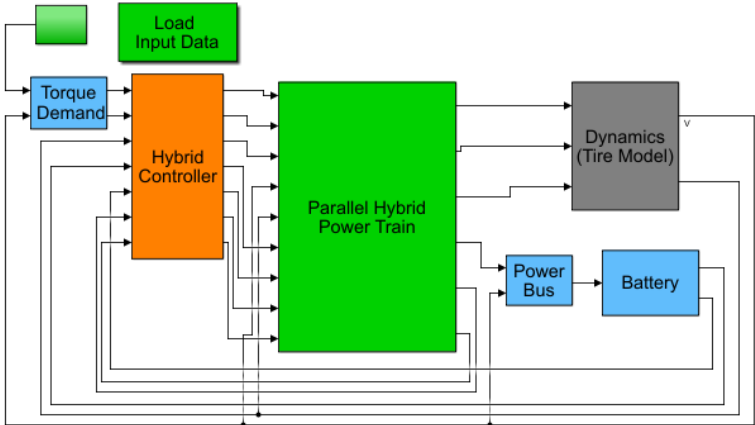


Figure 2.13: VESIM Model for modelling the powertrain of the plug-in hybrid electric vehicle.

to reproduce the vehicle characteristics generated by the factory controller of the Audi A3. Due to the combined contribution of the internal combustion engine and the motor of the Audi A3, the VESIM model computes the *miles-per-gallon of gasoline equivalent* (MPGe) according to the EPA standard. By feeding the baseline and the VD controller’s speed profiles to the VESIM model, we quantify the fuel consumption of the Audi A3, and evaluate the performance of the VD controller at different conflict

scenarios. Some of the most essential VESIM parameters required for the calibration purpose are summarized in Table A.3. The Audi A3 has several modes of operation:

1. **EV mode:** Motor only operation, where the engine remains turned off.
2. **Charge Battery Mode:** The engine provides the torque demanded by the driver and also provides torque to the IMG unit to charge the battery.
3. **Hold Battery Mode:** The SOC of the battery is maintained within a certain bandwidth of the initial SOC. Although the engine provides the torque demanded, the motor can contribute if the torque demand is higher than the maximum capacity of the engine.
4. **Hybrid Mode:** The vehicle can use both the engine and the IMG unit to provide the torque demanded by the driver.

We calibrate the VESIM model for each of the aforementioned modes of Audi A3 to capture appropriate engine and IMG characteristics. Fig. 2.13 shows a representation of such effort, where the speed and battery SOC profile of the Audi A3 and corresponding calibrated VESIM model for hold battery mode are illustrated. Note that, the hold battery mode is characterized by the SOC variation constrained within a certain SOC bandwidth. We observe that the calibrated VESIM model can trace the reference speed of the actual Audi A3's drive cycle very closely, which is illustrated by their complete overlap in Fig. 2.14. We obtain MPGe of 29.73 from the calibrated VESIM model compared to the Audi A3 MPGe of 30.92 for the same drive cycle, with 3.8 % deviation.

### 2.3.4 Integration of Powertrain Controller in VESIM

For deriving the optimal control policy of the PT controller, we first derive the engine's efficiency map from its brake-specific fuel consumption (BSFC) data, contrary to the motor's efficiency map which is readily available. With the engine's and motor's efficiency map, we solve the multiobjective optimization problem in Eq. (2.32) offline. We discretize the torque, engine/motor speed and the scalar  $\alpha$  with the resolution of 10 Nm, 100 RPM and 0.05 respectively, and use the optimization toolbox of MATLAB to

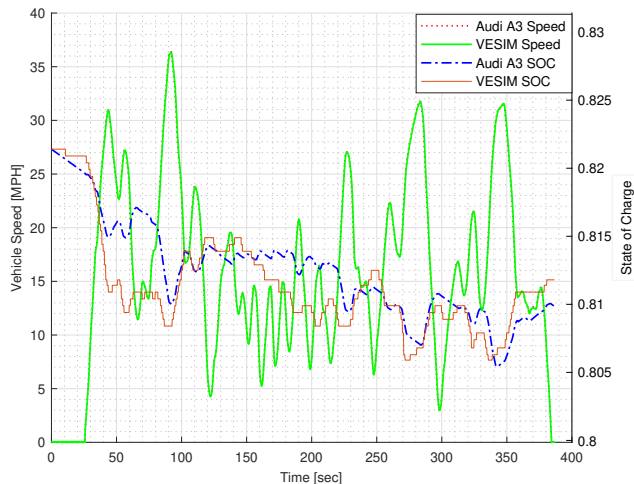


Figure 2.14: VESIM calibration model for hold battery mode.

solve Eq. (2.32). Finer resolution of  $\alpha$  increases the solution time significantly without yielding proportional changes to the solution matrix. The optimization process yields a Pareto efficiency set that we store in the CA-PHEV memory for later online use. For each torque demanded by the driver and corresponding engine/motor speed, the CA-PHEV searches the Pareto efficiency table to obtain the optimal torque split between the engine and the IMG unit.

The Pareto efficiency computed off-line is illustrated in Fig. 2.15. We note that when the driver’s torque demand is below 300  $Nm$ , the optimal solution is to use the motor exclusively to satisfy the torque demanded by the driver. This is because the electric motor considered here has high efficiency (almost 95%) in most of its operating regions compared to the engine, which has a peak efficiency of 35%.

### 2.3.5 Vehicle Dynamics and Powertrain Controller Performance

To evaluate the effectiveness of the proposed control architecture, we design a simulation scenario using the commercial software PTV VISSIM [184]. We create a simulation environment resembling the Mcity vehicle testing facility and define the network routes for all the vehicles. In terms of the nature of vehicle control, we consider

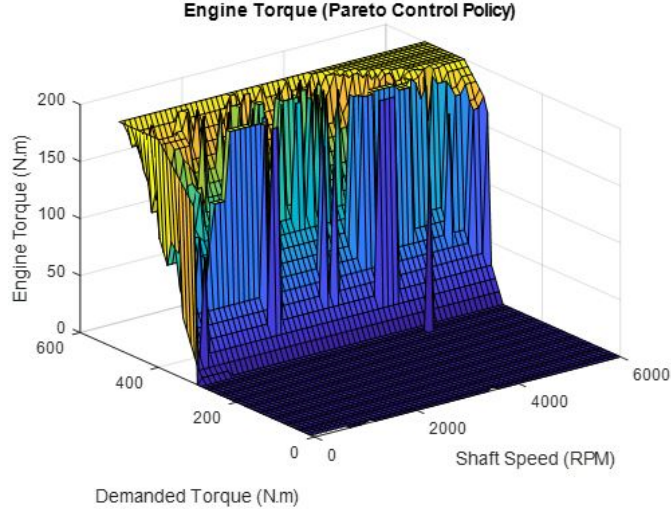


Figure 2.15: Pareto efficiency set of the powertrain controller.

two scenarios:

1. **Baseline Vehicle Dynamics:** All vehicles are human-driven without any connectivity and automation. The VISSIM employs the *Wiedemann* car following model [160] to emulate the behavior of the human-driven vehicles. However, the VISSIM built-in car following models is slightly different from the original Wiedemann model in [160] due to the inclusion of certain parameters to introduce additional randomness and heterogeneity in terms of driving behavior. We apply VISSIM’s *Wiedemann-74* car-following model for the urban traffic and *Wiedemann-99* for the freeway traffic. The conflict zones inside the corridor have conventional traffic signals, which the vehicles must abide by. We model the traffic signals (yield behavior) at the on-ramp merging, and the roundabout by imposing VISSIM’s *priority rule* object in the conflict areas. To model the speed reduction zone, we apply VISSIM’s *reduced speed area* object with specified route length and speed.
2. **Optimal Vehicle Dynamics:** In this case, we have CA-PHEVs (i.e., connected and automated PHEVs) traveling through the corridor. The CA-PHEVs employ the VD controller to optimize their speed profile for increasing fuel efficiency. We consider an automated conflict zone, where the conventional traffic signals are not present. We

modify one of VISSIM’s API, namely the DriverModel.dll to implement the VD controller written in C++ for the CA-PHEVs in the optimal controlled case. Within each CZ, we override each vehicle’s internal car-following model with the DriverModel.dll containing the VD controller logic. Outside the CZ, the vehicles can switch back to the VISSIM’s built-in Wiedemann car-following model. At each simulation time step, each vehicle access the external DriverModel.dll, and computes the optimal control output based on its location in the route.

To investigate the robustness of the VD controller through different conflict zones of the corridor, we consider three different traffic volumes in the VISSIM’s traffic network. The traffic flow in both the main route and the congestion routes are modified to achieve different traffic scenarios. Table A.1 presents the different traffic flows considered to achieve the low, medium, and high traffic volume. The parameters relevant to the VISSIM simulation environment are compiled in Table A.2. The impact of the PT controller on engine operation is shown in Fig. 2.17. For the baseline scenario, we use the calibrated VESIM model, while the PT-controlled CA-PHEVs were operated by the optimal VESIM model embedded with the Pareto efficiency table. We first evaluate the impact of the PT controller under different driving behavior. To this end, we use three standardized drive cycles, namely the highway fuel economy driving schedule (HWFET), urban dynamometer driving schedule (UDDS), and the US06 supplemental federal test procedure to represent the 60mph-highway, heavy-duty urban, and high acceleration aggressive driving behavior. We incorporate the aforementioned driving behaviors in a single drive cycle by stitching the considered drive cycles together to obtain a combined cycle of 25.72 miles. We characterize the performance of the proposed Pareto efficient powertrain controller compared to the baseline Audi A3 powertrain by tracing the drive cycles through the corresponding VESIM model. Fig. 2.16 shows the UDDS drive cycle traced by the VESIM for the baseline (Audi A3 powertrain) and the optimal controlled (Pareto efficient) case. Note that, in both cases, the VESIM model was able to trace the UDDS drive cycle completely, as represented by the complete

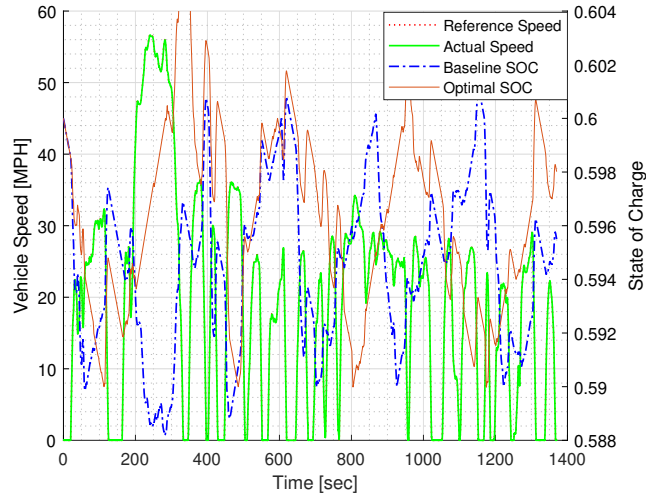


Figure 2.16: The UDDS drive cycle traced by the baseline (Audi A3) powertrain and the optimal controlled Pareto efficient powertrain.

overlap of the reference and actual vehicle speed profile in Fig. 2.16. The battery SOC for the baseline and the optimal PT controlled case are also illustrated at the right axis of Fig. 2.16. We observe that the battery SOC is constrained within a certain bandwidth of the initial SOC to represent the Audi A3’s hold-battery mode.

The energy consumption results (MPGe) of the Audi A3’s baseline powertrain and the optimal PT controlled case for the aforementioned standardized drive cycles are summarized in Table 2.2. We note that the optimal PT controller shows improvement in terms of energy efficiency compared to its baseline counterpart in all the standardized drive cycles considered here. The most fuel consumption benefit is obtained for the UDDS drive cycle and the least for HWFET.

Table 2.2: PT controller validation for standardized drive cycles.

Drive Cycle [miles]	US06 (8.0 )	UDDS (7.5)	HWFET (10.3)	Combined (25.7)
Baseline [MPGe]	26.4	28.2	32.5	29.1
PT Controller [MPGe]	27.8	30.4	38.1	31.8
Improvement [%]	7.7	17.1	5.3	9.1

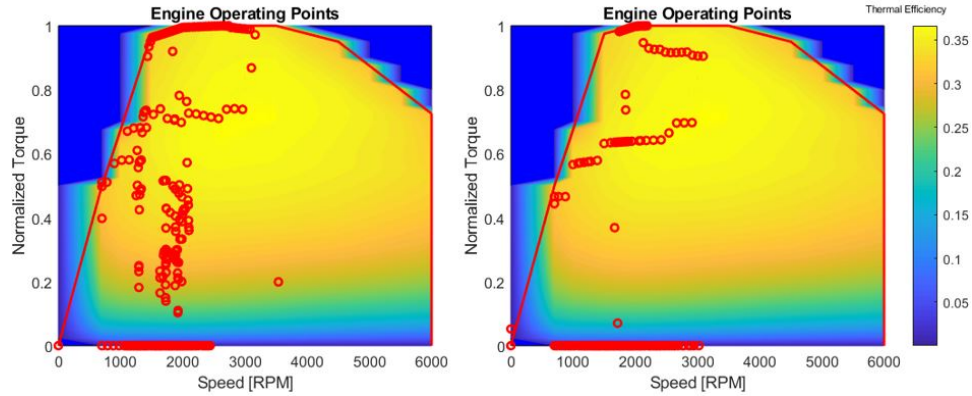


Figure 2.17: Engine operating points without and with the PT controller.

In Fig. 2.17, we observe that the PT controller operates the engine at the most efficient brake-specific fuel consumption regimes. In the baseline scenario, in contrast, there is a spread of operating points in non-efficient regimes. As the Pareto control policy yields an online equivalent solution to DP, the benefits of the PT controller would be apparent for any heuristic approach used in the baseline scenario.

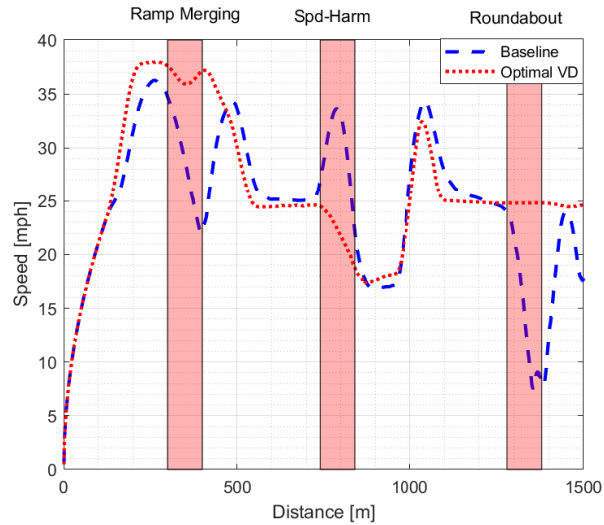


Figure 2.18: Average vehicle speed trajectories for high traffic volume.

Fig. 2.18 illustrates the average of vehicle speed profiles corresponding to PHEVs with the baseline scenario, and the average of speed profiles corresponding to the CA-PHEVs with the VD controller traveling through the corridor under a high

traffic scenario. Note that the average speed profile of the baseline scenario in Fig. 2.18 shows that CAVs cruise with low speed in the control zones at ramp-merging and roundabout. The control zones of on-ramp merging and roundabout denote the upstream area of the entry to these bottlenecks. Human-driven vehicles on the ramp have to yield to the incoming vehicles from the main road. The human-driven vehicles exhibit stop-and-go behavior if the main road is very congested. Therefore, the resulting average speed in the baseline scenario (Fig. 2.18) is low inside the control zones. On the other hand, with the VD controller, the CAVs can space themselves in such a way that they can enter the conflict zones without any stop-and-go driving behavior. As a result, the average speed of all CAVs is higher than the baseline in the control zones. Another interesting observation is that the average speed profile in the baseline scenario (Fig. 2.18) is high at the SRZ control zone marked as *Spd-Harm*. The SRZ is located at the end of a straight segment of Mcity (see Fig. 2.7) which allows the vehicles to pick up speed. Since the conventional human-driven vehicles do not have any information regarding the upcoming SRZ or the slower moving vehicle inside the SRZ, they pick up speed upstream of the SRZ and suddenly start decelerating at the entry of the SRZ. This behavior results in the backward propagating traffic wave. On the other hand, the CAVs know beforehand the state of the previous vehicles approaching the SRZ. Therefore, the CAVs adjust their speed inside the control zone of the SRZ in such a way that they have a smooth entry at the SRZ while eliminating the backward propagating traffic wave. We observe that under the optimal scenario of the VD controller, the average vehicle speed is more streamlined at the conflict zones compared to the average speed of the vehicles under the baseline scenario where speed oscillations at the upstream and downstream of the conflict zone is observed. The streamlined speed profile of the VD controller indicates a reduction in transient engine operation, resulting in 21.3% better fuel efficiency compared to the baseline for high traffic volume.

To further investigate and quantify the individual as well as the combined contribution of the VD and PT controller, we consider four different simulation cases where

the different combinations of the VD and PT controllers are active.

1. **VD and PT controller inactive (Baseline):** None of the VD and PT controllers are active in the CA-PHEV. The vehicle traverses the whole corridor by following the conventional traffic laws and uses the Wiedemann [160] car-following model. The engine and motor operating points are also determined by Audi A3's factory powertrain setting as determined by the baseline VESIM model.
2. **VD controller active:** The CA-PHEVs traverse the route with optimal VD controller by communicating with other CA-PHEVs, but using the Audi A3's factory powertrain model for selecting its torque set-point.
3. **PT controller active:** The CA-PHEVs use the optimal PT controller to select the torque distribution between their engine and the IMG unit to meet the driver's demand. However, the vehicle is driven by conventional human drivers without the help of connectivity and automation.
4. **VD and PT controller active:** The CA-PHEVs employ the VD controller within the CZ to optimize its speed profile. For each optimal desired speed, the vehicle demands torque from the powertrain. The vehicle then uses the optimal PT controller to select the optimal power split between the engine and the IMG unit to meet the torque demanded.

To evaluate the robustness of these control cases in different traffic congestion, we consider low, medium, and high traffic conditions. 2.3 summarizes the VD and PT controller's impact on fuel efficiency in three different traffic conditions. We observe a significant increase in fuel efficiency in all traffic scenarios considered. Note that, the VD controller shows comparatively better improvement for high traffic volume as it streamlines the extreme stop-and-go driving behavior associated with high congestion scenarios. On the other hand, the PT controller performs comparatively better in the low-traffic scenario. Although the VD and PT controller show energy improvement individually, their combination manages to obtain the most benefit in all traffic scenarios.

In Table 2.4, we summarize the mean and standard deviation of the distribution of the control cases under different traffic volumes. We observe that, for all the traffic volume cases, the VD controller reduces the standard deviation and increases the mean of the MPGe distribution compared to the baseline scenario. This implies that, by

Table 2.3: Fuel Efficiency Improvement for VD and PT controller.

Controllers / Traffic Level	Low	Medium	High
VD Controller Only [%]	17.3	17.7	21.3
PT Controller Only [%]	25.9	25.4	21.8
PT & VD Controller Combined [%]	34.0	32.7	29.2

Table 2.4: Mean and standard deviation of the MPGe distribution for different traffic flow scenarios.

	Baseline	VD Active	PT Active	VD+PT Active
	<b>Low Traffic</b>			
Mean [MPGe]	19.5	23.5	26.3	29.8
Std. Deviation	1.5	1.3	1.9	2.8
	<b>Medium Traffic</b>			
Mean [MPGe]	19.6	23.7	26.2	29.2
Std. Deviation	1.7	1.5	1.8	2.9
	<b>High Traffic</b>			
Mean [MPGe]	21.9	27.8	28.1	30.9
Std. Deviation	1.8	1.51	2.5	1.7

streamlining the vehicle speed profiles, the VD controller enables a more closely packed distribution of fuel consumption. On the other hand, the PT controller only case shows energy improvement compared to the baseline case for all traffic volumes as evident by the higher mean of the distribution but shows an increase in the standard deviation. Finally, the combined effect of the VD and PT controller is observed for the increase in the mean MPGe. However, the standard deviation of the distribution increases for both the low and medium traffic volume cases. Note that, for low and medium traffic volume, the increase in average MPGe for the combined VD and PT controlled case compared to the baseline case is additive, i.e., the MPGe increase for only the case of the VD controller, and the MPGe increase for only the PT controlled case can be added to obtain the MPGe increase for their combined control. The high traffic volume case, however, slightly varies from this observation.

In this section, a two-level control architecture to optimize simultaneously the

vehicle-level and powertrain-level operation of a PHEV is presented. The proposed architecture is applied to the operation of CA-PHEVs over a range of real-world driving scenarios, and its effectiveness is validated with simulation analysis.

## 2.4 Experimental Validation of Optimal Controllers: From Simulation to Field Test

Before CAVs incorporated with the decentralized vehicle dynamics controller can be deployed on public roads, they need to be tested extensively. In this section, I present a sequential experimentation methodology to implement the optimal control framework, developed in Sections 2.1 and 2.2, in an Audi A3 etron plug-in hybrid electric vehicle and demonstrate that the vehicle’s efficiency and travel time in a real-world traffic corridor can be improved. The remaining exposition in the section includes the development, integration, implementation, and validation of the experimentation framework that includes a (1) hi-fidelity simulation environment, (2) hardware-in-the-loop (HIL) testing, (3) connectivity enabled virtual reality-based bench-test, and (4) field test in Mcity. I show that by adopting such an inexpensive, yet effective process, we can efficiently integrate and test the control framework, establish proper connectivity and data transmission between different modules of the system, and reduce uncertainty stemming from the test environment.

### 2.4.1 A Sequential Test Strategy for Connected Automated Vehicles

Our goal is to validate the effectiveness of the VD controller and investigate its performance in a real-world scenario. To this end, I develop a systematic and sequential approach to validate the VD controller performance. The controller validation is initiated in the simulation environment and completed with a real-world field test at MCity. These sequential steps can be briefly summarized as follows:

1. **Simulation Environment:** We create a simulation environment of Mcity in commercial software (i.e., PTV VISSIM), and develop the baseline and optimal scenarios. The baseline scenario considers the case of 0% penetration rate of CAVs. The optimal scenario corresponds to the 100% penetration rate of CAVs, and they all are controlled by the VD controller.

2. **Hardware-in-the-Loop Test:** We make necessary modifications to the Audi A3 in terms of vehicle hardware and software to be able to implement the VD controller output (recommended speed). We feed the baseline and optimal controlled speed profiles generated in the simulation environment in step 1 to the Audi A3, and trace them in a chassis-dyno setup.
3. **Bench Test:** We integrate the controller in the Audi A3’s head unit. We develop a bench-test method and conduct a basic system validation. Here, we employ the message queuing telemetry transport (MQTT) protocol, which is a publish-subscribe based messaging protocol of IoT, in conjunction with a simulation-based virtual traffic environment. We establish both the controller integration and the V2X communication framework.
4. **Field Test:** After following these steps, the Audi A3 integrated with the proposed VD controller can be taken to the test facility. Steps 1-4 not only reduce the possibility of technical complications during the field test but also provide an extra layer of safety to the driver and the test vehicle components. Therefore, these prerequisite steps can be considered essential before the on-field vehicle test session. Finally, we conduct the field test in a V2X enabled virtual reality-based test facility in Mcity with the Audi A3 (Fig. 2.12). We provide a detailed exposition of the various aspects of the field test in the following sections.

In what follows, we provide a detailed exposition of each of the aforementioned steps.

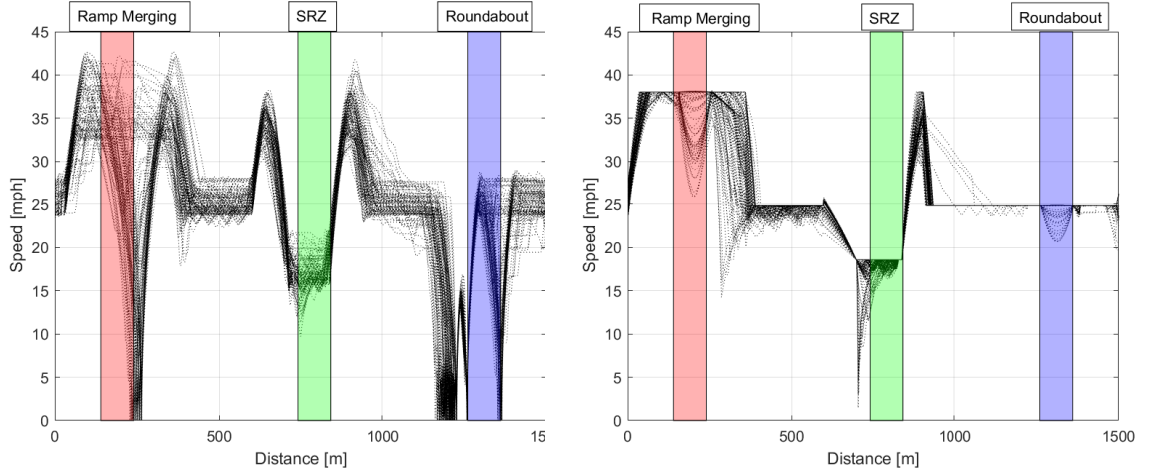
#### 2.4.2 Simulation Framework

To implement the control framework for optimizing vehicle dynamics presented in Sections 2.1,2.2, we use the microscopic multi-modal commercial traffic simulation software PTV VISSIM. The attributes of the simulation environment are similar to the setup presented in Section 2.2.3, thus the detailed exposition is omitted here. The corridor through which the Audi A3 travels has a length of 1500 *m* length within Mcity. The control zone of each conflict scenario is selected in such a way that no sharp turns or bends fall inside the controlled region. The vehicle dynamics parameters are calibrated by the data collected through driving the vehicle inside the Mcity facility. Medium to a high level of traffic congestion is considered for investigating the robustness of the controller. Table A.2 contains the essential parameter required for setting up the simulation environment.

The speed profiles of human-driven vehicles (baseline scenario) with Wiedemann human driver model [160] in the test route are shown in Fig. 2.19a. We notice significant stop-and-go driving at the on-ramp merging and roundabout conflict zones because the conventional human-driven vehicles have to yield to the incoming main-road vehicles. The human-driven vehicles can either show stop-and-go behavior if the main road is very congested or have a free merging if the main road is empty. Moreover, we observe an increase in vehicle speed in the region before the SRZ. The SRZ is located near the end of a straight segment of Mcity (see Fig. 2.7) which allows the vehicles to gain speed. Since the human-driven vehicles do not have any information regarding the upcoming SRZ or the slower moving vehicles in the SRZ, they pick up speed until the entry of the SRZ and start decelerating at the entry of the SRZ. We also observe that the stop-and-go driving behavior at each conflict scenario has negative implications upstream and downstream of the route. Due to the presence of high-speed variation inside the CZ, backward propagating traffic waves may result, which impacts the energy efficiency of the vehicles traveling outside the CZ.

In Fig. 2.19b, we show the speed profiles of simulated CAVs under the optimal VD controller. We observe that the CAVs can be coordinated using the VD controller to space themselves out in such a way that they can pass through the conflict zones without stop-and-go driving. The VD controller smooths the traffic flow and eliminates traffic congestion. We also note that in the SRZ, the speed of the CAVs is harmonized contributing to some additional benefits in fuel consumption. In this case, the CAVs know beforehand the state of the previous CAVs approaching the SRZ. Therefore, the CAVs can adjust their speed inside the control zone of the SRZ in such a way that they have a smooth entry at the SRZ and negate the backward propagating traffic wave. Moreover, we observe that the driving behavior of the CAVs located upstream and downstream of each CZ is streamlined, which adds additional energy efficiency benefits to the vehicles traveling outside the CZ.

Table 2.5 summarizes the performance evaluation of the VD controller in terms



(a) Speed profile of baseline vehicles in simulation for high traffic volume. (b) Speed profile of optimal controlled CAVs in simulation for high traffic volume.

of fuel consumption and shows the average improvements in each conflict zone in terms MPGe of the CAVs under medium and heavy traffic volumes. The human-driven vehicles in the baseline simulation scenario exhibit stop-and-go driving, which in turn increases the transient engine operation [185]. On the other hand, the optimal speed profiles of the VD controller in Fig. 2.19b reduce the CAVs’ transient engine operation by eliminating the stop-and-go driving behavior.

Table 2.5: Summary of fuel consumption [MPGe] comparison in simulation.

Conflict Scenario	On-Ramp	SRZ	Roundabout
Improvement (MPGe)[%]	15.6	21.2	35.3

Table 2.6: Summary of travel time comparison in simulation.

Conflict Scenario	On-Ramp	SRZ	Roundabout	Corridor
Avg. Travel Time (Baseline) [s]	24.8	19.82	18.71	176.9
Avg. Travel Time (VD Controlled) [s]	15.9	19.78	13.4	131.1
Improvement [%]	35.5	0.17	28.1	25.9

Table 2.6 reports the average travel time of the CAVs to cross each of the conflict zones for both the baseline and the optimal VD controlled scenarios. We observe that,

in the scenario corresponding to the VD controller, we have on average 26% reduction in travel time for the whole corridor.

Note that, the simulation in VISSIM only outputs the speed profile of the vehicle in the network, and does not yield any fuel consumption result specific to the Audi A3. Since, the Audi A3 is PHEV, fuel consumption models for conventional vehicles are not applicable. Therefore, we adopt a hybrid electric vehicle simulation model VESIM model, reported in [186] and references therein, calibrated appropriately to emulate the fuel consumption of the Audi A3 (see Fig. 2.13). Due to the combined contribution of the internal combustion engine and the motor of the Audi A3, the VESIM model calculates the miles-per-gallon of gasoline-equivalent, MPGe according to the EPA standard. By feeding the baseline and the VD-controlled speed profiles to the VESIM model, we quantify the fuel consumption of the Audi A3, and evaluate the performance of the VD controller at different conflict scenarios.

### 2.4.3 Hardware-in-the-Loop (HIL) Test

We investigate the performance of the VD controller in a HIL environment through the chassis-dyno setup. In our application, only limited ECU variables of the Audi A3 can be monitored and, if necessary, bypassed. The rest of the variables are solely controlled by the Audi A3's software system and cannot be accessed externally. To bypass the control input (acceleration) expected from the driver pedal, we override the ECU variables responsible for the Audi A3's cruise controller. We also override the ECU variables relevant to the torque-regeneration module of the integrated motor-generator (IMG) unit to introduce braking (deceleration) force when required. That is, we use the brake regeneration functionality of the IMG unit of the Audi A3 to apply braking force when decelerating. However, the braking power generated by the IMG unit in this way is not as accurate as of the typical hydraulic/mechanical brakes. Note that, applying brake through IMG is only possible when the state of the charge (SOC) of the battery is below a certain threshold to allow charging. If the battery SOC is above

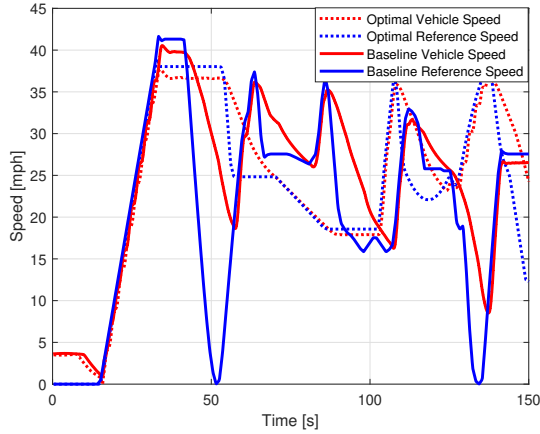


Figure 2.20: Medium traffic volume.

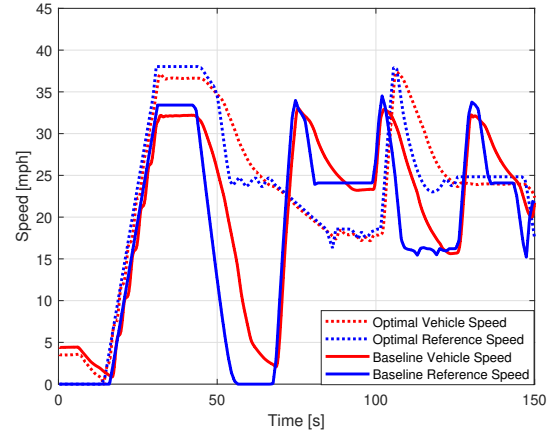


Figure 2.21: High traffic volume.

this certain threshold value, braking through IMG is not possible. The bypass of the aforementioned ECU variables has been realized by the ETAS ES910 rapid prototyping device. We calibrate the override coefficients to improve the tracking performance of the vehicle. Afterward, we feed the speed profiles generated by the simulation environment for both the baseline and optimal controlled case. We consider three different traffic volumes (e.g., low, medium, and high) to investigate the robustness of the VD controller performance, and record and analyze the fuel consumption data.

The speed profiles generated by the hardware in the loop testing in the chassis-dyno setup are illustrated in Figs. 2.20 and 2.21 for medium and high traffic volume respectively. We observe that the vehicle can trace the reference speed well while accelerating. While decelerating, we find a discrepancy between the reference speed and the actual vehicle speed. As we mentioned earlier, we use the brake regeneration functionality of the IMG unit of the test vehicle to apply braking force when decelerating. However, the braking power generated by the IMG unit in this way is not as accurate as of the typical hydraulic brakes. Table 2.7 summarizes the fuel consumption result for low, medium and heavy traffic volumes.

Table 2.7: Summary of energy improvement in HIL Test.

Traffic	Baseline [MPGe]	Optimal [MPGe]	Improvement[%]
Low	27.7	37.1	33.7
Medium	36.6	49.0	34.2
High	36.1	50.8	41.0

#### 2.4.4 Bench Test of Integrated System

We develop an IoT-based virtual reality framework to implement and debug the proposed VD controller on the bench. This particular bench test acts as a prerequisite to the actual field test and performs general system validation of the integrated VD controller. In Fig. 2.22, we illustrate the proposed framework, which enables system validation before the field test. The framework we employ here can be carried out in a single computer without requiring any additional hardware or devices, which significantly reduces the setup and execution time. The bench-test architecture in Fig. 2.22



Figure 2.22: Bench test model emulating the virtual reality based field test.

can be subdivided predominantly into two platforms, namely the simulation environment and the emulated head unit of the Audi A3. The connectivity of the platforms is established using the MQTT connectivity protocol. First, virtual vehicle information

generated from the aforementioned VISSIM simulator is stored offline. To mimic the data transfer process via the V2X communication framework, a python script reads the stored virtual vehicle information, parses them into suitable Basic Safety Message (BSM) strings, and publishes them sequentially to an MQTT topic in the BSM format as expected during the actual field test. An MQTT subscription thread runs in the emulated head unit, which subscribes to the specific MQTT topic to receive the incoming BSMs of virtual vehicles. Once received, the head unit reads the published BSMs instantaneously, and uses its hard-coded decoder algorithm to parse and assign the necessary information to its internal memory. Afterward, the head unit passes this stored information to the integrated VD controller to compute the optimal speed profile online. Note that, this is an open-loop process, namely, the test-vehicle information is not transmitted back to the simulation environment as the simulator works offline. With some simple modification, the process could be transformed into a closed-loop one where the BSMs from the test vehicles are transmitted back to the simulator, and the virtual vehicles inside the simulator could react to the state of the test vehicle.

**2.4.5 Virtual Reality Based Field Test**

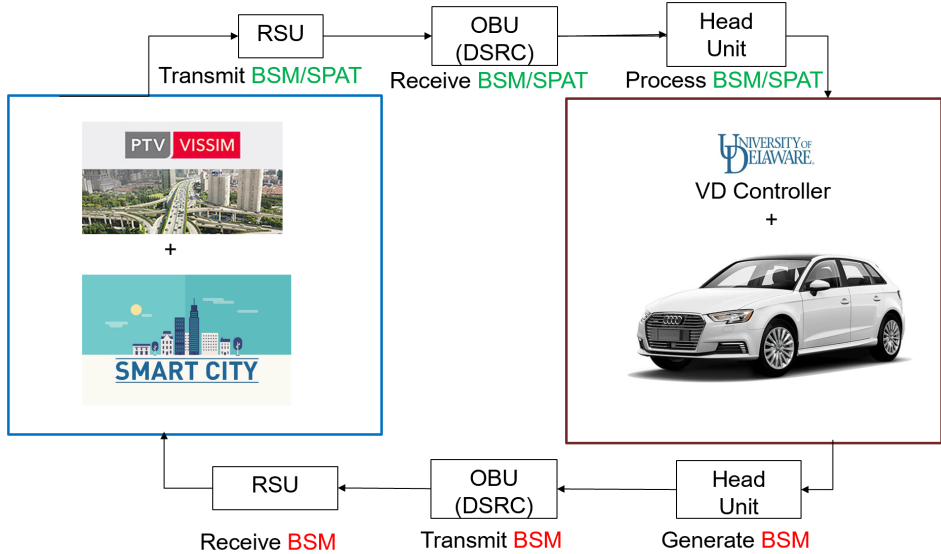


Figure 2.23: Workflow of virtual reality based V2X enabled field test in Mcity.

The general architecture of the virtual reality-based test environment of Mcity is shown in Fig. 2.23. The test environment is composed of three main subsystems as follows:

1. **Test Vehicle:** The Audi A3 is placed inside Mcity and is retrofitted with an onboard unit (OBU). The OBU considered here is a dedicated short-range communication (DSRC) device from COHDA Wireless (model MK5). The COHDA MK5 model has a latency of 1500 ns and a GNSS accuracy of 2.5 m. A GPS device (model BU-353-S4) with 5 Hz data output rate is used to get the latitude and longitudinal coordinates of the Audi A3 during the test. The head unit of the Audi A3 is emulated by a Linux machine, which is connected to the Audi A3's ECU through ETAS ES-910 rapid prototyping device.
2. **Infrastructure Equipment:** The infrastructure equipment includes roadside units (RSUs), traffic signal controllers, and vehicle detectors. The RSUs act as a two-way communication channel between the Audi A3 at the test facility, and the simulation platform located at the main control center.
3. **Simulation Platform:** The virtual environment is provided by a simulation platform located at the main control center. The simulator can generate virtual vehicles and provide their information to real-world structures. The simulation platform uses the commercial software PTV-VISSIM [184], where different test scenarios can be saved as different projects. We construct the VESIM model based on the parameters presented in Table A.2. The VISSIM APIs, namely the SignalControl.DLL, DriverModel.DLL, and COM interfaces are used for interactions with the real-world environment and the simulation managing application. We modify the DriverModel.DLL to integrate the proposed VD controller applicable to all the virtual vehicles within the simulation platform. To enable the VISSIM simulator to receive and transmit BSMs, we embed the DriverModel.DLL with the appropriate BSM encoder and decoder. At each time step, each virtual vehicle communicates with one another internally and derives its optimal speed. Information from simulated virtual vehicles is then encoded and sent out by the DriverModel.DLL to the real-world Audi A3.

The workflow of the vehicle testing procedure through virtual reality in Mcity is shown in Fig. 2.23. The Audi A3 communicates with the RSUs through the OBU and receives basic safety messages (BSMs) coming from the simulation platform, and the signal phase and timing (SPaT) messages coming from the infrastructure. The Audi A3 computes its optimal desired speed and passes this speed recommendation onto its ECU through CAN. At the same time, the Audi A3 broadcasts its state information (GPS location and speed) back to the RSUs through the OBU. Note that the

OBU considered here is a DSRC device that transmits messages to/from the RSU. The RSU's data processor receives and processes the incoming data from the Audi A3, and sends the processed information to the simulation platform at the main control center. All of the traffic network and infrastructure attributes of the vehicle test facility are virtually designed and modeled in a simulation environment. Virtual vehicles are generated and their trajectories are updated based on the preset simulation setting and the information received from the Audi A3. Finally, the virtual vehicles in the simulation platform broadcast their information as BSMs to the RSUs, which is then received by the OBU of the Audi A3 and the process repeats itself. Through this communication framework, both the virtual vehicles in the simulation environment and the Audi A3 in Mcity can interact with each other in real-time throughout the test session. Therefore, the behavior of both virtual and Audi A3 are completely synchronized. However, there are some drawbacks to this approach. First, significant efforts have to be taken for creating a proper simulation environment and communication framework between the real and virtual world. Second, preparing the Audi A3 for such an environment might not be straightforward, and would require significant involvement of the test facility itself. Lastly, the developed framework might not be easily transferable to other vehicle test facilities without significant modifications.

#### 2.4.5.1 Audi A3 System Architecture

The system architecture inside the HU of the Audi A3 consists of the following subsystems,

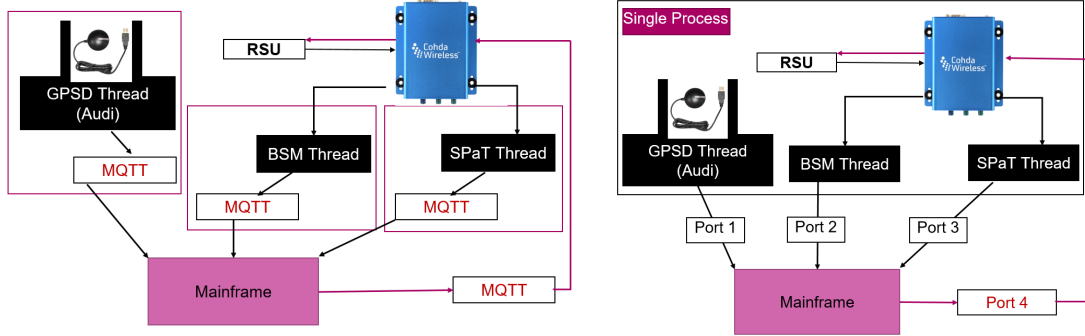
1. **GPS thread:** Collects and transmits the vehicle's latitude, longitude, and velocity information.
2. **BSM thread:** Collects the incoming BSMs from the DSRC device, parses them into usable values, and transmits them to the main process.
3. **SPaT thread:** Collects the incoming SPaT information from the DSRC device, parses them into usable information, and transmits them to the main process.

4. **Mainframe:** Based on the connectivity protocol, the mainframe can have a single or multiple subscription threads to receive the incoming information from the previous threads. The mainframe houses the integrated VD controller which uses the incoming information. Once the VD controller outputs an optimal recommended speed, the mainframe transmits it to the vehicle through CAN.

Based on the choice of connectivity framework, we develop two architectures as shown in Fig. 2.24a and Fig. 2.24b.

#### 2.4.5.2 MQTT and Socket Based Connectivity Protocols

MQTT (MQ Telemetry Transport) is a connectivity protocol used to publish/subscribe messaging transport. In the architecture illustrated in Fig. 2.24a, the GPS, BSM, and SPaT information acquisition and transmission threads run as individual processes. Each of these processes is eventually connected to the mainframe of the head unit through basic MQTT protocol. The MQTT protocol is realized by an inner publish and subscription thread, which means that for every data transmission, the sender has to publish the data to a specific topic, which is, in turn, retrieved by the receiver through subscription to that specific topic. Due to the requirement of several publish/subscription threads, the resulting system structure becomes complicated with additional data transmission and processing delays. The system delay can have a negative impact as it may prevent the real-time synchronization of virtual vehicles in the simulation platform and the Audi A3. To reduce the system delay associated with the MQTT-based architecture, we adopt an improved version of the communication framework (Fig. 2.24b). In this updated version, we unify all the different threads (GPS, BSM, and SPaT) under a single process. We eliminate the publish/subscription-based MQTT protocol, and use a significantly faster connection through direct sockets. A socket is essentially defined as a connection having a unique IP address and relevant port number. By tapping into the IP address of the DSRC device, and using different ports to handle the BSM and SPaT information, we have greatly simplified the data acquisition and transmission procedure. The resulting framework has been tested to be



(a) Workflow of MQTT Connectivity for individual processes. (b) Workflow of socket-based connectivity for the unified architecture.

Figure 2.24: Communication protocol for the Audi A3 etron.

significantly faster than the older version. For example, the head unit’s data transmission frequency with the MQTT protocol is 1 Hz, whereas it increased to greater than 100 Hz with the socket-based protocol. The aforementioned modifications have been implemented to collect the optimal control field test data for the on-ramp merging, SRZ, and the roundabout presented in this section.

### 2.4.5.3 Optimal Vehicle Dynamics Controller Integration

We integrate the VD controller algorithm in the emulated head unit of Audi A3, and link it up with the BSM and SPAT encoder/decoder. Therefore, the VD controller can receive the essential information necessary for Audi A3’s optimal speed calculation. To calculate the optimal speed trajectory, the Audi A3’s head unit has to find the answers to the following sequential questions:

1. Which control scenario does the test vehicle currently belong to?
2. Which particular virtual vehicle is acting as the putative leader in this specific control scenario?
3. What is the merging time of that particular putative leader?

Note that, the answer to the above questions can not be obtained directly from the incoming virtual vehicle information available from the regular BSM string as specified in the SAE-J2735 standard [187]. Therefore, we override some of the data sent by the regular BSM string to include the specific data useful to answer the aforementioned

questions. For example, we override the regular data to be transmitted through the BSM's elevation, vehicle length, and vehicle width variables to contain respectively the vehicle's merging time, vehicle's distance to the conflict zone, and vehicle's current CZ information. This updated BSM information is fed to the head unit of the Audi A3 where the optimal control input is computed through a workflow illustrated in Fig. 2.25.

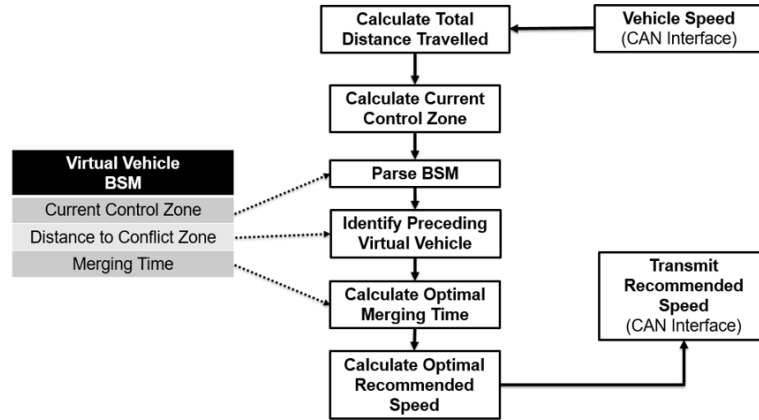


Figure 2.25: Workflow of VD Controller implementation within the head unit of Audi A3.

From the initialization of the test session, the Audi A3 continuously computes its total distance traveled by integrating its current speed over each time step. Based on the total distance traveled and the hard-coded location values of the conflict zones, the Audi A3 determines whether it has entered the CZ of a particular conflict scenario. Once the Audi A3 is within a specific CZ, it uses the CZ information from the incoming BSM strings of the virtual vehicles and sorts out the virtual vehicles pertaining only to that particular CZ. Afterward, the Audi A3 sorts the virtual vehicles pertaining to the corresponding CZ by the distance to conflict zone information to find the preceding virtual vehicle. Finally, the Audi A3 uses the merging time,  $t_{i-1}^{m,z}$  of the determined preceding virtual vehicle to calculate its optimal speed input using Eq. (3.12). If there are no preceding virtual vehicles at any time  $t$ , the Audi A3 computes the optimal speed

trajectory based on its estimated arrival time. The optimal speed input is transmitted to the vehicle’s ECU via CAN-Bus.

We summarize the field test results in Mcity in Table 2.8 and Table 2.9 which quantifies the Audi A3’s performance in terms of fuel efficiency and travel time. The VD-controlled Audi A3 shows improved fuel efficiency over the baseline scenario (human-driven Audi A3) exhibiting an overall 20 % improvement. A representative baseline and VD controlled speed profile of the Audi A3 from the field test in Mcity is shown in Fig. 2.26. We observe that the optimal VD controlled speed profile is comparatively smoother than the baseline one.

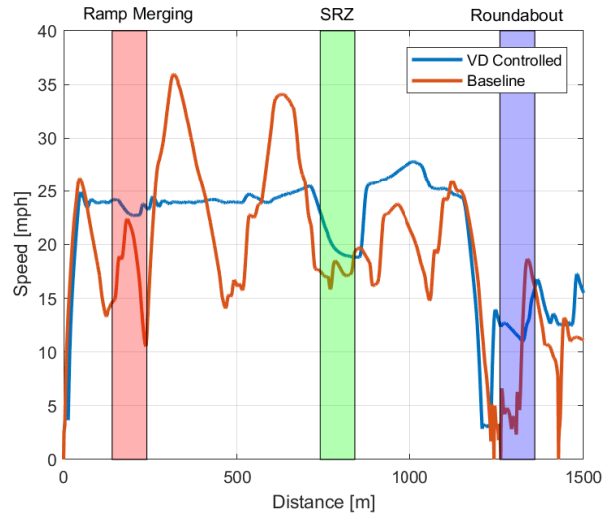


Figure 2.26: Speed profile of the Audi A3 etron considering the baseline and optimal VD controlled case at the field test in Mcity.

The optimal VD controller also shows improvement in terms of travel time through each of the conflict zones. Essentially, by optimizing the speed profile, and eliminating the stop-and-go behavior at the bottlenecks, the VD controller achieves 17% reduction in travel time in the whole corridor.

In this section, the effectiveness of the VD controller is validated systematically through a sequence of approaches, leading up to the virtual reality-based real-world field test. The Audi A3’s performance for baseline and optimal VD controlled scenarios

Table 2.8: Summary of MPGe Improvement in Field Test.

	<b>Optimal [MPGe]</b>	<b>Baseline [MPGe]</b>	<b>Improvement[%]</b>
<b>On-Ramp</b>	57.3	47.5	20.6
<b>SRZ</b>	63.3	48.6	30.2
<b>Roundabout</b>	65.4	57.7	13.3
<b>Total</b>	64.8	54.0	20.0

Table 2.9: Summary of travel time comparison of field test.

<b>Conflict Scenario</b>	<b>On- Ramp</b>	<b>SRZ</b>	<b>Roundabout</b>	<b>Corridor</b>
<b>Avg. Travel Time (Baseline) [s]</b>	34.3	19.4	15.3	218.2
<b>Avg. Travel Time (VD Controlled) [s]</b>	32.4	19.2	9.38	180.2
<b>Improvement [%]</b>	5.6	1.0	38.8	17.4

has been quantified with real-world data, and a comparative analysis between different traffic scenarios and congestion levels is conducted. It can be concluded that the Audi A3 retrofitted with the optimal VD controller shows significant improvements in terms of fuel consumption and travel time.

## Chapter 3

### MOTION PRIMITIVES WITH CONSTRAINED OPTIMAL CONTROL

In the previous chapter, I presented some of our preliminary research efforts on the decentralized time- and energy-optimal coordination of CAVs traveling through major traffic congestion scenarios. In general, it is difficult to solve a constrained optimal control problem in real time due to its iterative nature. For example, the standard methodology to solve the low-level optimal control problem (see [28]) is to employ Hamiltonian analysis with interior point state and/or control constraints. Namely, we first start with the unconstrained arc and derive the solution to the low-level optimal control problem. If the solution violates any of the state or control constraints, then the unconstrained arc is pieced together with the arc corresponding to the violated constraint. The two arcs yield a set of algebraic equations which are solved simultaneously using the boundary conditions and interior constraints between the arcs. If the resulting solution, which includes the determination of the optimal switching time from one arc to the next one, violates another constraint, then the last two arcs are pieced together with the arc corresponding to the new violated constraint, and we re-solve the problem with the three arcs pieced together. The three arcs will yield a new set of algebraic equations that need to be solved simultaneously using the boundary conditions and interior constraints between the arcs. The resulting solution includes the optimal switching time from one arc to the next one. The process is repeated until the solution does not violate any other constraints. This recursive process of piecing the arcs together to derive the optimal solution to the low-level problem can be computationally expensive and might prevent real-time implementation.

In this chapter, I present a rigorous mathematical framework to efficiently handle the constrained optimal control problems. Specifically, in Section 3.1, I provide a condition-based control framework that can derive constrained motion primitives in real time by identifying the constraint activation cases a priori. In Section 3.2, I present a decentralized optimal control framework for CAV coordination (100% CAV penetration rate) through multiple traffic scenarios, where we formulate the upper-level CAV coordination problem with dynamic re-sequencing queue, and explicitly consider rear-end collision avoidance constraint in the low-level trajectory optimization problem.

### 3.1 A Condition-Based Framework for Constrained Optimal Control

In this section, I address the problem of trajectory optimization of CAVs in the presence of system constraints, which is difficult to solve in real time due to its iterative solution structure according to the standard Hamiltonian analysis. The objectives of this section are (i) to derive a set of a priori conditions to identify the different activation cases of state and control constraints, (ii) to simplify the iterative process of the Hamiltonian analysis required to solve the optimal constrained problem for deriving energy-optimal motion primitives, and (iii) to increase the computational efficiency of the derivation of the solution in (ii) by eliminating numerical computations and constructing closed-form analytical solution using (i).

#### 3.1.1 Comparison With Related Work

The framework that I present in this section advances the state of the art in the following ways. First, the solution to the state and control unconstrained control problem presented in [61] and [40] shows acceleration spikes (jerk) at the boundaries of the optimization horizon, possibly exceeding the vehicle’s physical limitation and giving rise to undesired driving experience. In addition, the unconstrained solution can only guarantee that none of the constraints are violated at the boundaries of the optimization horizon only. In our proposed framework, we can guarantee that none of the state

and control constraints are violated throughout the entire optimization horizon. Second, in contrast to some approaches reported in the literature, e.g., [71, 73, 86], where either the state or the control constrained optimal control problem was addressed, our framework addresses all state and control constraints cases. Moreover, we explicitly include the state and control constraints in the Hamiltonian analysis as opposed to using a feasibility zone [87]. Third, several approaches have considered free terminal time to address the state/control constraints within the optimization horizon [35, 87]. In contrast, in our framework, we incorporate the constraints in the low-level control problem with the fixed time horizon. Fourth, the solution of the constrained optimal control problem requires piecing the unconstrained and constrained arcs together resulting in recursive numerical computations until all of the constraint activation cases are resolved [28, 35, 157]. In our proposed framework, we eliminate this recursive procedure to derive a real-time implementable closed-form analytical solution. Finally, the solution of the constrained optimization problem using Hamiltonian analysis reported in some approaches, e.g., [28], [157] and [35], only addresses different constraint activation cases without addressing the explicit interdependence between multiple constraint activation. In this section, we explore the interdependence of the combination of the constraint activation cases and explicitly provide the conditions for their realization.

In summary, the key features of this section that advances the state of the art are: (1) an in-depth exposition of the properties of the different combinations of the state and control constraint activation cases and a set of a priori conditions to identify the constrained solution without any recursive steps, (2) elimination of the recursive solution structure for the state and control constrained optimal control problems for CAV coordination by considering the constraint activation conditions, and (3) an explicit expression of the junction point between the constrained and unconstrained arcs leading to a closed-form analytical solution of the constrained optimal control problem.

### 3.1.2 Constrained Optimal Control Problem

We consider CAVs travelling through a traffic network containing a four-way signal-free intersection, as shown in Fig. 3.1. Although our analysis can be applied to any traffic scenario, e.g., merging at roadways, roundabouts, and passing through speed reduction zones, we use an intersection (Fig. 3.1) as a reference to present the fundamental ideas and results of this section, since an intersection provides unique features making it technically more challenging compared to other traffic scenarios. We define the area illustrated by the red square of dimension  $S$  in Fig. 3.1 as the *merging zone* where the potential lateral collision of CAVs may occur. Upstream of the merging zone, we define a *control zone* of length  $L$  inside of which CAVs can communicate with each other using a vehicle-to-vehicle communication protocol [177]. The intersection also has a *coordinator* that communicates with the CAVs traveling inside the control zone. Note that the coordinator does not make any decisions for the CAVs. When a CAV enters the control zone, the coordinator receives its information and assigns a unique identity  $i \in \mathbb{N}$  to it. Let  $\mathcal{N}(t) = \{1, \dots, N(t)\}$ , where  $N(t) \in \mathbb{N}$  is the number of CAVs inside the control zone at time  $t \in \mathbb{R}^+$ , be the queue of CAVs to enter the merging zone shown in Fig. 3.1. The time that a CAV  $i \in \mathcal{N}(t)$  enters the control and merging zones is denoted by  $t_i^0$  and  $t_i^m$ , respectively, while the time that a CAV  $i$  exits the merging zone is denoted by  $t_i^f$ . In our exposition, we assume that the queue  $\mathcal{N}(t)$  and the optimal time to enter the merging zone  $t_i^m$  is given a priori and can be derived by solving an upper-level vehicle coordination problem subject to rear-end and lateral safety constraints, as detailed in [28, 167, 175]. Given  $t_i^m$  a priori, the objective of each CAV  $i \in \mathcal{N}(t)$  is to derive its optimal control input (acceleration/deceleration) to cross the intersection without any lateral or rear-end collision with the other CAVs, and without violating any of the state and control constraints. For each CAV  $i \in \mathcal{N}(t)$ , we employ the double integrator dynamics as considered in (2.3), and impose the same state, control and safety constraints as in (2.4), (2.7) and (2.5), respectively. In the modeling framework described above, we also consider perfect communication

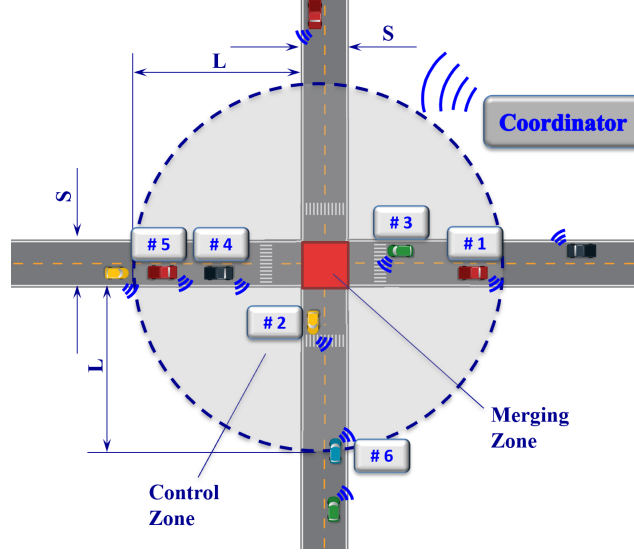


Figure 3.1: A traffic network of connected automated vehicles approaching a four-way signal-free intersection.

(Assumption 2.1.2), no lane changes or left/right turns (Assumption 2.1.1) and feasible initial condition (Assumption 2.1.3).

### 3.1.3 Low-level Optimal Control Problem

For each CAV  $i \in \mathcal{N}(t)$ ,  $t \in [t_i^0, t_i^m]$ , traveling inside the control zone, we formulate the following optimal control problem

$$\min_{u_i(t) \in U_i} \int_{t_i^0}^{t_i^m} \frac{1}{2} u_i^2(t) dt, \quad (3.1)$$

subject to : (2.3), (2.4),  $p_i(t_i^0) = 0$ ,  $p_i(t_i^m) = L$ ,

and given  $t_i^0$ ,  $v_i(t_i^0)$ ,  $t_i^m$ ,

where we consider the  $L^2$ -norm of the control input, i.e.,  $u_i^2(t)$ , as the cost function. By minimizing transient engine operation, we have direct benefits in fuel consumption in conventional vehicles (vehicles with internal combustion engines) [28]. Note that we do not explicitly include the lateral (2.7) and rear-end (2.5) safety constraints in (3.1). The lateral collision constraint is enforced by selecting the appropriate merging time  $t_i^m$

for each CAV  $i$  in the upper-level throughput maximization problem. The activation of rear-end safety constraint can be avoided under certain conditions [61].

In our formulation, the state constraints are

$$\mathbf{S}_i(t, \mathbf{x}_i(t)) := \begin{bmatrix} v_i(t) - v_{max} \\ v_{min} - v_i(t) \end{bmatrix} \leq 0. \quad (3.2)$$

Note that,  $\mathbf{S}_i(t, \mathbf{x}_i(t))$  is not an explicit function of the control input  $u_i(t)$ . Thus, to formulate the tangency constraints, we need to take successive time derivatives of  $\mathbf{S}_i(t, \mathbf{x}_i(t))$  until we obtain an expression that is explicitly dependent on  $u_i(t)$ ; see [188]. If  $q$  time derivatives are required, we refer to each constraint in  $\mathbf{S}_i^{(q)}(t, \mathbf{x}_i(t))$  as the  $q$ th-order state variable inequality constraint. In our case, we have 1st-order speed constraint, e.g.,  $\mathbf{S}_i^{(1)}(t, \mathbf{x}_i(t), u_i(t)) = \begin{bmatrix} u_i(t) \\ -u_i(t) \end{bmatrix}$ .

To derive an analytical solution of the optimal control problem in (3.1) for each CAV  $i \in \mathcal{N}(t)$ , we formulate the adjoined Hamiltonian function  $H_i(t, \mathbf{x}_i(t), u_i(t))$ ,  $t \in [t_i^0, t_i^m]$ , as follows,

$$\begin{aligned} H_i(t, \mathbf{x}_i(t), u_i(t)) &= \frac{1}{2}u_i^2(t) + \lambda_i^p(t) \cdot v_i(t) + \lambda_i^v(t) \cdot u_i(t) \\ &+ \boldsymbol{\mu}_i^T(t) \cdot \mathbf{C}_i(t, \mathbf{x}_i(t), u_i(t)) + \boldsymbol{\eta}_i^T(t) \cdot \mathbf{S}_i(t, \mathbf{x}_i(t)) \\ &= \frac{1}{2}u_i^2(t) + \lambda_i^p(t) \cdot v_i(t) + \lambda_i^v(t) \cdot u_i(t) \\ &+ \mu_i^a(t) \cdot (u_i(t) - u_{max}) + \mu_i^b(t) \cdot (u_{min} - u_i(t)) \\ &+ \eta_i^c(t) \cdot (v_i(t) - v_{max}) + \eta_i^d(t) \cdot (v_{min} - v_i(t)), \end{aligned} \quad (3.3)$$

where,  $\mathbf{C}_i(t, \mathbf{x}_i(t), u_i(t)) := [u_i(t) - u_{max} \quad u_{min} - u_i(t)]^T$  is the vector of control constraints in (2.4),  $\lambda_i^p(t)$ ,  $\lambda_i^v(t)$  are the co-state components corresponding to the state vector  $\mathbf{x}_i(t)$ , and  $\boldsymbol{\mu}_i(t)$  is the path co-vector for control constraints consisting of the

Lagrange multipliers with the following conditions,

$$\mu_i^a(t) = \begin{cases} > 0, & u_i(t) - u_{max} = 0, \\ = 0, & u_i(t) - u_{max} < 0, \end{cases} \quad (3.4)$$

$$\mu_i^b(t) = \begin{cases} > 0, & u_{min} - u_i(t) = 0, \\ = 0, & u_{min} - u_i(t) < 0, \end{cases} \quad (3.5)$$

and  $\boldsymbol{\eta}_i(t)$  is the path co-vector for state constraints consisting of the Lagrange multipliers,

$$\eta_i^c(t) = \begin{cases} > 0, & v_i(t) - v_{max} = 0, \\ = 0, & v_i(t) - v_{max} < 0, \end{cases} \quad (3.6)$$

$$\eta_i^d(t) = \begin{cases} > 0, & v_{min} - v_i(t) = 0, \\ = 0, & v_{min} - v_i(t) < 0. \end{cases} \quad (3.7)$$

The corresponding Euler-Lagrange equations at time  $t \in [t_i^0, t_i^m]$  are

$$\dot{\lambda}_i^p(t) = -\frac{\partial H_i}{\partial p_i} = 0, \quad (3.8)$$

$$\dot{\lambda}_i^v(t) = -\frac{\partial H_i}{\partial v_i} = \begin{cases} -\lambda_i^p(t), & v_i(t) - v_{max} < 0 \\ & \text{and } v_{min} - v_i(t) < 0, \\ -\lambda_i^p(t) - \eta_i^c(t), & v_i(t) - v_{max} = 0, \\ -\lambda_i^p(t) + \eta_i^d(t), & v_{min} - v_i(t) = 0, \end{cases} \quad (3.9)$$

and

$$\frac{\partial H_i}{\partial u_i} = u_i(t) + \lambda_i^v(t) + \mu_i^a(t) - \mu_i^b(t) = 0. \quad (3.10)$$

### 3.1.4 Unconstrained Solution

If the inequality state and control constraints (2.4) are not active, we have  $\mu_i^a(t) = \mu_i^b(t) = \eta_i^c(t) = \eta_i^d(t) = 0$ . Applying the necessary conditions, the optimal control  $u_i^*(t)$  can be derived from  $u_i^*(t) + \lambda_i^v(t) = 0$ ,  $i \in \mathcal{N}(t)$ . From (3.8) and (3.9) we have  $\lambda_i^p(t) = a_i$ , and  $\lambda_i^v(t) = -(a_i \cdot t + b_i)$ , where  $a_i$  and  $b_i$  are constants of integration

corresponding to each CAV  $i \in \mathcal{N}(t)$ . Therefore, the unconstrained optimal control input  $u_i^*(t)$  is

$$u_i^*(t) = a_i \cdot t + b_i, \quad t \in [t_i^0, t_i^m]. \quad (3.11)$$

Substituting the last equation into (2.3) we find the optimal speed and position for each CAV  $i \in \mathcal{N}(t)$ , namely

$$v_i^*(t) = \frac{1}{2}a_i \cdot t^2 + b_i \cdot t + c_i, \quad (3.12)$$

$$p_i^*(t) = \frac{1}{6}a_i \cdot t^3 + \frac{1}{2}b_i \cdot t^2 + c_i \cdot t + d_i, \quad t \in [t_i^0, t_i^m], \quad (3.13)$$

where  $c_i$  and  $d_i$  are constants of integration corresponding to each CAV  $i \in \mathcal{N}(t)$ . The constants of integration  $a_i$ ,  $b_i$ ,  $c_i$ , and  $d_i$  can be determined from (3.11)-(3.13) using the initial and boundary conditions imposed in (3.1). Note that, we can either compute  $a_i$ ,  $b_i$ ,  $c_i$ , and  $d_i$  only once at time  $t = t_i^0$  and apply the solution throughout optimization horizon  $[t_i^0, t_i^m]$ , or update the constants of integration by recomputing (3.11)-(3.13) at some discrete time step in  $[t_i^0, t_i^m]$  to account for any disturbance within the control zone. For the remainder of the section, we reserve the notations  $a_i$ ,  $b_i$ ,  $c_i$ , and  $d_i$  only for the unconstrained optimal solution given in (3.11)-(3.13).

**Remark 3.1.1.** For the case where the constants of integration  $a_i = 0$  and  $b_i = 0$ , we have the trivial solution of the unconstrained problem (3.11)-(3.13) as  $u_i^*(t) = 0$ ,  $v_i^*(t) = c_i$ ,  $p_i^*(t) = c_i \cdot t + d_i$ ,  $t \in [t_i^0, t_i^m]$ . This implies that if the speed is constant and the speed constraint is not active at time  $t = t_i^0$  (Assumption 2.1.3), none of the state and control constraints becomes active for  $t \in [t_i^0, t_i^m]$ . If  $a_i, b_i \neq 0$ , we have  $u_i^*(t_i^0) \neq 0$ .

In what follows, we only consider the non-trivial case (Remark 3.1.1) of the constrained optimization problem (3.1) where  $a_i, b_i \neq 0$ .

### 3.1.5 Analysis of the Constrained Optimal Control Problem

To derive the constrained analytical solution of (3.1), we follow the standard methodology used in optimal control problems with interior point state and/or control

constraints [85, 188]. Namely, we first start with the unconstrained arc and derive the solution using (3.11)-(3.13). If the solution violates any of the state or control constraints, then the unconstrained arc is pieced together with the arc corresponding to the activated constraint, and we re-compute the problem with the two arcs pieced together at the junction point between the constrained and unconstrained arcs of the constrained solution (3.1). The two arcs yield a set of algebraic equations which are solved simultaneously using the boundary conditions of (3.1) and the interior conditions between the arcs. If the resulting solution, which includes the determination of the junction point from one arc to the next one, violates another constraint, then the last two arcs are pieced together with the arc corresponding to the newly activated constraint, and we re-compute the problem with the three arcs pieced together. The three arcs will yield a new set of algebraic equations that need to be solved simultaneously using the boundary conditions of (3.1) and interior conditions between the arcs. The resulting solution includes the junction point from one arc to the next one. The process is repeated until the solution does not violate any other constraints.

This process can be computationally intensive for the following reasons. First, the recursive solution process to resolve all possible combinations of constraint activation might lead to intensive computation that prohibits real-time implementation. Second, each of the aforementioned recursion needs to be solved numerically due to the presence of implicit functions. To address both issues, we introduce a condition-based framework for the optimal control problem in (3.1) which leads to a closed-form analytical solution without this recursive procedure.

### 3.1.5.1 Condition of Constraint Exclusion

For the optimal control problem in (3.1), we have two state and two control constraints leading to 15 possible constraint combinations in total that can become active within the optimization horizon  $[t_i^0, t_i^m]$ . In this section, we show that it is only possible for a subset of the constraints to become active in  $[t_i^0, t_i^m]$ . Therefore, it is

not necessary to consider all the cases in (3.1). In what follows, we delve deeper into the nature of the unconstrained optimal solution given in (3.11)-(3.13) to derive useful information about the possible existence of constraint activation within the control zone.

**Lemma 3.1.1.** *For each CAV  $i \in \mathcal{N}(t)$ , let  $a_i$  and  $b_i$  be the constants of integration of the unconstrained solution of (3.1) corresponding to the optimal control input  $u_i^*(t)$ ,  $t \in [t_i^0, t_i^m]$ . If the speed  $v_i(t)$  is not specified at  $t_i^m$ , then*

$$a_i \cdot t_i^m + b_i = 0, \quad t_i^m > t_i^0 \geq 0. \quad (3.14)$$

*Proof.* For all  $i \in \mathcal{N}(t)$ , since the speed  $v_i(t)$  at  $t = t_i^m > t_i^0$  is not fixed, we have  $\lambda_i^v(t_i^m) = 0$  [189], which implies  $u_i^*(t_i^m) = 0$ , and the result follows.  $\square$

**Corollary 3.1.1.** *The constants of integration  $a_i$  and  $b_i$  of the unconstrained solution of (3.1) have opposite signs.*

*Proof.* Since  $t_i^m$  is positive and non-zero, the result follows from (3.14).  $\square$

**Corollary 3.1.2.** *The unconstrained optimal control input  $u_i^*(t)$  is linearly either increasing or decreasing with respect to time, and  $u_i^*(t_i^m) = 0$ .*

*Proof.* From (3.11),  $u_i^*(t)$  is a linear function with  $u_i^*(t_i^0) \neq 0$  for the non-trivial case (Remark 3.1.1), and  $u_i^*(t_i^m) = 0$  (Lemma 3.1.1), so the result follows.  $\square$

**Remark 3.1.2.** The constants of integration  $a_i$  and  $b_i$  of the unconstrained solution of (3.1) represents the slope of  $u_i^*(t)$ ,  $t \in [t_i^0, t_i^m]$ , and the initial value of the control input  $u_i^*(t)$  at time  $t = t_i^0$ , respectively.

**Lemma 3.1.2.** *Let  $v_i(t_i^0)$  be the initial speed of CAV  $i \in \mathcal{N}(t)$  when it enters the control zone at  $p_i(t_i^0)$  and travels up to the entry of the merging zone at  $p_i(t_i^m)$ . Then the nature of the unconstrained optimal control input  $u_i^*(t)$  can be characterized using the following conditions based on the boundary conditions of  $v_i(t_i^0), p_i(t_i^0)$  and  $p_i(t_i^m)$ :*

(i) The unconstrained optimal control input  $u_i^*(t)$  is linearly decreasing if  $v_i(t_i^0) < \frac{p_i(t_i^m) - p_i(t_i^0)}{t_i^m}$ . (ii) The unconstrained optimal control input  $u_i^*(t)$  is linearly increasing if  $v_i(t_i^0) > \frac{p_i(t_i^m) - p_i(t_i^0)}{t_i^m}$ .

*Proof.* From (3.12) and (3.13), we can write  $v_i(t_i^0) = \frac{1}{2}a_i \cdot (t_i^0)^2 + b_i \cdot t_i^0 + c_i$  and  $p_i(t_i^0) = \frac{1}{6}a_i \cdot (t_i^0)^3 + \frac{1}{2}b_i \cdot (t_i^0)^2 + c_i \cdot t_i^0 + d_i$ . Without loss of generality, if we let  $t_i^0 = 0$ , we have

$$c_i = v_i(t_i^0), \quad d_i = p_i(t_i^0). \quad (3.15)$$

Evaluating (3.13) at  $t = t_i^m$ , we have  $p_i(t_i^m) = \frac{1}{6}a_i \cdot (t_i^m)^3 + \frac{1}{2}b_i \cdot (t_i^m)^2 + c_i \cdot t_i^m + d_i$ . Substituting (3.14) and (3.15) in the above equation and solving for  $a_i$ , we have

$$a_i = \frac{3(v_i(t_i^0) \cdot t_i^m - (p_i(t_i^m) - p_i(t_i^0)))}{(t_i^m)^3}. \quad (3.16)$$

Since  $t_i^m > 0$ , we have a non-positive constant of integration  $a_i$ , if  $(v_i(t_i^0) \cdot t_i^m - (p_i(t_i^m) - p_i(t_i^0))) < 0$ . From Corollary 3.1.2 and Remark 3.1.2, a non-positive  $a_i$  indicates a negative slope for  $u_i^*(t)$ , which implies that  $u_i^*(t)$  is a linearly decreasing acceleration, and the proof is complete. The second part of Lemma 3.1.2 can be proved following similar steps, hence it is omitted.  $\square$

**Remark 3.1.3.** When the CAV  $i \in \mathcal{N}(t)$  travels with its initial speed  $v_i(t_i^0)$  throughout the control zone, we have  $v_i(t_i^0) \cdot t_i^m = (p_i(t_i^m) - p_i(t_i^0))$ . From (3.16), this implies that  $a_i = 0$ , referring to an optimal control input  $u_i^*(t)$  with horizontal slope. Since  $u_i^*(t_i^m) = 0$  (Lemma 3.1.1), we have  $u_i^*(t) = 0$ , for all  $t \in [t_i^0, t_i^m]$ .

**Lemma 3.1.3.** For the unconstrained optimal solution of (3.1), if either  $v_i(t) - v_{max} \leq 0$  or  $u_i(t) - u_{max} \leq 0$  becomes active at any time  $t \in [t_i^0, t_i^m]$ , neither  $v_{min} - v_i(t) \leq 0$  nor  $u_{min} - u_i(t) \leq 0$  can become active in  $[t_i^0, t_i^m]$ . The reverse also holds.

*Proof.* Let  $u_i^*(t) = a_i \cdot t + b_i > 0 > u_{min}$  at some time  $t \in [t_i^0, t_i^m]$ . Since  $u_i^*(t_i^m) = 0$  (Lemma 3.1.1) and  $u_i^*(t)$  is a linearly decreasing function (Corollary 3.1.2), we have  $u_i^*(t) > u_{min}$ , for all  $t \in [t_i^0, t_i^m]$ , i.e., the constraint  $u_{min} - u_i(t) \leq 0$  can not become

active at any time in  $t \in [t_i^0, t_i^m]$ . The corresponding quadratic optimal speed profile  $v_i^*(t)$  in (3.12) is a parabolic function of degree 2 with y-symmetric axis located at  $t_i^m$  in the speed-time graph. Applying the necessary and sufficient condition of optimality in (3.12), we have

$$\dot{v}_i^*(t) = a_i \cdot t + b_i = 0, \quad \ddot{v}_i^*(t) = a_i, \quad t \in [t_i^0, t_i^m]. \quad (3.17)$$

Solving the first equation of (3.17), we have the extremum point at  $t = -\frac{b_i}{a_i}$  which corresponds to the vertex of the parabola of (3.12) at  $t = t_i^m$ . Whether this point corresponds to the maximum or minimum of the (3.12) can be determined from the second part of (3.17). Since  $u_i^*(t)$  is decreasing,  $a_i < 0$  (Remark 3.1.2). Thus, the second equation of (3.17) indicates a maximum value at the vertex  $t_i^m$ , indicating a concave quadratic profile of  $v_i^*(t)$ . Since the extremum of the quadratic profile of  $v_i^*(t)$  is located at  $t_i^m$  and  $v_{min} < v_i(t_i^0) < v_{max}$  (Assumption 2.1.3), we have  $v_i^*(t) > v_{min}$  for all  $t \in [t_i^0, t_i^m]$ . Therefore, the constraints  $v_{min} - v_i(t) \leq 0$  can not become active at any time  $t \in [t_i^0, t_i^m]$ , and the proof of the first part of Lemma 3.1.3 is complete.

Conversely, let  $u_i^*(t) = a_i \cdot t + b_i < 0 < u_{max}$  at some  $t \in [t_i^0, t_i^m]$ . Since  $u_i^*(t_i^m) = 0$  (Lemma 3.1.1) and  $u_i^*(t)$  is linearly increasing in  $t \in [t_i^0, t_i^m]$  (Remark 3.1.2),  $u_{min} - u_i(t) \leq 0$  can not become active at any  $t \in [t_i^0, t_i^m]$ . In addition,  $u_i^*(t)$  yields a convex quadratic profile of  $v_i^*(t)$  with vertex at  $t = t_i^m$ . Since the extremum point is located at  $t_i^m$  and  $v_{min} < v_i(t_i^0) < v_{max}$  (Assumption 2.1.3), we have  $v_i^*(t) < v_{max}$  for any  $t \in [t_i^0, t_i^m]$ , which implies that the state constraint  $v_i(t) - v_{max} \leq 0$  cannot become active at any time  $t \in [t_i^0, t_i^m]$ .  $\square$

**Corollary 3.1.3.** *The sign of  $a_i$  corresponding to the unconstrained solution of (3.1) dictates the activation of either constraint set  $\{v_i(t) - v_{max} \leq 0, u_i(t) - u_{max} \leq 0\}$  or  $\{v_{min} - v_i(t) \leq 0, u_{min} - u_i(t) \leq 0\}$ .*

*Proof.* Since  $a_i$  is the slope of the optimal control input  $u_i^*(t)$  (Remark 3.1.2), the sign of  $a_i$  determines whether  $u_i^*(t)$  is positive and decreasing or negative and increasing, which, in turn, determines the constraint activation criteria in Lemma 3.1.3.  $\square$

**Remark 3.1.4.** The sign of  $a_i$  can provide direct insight on which of the state and control constraints becomes active, and thus it can reduce the cardinality of the set of possible constraint activation cases.

Based on Lemmas 3.1.2 and 3.1.3, we now present the following result which provides the condition under which the state and control constraints become active. Note that the result is based on the initial and final conditions of (3.1) which enable the determination of the possible constraint activation set without solving the unconstrained optimization problem in (3.1).

**Theorem 3.1.4.** *Let CAV  $i \in \mathcal{N}(t)$  enter the control zone with initial speed  $v_i(t_i^0)$  and travel with the unconstrained optimal control input  $u_i^*(t)$ ,  $t \in [t_i^0, t_i^m]$ . Then, (i)  $v_{min} - v_i(t) \leq 0$  and  $u_{min} - u_i(t) \leq 0$  do not become active in  $t \in [t_i^0, t_i^m]$ , if  $v_i(t_i^0) < \frac{(p_i(t_i^m) - p_i(t_i^0))}{t_i^m}$ , and (ii)  $v_i(t) - v_{max} \leq 0$  and  $u_i(t) - u_{max} \leq 0$  do not become active in  $t \in [t_i^0, t_i^m]$ , if  $v_i(t_i^0) > \frac{(p_i(t_i^m) - p_i(t_i^0))}{t_i^m}$ .*

*Proof.* If  $v_i(t_i^0) < \frac{(p_i(t_i^m) - p_i(t_i^0))}{t_i^m}$ , then from (3.16)  $a_i < 0$ , hence  $u_i^*(t)$  is linearly decreasing (Lemma 3.1.2). Therefore, from Lemma 3.1.3,  $v_{min} - v_i(t) \leq 0$  and  $u_{min} - u_i(t) \leq 0$  can not become active in  $t \in [t_i^0, t_i^m]$ , which concludes the proof of the first part.

For the second part of Theorem 1, suppose that  $v_i(t_i^0) > \frac{(p_i(t_i^m) - p_i(t_i^0))}{t_i^m}$ . Hence  $a_i > 0$  (Lemma 3.1.2), and  $u_i^*(t)$  is linearly increasing. Therefore, from Lemma 3.1.3,  $v_i(t) - v_{max}(t) \leq 0$  and  $u_i(t) - u_{max} \leq 0$  can not become active in  $t \in [t_i^0, t_i^m]$ , and the proof is complete.  $\square$

**Remark 3.1.5.** Theorem 3.1.4 aims at reducing the possible set of constraint activation cases. For example, if the condition in part (i) of Theorem 3.1.4 holds, then from the 15 possible cases of constraint activation, we only need to consider 3 cases: (a)  $v_i(t) - v_{max} \leq 0$ , (b)  $u_i(t) - u_{max} \leq 0$ , and (c) both  $v_i(t) - v_{max} \leq 0$  and  $u_i(t) - u_{max} \leq 0$ . Similarly, if the condition in part (ii) of Theorem 1 holds, then from the 15 possible cases of constraint activation, we only need to consider 3 cases: (a)  $v_{min} - v_i(t) \leq 0$ , (b)  $u_{min} - u_i(t) \leq 0$ , and (c) both  $v_{min} - v_i(t) \leq 0$  and  $u_{min} - u_i(t) \leq 0$ .

Although Theorem 3.1.4 aims at reducing the possible constraint activation cases, it does not lead to the identification of the exact constraint activation of the unconstrained solution of (3.1). In what follows, we provide the conditions that can be used to extend the results of Theorem 3.1.4 and identify the activation of any constraint case in  $[t_i^0, t_i^m]$ .

### 3.1.5.2 Conditions of Constraint Activation

We start our exposition with some results that contain essential properties of the state and control constraint activation.

**Lemma 3.1.5.** *If neither  $u_i(t) - u_{max} \leq 0$  nor  $u_{min} - u_i(t) \leq 0$  is active at  $t = t_i^0$ , then it is guaranteed that neither of them will become active for all  $t \in [t_i^0, t_i^m]$ .*

*Proof.* Suppose that the unconstrained optimal solution of (3.1) yields  $u_i^*(t) = a_i t + b_i$  with  $a_i < 0$ . From Corollary 3.1.2 and Remark 3.1.2,  $u_i^*(t)$  decreases with respect to  $t$ , and at  $t_i^m$ ,  $u_i^*(t_i^m) = 0$ . Therefore, if  $u_i^*(t_i^0) < u_{max}$ , then  $u_i^*(t) < u_{max}$  for all  $t \in [t_i^0, t_i^m]$ . The second part of Lemma 3.1.5 can be proved following similar steps, hence it is omitted.  $\square$

**Lemma 3.1.6.** *If either  $v_i(t) - v_{max} \leq 0$  or  $v_{min} - v_i(t) \leq 0$  becomes active at any time  $t \in [t_i^0, t_i^m]$ , then it will remain active until  $t = t_i^m$ .*

*Proof.* Suppose that the unconstrained optimal solution of (3.1) yields  $u_i^*(t) = a_i t + b_i$  with  $a_i < 0$ . From Corollary 3.1.2 and Remark 3.1.2,  $u_i^*(t)$  decreases with respect to  $t$ , and at  $t_i^m$ ,  $u_i^*(t_i^m) = 0$ , which implies that  $v_i^*(t)$  is monotonically increasing, i.e.,  $v_i^*(t_i^m) \geq v_i^*(t)$  in  $t \in [t_i^0, t_i^m]$ . Therefore,  $v_i(t) - v_{max} \leq 0$  will remain active until  $t = t_i^m$ . The second part of Lemma 3.1.6 can be proved following similar steps, hence it is omitted.  $\square$

**Remark 3.1.6.** Lemma 3.1.5 implies that the entry of the control-constrained arc can be only at  $t = t_i^0$ , while Lemma 3.1.6 implies that there is no exit point in  $[t_i^0, t_i^m]$  of the state-constrained arc after it becomes active.

The following results provide the conditions for which state and control constraint activation cases can be identified for the optimal control problem (3.1) a priori.

**Theorem 3.1.7.** *Let  $u_i^*(t) = a_i t + b_i$ ,  $t \in [t_i^0, t_i^m]$ , be the optimal control input of CAV  $i \in \mathcal{N}(t)$  for the unconstrained solution of (3.1). Then, (i) for  $a_i < 0$ ,  $v_i(t) - v_{max} \leq 0$  becomes active if  $t_i^m \leq \frac{3(p_i(t_i^m) - p_i(t_i^0))}{v_i(t_i^0) + 2v_{max}}$ , and (ii) for  $a_i > 0$ ,  $v_{min} - v_i(t) \leq 0$  becomes active if  $t_i^m \geq \frac{3(p_i(t_i^m) - p_i(t_i^0))}{v_i(t_i^0) + 2v_{min}}$ .*

*Proof.* For  $a_i < 0$ , suppose that there exists a time  $t_i^s \in (t_i^0, t_i^m]$  at which  $v_i(t) - v_{max} \leq 0$  becomes active. Then, from (3.12) and (3.15), we have  $\frac{1}{2}a_i \cdot (t_i^s)^2 + b_i \cdot t_i^s + v_i(t_i^0) = v_{max}$ . Solving the quadratic equation for  $t_i^s$ , we have  $t_i^s = \frac{-2b_i \pm \sqrt{4b_i^2 - 8a_i \cdot (v_i(t_i^0) - v_{max})}}{2a_i}$ , which yields  $t_i^s = t_i^m \pm \sqrt{\frac{4b_i^2 - 8a_i \cdot (v_i(t_i^0) - v_{max})}{4a_i^2}}$ . Since  $t_i^s \leq t_i^m$ , a feasible solution of  $t_i^s$  exists if we have  $\sqrt{4b_i^2 - 8a_i \cdot (v_i(t_i^0) - v_{max})} \geq 0$  resulting in  $a_i \leq \frac{2(v_i(t_i^0) - v_{max})}{(t_i^m)^2}$ . Combining with (3.16), the proof of the first statement of Theorem 3.1.7 follows.

For  $a_i > 0$ , suppose that there exists a time  $t_i^s \in (t_i^0, t_i^m]$  at which the state constraint  $v_{min} - v_i(t) \leq 0$  becomes active. Then, from (3.12) and (3.15), we have  $\frac{1}{2}a_i \cdot (t_i^s)^2 + b_i \cdot t_i^s + v_i(t_i^0) = v_{min}$ . Solving the above equation for  $t_i^s$ , we have  $t_i^s = \frac{-2b_i \pm \sqrt{4b_i^2 - 8a_i \cdot (v_i(t_i^0) - v_{min})}}{2a_i}$ , which yields  $t_i^s = t_i^m \pm \sqrt{\frac{4b_i^2 - 8a_i \cdot (v_i(t_i^0) - v_{min})}{4a_i^2}}$ . Since  $t_i^s \leq t_i^m$ , we need to have  $\sqrt{4b_i^2 - 8a_i \cdot (v_i(t_i^0) - v_{min})} \geq 0$ , and combining with (3.16), the proof of the second statement of Theorem 3.1.7 follows.  $\square$

**Theorem 3.1.8.** *Let  $u_i^*(t) = a_i \cdot t + b_i$ ,  $t \in [t_i^0, t_i^m]$ , be the optimal control input of CAV  $i \in \mathcal{N}(t)$  for the unconstrained solution of (3.1). Then, (i) for  $a_i < 0$ ,  $u_i(t) - u_{max} \leq 0$  becomes active if  $t_i^m \leq \frac{-3v_i(t_i^0) + \sqrt{9(v_i(t_i^0))^2 + 12u_{max} \cdot (p_i(t_i^m) - p_i(t_i^0))}}{2u_{max}}$ , and (ii) for  $a_i > 0$ ,  $u_{min} - u_i(t) \leq 0$  becomes active if  $t_i^m \geq \frac{-3v_i(t_i^0) + \sqrt{9(v_i(t_i^0))^2 + 12u_{min} \cdot (p_i(t_i^m) - p_i(t_i^0))}}{2u_{min}}$ .*

*Proof.* For  $a_i < 0$ , without loss of generality, we let  $t_i^0 = 0$ . Given  $v_i(t_i^0)$ ,  $p_i(t_i^0)$  and  $p_i(t_i^m)$ , we will show that  $t_i^m$  determines whether  $u_i(t) - u_{max} \leq 0$  becomes active or not. Let  $\hat{t}_i^m$  be the value for which  $u_i(t) - u_{max} \leq 0$  becomes active at  $t_i^0$ , and  $\hat{a}_i$ ,  $\hat{b}_i$  the corresponding constants of integration. Then from (3.14) and (3.16), we can write

$\hat{b}_i = -\frac{3(v_i(t_i^0) \cdot \hat{t}_i^m - L)}{(\hat{t}_i^m)^2} = u_{max}$ , where  $L = p_i(t_i^m) - p_i(t_i^0) = p_i(\hat{t}_i^m) - p_i(t_i^0)$ , which can be reduced to  $u_{max} \cdot (\hat{t}_i^m)^2 + 3v_i(t_i^0) \cdot \hat{t}_i^m - 3L = 0$ . The solution of the last equation yields  $\hat{t}_i^m = \frac{-3v_i(t_i^0) \pm \sqrt{9(v_i(t_i^0))^2 + 12u_{max} \cdot L}}{2u_{max}}$ . Since  $\hat{t}_i^m > 0$ ,  $\hat{t}_i^m = \frac{-3v_i(t_i^0) + \sqrt{9(v_i(t_i^0))^2 + 12u_{max} \cdot L}}{2u_{max}}$ . Hence, for any  $t_i^m$  such that  $t_i^m \leq \hat{t}_i^m$ ,  $u_i(t) - u_{max} \leq 0$  becomes active, and the proof of the first statement of Theorem 3.1.8 is complete.

For  $a_i > 0$ , without loss of generality, we let  $t_i^0 = 0$ . Let  $\hat{t}_i^m$  be a value that  $u_{min} - u_i(t) \leq 0$  becomes active at  $t_i^0$ , and  $\hat{a}_i$ ,  $\hat{b}_i$  the corresponding constants of integration. Then from (3.14) and (3.16), we can write  $\hat{b}_i = -\frac{3(v_i(t_i^0) \cdot \hat{t}_i^m - L)}{(\hat{t}_i^m)^2} = u_{min}$ , where  $L = p_i(t_i^m) - p_i(t_i^0) = p_i(\hat{t}_i^m) - p_i(t_i^0)$ , which can be reduced to  $u_{min} \cdot (\hat{t}_i^m)^2 + 3v_i(t_i^0) \cdot \hat{t}_i^m - 3L = 0$ . The solution of the last equation yields  $\hat{t}_i^m = \frac{-3v_i(t_i^0) \pm \sqrt{9(v_i(t_i^0))^2 + 12u_{min} \cdot L}}{2u_{min}}$ , from which we have the only admissible result  $\hat{t}_i^m = \frac{-3v_i(t_i^0) + \sqrt{9(v_i(t_i^0))^2 + 12u_{min} \cdot L}}{2u_{min}}$ . Hence, for any  $t_i^m$  such that  $t_i^m \geq \hat{t}_i^m$ ,  $u_{min} - u_i(t) \leq 0$  becomes active, and the proof of the second statement of Theorem 3.1.8 is complete. □

### 3.1.5.3 Interdependence of Constraint Activation Cases

We have discussed so far the conditions under which any of the state and control constraints become active. Using these conditions, we can derive the analytical solution of (3.1). However, the resulting solution might activate additional constrained arcs. Therefore, we need to be able to identify beforehand under which conditions any additional constrained arcs may become active. Next, we provide a set of conditions based on the junction point where the transition between the constrained and unconstrained arcs occurs.

**Theorem 3.1.9.** *For CAV  $i \in \mathcal{N}(t)$ , let  $\tau_s^* \in (t_i^0, t_i^m]$  be the junction point of the state constrained arc where either  $v_i(t) - v_{max} \leq 0$  or  $v_{min} - v_i(t) \leq 0$  becomes active. Then, (i)  $v_i(t) - v_{max} \leq 0$  may cause  $u_i(t) - u_{max} \leq 0$  to become active, if  $\tau_s^* \leq \frac{-3v_i(t_i^0) + \sqrt{9(v_i(t_i^0))^2 + 12u_{max} \cdot (p_i^*(\tau_s^*) - p_i(t_i^0))}}{2u_{max}}$ , and (ii)  $v_{min} - v_i(t) \leq 0$  may cause  $u_{min} - u_i(t) \leq 0$  to become active, if  $\tau_s^* \geq \frac{-3v_i(t_i^0) + \sqrt{9(v_i(t_i^0))^2 + 12u_{min} \cdot (p_i^*(\tau_s^*) - p_i(t_i^0))}}{2u_{min}}$ .*

*Proof.* Suppose that  $v_i(t) - v_{max} \leq 0$  becomes active at  $\tau_s^*$ , where  $t_i^0 < \tau_s^* \leq t_i^m$ . Then from (2.3),  $u_i^*(t) = 0$  in  $t \in [\tau_s^*, t_i^m]$  and  $p_i(\tau_s^*) = p_i(t_i^m) - v_{max} \cdot (t_i^m - \tau_s^*)$ . We will determine whether any control constraint  $u_i(t) - u_{max} \leq 0$  becomes active in  $t \in [t_i^0, \tau_s^*]$ . From Lemma 3.1.5, the control constraint becomes active at  $t = t_i^0$ . Let  $\hat{t}_i^m$  be the value that  $u_i(t) - u_{max} \leq 0$  becomes active at  $t_i^0$ , and  $\hat{a}_i, \hat{b}_i$  the corresponding constants of integration. Without loss of generality, if we let  $t_i^0 = 0$ , then from (3.14) and (3.16) we can write,  $\hat{b}_i = -\frac{3(v_i(t_i^0) \cdot \hat{t}_i^m - (p_i^*(\tau_s^*) - p_i(t_i^0)))}{(\hat{t}_i^m)^2} = u_{max}$ , where  $p_i(\tau_s^*) - p_i(t_i^0) = p_i(\hat{t}_i^m) - p_i(t_i^0)$ , which can be reduced to  $u_{max} \cdot (\hat{t}_i^m)^2 + 3v_i(t_i^0) \cdot \hat{t}_i^m - 3(p_i^*(\tau_s^*) - p_i(t_i^0)) = 0$ . The solution of the last equation yields  $\hat{t}_i^m = \frac{-3v_i(t_i^0) \pm \sqrt{9(v_i(t_i^0))^2 + 12u_{max} \cdot (p_i^*(\tau_s^*) - p_i(t_i^0))}}{2u_{max}}$ . Since  $\hat{t}_i^m > 0$ ,  $\hat{t}_i^m = \frac{-3v_i(t_i^0) + \sqrt{9(v_i(t_i^0))^2 + 12u_{max} \cdot (p_i^*(\tau_s^*) - p_i(t_i^0))}}{2u_{max}}$ . Hence, for any  $\tau_s^*$  such that  $\tau_s^* \leq \hat{t}_i^m$ ,  $u_i(t) - u_{max} \leq 0$  becomes active, and the proof of the first statement of Theorem 3.1.9 is complete.

Suppose that  $v_{min} - v_i(t) \leq 0$  becomes active at  $\tau_s^*$ , where  $t_i^0 < \tau_s^* \leq t_i^m$ . Then from (2.3),  $u_i^*(t) = 0$  in  $t \in [\tau_s^*, t_i^m]$  and  $p_i(\tau_s^*) = p_i(t_i^m) - v_{min} \cdot (t_i^m - \tau_s^*)$ . Let  $\hat{t}_i^m$  be the value that  $u_{min} - u_i(t) \leq 0$  becomes active at  $t_i^0$ , and  $\hat{a}_i, \hat{b}_i$  the corresponding constants of integration. Without loss of generality, if we let  $t_i^0 = 0$ , then from (3.14) and (3.16) we can write,  $\hat{b}_i = -\frac{3(v_i(t_i^0) \cdot \hat{t}_i^m - (p_i^*(\tau_s^*) - p_i(t_i^0)))}{(\hat{t}_i^m)^2} = u_{min}$ , where  $p_i(\tau_s^*) - p_i(t_i^0) = p_i(\hat{t}_i^m) - p_i(t_i^0)$ , which can be reduced to  $u_{min} \cdot (\hat{t}_i^m)^2 + 3v_i(t_i^0) \cdot \hat{t}_i^m - 3(p_i^*(\tau_s^*) - p_i(t_i^0)) = 0$ . The solution of the last equation yields  $\hat{t}_i^m = \frac{-3v_i(t_i^0) \pm \sqrt{9(v_i(t_i^0))^2 + 12u_{min} \cdot (p_i^*(\tau_s^*) - p_i(t_i^0))}}{2u_{min}}$ , where  $\hat{t}_i^m = \frac{-3v_i(t_i^0) + \sqrt{9(v_i(t_i^0))^2 + 12u_{min} \cdot (p_i^*(\tau_s^*) - p_i(t_i^0))}}{2u_{min}}$  is the only admissible result. Hence, for any  $\tau_s^*$  such that  $\tau_s^* \geq \hat{t}_i^m$ ,  $u_{min} - u_i(t) \leq 0$  becomes active, and the proof of the second statement of Theorem 3.1.9 is complete.  $\square$

**Theorem 3.1.10.** *For CAV  $i \in \mathcal{N}(t)$ , let  $\tau_c^* \in (t_i^0, t_i^m]$  be the junction point of the control constrained arc where either  $u_i(t) - u_{max} \leq 0$  or  $u_{min} - u_i(t) \leq 0$  becomes active. Then, (i)  $u_i(t) - u_{max} \leq 0$  may cause  $v_i(t) - v_{max} \leq 0$  to become active, if  $t_i^m \geq \tau_c^* - \frac{2(v_i(\tau_c^*) - v_{max})}{u_{max}}$ , and (ii)  $u_{min} - u_i(t) \leq 0$  may cause  $v_{min} - v_i(t) \leq 0$  to become active, if  $t_i^m \geq \tau_c^* - \frac{2(v_i(\tau_c^*) - v_{min})}{u_{min}}$ .*

*Proof.* Suppose that  $u_i(t) - u_{max} \leq 0$  becomes active at  $t_i^0$  (Remark 3.1.6) with an

exit time at  $\tau_c^* \in (t_i^0, t_i^m]$ . Then from (2.3),  $u_i^*(t) = u_{max}$  in  $t \in [t_i^0, \tau_c^*]$ . Consequently, we have  $v_i(\tau_c^*) = v_i(t_i^0) + u_{max} \cdot \tau_c^*$ . We will determine whether any state constraint  $v_i(t) - v_{max} \leq 0$  becomes active for the unconstrained arc within  $t \in [\tau_c^*, t_i^m]$ . Suppose that there exists a time  $t_i^s \in (\tau_c^*, t_i^m]$  at which  $v_i(t) - v_{max} \leq 0$  becomes active in  $[\tau_c^*, t_i^m]$ . Without loss of generality, if we let  $\tau_c^* = 0$ , then the constants of integration  $\hat{a}_i, \hat{b}_i$  are given by  $\hat{a}_i = -\frac{u_{max}}{\hat{t}_i^m}$  and  $\hat{b}_i = u_{max}$  (Remark 3.1.2), where  $\hat{t}_i^m := t_i^m - \tau_c^*$ . From (3.12) and (3.15), we have  $\frac{1}{2}\hat{a}_i \cdot (t_i^s)^2 + \hat{b}_i \cdot t_i^s + v_i(\tau_c^*) = v_{max}$ . Solving the quadratic equation for  $t_i^s$ , we have  $t_i^s = \frac{-2\hat{b}_i \pm \sqrt{4\hat{b}_i^2 - 8\hat{a}_i \cdot (v_i(\tau_c^*) - v_{max})}}{2\hat{a}_i}$ , which yields  $t_i^s = \hat{t}_i^m \pm \sqrt{\frac{4\hat{b}_i^2 - 8\hat{a}_i \cdot (v_i(\tau_c^*) - v_{max})}{4\hat{a}_i^2}}$ . Since we require  $t_i^s \leq \hat{t}_i^m$ , we need to have  $\sqrt{4\hat{b}_i^2 - 8\hat{a}_i \cdot (v_i(\tau_c^*) - v_{max})} \geq 0$  resulting in  $\hat{a}_i \leq \frac{2(v_i(\tau_c^*) - v_{max})}{(\hat{t}_i^m)^2}$ . By using the value of  $\hat{a}_i$  in the above equation and simplifying, the proof of the first statement of Theorem 3.1.7 follows.

For the second statement of Theorem 3.1.10, suppose that there exists a time  $t_i^s \in (\tau_c^*, t_i^m]$  at which  $v_{min} - v_i(t) \leq 0$  becomes active in  $[\tau_c^*, t_i^m]$ . Without loss of generality, if we let  $\tau_c^* = 0$ , then the constants of integration  $\hat{a}_i, \hat{b}_i$  are given by  $\hat{a}_i = -\frac{u_{min}}{\hat{t}_i^m}$  and  $\hat{b}_i = u_{min}$  (Remark 3.1.2), where  $\hat{t}_i^m := t_i^m - \tau_c^*$ . From (3.12) and (3.15), we have  $\frac{1}{2}\hat{a}_i \cdot (t_i^s)^2 + \hat{b}_i \cdot t_i^s + v_i(\tau_c^*) = v_{min}$ . Solving the quadratic equation for  $t_i^s$ , we have  $t_i^s = \frac{-2\hat{b}_i \pm \sqrt{4\hat{b}_i^2 - 8\hat{a}_i \cdot (v_i(\tau_c^*) - v_{min})}}{2\hat{a}_i}$ , which yields  $t_i^s = \hat{t}_i^m \pm \sqrt{\frac{4\hat{b}_i^2 - 8\hat{a}_i \cdot (v_i(\tau_c^*) - v_{min})}{4\hat{a}_i^2}}$ . Since  $t_i^s \leq \hat{t}_i^m$ , we need to have  $\sqrt{4\hat{b}_i^2 - 8\hat{a}_i \cdot (v_i(\tau_c^*) - v_{min})} \geq 0$  resulting in  $\hat{a}_i \leq \frac{2(v_i(\tau_c^*) - v_{min})}{(\hat{t}_i^m)^2}$ . By using the value of  $\hat{a}_i$  in the above equation and simplifying, the proof of the second statement of Theorem 3.1.7 follows.  $\square$

**Remark 3.1.7.** The conditions in Theorems 4 and 5 depend on the junction points  $\tau_s^*$  and  $\tau_c^*$  of the corresponding constraint activation cases, which can be derived analytically from the known boundary conditions of (3.1). Since the derivation of such an analytical solution requires additional information, we provide the analysis in the following section.

### 3.1.6 Analytical Solution of the Constrained Optimal Control Problem

To derive the analytical solution of (3.1), we present a condition-based framework consisting of the following steps. We first evaluate the condition stated in Theorem 3.1.4 to reduce the set of possible constraint activation cases (Remark 3.1.5). Then using the above result, we evaluate the conditions presented in Theorems 3.1.7 and 3.1.8 to determine whether any constraint has become active. If none of the constraints in (2.4) becomes active, we simply derive the unconstrained solution using (3.11)-(3.13) and terminate the process. However, if the conditions in Theorems 3.1.7 and 3.1.8 indicate the activation of any constraint cases, we need to evaluate further the conditions in Theorems 3.1.9 and 3.1.10 to determine whether any additional constraints may become active within the constrained solution as a result of the constraint cases identified from Theorems 3.1.7 and 3.1.8. Once the nature of the final constraint activation case is identified using Theorems 3.1.9 and 3.1.10, we then piece together the relevant unconstrained and constrained arcs that yield a set of algebraic equations which are solved simultaneously using the boundary conditions of (3.1) and interior conditions between the arcs.

Since we piece together multiple constrained and unconstrained arcs, we denote the constants of integration corresponding to each arc by  $a_i^{(p)}, b_i^{(p)}, c_i^{(p)}, d_i^{(p)}$ ,  $p = 1, 2, \dots, N_{arc}$ , where  $N_{arc} \in \mathbb{N}$  is the total number of arcs pieced together in the constrained solution and  $p$  represents the position of the arcs in terms of their appearance in the optimal solution starting from  $t_i^0$  to  $t_i^m$ . For  $N_{arc}$  arcs, we have  $(N_{arc} - 1)$  junction points. At any junction point  $\tau$ , the states are continuous, namely,

$$p_i(\tau^-) = p_i(\tau^+), \quad v_i(\tau^-) = v_i(\tau^+), \quad (3.18)$$

where,  $\tau^-$  and  $\tau^+$  represent the time instance right before and right after  $\tau$ , respectively.

In what follows, we present the closed form analytical solution of different cases of state and control constraint activation to derive the optimal input  $u_i^*(t)$ ,  $t \in [t_i^0, t_i^m]$ , for each CAV  $i \in \mathcal{N}(t)$ .

**Case 1.** 1 Only the state constraint  $v_i(t) - v_{max} \leq 0$  becomes active.

In this case, we have  $\mu_i^a(t) = \mu_i^b(t) = \eta_i^d(t) = 0$ . From (3.8), (3.9), and (3.10), we have  $u_i(t) + \lambda_i^v(t) = 0$ ,  $\dot{\lambda}_i^p(t) = 0$ , and  $\dot{\lambda}_i^v(t) = -\lambda_i^p(t) - \eta_i^c(t)$ . By Lemma 3.1.6, CAV  $i \in \mathcal{N}(t)$  exits the constrained arc at  $t = t_i^m$  which leads to a single junction point. Let  $\tau_s, t_i^0 < \tau_s < t_i^m$ , be the junction point and let  $\tau_s^-$  and  $\tau_s^+$  be the time instance just before and after time  $\tau_s$ . The optimal speed and control input on the constrained arc are

$$v_i^*(t) = v_{max}, \quad u_i^*(t) = 0, \quad t \in [\tau_s, t_i^m]. \quad (3.19)$$

The jump conditions of the costates and the Hamiltonian at  $\tau_s$  are

$$\lambda_i^p(\tau_s^-) = \lambda_i^p(\tau_s^+) + \pi_i \cdot \frac{\partial}{\partial p_i(t)} \left[ v_i(t) - v_{max} \right] \Bigg|_{t=\tau_s}, \quad (3.20a)$$

$$\lambda_i^v(\tau_s^-) = \lambda_i^v(\tau_s^+) + \pi_i \cdot \frac{\partial}{\partial v_i(t)} \left[ v_i(t) - v_{max} \right] \Bigg|_{t=\tau_s}, \quad (3.20b)$$

$$H_i(\tau_s^-) = H_i(\tau_s^+) - \pi_i \cdot \frac{\partial}{\partial t} \left[ v_i(t) - v_{max} \right] \Bigg|_{t=\tau_s}, \quad (3.20c)$$

where  $\pi_i$  is a constant Langrange multiplier determined so that  $v_i(t) - v_{max} = 0$  is satisfied. Note that, (3.20a)-(3.20c) imply possible discontinuity of the costates and the Hamiltonian at  $t = \tau_s$ . The state variables are continuous at  $t = \tau_s$ . From (3.20c), we have

$$\begin{aligned} & \frac{1}{2} u_i^2(\tau_s^-) + \lambda_i^p(\tau_s^-) \cdot v_i(\tau_s^-) + \lambda_i^v(\tau_s^-) \cdot u_i(\tau_s^-) + \eta_i^c(\tau_s^-) \cdot (v_i(\tau_s^-) - v_{max}) \\ &= \frac{1}{2} u_i^2(\tau_s^+) + \lambda_i^p(\tau_s^+) \cdot v_i(\tau_s^+) + \lambda_i^v(\tau_s^+) \cdot u_i(\tau_s^+) + \eta_i^c(\tau_s^+) \cdot (v_i(\tau_s^+) - v_{max}). \end{aligned} \quad (3.21)$$

From the continuity of the states and since  $v_i(\tau_s^+) = v_{max}$ ,  $u_i(\tau_s^+) = 0$ , we have  $\lambda_i^p(\tau_s^-) \cdot v_i(\tau_s^-) = \lambda_i^p(\tau_s^+) \cdot v_i(\tau_s^+)$ . The Lagrange multiplier  $\eta_i^c(t)$  in (3.6), yields  $\eta_i^c(\tau_s^-) \cdot (v_i(\tau_s^-) - v_{max}) = \eta_i^c(\tau_s^+) \cdot (v_i(\tau_s^+) - v_{max}) = 0$ . By combining the above equations, (3.21) reduces to  $\frac{1}{2} u_i^2(\tau_s^-) + \lambda_i^v(\tau_s^-) \cdot u_i(\tau_s^-) = 0$ , which implies that either

$u_i(\tau_s^-) = 0$  or  $\frac{1}{2}u_i(\tau_s^-) + \lambda_i^v(\tau_s^-) = 0$ , or both. Since the second term contradicts  $u_i(t) + \lambda_i^v(t) = 0$ , we have  $u_i(\tau_s^-) = 0$ . The Lagrange multiplier  $\eta_i^c(t)$  is

$$\eta_i^c(t) = \begin{cases} 0, & \text{if } v_i(t) < v_{max}, t \in [t_i^0, \tau_s), \\ -\lambda_i^p(t), & \text{if } v_i(t) = v_{max}, t \in [\tau_s, t_i^m]. \end{cases}$$

Using the Euler-Lagrange equations, interior conditions, the initial and final boundary conditions, and the terminal condition of the costates, we can formulate a set of equations by piecing the unconstrained and constrained arcs together at time  $t = \tau_s$ . This results in a total number of 9 equations that we need to solve simultaneously to compute  $4 + 4 + 1 = 9$  variables corresponding to the constants of integration of unconstrained and constrained arc, and the junction point  $\tau_s^*$  respectively. From (3.11)-(3.13) and the boundary conditions in (3.1), we receive the following 4 equations:  $\frac{1}{2}a_i^{(1)} \cdot (t_i^0)^2 + b_i^{(1)} \cdot t_i^0 + c_i^{(1)} = v_i(t_i^0)$ ,  $\frac{1}{6}a_i^{(1)} \cdot (t_i^0)^3 + \frac{1}{2}b_i^{(1)} \cdot (t_i^0)^2 + c_i^{(1)} \cdot t_i^0 + d_i^{(1)} = p_i(t_i^0)$ ,  $a_i^{(2)} \cdot t_i^m + b_i^{(2)} = 0$ ,  $\frac{1}{6}a_i^{(2)} \cdot (t_i^m)^3 + \frac{1}{2}b_i^{(2)} \cdot (t_i^m)^2 + c_i^{(2)} \cdot t_i^m + d_i^{(2)} = p_i(t_i^m)$ . From the state and control continuity at the junction point  $\tau_s$ , we receive the remaining 5 equations are,

$$\frac{1}{2}a_i^{(1)} \cdot (\tau_s)^2 + b_i^{(1)} \cdot \tau_s + c_i^{(1)} = v_{max}, \quad (3.22a)$$

$$a_i^{(1)} \cdot \tau_s + b_i^{(1)} = 0, \quad (3.22b)$$

$$\frac{1}{6}a_i^{(1)} \cdot (\tau_s)^3 + \frac{1}{2}b_i^{(1)} \cdot (\tau_s)^2 + c_i^{(1)} \cdot \tau_s + d_i^{(1)} + v_{max} \cdot (t_i^m - \tau_s) = p_i(t_i^m), \quad (3.22c)$$

$$\frac{1}{2}a_i^{(2)} \cdot (\tau_s)^2 + b_i^{(2)} \cdot \tau_s + c_i^{(2)} = v_{max}, \quad (3.22d)$$

$$a_i^{(2)} \cdot \tau_s + b_i^{(2)} = 0, \quad (3.22e)$$

where  $a_i^{(1)}, b_i^{(1)}, c_i^{(1)}, d_i^{(1)}$  and  $a_i^{(2)}, b_i^{(2)}, c_i^{(2)}, d_i^{(2)}$  are the constants of integration for the unconstrained and constrained arcs, respectively. The recursive process to solve the above set of equations cannot be computed in real time. Additionally, the computational speed and convergence of numerical methods are also sensitive to the initial guess of the variables, which impose additional burden on the real-time computation effort. However, if the junction point  $\tau_s^*$  can be derived as an explicit function of the initial and final boundary conditions, then the above set of equations can lead to a closed-form solution that can be solved analytically in real time.

**Lemma 3.1.11.** For CAV  $i \in \mathcal{N}(t)$ , let  $\tau_s^*$  be the junction point between the unconstrained and constrained arc of the state constrained  $v_i(t) - v_{max} \leq 0$  solution. Then  $\tau_s^*$  is an explicit function of  $p_i(t_i^m)$ ,  $v_{max}$ ,  $t_i^m$ , and  $v_i(t_i^0)$ , and can be expressed as 
$$\tau_s^* = \frac{3(p_i(t_i^m) - v_{max} \cdot t_i^m)}{(v_i(t_i^0) - v_{max})}.$$

*Proof.* If  $v_i(t) - v_{max} \leq 0$  becomes active, we have an unconstrained arc (with constant parameters  $a_i^{(1)}, b_i^{(1)}, c_i^{(1)}, d_i^{(1)}$ ) followed by a constrained arc (with constant parameters  $a_i^{(2)}, b_i^{(2)}, c_i^{(2)}, d_i^{(2)}$ ) pieced together at the junction point  $t = \tau_s^*$ . The constrained arc yields at  $t = \tau_s^*$  and  $t = t_i^m$ ,

$$a_i^{(2)} \cdot \tau_s^* + b_i^{(2)} = 0, \quad (3.23a)$$

$$a_i^{(2)} \cdot t_i^m + b_i^{(2)} = 0, \quad (3.23b)$$

$$\frac{1}{2}a_i^{(2)} \cdot (t_i^m)^2 + b_i^{(2)} \cdot (t_i^m) + c_i^{(2)} = v_{max}, \quad (3.23c)$$

$$\frac{1}{6}a_i^{(2)} \cdot (\tau_s^*)^3 + \frac{1}{2}b_i^{(2)} \cdot (\tau_s^*)^2 + c_i^{(2)} \cdot (\tau_s^*) + d_i^{(2)} + v_{max} \cdot (t_i^m - \tau_s^*) = p_i(t_i^m). \quad (3.23d)$$

From (3.23a) and (3.23b), we have  $a_i^{(2)} = 0$  and  $b_i^{(2)} = 0$ . Substituting in (3.23c), we have  $c_i^{(2)} = v_{max}$ . Finally, from (3.23d) we have  $d_i^{(2)} = (p_i(t_i^m) - v_{max} \cdot t_i^m)$ . The unconstrained arc at the initial condition  $t = t_i^0$  yields the following equations:  $\frac{1}{2}a_i^{(1)} \cdot (t_i^0)^2 + b_i^{(1)} \cdot (t_i^0) + c_i^{(1)} = v_i(t_i^0)$ ,  $\frac{1}{6}a_i^{(1)} \cdot (t_i^0)^3 + \frac{1}{2}b_i^{(1)} \cdot (t_i^0)^2 + c_i^{(1)} \cdot (t_i^0) + d_i^{(1)} = p_i(t_i^0)$ . Solving the above two equations by considering  $t_i^0 = 0$ , without loss of generality, we have  $c_i^{(1)} = v_i(t_i^0)$  and  $d_i^{(1)} = 0$ . At  $\tau_s^*$ , we have the following set of equations for the unconstrained arc,

$$a_i^{(1)} \cdot \tau_s^* + b_i^{(1)} = 0, \quad (3.24a)$$

$$\frac{1}{2}a_i^{(1)} \cdot (\tau_s^*)^2 + b_i^{(1)} \cdot \tau_s^* + (v_i(t_i^0) - v_{max}) = 0, \quad (3.24b)$$

$$\frac{1}{6}a_i^{(1)} \cdot (\tau_s^*)^3 + \frac{1}{2}b_i^{(1)} \cdot (\tau_s^*)^2 + (v_i(t_i^0) - v_{max}) \cdot \tau_s^* - (p_i(t_i^m) - v_{max} \cdot t_i^m) = 0. \quad (3.24c)$$

Substituting  $\tau_s^* = -\frac{b_i^{(1)}}{a_i^{(1)}}$  from (3.24a) in (3.24b), we have  $\frac{(b_i^{(1)})^2}{a_i^{(1)}} = 2(v_i(t_i^0) - v_{max})$ . Substituting  $\tau_s^* = -\frac{b_i^{(1)}}{a_i^{(1)}}$  from (3.24a) in (3.24c), we have  $\frac{1}{3}\frac{(b_i^{(1)})^3}{(a_i^{(1)})^2} + \frac{(b_i^{(1)})}{a_i^{(1)}} \cdot (v_{max} - v_i(t_i^0)) - (p_i(t_i^m) - v_{max} \cdot t_i^m) = 0$ . From the last two equations, we obtain 
$$\tau_s^* = -\frac{3(p_i(t_i^m) - v_{max} \cdot t_i^m)}{(v_{max} - v_i(t_i^0))},$$

where  $\tau_s^*$  is an explicit function of the known parameters  $p_i(t_i^m)$ ,  $v_{max}$ ,  $v_i(t_i^0)$  and  $t_i^m$ . □

**Case 2.** Only the control constraint  $u_i(t) - u_{max} \leq 0$  becomes active.

In this case, we have  $\mu_i^b(t) = \eta_i^c(t) = \eta_i^d(t) = 0$ . From (3.8), (3.9), and (3.10), we have  $u_i(t) + \lambda_i^v(t) + \mu_i^a(t) = 0$ ,  $\dot{\lambda}_i^p(t) = 0$ , and  $\dot{\lambda}_i^v(t) = -\lambda_i^p(t)$ . By Lemma 3.1.5, CAV  $i \in \mathcal{N}(t)$  enters the constrained arc at time  $t = t_i^0$  and has a single exit junction point. Let  $\tau_c$ ,  $t_i^0 < \tau_c < t_i^m$ , be the junction point where the control constrained arc transitions into the unconstrained arc, and let  $\tau_c^-$  and  $\tau_c^+$  be the immediate left and the right instance of  $\tau_c$ . The optimal control input  $u_i^*(t)$  at the junction point is  $u_i^*(\tau_c) = u_{max}$ . The jump conditions are

$$\lambda_i^p(\tau_c^-) - \lambda_i^p(\tau_c^+) = 0, \quad (3.25)$$

$$\lambda_i^v(\tau_c^-) - \lambda_i^v(\tau_c^+) = 0, \quad (3.26)$$

$$H_i(\tau_c^+) - H_i(\tau_c^-) = 0, \quad (3.27)$$

which imply continuity of the costates and the Hamiltonian at the junction point  $t = \tau_c$ . The last jump condition leads to  $\frac{1}{2}u_i^2(\tau_c^-) + \lambda_i^p(\tau_c^-) \cdot v_i(\tau_c^-) + \lambda_i^v(\tau_c^-) \cdot u_i(\tau_c^-) + \mu_i^a(\tau_c^-) \cdot (u_i(\tau_c^-) - u_{max}) = \frac{1}{2}u_i^2(\tau_c^+) + \lambda_i^p(\tau_c^+) \cdot v_i(\tau_c^+) + \lambda_i^v(\tau_c^+) \cdot u_i(\tau_c^+) + \mu_i^a(\tau_c^+) \cdot (u_i(\tau_c^+) - u_{max})$ . From the continuity of the state and costate  $\lambda_i^p$  at  $t = \tau_c$ , we have  $\lambda_i^p(\tau_c^-) \cdot v_i(\tau_c^-) = \lambda_i^p(\tau_c^+) \cdot v_i(\tau_c^+)$ . Moreover, (3.4) yields  $\mu_i^a(\tau_c^-) \cdot (u_i(\tau_c^-) - u_{max}) = \mu_i^a(\tau_c^+) \cdot (u_i(\tau_c^+) - u_{max}) = 0$ , which after simplification leads to either  $u_i(\tau_c^+) = u_i(\tau_c^-)$  or  $\frac{1}{2}(u_i(\tau_c^+) + u_i(\tau_c^-)) + \lambda_i^v(\tau_c^+) = 0$ , or both. Both equations lead to  $u_i(\tau_c^+) = u_i(\tau_c^-) = u_{max}$ . The Lagrange multiplier  $\mu_i^a(t)$  is  $\mu_i^a(t) = \begin{cases} -\lambda_i^v(t) - u_{max}, & \text{if } t \in [t_i^0, \tau_c), \\ 0, & \text{if } t \in [\tau_c, t_i^m]. \end{cases}$

Using the Euler-Lagrange equations, jump conditions at the junction point, the initial and final boundary conditions, and the costate condition at  $t = t_i^m$ , we can formulate a set of equations by piecing the constrained and unconstrained arcs together at  $t = \tau_c$ . In this case, we have a constrained arc with constant parameters  $a_i^{(1)}, b_i^{(1)}, c_i^{(1)}, d_i^{(1)}$ , followed by an unconstrained arc with constant parameters  $a_i^{(2)}, b_i^{(2)}, c_i^{(2)}, d_i^{(2)}$  pieced

together at junction point  $\tau_c$ , leading to  $4 + 4 + 1 = 9$  variables that need to be determined. At time  $t = t_i^0$  and  $t = \tau_c$ , we have the following set of equations for the constrained arc,

$$a_i^{(1)} \cdot t_i^0 + b_i^{(1)} = u_{max}, \quad (3.28a)$$

$$a_i^{(1)} \cdot \tau_c + b_i^{(1)} = u_{max}, \quad (3.28b)$$

$$\frac{1}{2}a_i^{(1)} \cdot (t_i^0)^2 + b_i^{(1)} \cdot t_i^0 + c_i^{(1)} = v_i(t_i^0), \quad (3.28c)$$

$$\frac{1}{6}a_i^{(1)} \cdot (t_i^0)^3 + \frac{1}{2}b_i^{(1)} \cdot (t_i^0)^2 + c_i^{(1)} \cdot t_i^0 + d_i^{(1)} = p_i(t_i^0). \quad (3.28d)$$

From (3.28a) and (3.28b), considering  $t_i^0 = 0$  without loss of generality, we have  $a_i^{(1)} = 0$  and  $b_i^{(1)} = u_{max}$ . Substituting in (3.28c), we have  $c_i^{(1)} = v_i(t_i^0)$ . Finally, solving (3.28d),  $d_i^{(1)} = p_i(t_i^0)$ . The following set of equations aim to determine the remaining constants of integration  $a_i^{(2)}, b_i^{(2)}, c_i^{(2)}, d_i^{(2)}$  of the exiting unconstrained arc and the junction point  $\tau_c^*$ .

$$a_i^{(2)} \cdot \tau_c + b_i^{(2)} = u_{max}, \quad (3.29a)$$

$$a_i^{(2)} \cdot t_i^m + b_i^{(2)} = 0, \quad (3.29b)$$

$$\frac{1}{2}a_i^{(2)} \cdot \tau_c^2 + (b_i^{(2)} - u_{max}) \cdot \tau_c + c_i^{(2)} - v_i^0 = 0, \quad (3.29c)$$

$$\frac{1}{6}a_i^{(2)} \cdot \tau_c^3 + \frac{1}{2}(b_i^{(2)} - u_{max}) \cdot \tau_c^2 + (c_i^{(2)} - v_i^0) \cdot \tau_c + d_i^{(2)} - p_i(t_i^0) = 0, \quad (3.29d)$$

$$\frac{1}{6}a_i^{(2)} \cdot (t_i^m)^3 + \frac{1}{2}b_i^{(2)} \cdot (t_i^m)^2 + c_i^{(2)} \cdot t_i^m + d_i^{(2)} = p_i(t_i^m). \quad (3.29e)$$

**Lemma 3.1.12.** *For CAV  $i \in \mathcal{N}(t)$ , let  $\tau_c^*$  be the junction point between the unconstrained and control constraint  $u_i(t) - u_{max} \leq 0$  solution. Then  $\tau_c^*$  can be expressed as an explicit function of  $p_i(t_i^m)$ ,  $p_i(t_i^0)$ ,  $u_{max}$ ,  $t_i^m$ , and  $v_i(t_i^0)$ .*

*Proof.* If  $u_i(t) - u_{max} \leq 0$  becomes active, we have a constrained arc (with constant parameters  $a_i^{(1)}, b_i^{(1)}, c_i^{(1)}, d_i^{(1)}$ ) followed by an unconstrained arc (with constant parameters  $a_i^{(2)}, b_i^{(2)}, c_i^{(2)}, d_i^{(2)}$ ) pieced together at the junction point  $t = \tau_c^*$ . Solving (3.29a) and (3.29c)-(3.29e), we have  $a_i^{(2)} = -\sqrt{\frac{(u_{max})^3}{3(t_i^m)^2 \cdot u_{max} + 6t_i^m \cdot v_i(t_i^0) - 6L}}$ , where  $L = p_i(t_i^m) - p_i(t_i^0)$ . From (3.29a) and (3.29b),  $\tau_c^* = \frac{u_{max}}{a_i^{(2)}} + t_i^m$ . Finally, substituting  $a_i^{(2)}$

into the last equation, the junction point  $\tau_c^*$  is given by  $\tau_c^* = t_i^m - \frac{u_{max}}{\sqrt{\frac{(u_{max})^3}{3(t_i^m)^2 \cdot u_{max} + 6t_i^m \cdot v_i(t_i^0) - 6L}}}$ , and can be simplified to  $\tau_c^* = t_i^m - \sqrt{\frac{3(t_i^m)^2 \cdot u_{max} + 6t_i^m \cdot v_i(t_i^0) - 6L}{u_{max}}}$ , which is an explicit function of the known boundary parameters  $t_i^m$ ,  $p_i(t_i^m)$ ,  $p_i(t_i^0)$ ,  $v_i(t_i^0)$ , and  $u_{max}$ .  $\square$

**Case 3.** Both state constraint  $v_i(t) - v_{max} \leq 0$  and the control constraint  $u_i(t) - u_{max} \leq 0$  become active.

If both  $u_i(t) - u_{max} \leq 0$  and  $v_i(t) - v_{max} \leq 0$  become active, we derive the analytical solution combining the steps described in the previous two cases. In this case, we have  $\mu_i^b(t) = \eta_i^d(t) = 0$ . From (3.8), (3.9), and (3.10), we have  $u_i(t) + \lambda_i^v(t) + \mu_i^a(t) = 0$ ,  $\dot{\lambda}_i^p(t) = 0$ , and  $\dot{\lambda}_i^v(t) = -\lambda_i^p(t) - \eta_i^c(t)$ . Let  $\tau_c$  be the junction point that CAV  $i \in \mathcal{N}(t)$  exits the control constrained arc and  $\tau_s$  be the junction point that CAV  $i$  enters the state constrained arc such that  $t_i^0 < \tau_c < \tau_s < t_i^m$ . The optimal control input at the control constrained arc is  $u_i^*(t) = u_{max}$ , for all  $t \in [t_i^0, \tau_c]$ . In the state constrained arc, we have  $v_i^*(t) = v_{max}$ ,  $u_i^*(t) = 0$ , for all  $t \in [\tau_s, t_i^m]$ . From the jump conditions at the junction points  $\tau_c$  and  $\tau_s$ , we have continuity in the state and control input. The Lagrange multipliers  $\mu_i^a(t)$  and  $\eta_i^c(t)$  are given by

$$\mu_i^a(t) = \begin{cases} 0, & t \in (\tau_c, t_i^m], \\ -\lambda_i^v(t) - u_{max}, & t \in [t_i^0, \tau_c], \end{cases}, \quad (3.30)$$

$$\eta_i^c(t) = \begin{cases} 0, & t \in [t_i^0, \tau_s), \\ -\lambda_i^p(t), & t \in [\tau_s, t_i^m]. \end{cases}. \quad (3.31)$$

Solving (3.28a)-(3.28d), considering  $t_i^0 = 0$  without loss of generality, the constants of integration  $a_i^{(1)}, b_i^{(1)}, c_i^{(1)}, d_i^{(1)}$  of the control constrained arc are  $a_i^{(1)} = 0$ ,  $b_i^{(1)} = u_{max}$ ,  $c_i^{(1)} = v_i^0$  and  $d_i^{(1)} = p_i(t_i^0)$ . The unconstrained arc with constants of integration

$a_i^{(2)}, b_i^{(2)}, c_i^{(2)}$ , and  $d_i^{(2)}$  can consists of the following set of equations,

$$a_i^{(2)} \cdot \tau_c + b_i^{(2)} = u_{max}, \quad (3.32a)$$

$$\frac{1}{2}a_i^{(2)} \cdot \tau_c^2 + (b_i^{(2)} - u_{max}) \cdot \tau_c + c_i^{(2)} - v_i^0 = 0, \quad (3.32b)$$

$$\frac{1}{6}a_i^{(2)} \cdot \tau_c^3 + \frac{1}{2}(b_i^{(2)} - u_{max}) \cdot \tau_c^2 + (c_i^{(2)} - v_i^0) \cdot \tau_c + (d_i^{(2)} - p_i(t_i^0)) = 0, \quad (3.32c)$$

$$a_i^{(2)} \cdot \tau_s + b_i^{(2)} = 0, \quad (3.32d)$$

$$\frac{1}{2}a_i^{(2)} \cdot \tau_s^2 + b_i^{(2)} \cdot \tau_s + c_i^{(2)} - v_{max} = 0, \quad (3.32e)$$

$$\frac{1}{6}a_i^{(2)} \cdot (\tau_s)^3 + \frac{1}{2}b_i^{(2)} \cdot (\tau_s)^2 + c_i^{(2)} \cdot \tau_s + d_i^{(2)} + v_{max} \cdot (t_i^m - \tau_s) = p_i(t_i^m). \quad (3.32f)$$

Finally, the state-constrained arc with constants of integration  $a_i^{(3)}, b_i^{(3)}, c_i^{(3)}, d_i^{(3)}$  consists of the following set of equations,

$$a_i^{(3)} \cdot t_i^m + b_i^{(3)} = 0, \quad (3.33a)$$

$$a_i^{(3)} \cdot \tau_s + b_i^{(3)} = 0, \quad (3.33b)$$

$$\frac{1}{2}a_i^{(3)} \cdot \tau_s^2 - b_i^{(3)} \cdot \tau_s - c_i^{(3)} - v_{max} = 0, \quad (3.33c)$$

$$\frac{1}{6}a_i^{(3)} \cdot (t_i^m)^3 + \frac{1}{2}b_i^{(3)} \cdot (t_i^m)^2 + c_i^{(3)} \cdot t_i^m + d_i^{(3)} - p_i(t_i^m) = 0. \quad (3.33d)$$

From (3.33a)-(3.33d), we have  $a_i^{(3)} = 0$ ,  $b_i^{(3)} = 0$ ,  $c_i^{(3)} = v_{max}$  and  $d_i^{(3)} = p_i(t_i^m) - v_{max} \cdot t_i^m$ . The remaining constants of integration  $a_i^{(2)}, b_i^{(2)}, c_i^{(2)}, d_i^{(2)}$  of the unconstrained arc, and the junction points  $\tau_s^*$  and  $\tau_c^*$  can be determined by solving the set of equations (3.32a)-(3.32f).

**Lemma 3.1.13.** *The junction point  $\tau_s^*$  between the unconstrained and the constrained arc if  $v_i(t) - v_{max} \leq 0$  becomes active, and the junction point  $\tau_c^*$  between the unconstrained and the constrained arc if  $u_i(t) - u_{max} \leq 0$  also becomes active are explicit functions of  $p_i(t_i^m)$ ,  $v_{max}$ ,  $u_{max}$ ,  $t_i^m$ , and  $v_i(t_i^0)$ .*

*Proof.* If  $u_i(t) - u_{max} \leq 0$  becomes active, we have a constrained arc with constants of integration  $a_i^{(1)}, b_i^{(1)}, c_i^{(1)}, d_i^{(1)}$  followed by an unconstrained arc with constants of integration  $a_i^{(2)}, b_i^{(2)}, c_i^{(2)}, d_i^{(2)}$ , pieced together at the junction point  $t = \tau_c^*$ . If

$v_i(t) - v_{max} \leq 0$  becomes active, we have a constrained arc with constants of integration  $a_i^{(2)}, b_i^{(2)}, c_i^{(2)}, d_i^{(2)}$  followed by a constrained arc with constants of integration  $a_i^{(3)}, b_i^{(3)}, c_i^{(3)}, d_i^{(3)}$  pieced together at the junction point  $t = \tau_s^*$ . Solving (3.28a)-(3.28d) for the control constrained arc with  $t_i^0 = 0$ , we have  $a_i^{(1)} = 0$ ,  $b_i^{(1)} = u_{max}$ ,  $c_i^{(1)} = v_i(t_i^0)$  and  $d_i^{(1)} = p_i(t_i^0)$ . Solving (3.33a)-(3.33d) for the state constrained arc, considering  $t_i^0 = 0$  without loss of generality, we have  $a_i^{(3)} = 0$ ,  $b_i^{(3)} = 0$ ,  $c_i^{(3)} = v_{max}$  and  $d_i^{(3)} = p_i(t_i^m) - v_{max} \cdot t_i^m$ . From (3.32a) and (3.32d), we have  $\tau_c^* = \frac{u_{max} - b_i^{(2)}}{a_i^{(2)}}$  and  $\tau_s^* = -\frac{b_i^{(2)}}{a_i^{(2)}}$  respectively. Substituting the latter into (3.32b), (3.32c), (3.32e) and (3.32f), and solving the system of equations, we have  $a_i^{(2)} = -u_{max}^2 \cdot \sqrt{-\frac{1}{\phi}}$ , and  $b_i^{(2)} = \frac{u_{max}(-2v_i(t_i^0)\sqrt{-\frac{1}{\phi}} + 2v_{max}\sqrt{-\frac{1}{\phi}} + 1)}{2}$ , where,  $\phi(t_i^m, p_i(t_i^m), v_i(t_i^0), u_{max}, v_{max}) = -24(t_i^m \cdot u_{max} \cdot v_{max} - p_i(t_i^m) \cdot u_{max} + v_i(t_i^0) \cdot v_{max}) + 12(v_i^2(t_i^0) + v_{max}^2)$ . Substituting the last results into (3.32a) and (3.32d), the junction points  $\tau_s^*$  and  $\tau_c^*$  are given as explicit functions of the known parameters  $t_i^m$ ,  $p_i(t_i^m)$ ,  $v_i(t_i^0)$ ,  $u_{max}$  and  $v_{max}$ .  $\square$

**Case 4.** Only the state constraint  $v_{min} - v_i(t) \leq 0$  becomes active.

In this case, we have  $\mu_i^a(t) = \mu_i^b(t) = \eta_i^c(t) = 0$ . From (3.8), (3.9), and (3.10), we have  $u_i(t) + \lambda_i^v(t) = 0$ ,  $\dot{\lambda}_i^p(t) = 0$ , and  $\dot{\lambda}_i^v(t) = -\lambda_i^p(t) - \eta_i^d(t)$ . Let  $t = \tau_s$  be the junction point that  $v_{min} - v_i(t) \leq 0$  becomes active. The optimal speed and control at the junction point are  $v_i^*(t) = v_{min}$ ,  $u_i^*(t) = 0$ , for all  $t \in [\tau_s, t_i^m]$ . The jump conditions are

$$\lambda_i^p(\tau_s^-) = \lambda_i^p(\tau_s^+) + \pi_i \cdot \frac{\partial}{\partial p_i(t)} \left[ v_{min} - v_i(t) \right] \Big|_{t=\tau_s}, \quad (3.34a)$$

$$\lambda_i^v(\tau_s^-) = \lambda_i^v(\tau_s^+) + \pi_i \cdot \frac{\partial}{\partial v_i(t)} \left[ v_{min} - v_i(t) \right] \Big|_{t=\tau_s}, \quad (3.34b)$$

$$H_i(\tau_s^-) = H_i(\tau_s^+) - \pi_i \cdot \frac{\partial}{\partial t} \left[ v_{min} - v_i(t) \right] \Big|_{t=\tau_s}, \quad (3.34c)$$

where  $\pi_i$  is a constant Langrange multiplier determined so that  $v_{min} - v_i(t) = 0$  is satisfied. Note that, (3.34a)-(3.34c) imply possible discontinuity of the costates and the Hamiltonian at  $t = \tau_s$ . The state variables are continuous at  $t = \tau_s$ . From (3.34a)

and (3.34c), the position costate and the Lagrangian of the Hamiltonian is continuous at  $t = \tau_s$ .

**Lemma 3.1.14.** *If the state constraint  $v_{min} - v_i(t) \leq 0$  becomes active, then the control input  $u_i(t)$  is continuous at the junction point  $t = \tau_s$ .*

*Proof.* From (3.34c), we have

$$\begin{aligned} & \frac{1}{2}u_i^2(\tau_s^-) + \lambda_i^p(\tau_s^-) \cdot v_i(\tau_s^-) + \lambda_i^v(\tau_s^-) \cdot u_i(\tau_s^-) + \eta_i^d(\tau_s^-) \cdot (v_{min} - v_i(\tau_s^-)) \\ &= \frac{1}{2}u_i^2(\tau_s^+) + \lambda_i^p(\tau_s^+) \cdot v_i(\tau_s^+) + \lambda_i^v(\tau_s^+) \cdot u_i(\tau_s^+) + \eta_i^d(\tau_s^+) \cdot (v_{min} - v_i(\tau_s^+)). \end{aligned} \quad (3.35)$$

Since  $v_i(\tau_s^+) = v_{min}$  and  $u_i(\tau_s^+) = 0$ , and from the continuity of state (3.18) and  $\lambda_i^p$  (3.34a), we have  $\lambda_i^p(\tau_s^-) \cdot v_i(\tau_s^-) = \lambda_i^p(\tau_s^+) \cdot v_i(\tau_s^+)$ . From (3.6), we have  $\eta_i^d(\tau_s^-) \cdot (v_{min} - v_i(\tau_s^-)) = \eta_i^d(\tau_s^+) \cdot (v_{min} - v_i(\tau_s^+)) = 0$ . Hence, (3.1.6) reduces to  $\frac{1}{2}u_i^2(\tau_s^-) + \lambda_i^v(\tau_s^-) \cdot u_i(\tau_s^-) = 0$ , which implies that either  $u_i(\tau_s^-) = 0$  or  $\frac{1}{2}u_i(\tau_s^-) + \lambda_i^v(\tau_s^-) = 0$ , or both. Since the second term can not hold, we have  $u_i(\tau_s^-) = u_i(\tau_s^+) = 0$ .  $\square$

The Lagrange multiplier  $\eta_i^d(t)$  can be expressed as,

$$\eta_i^d(t) = \begin{cases} 0, & \text{if } t \in [t_i^0, \tau_s), \\ -\lambda_i^p(t), & \text{if } t \in [\tau_s, t_i^m]. \end{cases} \quad (3.36)$$

Using the Euler-Lagrange equations, interior conditions, initial and final boundary conditions, and the costate condition at  $t = t_i^m$ , we can formulate a set of equations similar to Case 1 to solve for  $4 + 4 + 1 = 9$  variables corresponding to the constants of integration of the unconstrained and constrained arc, and the junction point  $\tau_s$ . The set of equations of the unconstrained arc with constants of integration  $a_i^{(1)}, b_i^{(1)}, c_i^{(1)}, d_i^{(1)}$  are,  $\frac{1}{2}a_i^{(1)} \cdot (t_i^0)^2 + b_i^{(1)} \cdot t_i^0 + c_i^{(1)} = v_i(t_i^0)$ ,  $\frac{1}{6}a_i^{(1)} \cdot (t_i^0)^3 + \frac{1}{2}b_i^{(1)} \cdot (t_i^0)^2 + c_i^{(1)} \cdot t_i^0 + d_i^{(1)} = p_i(t_i^0)$ ,  $\frac{1}{2}a_i^{(1)} \cdot (\tau_s)^2 + b_i^{(1)} \cdot \tau_s + c_i^{(1)} = v_{min}$ ,  $a_i^{(1)} \cdot \tau_s + b_i^{(1)} = 0$ , and  $\frac{1}{6}a_i^{(1)} \cdot (\tau_s)^3 + \frac{1}{2}b_i^{(1)} \cdot (\tau_s)^2 + c_i^{(1)} \cdot \tau_s + d_i^{(1)} + v_{min} \cdot (t_i^m - \tau_s) = p_i(t_i^m)$ . The set of equations of the state constrained arc with the constants of integration  $a_i^{(2)}, b_i^{(2)}, c_i^{(2)}, d_i^{(2)}$  are  $\frac{1}{2}a_i^{(2)} \cdot (\tau_s)^2 + b_i^{(2)} \cdot \tau_s + c_i^{(2)} = v_{min}$ ,  $a_i^{(2)} \cdot t_i^m + b_i^{(2)} = 0$ ,  $a_i^{(2)} \cdot \tau_s + b_i^{(2)} = 0$ , and  $\frac{1}{6}a_i^{(2)} \cdot (t_i^0)^3 + \frac{1}{2}b_i^{(2)} \cdot (t_i^0)^2 + c_i^{(2)} \cdot t_i^0 + d_i^{(2)} =$

$p_i(t_i^m)$ , which yield  $a_i^{(2)} = 0$ ,  $b_i^{(2)} = 0$ ,  $c_i^{(2)} = v_{min}$  and  $d_i^{(2)} = p_i(t_i^m) - v_{min} \cdot t_i^m$ . The remaining constants of integration  $a_i^{(1)}, b_i^{(1)}, c_i^{(1)}, d_i^{(1)}$  and the junction point  $\tau_s^*$  can be determined numerically by solving simultaneously the above set of equations.

**Lemma 3.1.15.** *For CAV  $i \in \mathcal{N}(t)$ , let  $\tau_s^*$  be the junction point between the unconstrained and constrained arc of the state constrained  $v_{min} - v_i(t) \leq 0$  solution. Then  $\tau_s^*$  is an explicit function of  $p_i(t_i^m)$ ,  $v_{min}$ ,  $t_i^m$  and  $v_i(t_i^0)$ , and can be expressed as*

$$\tau_s^* = \frac{3(p_i(t_i^m) - v_{min} \cdot t_i^m)}{(v_i(t_i^0) - v_{min})}$$

*Proof.* The proof is similar to the proof of Lemma 3.1.11, hence it is omitted.  $\square$

**Case 5.** Only the control constraint  $u_{min} - u_i(t) \leq 0$  becomes active.

In this case, we have  $\mu_i^a(t) = \eta_i^c(t) = \eta_i^d(t) = 0$ . From (3.8), (3.9), and (3.10), we have  $u_i(t) + \lambda_i^v(t) - \mu_i^b(t) = 0$ ,  $\dot{\lambda}_i^p(t) = 0$ , and  $\dot{\lambda}_i^v(t) = -\lambda_i^p(t)$ . Let  $\tau_c > t_i^0$  be the junction point that CAV  $i \in \mathcal{N}(t)$  transitions from the constrained arc to the unconstrained arc. The optimal control at the junction point  $\tau_c$  is  $u_i^*(\tau_c) = u_{min}$ . From the jump conditions, we have  $\lambda_i^p(\tau_c^-) = \lambda_i^p(\tau_c^+)$ ,  $\lambda_i^v(\tau_c^-) = \lambda_i^v(\tau_c^+)$ , and  $H_i(\tau_c^+) = H_i(\tau_c^-)$ .

**Lemma 3.1.16.** *If the control constraint  $u_{min} - u_i(t) \leq 0$  becomes active, then the control input  $u(t)$  is continuous at the junction point  $t = \tau_c$ .*

*Proof.* Since  $H_i(\tau_c^+) = H_i(\tau_c^-)$ , we have  $\frac{1}{2}u_i^2(\tau_c^-) + \lambda_i^p(\tau_c^-) \cdot v_i(\tau_c^-) + \lambda_i^v(\tau_c^-) \cdot u_i(\tau_c^-) + \mu_i^b(\tau_c^-) \cdot (u_{min} - u_i(\tau_c^-)) = \frac{1}{2}u_i^2(\tau_c^+) + \lambda_i^p(\tau_c^+) \cdot v_i(\tau_c^+) + \lambda_i^v(\tau_c^+) \cdot u_i(\tau_c^+) + \mu_i^b(\tau_c^+) \cdot (u_{min} - u_i(\tau_c^+))$ . From the continuity of the state (3.18) and  $\lambda_i^p$  at  $t = \tau_c$ , we have  $\lambda_i^p(\tau_c^-) \cdot v_i(\tau_c^-) = \lambda_i^p(\tau_c^+) \cdot v_i(\tau_c^+)$ . From (3.4) we have  $\mu_i^b(\tau_c^-) \cdot (u_{min} - u_i(\tau_c^-)) = \mu_i^b(\tau_c^+) \cdot (u_{min} - u_i(\tau_c^+)) = 0$ . After simplifying, we have either  $u_i(\tau_c^+) = u_i(\tau_c^-)$  or  $\frac{1}{2}(u_i(\tau_c^+) + u_i(\tau_c^-)) + \lambda_i^v(\tau_c^+) = 0$ . Both the equations lead to the continuity in control input  $u_i(t)$  at time  $t = \tau_c$ , i.e.,  $u_i(\tau_c^+) = u_i(\tau_c^-)$ .  $\square$

The Lagrange multiplier  $\mu_i^b(t)$  can be expressed as,

$$\mu_i^b(t) = \begin{cases} \lambda_i^v(t) + u_{min}, & \text{if } t \in [t_i^0, \tau_c), \\ 0, & \text{if } t \in [\tau_c, t_i^m]. \end{cases} \quad (3.37)$$

Using the Euler-Lagrange equations, interior condition, initial and final boundary conditions, and the condition of costates at  $t = t_i^m$ , we have a set of equations of the constrained arc:  $a_i^{(1)} \cdot t_i^0 + b_i^{(1)} = u_{min}$ ,  $a_i^{(1)} \cdot \tau_c + b_i^{(1)} = u_{min}$ ,  $\frac{1}{2}a_i^{(1)}(t_i^0)^2 + b_i^{(1)} \cdot t_i^0 + c_i^{(1)} = v_i(t_i^0)$ , and  $\frac{1}{6}a_i^{(1)}(t_i^0)^3 + \frac{1}{2}b_i^{(1)} \cdot (t_i^0)^2 + c_i^{(1)} \cdot t_i^0 + d_i^{(1)} = 0$ ., resolving which with  $t_i^0 = 0$  yields,  $a_i^{(1)} = 0$ ,  $b_i^{(1)} = u_{min}$ ,  $c_i^{(1)} = v_i(t_i^0)$ ,  $d_i^{(1)} = p_i(t_i^0)$ , where  $a_i^{(1)}$ ,  $b_i^{(1)}$ ,  $c_i^{(1)}$ ,  $d_i^{(1)}$  are the constants of integration for the constrained arc. In addition, we have a set of equations of the unconstrained arc:  $a_i^{(2)} \cdot \tau_c - b_i^{(2)} + u_{min} = 0$ ,  $a_i^{(2)} \cdot t_i^m + b_i^{(2)} = 0$ ,  $\frac{1}{2}a_i^{(2)} \cdot \tau_c^2 + (b_i^{(2)} - u_{min}) \cdot \tau_c + c_i^{(2)} - v_i(t_i^0) = 0$ ,  $\frac{1}{6}a_i^{(2)} \cdot \tau_c^3 + \frac{1}{2}(b_i^{(2)} - u_{min}) \cdot \tau_c + (c_i^{(2)} - v_i(t_i^0)) \cdot \tau_c + d_i^{(2)} = 0$ , and  $\frac{1}{6}a_i^{(2)} \cdot (t_i^m)^3 + \frac{1}{2}b_i^{(2)} \cdot (t_i^m)^2 + c_i^{(2)} \cdot t_i^m + d_i^{(2)} - p_i(t_i^m) = 0$ , where  $a_i^{(2)}$ ,  $b_i^{(2)}$ ,  $c_i^{(2)}$ ,  $d_i^{(2)}$  are the constants of integration of the unconstrained arc.

**Lemma 3.1.17.** *For CAV  $i \in \mathcal{N}(t)$ , let  $\tau_s^*$  be the junction point between the unconstrained and constrained arc of the control constrained ( $u_{min} - u_i(t) \leq 0$ ) solution of (3.1). Then  $\tau_c^*$  can be expressed as an explicit function of  $p_i(t_i^m)$ ,  $p_i(t_i^0)$ ,  $u_{min}$ ,  $t_i^m$ , and  $v_i(t_i^0)$ .*

*Proof.* The proof is similar to the proof of Lemma 3.1.12, hence it is omitted.  $\square$

**Case 6.** Both state constraint  $v_{min} - v_i(t) \leq 0$  and the control constraint  $u_{min} - u_i(t) \leq 0$  become active.

In this case, we can derive the analytical solution following similar steps to Case 3. A control constrained  $u_{min} - u_i(t) \leq 0$  arc with constants of integration  $a_i^{(1)}, b_i^{(1)}, c_i^{(1)}, d_i^{(1)}$  is pieced together with an unconstrained arc with constants of integration  $a_i^{(2)}, b_i^{(2)}, c_i^{(2)}, d_i^{(2)}$  at the junction point  $\tau_c$ . The unconstrained arc is pieced together with the state constrained  $v_{min} - v_i(t) \leq 0$  arc with constants of integration

$a_i^{(3)}, b_i^{(3)}, c_i^{(3)}, d_i^{(3)}$  at the junction point  $\tau_s$ . The constants of integration of the constrained and unconstrained arcs, and the junction points  $\tau_s^*$  and  $\tau_c^*$  can be determined by a set of equations similar to those derived in Case 3.

**Lemma 3.1.18.** *The junction point  $\tau_s^*$  between the unconstrained and the constrained arc when  $v_{min} - v_i(t) \leq 0$  becomes active, and the junction point  $\tau_c^*$  between the unconstrained and the constrained arc when  $u_{min} - u_i(t) \leq 0$  also becomes active are explicit functions of  $p_i(t_i^m)$ ,  $v_{min}$ ,  $u_{min}$ ,  $t_i^m$ , and  $v_i(t_i^0)$ .*

*Proof.* The proof is similar to the proof of Lemma 3.1.13, hence it is omitted.  $\square$

### 3.1.7 Simulation Results and Summary

We validate the analytical solution of the optimal control problem (3.1) through numerical simulation in MATLAB. In this section, we present the results considering  $t_i^m = 10$  s, where only the state constraint  $v_i(t) - v_{max} \leq 0$  and control constraint  $u_i(t) - u_{max} \leq 0$  can become active (Theorem 3.1.4). Similar results to those presented here can be also derived for the case where  $v_{min} - v_i(t) \leq 0$  and  $u_{min} - u_i(t) \leq 0$  become active. We consider the initial and final position of CAV  $i \in \mathcal{N}(t)$  to be  $p_i(t_i^0) = 0$  m and  $p_i(t_i^m) = 200$  m, and the initial speed  $v_i(t_i^0) = 14.3$  m/s. For each CAV  $i \in \mathcal{N}(t)$ , we enforce the maximum speed limit and acceleration to be  $v_{max} = 22$  m/s and  $u_{max} = 1.8$  m/s<sup>2</sup> respectively. The standard procedure to solve the optimal control problem (3.1) is to identify whether any of the state or control constraints become active and derive the constrained solution in a recursive manner until none of the constraints are active, as shown in Fig. 3.2. The unconstrained solution (blue trajectory in Fig. 3.2) activates the state constraint  $v_i(t) - v_{max} \leq 0$  only. The acceleration corresponding to the state-constrained ( $v_i(t) - v_{max} \leq 0$ ) solution is shown by the red trajectory in Fig. 3.2, where the unconstrained and constrained arcs are pieced together at the junction point at  $t = 7.79$  s. However, the state-constrained solution (red trajectory in Fig. 3.2) has to be re-derived since the control constraint  $u_i(t) - u_{max} \leq 0$ , which was not active before, becomes active now as shown by the red trajectory in Fig. 3.2. The constrained optimal

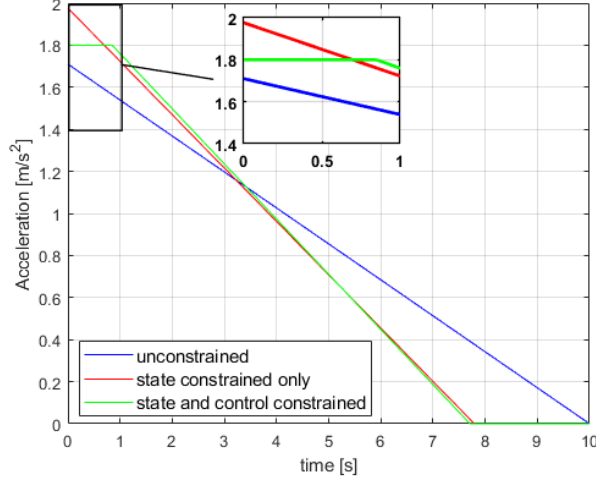


Figure 3.2: Optimal control trajectory for the unconstrained (blue), state constraint  $v_i(t) - v_{max} \leq 0$  only (red) and both state-control constraint (green) case.

control input is derived by piecing the state and control constrained arcs together, and it is shown by the green trajectory in Fig. 3.2.

In our condition-based framework, we do not need to consider the intermediate iterative steps above, i.e., the unconstrained (blue trajectory) and state constrained solution (red trajectory) in Fig. 3.2. We can directly derive the final closed-form analytical solution (green trajectory in Fig. 3.2) by sequentially checking the conditions in Theorems 3.1.4-3.1.10. First, we start with Theorem 3.1.4 to reduce the possible constraint activation set. Since the first statement of Theorem 3.1.4 holds for  $t_i^m = 10$  s and the boundary conditions, we only need to consider whether  $v_i(t) - v_{max} \leq 0$  or  $u_i(t) - u_{max} \leq 0$  become active, which reduces the possible constraint activation cases from 15 to 3. Then, we use Theorems 3.1.7 and 3.1.8 to identify the specific constraint activation case. In this case, part (i) of Theorem 3.1.7 holds, indicating that  $v_i(t) - v_{max} \leq 0$  becomes active in  $(t_i^0, t_i^m]$ . However, part (i) of Theorem 3.1.8 does not hold indicating that  $u_i(t) - u_{max} \leq 0$  will not become active. Using the result obtained above, we then check part (i) of Theorem 3.1.9 which readily indicates that an additional and initially non-existent control constraint  $u_i(t) - u_{max} \leq 0$  becomes active within the state-constrained solution, as shown by the red trajectory in Fig. 3.2. Using

the result of Theorem 3.1.9, we apply the analysis presented in Case 3 to determine the complete state and control constrained-optimal solution. Here, the aforementioned condition-based framework requires 0.001107 s to solve in an Intel Core i7-6700 CPU @ 3.40 GHz using MATLAB R2017b. Note that, if the first statement of Theorem 3.1.9 does not hold, then none of the control constraints can become active, and thus we can use the analysis presented in Case 1 to determine the optimal solution.

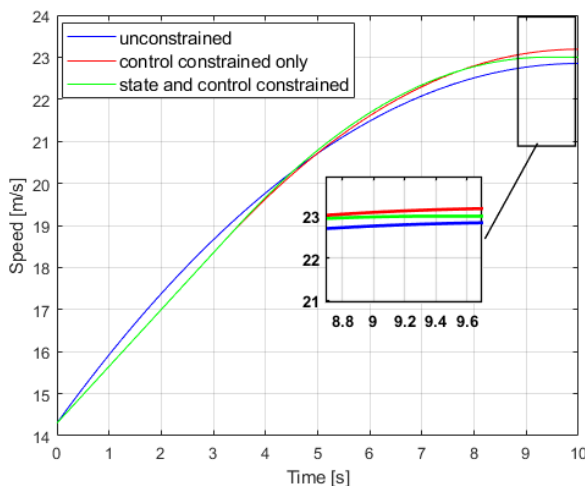


Figure 3.3: Optimal speed trajectory for the unconstrained (blue), control constraint  $u_i(t) - u_{max} \leq 0$  only (red) and both state-control constraint (green) case.

Next, we consider a different scenario to show the impact when the control constraint ( $u_i(t) - u_{max} \leq 0$ ) becomes active (Fig. 3.3). In this case, we set the maximum speed  $v_{max}$  and acceleration  $u_{max}$  to be 23 m/s and 1.35 m/s<sup>2</sup> respectively. Following the above procedure, we check part (i) of Theorem 3.1.7 and 3.1.8. Since only part (i) of Theorem 3.1.8 holds, we conclude that the control constraint  $u_i(t) - u_{max} \leq 0$  will become active. We then check part (i) of Theorem 3.1.10 to check whether any additional state constraint will become active within the control constrained solution. In this case, part (i) of Theorem 3.1.10 holds, as evident from the control constrained state trajectory (red trajectory) in Fig. 3.3. Therefore, we use the analysis presented in Case 3 to derive the complete state- and control- constrained solution as illustrated by the green trajectory in Fig. 3.3. Note that, in Fig. 3.3, in the unconstrained

solution (blue trajectory) none of the state constraints become active. However, the control-constrained solution (red trajectory) activates the state constraint  $v_i(t) - v_{max} \leq 0$ . Based on our condition-based framework, we can avoid the computation of the intermediate solutions, i.e., the unconstrained trajectory (blue trajectory in Fig. 3.3) and the control constrained trajectory (red trajectory in Fig. 3.3), and directly derive the final constrained trajectory as illustrated by the green trajectory in Fig. 3.3.

In this section, I addressed the state and control constrained optimal framework for coordinating CAVs at different traffic scenarios, and provided a condition-based framework to determine the constrained solution without requiring to follow the standard recursive process. I mathematically characterized the activation cases of different state and control constraint combinations and provided a set of conditions to identify the nature of constraint activation a priori. Using these conditions, I derived the closed-form analytical solution of the constrained optimal control problem that can be computed and implemented in real time. I validated a subset of constraint activation cases through numerical simulation and showed how the proposed framework can identify the interdependent constraint activation based on the boundary conditions. By eliminating the intermediate steps of solving the constrained optimal control problem, the proposed condition-based framework improves on the standard methodology to solve the constrained optimal control problem.

### 3.2 Decentralized Optimal Coordination with Safety Constraints

In this section, I address the problem of constrained optimal control with hard safety constraints of collision avoidance while coordinating a group of CAVs through a corridor consisting of multiple traffic scenarios to improve energy consumption and travel time. I formulate a two-level optimization problem in which we maximize traffic throughput in the upper-level problem, and derive a closed-form analytical solution that yields the optimal control input for each CAV, in terms of fuel consumption, in the low-level problem. The key contribution of this research is the formulation and

analytical solution of an optimal control problem for coordinating CAVs in a traffic corridor with the explicit incorporation of the rear-end safety constraint.

### 3.2.1 Modeling Framework: Decentralized Coordination

Let us consider a traffic corridor (Fig. 3.4) that consists of several conflict zones (e.g., a merging area, an intersection, and a roundabout), where a potential lateral collision of vehicles may occur. Upstream of each conflict zone, there exists a control zone, inside of which, the vehicles can communicate with each other. The dimension of each control zone is restricted by the communication range of an associated coordinator, which records the vehicle queue inside the control zone. The communication range of the coordinator can be adjustable and its length could be extended as needed. For clarity, we illustrate the boundary of the corridor as indicated by dashed lines and the limits of each control zone by shaded rectangles (Fig. 3.4). Note that we only coordinate CAVs inside the control zone of each conflict zone.

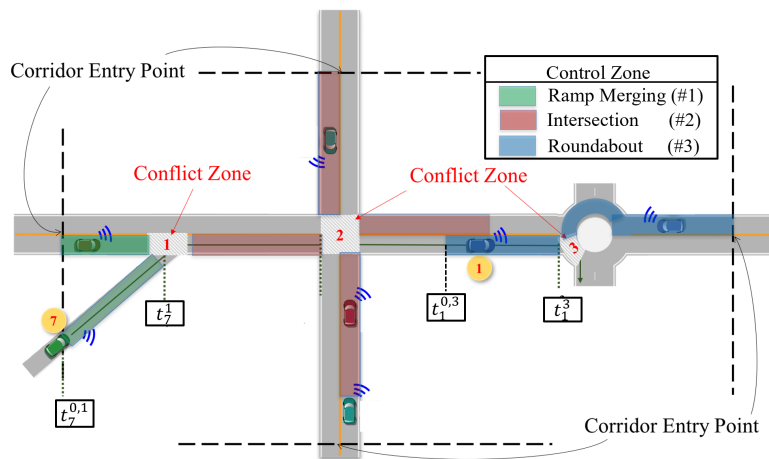


Figure 3.4: Corridor with connected and automated vehicles.

Let  $\mathcal{N}_z(t) = \{1, 2, \dots, N_z(t)\}$  be a queue of CAVs inside the control zone of a conflict zone  $z$ , where  $N_z(t) \in \mathbb{N}$  is the number of CAVs in the control zone of  $z$  at time  $t \in \mathbb{R}^+$ . When a CAV enters the control zone, it broadcasts its route information to the coordinator of this conflict zone. The coordinator then assigns a unique integer

$i \in \mathbb{N}$  that serves as the identification of CAVs inside the corridor. Let  $t_i^{0,z}$  be the initial time that CAV  $i$  enters the control zone of  $z \in \mathcal{Z}$ , and  $t_i^z$  be the time for CAV  $i$  that enters  $z$ . For example, for CAV #7 (Fig. 3.4),  $t_7^{0,1}$  is the time that it enters the control zone of conflict zone #1, which is also the time that it enters the corridor, and  $t_7^1$  is the time that it enters the conflict zone #1. Similarly, CAV #1 enters the control zone of conflict zone #3 at  $t_1^{0,3}$ , and enters the conflict zone #3 at  $t_1^3$ . The CAV index given by the coordinator is removed from the queue  $\mathcal{N}_z$  once the vehicle  $i$  exits the conflict zone  $z$ .

To avoid any possible lateral collision, there are several ways to compute  $t_i^z$  for each CAV  $i$ . In what follows, we present a decentralized framework in which we formulate an upper-level optimal control problem for determining the time  $t_i^z$  that each CAV  $i$  will enter the conflict zone  $z \in \mathcal{Z}$ , and then address a lower-level control problem that will yield for each CAV the optimal control input (acceleration/deceleration) to achieve the assigned time  $t_i^z$  (upon arrival of CAV  $i$ ) without collision.

Similar to the previous section, for each CAV  $i \in \mathcal{N}(t)$ , we employ the double integrator dynamics as considered in (2.3), and impose the state and control constraints as in (2.4). Let  $x_i(t) = [p_i(t) \ v_i(t)]^T$  denote the state of each CAV  $i$ , with initial value at the entry of the control zone of conflict zone  $z \in \mathcal{Z}$  given as  $x_i^{0,z} = [p_i^{0,z} \ v_i^{0,z}]^T$ , where  $p_i^{0,z} = p_i(t_i^{0,z})$  and  $v_i^{0,z} = v_i(t_i^{0,z})$ . For each CAV  $i \in \mathcal{N}_z(t)$ , the lateral collision is possible within the set  $\Gamma_i \triangleq \{t \mid t \in [t_i^z, t_i^z + \rho]\}$ , where,  $\rho$  is the safety time headway to avoid lateral collision. Lateral collision between any two CAVs  $i, j \in \mathcal{N}_z(t)$  can be avoided if the following constraint holds,

$$\Gamma_i \cap \Gamma_j = \emptyset, \quad \forall t \in [t_i^z, t_i^z + \rho], \quad i, j \in \mathcal{N}_z(t). \quad (3.38)$$

To ensure the absence of rear-end collision of two consecutive CAVs traveling on the same lane, we impose the following condition

$$s_i(t) = p_k(t) - p_i(t) \geq \delta(t), \quad \forall t \in [t_i^{0,z}, t_i^z]. \quad (3.39)$$

Here,  $s_i(t)$  denotes the distance between CAV  $i$  and CAV  $k$  which is physically immediately ahead of  $i$ . The minimum safe distance  $\delta(t)$  is a function of speed  $v_i(t)$ . Since we consider an urban traffic corridor, the average speed does not exhibit significant variations. Therefore, we can consider that the safe distance  $\delta(t) = \delta$  is constant. In the modeling framework described above, we consider perfect communication (Assumption 2.1.2), no lane changes or left/right turns (Assumption 2.1.1) and feasible initial condition (Assumption 2.1.3).

**Definition 3.2.1.** Let  $i - 1, i \in \mathcal{N}_z(t)$  be two CAVs inside the control zone traveling towards the corresponding conflict zone  $z$ . Depending on the physical location and trajectory inside the control zone with respect to CAV  $i$ , CAV  $i - 1$  belongs to one of the following three subsets of  $\mathcal{N}_z(t)$  with respect to CAV  $i \in \mathcal{N}_z(t)$ :

1.  $\mathcal{R}_i^z$  contains all CAVs that travel in the same lane with CAV  $i$  towards the conflict zone  $z$ , having travel paths that can cause rear-end collision.
2.  $\mathcal{C}_i^z$  contains all CAVs from different roads having travel paths that can cause lateral collision with CAV  $i$  in conflict zone  $z$ .
3.  $\mathcal{O}_i^z$  contains all CAVs from different roads having travel paths that cannot cause lateral or rear-end collision with CAV  $i$  in conflict zone  $z$ .

Upon arrival at the entry of the control zone of conflict zone  $z \in \mathcal{Z}$  at time  $t_i^{0,z}$ , CAV  $i \in \mathcal{N}_z(t)$  needs to compute the time  $t_i^z$ . In general, a value of  $t_i^z$  that satisfies the safety constraints (3.38) and (3.39) may depend on the preceding CAV in the control zone. Next, we address the question of identifying the appropriate  $t_i^z$  for each CAV through an upper-level optimization problem.

### 3.2.2 Throughput Maximization with Dynamic Resequencing

To fully utilize the capacity of the traffic network of CAVs, we formulate a throughput maximization problem, in terms of minimizing the gaps between CAVs in the conflict zones, i.e., minimizing the total time to process CAVs in the network, subject to the constraints (2.4), (3.38) and (3.39). Note that for  $i = 1$ , the safety constraint is not active since there is no prior CAV in the control zone, which implies that

$t_1^z$  is not constrained and can be determined outside the optimization framework. Thus, for each control zone of conflict zone  $z \in \mathcal{Z}$ , we formulate the following optimization problem:

$$\min_{\mathbf{t}_{(2:N_z(t))}} \sum_{i=2}^{N_z(t)} (t_i^z - t_{i-1}^z) = \min_{\mathbf{t}_{(N_z(t))}} (t_{N_z(t)}^z - t_1^z), \quad (3.40)$$

subject to : (2.3), (2.4), (3.38), (3.39),

where,  $\mathbf{t}_{(2:N_z(t))} = [t_2^z, \dots, t_{N_z(t)}^z]$ . The solution of (3.40) yields the optimal time  $t_i^{z*}$ ,  $i \geq 2$ ,  $z \in \mathcal{Z}$ , which designates the entry times of each CAV in each conflict zone to maximize the throughput of the corresponding bottleneck.

In what follows, we discuss how the lateral collision safety constraint is addressed in the solution of (3.40). We also show that the solution has an iterative structure and depends only on the state and control constraint (2.4) as well as the safety constraint (3.39).

To obtain the optimal solution of  $t_i^{z*}$  for CAV  $i \in \mathcal{N}_z(t)$  at the conflict zone  $z \in \mathcal{Z}$ , we first consider the case when  $\mathcal{C}_i^z(t)$  is empty, thus the entry time for CAV  $i$  at  $z$  depends only on some CAV  $k = (i-1) \in \mathcal{R}_i^z$ , where  $k$  is physically immediately ahead of  $i$  on the roadway segment inside the control zone. In this case, the minimum time  $t_i^z$  for CAV  $i$  to enter the conflict zone  $z$  is designated by the rear-end safety constraint (3.39), and in particular, by the safe headway,  $\rho$ , that a CAV  $i$  should maintain while following CAV  $k$ , i.e.,  $t_i^z = t_k^z + \rho$ . In this context, we need to find the bound of  $t_i^z$  to ensure feasibility of the solution. Consider the maximum and minimum speeds that CAV  $i$  could achieve. The value of  $t_i^z$  is then given by

$$t_i^z = \max \{ \min \{ t_k^z + \rho, t_i^{z,max} \}, t_i^{z,min} \}, \quad (3.41)$$

where  $t_i^{z,max}$  and  $t_i^{z,min}$  is the longest and shortest possible travel time of a CAV  $i$  between the entry and exit of the control zone of the conflict zone  $z \in \mathcal{Z}$  corresponding to the minimum,  $v_{min}$ , and maximum,  $v_{max}$ , speed limit respectively. Note that condition (3.41) ensures that the time  $t_i^z$  that CAV  $i$  will be entering the conflict zone  $z$  is feasible

and can be attained based on the imposed speed limits in the corridor. From (3.41), the safety constraint between CAVs traveling in the same lane is guaranteed at  $t_i^z$ . We now turn our attention to the case where possible lateral collision might occur if  $\mathcal{C}_i^z(t)$  is non-empty. In this case, the minimum time  $t_i^{z*}$  for CAV  $i$  to enter the conflict zone  $z$  is constrained by both the lateral collision (3.38) and rear-end collision (3.39) constraints.

**Definition 3.2.2.** We define the set  $\mathcal{A}_i^z \subset \mathcal{C}_i^z$ ,  $\mathcal{A}_i^z := \{j \in \mathcal{C}_i^z \mid t_j^z \geq t_i^z\}$ , that includes any CAV  $j \in \mathcal{C}_i^z$  whose entry time at conflict zone  $z$  is later than  $t_i^z$ , and the set  $\mathcal{L}_i^z \subset \mathcal{A}_i^z$ ,  $\mathcal{L}_i^z := \{j \in \mathcal{A}_i^z \mid t_j^z + \rho \leq t_{j+1}^z - \rho\}$ , that includes any CAV  $j \in \mathcal{C}_i^z$  whose entry time satisfy (3.39).

Considering possible lateral collisions at conflict zone  $z$ , for all  $z \in \mathcal{Z}$ , we obtain the following result.

**Theorem 3.2.3.** *The solution  $t_i^{z*}, \forall i \geq 2, \forall z \in \mathcal{Z}$ , of (3.40) is recursively determined through*

$$t_i^{z*} = \begin{cases} \max\{\max\{t_c^z\} + \rho_i, t_i^z\}, & \text{if } \forall c \in \mathcal{C}_i^z \text{ and } \nexists c \in \mathcal{A}_i^z, \\ t_i^z, & \text{if } \exists a \in \mathcal{A}_i^z \text{ and } t_i^z + \rho \leq \min\{t_a^z\}, \\ \min\{t_b^z\} + \rho_i, & \text{if } \exists b \in \mathcal{L}_i^z \text{ and } t_i^z + \rho_i > \min\{t_a^z\}, \\ \max\{t_a^z\} + \rho_i, & \text{if } \exists a \in \mathcal{A}_i^z \text{ and } \nexists a \in \mathcal{L}_i^z. \end{cases} \quad (3.42)$$

*Proof.* Based on Definition 3.2.1, there are three cases to consider for  $t_i^{z*}$ .

*Case 1:* If  $\mathcal{A}_i^z \neq \emptyset$ , all CAVs in  $\mathcal{C}_i^z$  will be entering the conflict zone  $z$  earlier than  $t_i^z$ , which, by Definition 3.2.1, implies  $t_i^{z*} = \begin{cases} t_i^z, \\ \max\{t_c^z\} + \rho, \end{cases} \forall c \in \mathcal{C}_i^z$ . Hence, we have  $t_i^{z*} = \max\{\max\{t_c^z\} + \rho, t_i^z\}, \forall c \in \mathcal{C}_i^z$ .

*Case 2:* If  $\mathcal{A}_i^z \neq \emptyset$  and  $\mathcal{L}_i^z \neq \emptyset$ , we consider two cases: (i) if the earliest entry time of CAVs in the set  $\mathcal{A}_i^z$  is later than  $t_i^z$  plus a safe headway  $\rho$ , then the minimum entry time of CAV  $i$  is  $t_i^z$ , which satisfies the safety constraints to avoid both lateral

and rear-end collisions; (ii) the optimal value of  $t_i^z$  is the earliest possible time slot between the entry times of two consecutive CAVs in the set  $\mathcal{L}_i^z$ . Hence, we have

$$t_i^{z*} = \begin{cases} t_i^z, & \text{if } t_i^z + \rho \leq \min\{t_a^z\}, \\ \min\{t_b^z\} + \rho, & \text{if } t_i^z + \rho > \min\{t_a^z\}, \end{cases} \quad \forall a \in \mathcal{A}_i^z, \forall b \in \mathcal{L}_i^z. \quad (3.43)$$

*Case 3:* Finally, if  $\mathcal{L}_i^z \neq \emptyset$ , this implies that there is no available time slot between the entry times of two CAVs in  $\mathcal{A}_i^z$ . In this case, CAV  $i$  will be entering the conflict zone after the last CAV in  $\mathcal{A}_i^z$  to avoid lateral collision, which implies  $t_i^{z*} = \max\{t_a^z\} + \rho, \forall a \in \mathcal{A}_i^z$ , if there not exist  $a \in \mathcal{L}_i^z$ . Combining the above results, we obtain  $t_i^{z*}$  in (3.42), which completes the proof.  $\square$

Theorem 3.2.3 yields the sequence that the CAVs will be traveling through each control zone. Each CAV  $i$  follows the above policy to determine the time  $t_i^{z*}$  that it will be entering the conflict zone  $z \in \mathcal{Z}$  upon arrival at the entry of the control zone. Once the entry time  $t_i^{z*}$  is computed, it is stored in the coordinator and it is not changed. Thus, the next CAV  $i + 1$ , upon its arrival at the entry of the control zone, will search for feasible times to cross the conflict zone based on the available time slots. The recursion is initialized when the first CAV enters the boundary of the corridor, i.e., it is assigned  $i = 1$ . In this case,  $t_1^z, \forall z \in \mathcal{Z}$ , can be externally assigned as the desired entry time of this CAV whose behavior is unconstrained.

### 3.2.3 Energy-Optimal Motion Primitives with Safety Constraints

When a CAV  $i$  enters the corridor, it communicates with the other CAVs (Assumption 1) and the coordinator broadcasts information without any errors or delays (Assumption 3). The coordinator assigns a unique identity to each CAV and receives back some information at the time each CAV arrives at the entry of the corridor, as defined next.

**Definition 3.2.4.** For each CAV  $i$ , we define the *information set*  $Y_i(t)$  as

$$Y_i(t) \triangleq \{p_i(t), v_i(t), o_i, t_i^{z*}\}, z \in \mathcal{Z}, t \in [t_i^0, t_i^z], \quad (3.44)$$

where  $p_i(t)$ ,  $v_i(t)$  are the position and speed of CAV  $i$  inside the corridor,  $o_i$  is the route that CAV  $i$  travels inside the corridor, and  $t_i^{z*}$  is the time for CAV  $i$  to enter the conflict zone  $z$  given by (3.42).

As discussed in the previous section, the time  $t_i^{z*}$  for CAV  $i$  is determined recursively based on the information received from the coordinator. Therefore, once CAV  $i$  enters each of the control zones, immediately all information in  $Y_i(t)$  becomes available for  $i$  and is stored in the coordinator accessible for the next arriving CAV  $i + 1$ .

In the low-level optimal control problem, the objective is to minimize the control input (acceleration/deceleration) for each CAV  $i \in \mathcal{N}_z(t)$  from the time  $t_i^{0,z}$  that  $i$  enters the control zone until the time  $t_i^z$  that it exits the control zone under the hard safety constraint to avoid rear-end collision. By minimizing each CAV's acceleration/deceleration, we minimize transient engine operation. Thus, we can have direct benefits in fuel consumption and emissions since internal combustion engines are optimized over steady-state operating points (constant torque and speed). Therefore, the optimization problem for each CAV  $i \in \mathcal{N}_z(t)$  is to minimize the  $L^2$ -norm of the control input in  $[t_i^{0,z}, t_i^z]$ , formulated as follows:

$$\min_{u_i(t) \in U_i} J_i(u(t)) = \min_{u_i(t) \in U_i} \frac{1}{2} \int_{t_i^{0,z}}^{t_i^z} u_i^2(t) dt, \quad (3.45)$$

subject to : (2.3), (2.4), (3.39),

given  $t_i^{0,z}$ ,  $p_i(t_i^{0,z}) = 0$ ,  $v_i^{0,z}$ ,  $t_i^{z*}$ , and  $p_i(t_i^{z*}) = p_z$ .

Note that we do not include the lateral collision constraint (3.38) in (3.45), since it has been addressed in the upper-level optimization problem. On the contrary, we explicitly include the rear-end safety constraint. The problem formulation with the state and control constraints requires the constrained and unconstrained arcs of the

state and control input to be pieced together to satisfy the Euler-Lagrange equations and necessary condition of optimality. Let  $\mathbf{S}(t, \mathbf{x}_i(t), u_i(t)) = [v_i(t) - v_{max} \quad v_{min}(t) - v_i(t) \quad p_i(t) - p_k(t) - \delta]^T$  be the vector of constraints that are not explicit functions of the control input  $u_i(t)$ . We take successive total time derivatives of  $\mathbf{S}(t, \mathbf{x}_i(t), u_i(t))$  until we obtain an expression that is explicitly dependent on  $u_i(t)$ . If  $q$  time derivatives are required for a specific constraint of  $\mathbf{S}_i(t, \mathbf{x}_i(t), u_i(t))$ , we refer to that constraint as a  $q$ th-order state variable inequality constraint [188]. Note that we have 1st-order speed constraint and 2nd-order rear-end safety constraint in  $\mathbf{S}_i(t, \mathbf{x}_i(t), u_i(t))$ . The 2nd-order rear-end safety constraint plays the role of a control variable constraint on the constrained arc,

$$S_i^{(2)}(x_i(t), u_i(t), t) = u_i(t) - u_k(t) = 0. \quad (3.46)$$

From (3.45), the CAV dynamics (2.3), state and control constraints (2.4), and the rear-end safety constraint (3.39) for each CAV  $i \in \mathcal{N}_z(t)$ , we formulate the Hamiltonian function

$$\begin{aligned} H_i(t, p_i(t), v_i(t), u_i(t)) &= \frac{1}{2}u_i(t)^2 + \lambda_i^p \cdot v_i(t) + \lambda_i^v \cdot u_i(t) \\ &+ \eta_i^a \cdot u_i(t) - \eta_i^b \cdot u_i(t) + \eta_i^c \cdot (u_i(t) - u_k(t)) \\ &+ \mu_i^d \cdot (u_i(t) - u_{max}) + \mu_i^e \cdot (u_{min} - u_i(t)), \end{aligned} \quad (3.47)$$

where  $\lambda_i^p$ ,  $\lambda_i^v$  are the co-state components, and  $\eta_i^a, \eta_i^b, \eta_i^c, \mu_i^d, \mu_i^e$  are the Lagrange multipliers satisfying the complimentary slackness conditions based on the state and control constraints in (2.4) and (3.39).

The Euler-Lagrange equations become

$$\dot{\lambda}_i^p(t) = -\frac{\partial H_i}{\partial p_i} = 0, \quad \dot{\lambda}_i^v(t) = -\frac{\partial H_i}{\partial v_i} = -\lambda_i^p. \quad (3.48)$$

The necessary condition for optimality is

$$\frac{\partial H_i}{\partial u_i} = u_i(t) + \lambda_i^v + \eta_i^a - \eta_i^b + \eta_i^c + \mu_i^d - \mu_i^e = 0. \quad (3.49)$$

When the inequality state and control constraints are not active,  $\eta_i^a = \eta_i^b = \eta_i^c = \mu_i^d = \mu_i^e = 0$ , applying the necessary condition (3.49), the optimal control is

$$u_i(t) + \lambda_i^v = 0, \quad i \in \mathcal{N}_z(t). \quad (3.50)$$

From (3.48) we have  $\lambda_i^p(t) = a_i$ , and  $\lambda_i^v(t) = -(a_i \cdot t + b_i)$ . The coefficients  $a_i$ ,  $b_i$  are constants of integration corresponding to each CAV  $i$ . From (3.50) the optimal control input (acceleration/deceleration), speed and position as a function of time are given by

$$u_i^*(t) = (a_i \cdot t + b_i), \quad \forall t \geq t_i^{0,z}, \quad (3.51)$$

$$v_i^*(t) = \frac{1}{2}a_i \cdot t^2 + b_i \cdot t + c_i, \quad \forall t \geq t_i^{0,z}, \quad (3.52)$$

$$p_i^*(t) = \frac{1}{6}a_i \cdot t^3 + \frac{1}{2}b_i \cdot t^2 + c_i \cdot t + d_i, \quad \forall t \geq t_i^{0,z}, \quad (3.53)$$

where  $c_i$  and  $d_i$  are constants of integration which can be computed at each time  $t$ ,  $t_i^0 \leq t \leq t_i^z$ , using the values of the control input, speed, and position of each CAV  $i$  at  $t$ , the position  $p_i(t_i^z)$ , and  $\lambda_i^v(t_i^z) = 0$ . The simple nature of the optimal control and states in (3.51) through (3.53) makes the online solution of (3.45) computationally feasible, even with the additional burden of checking for active constraints. In what follows, we address the optimization problem (3.45) with the activation of the constrained case corresponding to the rear-end collision only. The other constrained cases related to the state, i.e., speed,  $v_i$ , and control,  $u_i$  as in (2.4), are similar to the cases presented in Section 3.1, and thus are omitted.

Suppose a CAV starts from a feasible state and control at  $t = t_i^0$  and at some time  $t = t_1$ , the rear-end safety constraint  $(p_i(t) - p_k(t) + \delta) \leq 0$  is activated. In this case,  $\eta_i^a = \eta_i^b = \mu_i^d = \mu_i^e = 0$ . From (3.49), the optimal control is given by

$$u_i(t) + \lambda_i^v + \mu_i^c(t) = 0, \quad \forall t \geq t_1. \quad (3.54)$$

The  $q$ -component vector function of tangency constraints  $N(x_i(t), t)$  is

$$N(x_i(t), t) = \begin{bmatrix} S_i(x_i(t), t) \\ S_i^{(q-1)}(x_i(t), t) \end{bmatrix} = \begin{bmatrix} (p_i(t) - p_k(t) + \delta) \\ v_i(t) - v_k(t) \end{bmatrix}. \quad (3.55)$$

The state trajectory entering onto the 2nd-order rear-end safety constraint boundary must satisfy the following tangency conditions

$$N(x_i(t), t) = \begin{bmatrix} p_i(t) - p_k(t) + \delta \\ v_i(t) - v_k(t) \end{bmatrix} = 0, \quad (3.56)$$

where,  $N(x_i(t), t)$  is the  $q$ -component vector function of the 2nd order safety tangency constraints. The tangency constraints in (3.56) also apply to the state trajectory at the exit of the constraint arc. Since the optimal solution of the preceding CAV  $k \in \mathcal{N}_z(t)$  is known a priori, from (3.46) and (3.56), the optimal solution for CAV  $i \in \mathcal{N}_z(t)$  in the constrained arc is derived from  $\mathbf{S}_i(t, \mathbf{x}_i(t), u_i(t)) = 0$  and is

$$u_i^*(t) = u_k^*(t), \quad v_i^*(t) = v_k^*(t), \quad \text{and} \quad p_i^*(t) = p_k^*(t) - \delta. \quad (3.57)$$

The equations in (3.56) form a set of interior boundary conditions where the co-states  $\lambda_i^p(t)$  and  $\lambda_i^v(t)$ , in general, have discontinuity at the junction points, i.e., entry and exit points of the state trajectory between the constrained and the unconstrained arcs. However, the control trajectory may or may not have discontinuities at the junction points. Next, we address the jump conditions at the entry junction point  $t = t_1$ . At time  $t = t_1$ , when the safety constraint is activated, we have a junction point between the unconstrained and constrained arcs. Let  $t_1^-$  represents the time instance just before  $t_1$ , and  $t_1^+$  signifies just after  $t_1$ . The state trajectories are continuous at the junction points. Thus, we have

$$p_i(t_1^-) = p_i(t_1^+), \quad v_i(t_1^-) = v_i(t_1^+). \quad (3.58)$$

The jump conditions at  $t_1$  can be written as

$$\lambda_i^p(t_1^-) = \lambda_i^p(t_1^+) + \pi^T \cdot \left. \frac{\partial N(x_i(t), t)}{\partial p_i(t)} \right|_{t=t_1}, \quad (3.59)$$

$$\lambda_i^v(t_1^-) = \lambda_i^v(t_1^+) + \pi^T \cdot \left. \frac{\partial N(x_i(t), t)}{\partial v_i(t)} \right|_{t=t_1}, \quad (3.60)$$

$$H(t_1^-) = H(t_1^+) - \pi^T \cdot \left. \frac{\partial N(x_i(t), t)}{\partial t} \right|_{t=t_1}, \quad (3.61)$$

$$\frac{\partial H(t_1^-)}{u_i(t)} = \frac{\partial H(t_1^+)}{u_i(t)}. \quad (3.62)$$

In (3.59)-(3.62),  $\pi^T = [\pi_1 \ \pi_2]$  is a vector of constant Lagrange multipliers to be determined so that the condition in (3.56) is satisfied. From (3.61), using (3.57)-(3.62), we obtain  $\frac{1}{2}(u_i(t_1^-)^2 - u_i(t_1^+)^2) + \lambda_i^v(t_1^+) \cdot (u_i(t_1^-) - u_i(t_1^+)) = 0$ . This yields two cases: either  $(u_i(t_1^-) - u_i(t_1^+)) = 0$  or  $\frac{1}{2}(u_i(t_1^-) + u_i(t_1^+)) + \lambda_i^v(t_1^+) = 0$ . Both conditions lead to  $u_i(t_1^-) = u_i(t_1^+)$ , which indicates that the control trajectory is continuous at the entry junction point at  $t = t_1$ . Finally, using the continuity in control and (3.60) in (3.62), we obtain  $\eta_i^c(t_1^+) = \pi_2$ . With two junction points at time  $t = t_1$  and  $t = t_2$ , we have a constrained arc between two unconstrained arcs. Since we have multiple arcs pieced together at the junction points, we differentiate the constants of integration for the state and control trajectory by adding a superscript  $h$  representing the order of appearance of the arcs. Therefore, we represent the constants of integration as  $(a_i^h, b_i^h, c_i^h, d_i^h)$ , where  $h = 1, 2$  corresponds to the first and the last unconstrained arc respectively. The control trajectory of CAV  $i$  considering the constrained and unconstrained arcs can be written as,

$$u_i^*(t) = \begin{cases} a_i^1 \cdot t + b_i^1, & t_i^{0,z} \geq t \leq t_1, \\ u_k^*(t), & t_1 < t < t_2, \\ a_i^3 \cdot t + b_i^3, & t_2 \geq t \leq t_i^z. \end{cases} \quad (3.63)$$

The constants of integration, along with the junction points  $t_1$  and  $t_2$  can be computed by solving (3.51)-(3.53) and (3.57)-(3.63) with appropriate initial, boundary and transversality conditions.

### 3.2.4 Simulation Results and Summary

To validate the effectiveness of the rear-end safety constrained formulation, we present two cases in Fig. 3.5, where a leading CAV  $k$  and a following CAV  $i$  are both cruising with the optimal control input. In the left panel of Fig. 3.5, the following CAV  $i$  derives its control input according to (3.51) and activates the rear-end safety constraint with respect to the immediately preceding CAV  $k$  with two junction points. In the right panel of Fig. 3.5, CAV  $i$  derives its control input using (3.63) subject to safety constrained optimization.

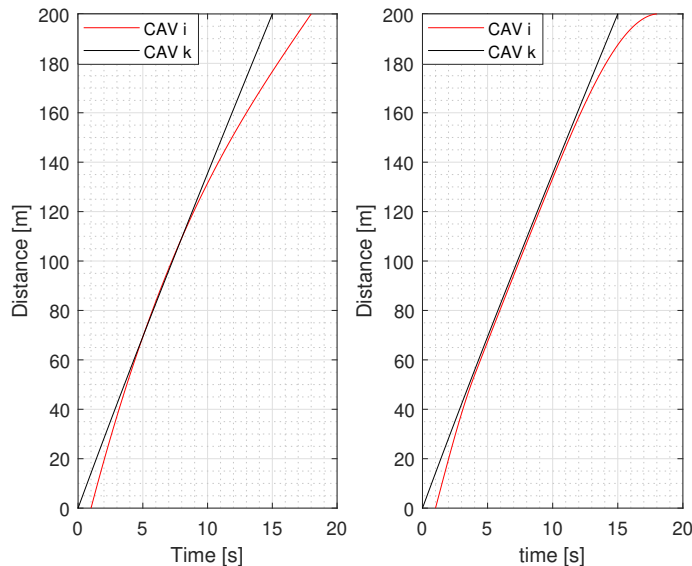


Figure 3.5: Unconstrained (left) and rear-end safety constrained state trajectory (right) of CAV  $i$  with respect to its immediately preceding vehicle  $k$ .

To validate the proposed approach for multiple traffic scenarios, we use a simulation network of Mcity created in PTV VISSIM environment. We define a corridor consisting of four conflict zones: (1) a merging roadway, (2) a speed reduction zone, (3) a roundabout, and (4) an intersection. Vehicles enter the network on the ramp, join the traffic on the highway with desired speed of  $22\text{ m/s}$ , and then enter the speed reduction zone where the speed limit drops to  $11\text{ m/s}$ . The vehicles exit the highway segment and travel through the roundabout, where the desired speed of  $13\text{ m/s}$  is imposed until the exit of the roundabout, to the intersection (conflict zone #4).

To evaluate the network performance with the proposed control framework, we define two scenarios as follows:

**Scenario 1:** baseline, i.e., 0% CAV penetration rate. All vehicles in the network are non-connected and non-automated. In this case, the Wiedemann car following model [160] built in VISSIM is applied.  $1.2\text{ s}$  time headway is adopted to estimate the minimum allowable following distance.

**Scenario 2:** optimal control, i.e., 100% CAV penetration rate. The proposed



Figure 3.6: The corridor in Mcity.

control framework is integrated to generate the optimal acceleration/deceleration profile for each CAV in the network.

The CAV speed trajectories under 0% and 100% CAV penetration rate in the corridor are illustrated in Fig. 3.7. In the baseline scenario with 0% CAV penetration rate, CAVs traveling along the corridor need to yield to mainline traffic and wait in the signalized intersection. Thus, we observe high fluctuations in their speed profiles under the baseline scenario at the proximity of the conflict zones (see the upper panel of Fig. 3.7). In the optimal control scenario under 100% CAV penetration rate, CAVs travel through the corridor without stop-and-go driving (see lower panel of Fig. 3.7). The latter enables CAVs to have a smoother speed trajectory affecting the uncontrolled upstream and downstream area of the control zone. We observe 9% improvement in terms of travel time and an average of 47% savings in total fuel consumption in the optimal control scenario compared to the baseline one.

We plot the accumulated fuel consumption for all the vehicles traveling through

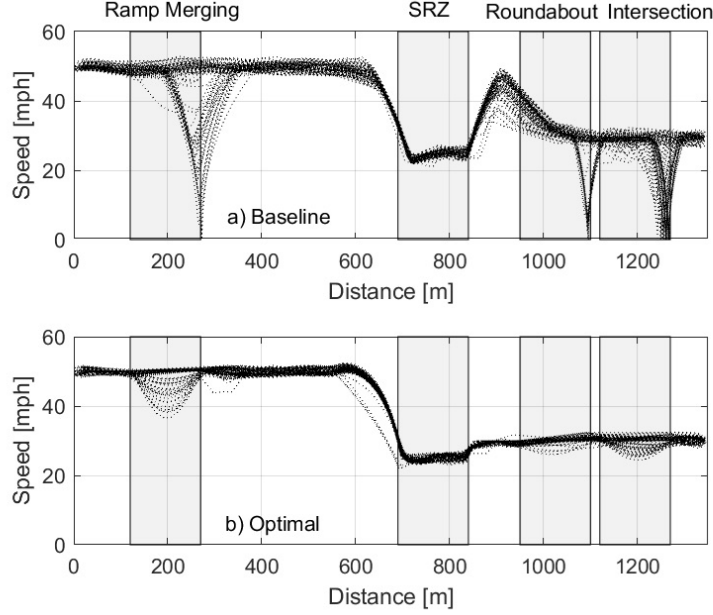


Figure 3.7: Vehicle trajectories inside the corridor for (a) baseline and (b) optimal controlled case. The control zone for each of the conflict zones are shown for comparison.

the corridor considered here in one simulation replication in Fig. 3.8 to show energy consumption under both scenarios. With smooth acceleration/deceleration profiles throughout the entire corridor, vehicles’ stop-and-go driving behavior is eliminated under Scenario 2 with 100% CAV penetration rate. Thus, transient engine operation is minimized, leading to direct fuel consumption savings compared to the baseline scenario as shown in Fig. 3.8.

With vehicle trajectory data collected every 1 s, fuel consumption is estimated by using the polynomial metamodel proposed in [190] that relates vehicle fuel consumption as a function of speed  $v(t)$  and acceleration  $u(t)$ . Overall, through the optimal control algorithm, an average of 47% savings in total fuel consumption for vehicles traveling along the corridor is obtained. The reasons are mainly twofold: 1) while CAVs are immediately preparing for the speed reduction zone/roundabout/intersection with smooth maneuver, human-driven vehicles keep accelerating or cruising at a much higher speed until they are aware of downstream conflict zones. We observe that in Fig. 3.7 deceleration is the major behavior around the conflict zones in the baseline scenario; 2)

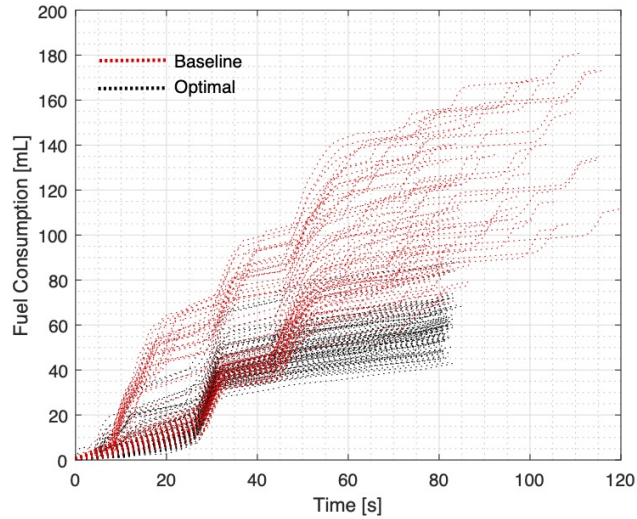


Figure 3.8: Accumulated fuel consumption over time for the baseline and optimal controlled vehicles.

CAVs are coordinated with each other to create enough gaps for merging and crossing the intersection, whereas human-driven vehicles need to stop and accelerate again to cross these conflict zones.

To summarize, in this chapter, the problem related to the optimal control and coordination of CAVs is addressed for traffic scenarios with state, control, and safety constraints. Specifically, the theorems and results have been detailed that would enable us to compute the state and control constrained optimal control policy for the CAVs with a real-time implementable closed-form analytic solution. I have also extended the optimal coordination approach in a traffic network of multiple scenarios, where the CAVs can dynamically re-sequence their optimal coordination queue, and cross the traffic scenarios without any rear-end and lateral safety collision. In the next chapter, we delve into the domain of a mixed traffic environment.

## Chapter 4

### OPTIMAL CONTROL IN A MIXED TRAFFIC ENVIRONMENT

In the previous chapters, we explored in detail the problem of optimal control and coordination of CAVs through traffic scenarios with system constraints. However, we have considered 100% CAV penetration which enabled us to have full control of all the agents present within the traffic network. In reality, such an idealized framework is not implementable in the current transportation condition due to the presence of HDVs. Therefore, consideration of a mixed traffic environment, where CAVs and HDVs can safely co-exist, is necessary. In general, a mixed traffic environment poses significant modeling and control challenges regarding the following aspects.

1. **State Estimation Problem:** HDVs do not transmit their state information to any external agents. Therefore, the CAVs need to estimate the neighboring HDVs' state either using their onboard sensors or from an appropriate infrastructure such as roadside units, coordinators, loop detectors, etc.
2. **Dynamics Prediction Problem:** Although several car-following models exist in the literature [101, 160, 191] to model the HV dynamics, no car-following model can capture fully the human driving behavior. This leads to the problem of predicting the HV dynamics properly which is required for the CAVs to derive a closed-form analytic solution. The uncertainty arising out of such unpredictable HV dynamics also needs to be considered by the CAVs.
3. **Vehicle Control Problem:** The HDVs we consider in our modeling framework do not have any driving automation (Level 0 automation), and are controlled only by the human input, which prevents the implementation of a distributed control framework in a centralized or decentralized way.

In this chapter, I address the problem of controlling CAVs in a mixed traffic environment and investigate the implication regarding vehicle- and network-level performance.

#### 4.1 Safety-Aware Control at a Mixed Traffic Signalized Junction

A typical urban signalized intersection poses significant modeling and control challenges in a mixed traffic environment with connected automated vehicles (CAVs)

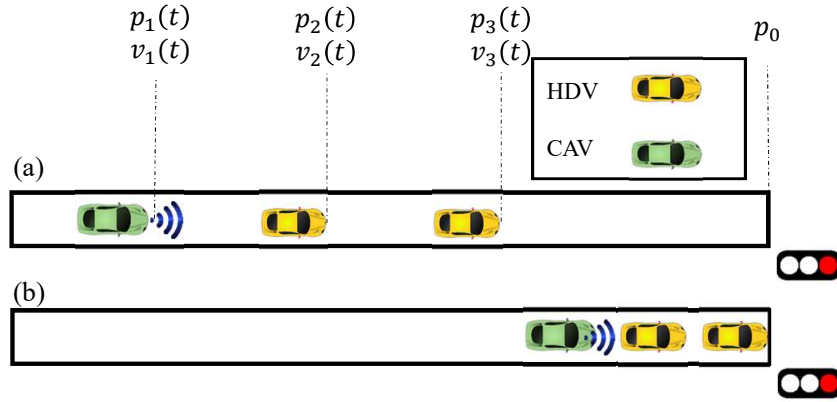


Figure 4.1: A connected and automated vehicle (CAV) and human-driven vehicles (HDV) approaching a signalized intersection at red-light signal phase.

and human-driven vehicles (HDVs). Furthermore, the use of conventional traffic lights is still the most prevalent way of traffic control at urban intersections that adds an extra layer of complexity in modeling the HDV behavior due to the presence of the zone of the yellow light dilemma [192]. Thus, it is essential to develop an efficient control framework considering the inclusion and interaction of CAVs with HDVs approaching the signalized intersections to provide safety assurance under unknown HDV behavior.

In this section, we address the problem of deriving safe trajectories for CAVs in a mixed traffic environment that prioritize rear-end collision avoidance when the preceding HDVs approach the yellow- and red signal phases of the intersection. We present a predictive control framework for the CAVs that employs a recursive least squares algorithm to approximate in real time the driving behavior of the preceding HDVs and then use this approximation to derive its safety-aware trajectory in a finite horizon. We validate the effectiveness of our proposed framework through numerical simulation and analyze the robustness of the control framework.

### 4.1.1 Optimal Control at a Signalized Intersection

We consider a group of vehicles consisting of multiple HDVs traveling on a single-lane road and followed by a CAV while approaching an urban signalized intersection with a red (or yellow then red) traffic phase (Fig. 4.1). Note that, the general idea of our formulation can be extended to different cases such as yield/stop traffic signs, downstream traffic congestion, and pedestrian crossing, where the preceding HDVs' motion can change abruptly to come to a full stop. To facilitate our exposition, we provide the following definitions.

**Definition 4.1.1.** Suppose that the red signal phase is active at some time instant  $t = t^0$ . The set  $\mathcal{N}$  of the vehicles approaching the intersection at  $t = t^0$  is  $\mathcal{N} = \{N, N - 1, \dots, 1\}$ , where  $N \in \mathbb{N}$  is the total number of vehicles under consideration. Here, the vehicles are assigned integer indices by the order of their respective distances from some fixed stopping position  $p_0$  located downstream near the signal head. The indices  $N, N - 1, \dots, 2$  represent the HDVs followed by the CAV denoted by the index 1.

**Definition 4.1.2.** The set of HDVs at time instant  $t = t^0$  is  $\mathcal{N}_{\text{HDV}} = \mathcal{N} \setminus \{1\}$ .

When the red signal phase is active at some time instant  $t = t^0$ , the HDV- $N$  in  $\mathcal{N}$  must stop behind the position  $p_0$ . The objective of the CAV-1 is to derive an optimal trajectory to stop behind HDV-2 such that no rear-end collision takes place.

**Remark 4.1.1.** In our formulation, we require that the set of HDVs  $\mathcal{N}_{\text{HDV}}$  is non-empty at time instant  $t = t^0$  when the red signal phase of the intersection is active. If  $\mathcal{N}_{\text{HDV}}$  is empty, then the problem of avoiding rear-end collision becomes redundant.

#### 4.1.1.1 Communication Structure

The CAV-1 is retrofitted with appropriate sensors and communication devices to estimate in real time the state information of the preceding HDVs in  $\mathcal{N}_{\text{HDV}}$  through

vehicle-to-everything communication protocol and intelligent roadside units [193]. We refer to the unidirectional flow of information from the preceding HDVs in  $\mathcal{N}_{\text{HDV}}$  to the trailing CAV-1 as the multi-predecessor communication topology. In contrast, the trajectory of each HDV  $i$  in  $\mathcal{N}_{\text{HDV}}$  is solely dictated by the perception of the state information of the immediate preceding vehicle  $i + 1$  in  $\mathcal{N}_{\text{HDV}}$ . For the leading vehicle HDV- $N$  that does not have a preceding vehicle, its driving actions depend on the relative distance to the stopping point.

#### 4.1.1.2 Vehicle Dynamics and Constraints at Mixed Traffic

We consider a discrete-time double integrator model, similar to (2.3), with a sampling time  $\tau \in \mathbb{R}^+$  to represent the dynamics of each vehicle  $i \in \mathcal{N}$  as follows

$$p_i(t + 1) = p_i(t) + v_i(t)\tau + \frac{1}{2}u_i(t)\tau^2, \quad (4.1a)$$

$$v_i(t + 1) = v_i(t) + u_i(t)\tau, \quad (4.1b)$$

where  $p_i(t) \in \mathcal{P}_i$ ,  $v_i(t) \in \mathcal{V}_i$ , and  $u_i(t) \in \mathcal{U}_i$  denote the position, speed and acceleration of each vehicle  $i$  in  $\mathcal{N}$ . The sets  $\mathcal{P}_i$ ,  $\mathcal{V}_i$ , and  $\mathcal{U}_i$ ,  $i \in \mathcal{N}(t)$ , are complete and totally bounded subsets of  $\mathbb{R}$ . Note that in the discrete-time dynamics model (4.1), we assume that the acceleration  $u_i(t)$  of each vehicle  $i$  in  $\mathcal{N}$  remains constant in the time period of length  $\tau$  between time instants  $t$  and  $t + 1$ , which is different to some previous approaches that assume constant speed between time instants  $t$  and  $t + 1$  [148, 194]. To ensure that the control input and vehicle speed are within a given admissible range, we impose the state and control constraints as in (2.4).

The control input  $u_i(t)$  of each vehicle  $i \in \mathcal{N}$  in (4.1) can take different forms based on the consideration of connectivity and automation. For CAV-1 in  $\mathcal{N}$ , we consider a switching control framework based on the following cases: if at time instant  $t = t^0$  (Remark 4.1.1) (a)  $\mathcal{N}_{\text{HDV}}$  is empty, then CAV-1 derives its control input by using its default adaptive cruise controller (see [164]), (b) if  $\mathcal{N}_{\text{HDV}}$  is not empty, then CAV-1

derives and implements the control input  $u_1(t)$  using the proposed control framework discussed in Section 4.1.2.

For each HDV  $i \in \mathcal{N}_{\text{HDV}}$ , however, we consider a car-following model to represent the predecessor-follower coupled dynamics (Fig. 4.1) with its preceding vehicle  $i + 1$  that has the following generic structure

$$u_i(t) = f_i(\Delta p_i(t), v_i(t), \Delta v_i(t)), \quad (4.2)$$

where  $f_i(\cdot)$  represents the behavioral function of the car-following model of vehicle  $i \in \mathcal{N}_{\text{HDV}}$ , and  $\Delta p_i(t) := p_{i+1}(t) - p_i(t) - l_c$  and  $\Delta v_i(t) := v_{i+1}(t) - v_i(t)$  denote the headway and approach rate of vehicle  $i$  with respect to its preceding vehicle  $i + 1$ , respectively. We consider two edge cases that may arise from the above definitions: (a) if there is no vehicle  $i + 1$  preceding vehicle  $i$  within a certain look-ahead distance  $d_f$ , then we consider  $\Delta p_i(t) = d_f$  and  $\Delta v_i(t) = v_i(t)$ , and (b) if there is an obstruction/red signal phase immediately ahead of vehicle  $i$  at a distance  $d_s$ , then  $\Delta p_i(t) = d_s$  and  $\Delta v_i(t) = -v_i(t)$ . There are several car-following models reported in the literature that can emulate a varied class of human driving behavior [195].

The parameters of a car-following model can be recovered from historical data using offline identification methods [161]. However, since the historical data might not be available and the human driving behavior usually changes over time, offline identification methods do not work well in practice. As a result, in our proposed framework, we consider that the CAV does not have full prior knowledge of the behavioral function  $f_i(\cdot)$  of the preceding HDVs. Instead, the CAV assumes a specific type of car-following model for the HDV, then estimates the model parameters for each HDV online using real-time collected data.

To capture the car-following characteristics of the preceding HDV-2's dynamics from the CAV-1's control point of view, we define the states associated with tracking

the position error  $e_p(t)$  and speed error  $e_v(t)$  as

$$e_p(t) = p_2(t) - p_1(t) - l_c, \quad (4.3a)$$

$$e_v(t) = v_2(t) - v_1(t). \quad (4.3b)$$

We consider the dynamic safe following headway  $s_i(t)$  between two consecutive vehicles  $i$  and  $(i+1) \in \mathcal{N}$  as  $s_i(t) = \rho_i v_i(t) + s_0$ , where  $\rho_i \in \mathbb{R}^+$  denotes a desired time headway that each vehicle  $i \in \mathcal{N}$  maintains while following the preceding vehicle, and  $s_0 \in \mathbb{R}^+$  is the standstill distance denoting the minimum bumper-to-bumper gap at stop. The rear-end collision avoidance constraint between CAV-1 and its immediately preceding HDV-2 can thus be written as

$$e_p(t) \geq s_1(t). \quad (4.4)$$

We now formalize the main objective of the CAV-1 control framework.

**Problem 4.1.1.** *Given the multi-predecessor communication topology (Section 4.1.1.1), the main objective of CAV-1 is to derive its optimal control input  $u_1^*(t)$  such that CAV-1 drives the states  $e_p(t)$ ,  $e_v(t)$  to respective reference states, and the control input  $u_1(t)$  is minimized with online estimation of the car-following parameters in (4.2) subject to the state, control and safety constraints in (2.4)-(4.4).*

#### 4.1.2 Data-Driven Predictive Control Framework

In our approach, we adopt a receding horizon predictive control framework with multi-predecessor communication topology and data-driven estimation of HDVs' car-following parameters for state prediction to address Problem 4.1.1, as shown in Figure 4.2. In the receding horizon control, the optimal control input at the current time step is obtained by solving a predictive control problem with a horizon  $T_p$  while only the first element of the obtained control input sequence is implemented. Afterward, the horizon moves forward one step, and the above process is repeated until a final horizon is reached. The essential steps of the proposed framework are outlined as follows.

1. **Data-driven parameter estimation:** At each time instant  $t$ , the current states  $p_i(t), v_i(t)$  of each preceding HDV  $i$  in  $\mathcal{N}_{\text{HDV}}$  is communicated to CAV-1. Since

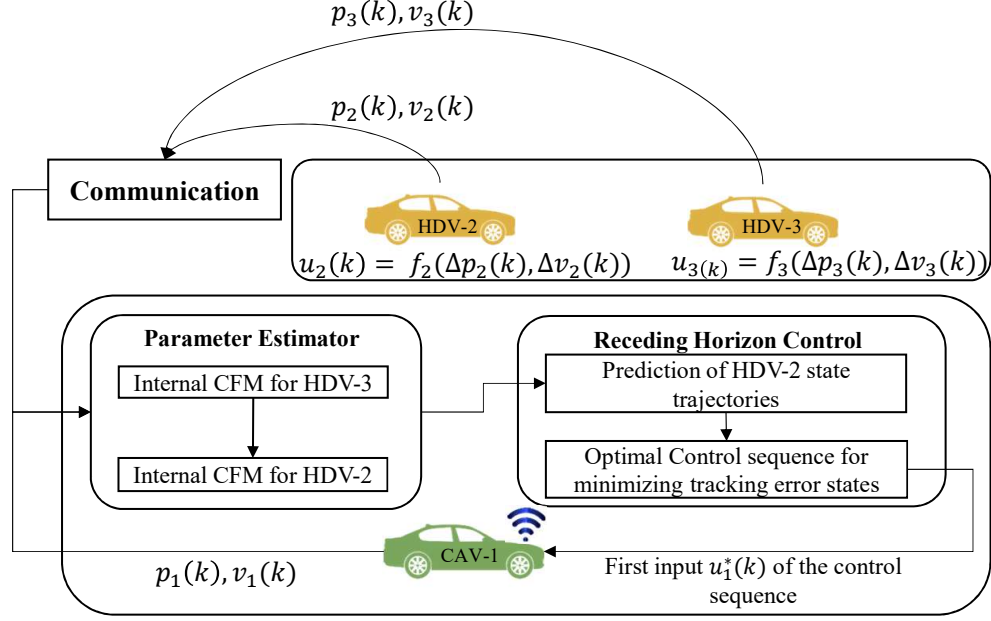


Figure 4.2: The structure of the proposed control framework to address Problem 4.1.1.

the exact car-following model  $f_i$  of each HDV  $i$  in  $\mathcal{N}_{\text{HDV}}$  is unknown to CAV-1, it considers a specific type of car-following model to represent the driving behavior of each HDV, and estimates the parameters of the car-following model for each HDV online.

2. **Predictive control problem:** CAV-1 then uses the estimated car-following model from Step 1 to predict the future state trajectories of the immediately preceding HDV-2 and derives its own optimal control input sequence  $U_1^*(t) := [u_1^*(t), u_1^*(t+1), \dots, u_1^*(t+T_p-1)]^T$  using the receding horizon control framework discussed above. Finally, CAV-1 implements only the first control input  $u_1^*(t)$ .

In what follows, we provide a detailed exposition of the steps of the proposed control framework discussed above.

#### 4.1.2.1 Online Car-following Model Parameter Estimation

In this section, we use a recursive least-squared formulation [196] to estimate the parameters of the internal car-following model residing in CAV-1's mainframe to

represent the driving behavior of each of the preceding HDVs. To this end, we consider the CTH-RV model [197]

$$v_i(t+1) = v_i(t) + \eta_i(\Delta p_i(t) - \rho_i v_i(t))\tau + \nu_i(v_1(t) - v_i(t))\tau, \quad (4.5)$$

where the model parameters  $\eta_i$  and  $\nu_i$  are the control gains on the constant time headway and the approach rate, and  $\rho_i$  is the desired safe time headway for each HDV  $i$  in  $\mathcal{N}_{\text{HDV}}$ , respectively. We employ the linear CTH-RV model instead of other complex nonlinear models so that the resulting control problem presented in the next section is thus convex and can be solved efficiently in real-time. Moreover, it is also observed that CTH-RV model is highly comparable to other nonlinear car-following models in terms of data fitting [198].

Suppose that we measure the speed  $v_i(t)$ , headway gap  $\Delta p_i(t)$  and approach rate  $\Delta v_i(t)$  for each preceding HDV  $i$  in  $\mathcal{N}_{\text{HDV}}$  with sampling rate  $\tau$ . We recast (4.5) as

$$v_i(t+1) = \gamma_{i,1}v_i(t) + \gamma_{i,2}\Delta p_i(t) + \gamma_{i,3}v_1(t), \quad (4.6)$$

where  $\gamma_{i,1} := (1 - (\eta_i\rho_i + \nu_i)\tau)$ ,  $\gamma_{i,2} := \eta_i\tau$  and  $\gamma_{i,3} := \nu_i\tau$  are the parameters that can be estimated using the RLS algorithm [196]. The original model parameters  $\eta_i, \nu_i$  and  $\rho_i$  are then uniquely determined from  $\gamma_{i,1}, \gamma_{i,2}, \gamma_{i,3}$  as long as  $\gamma_{i,2} \neq 0$ . Next, we can write (4.6) in matrix form as

$$v_i(t+1) = \gamma_i^T \phi_i(t), \quad (4.7)$$

where  $\phi_i(t) := [v_i(t), \Delta p_i(t), v_1(t)]^T$  is the regressor vector and  $\gamma_i := [\gamma_{i,1}, \gamma_{i,2}, \gamma_{i,3}]^T$  is the parameter vector. We can estimate  $\gamma_i$  using the following recursive least squares

algorithm as follows [196]

$$\hat{\gamma}_i(t) = \hat{\gamma}_i(t-1) + L_i(t)[v_i(t) - \hat{v}_i(t)], \quad (4.8a)$$

$$\hat{v}_i(t) = \hat{\gamma}_i^T(t-1)\phi_i(t), \quad (4.8b)$$

$$L_i(t) = \frac{P_i(t-1)\phi_i(t)}{\xi + \phi_i^T(t)P_i(t-1)\phi_i(t)}, \quad (4.8c)$$

$$P_i(t) = \frac{1}{\xi} \left[ P_i(t-1) - \frac{P_i(t-1)\phi_i(t)\phi_i^T(t)P_i(t-1)}{\xi + \phi_i^T(t)P_i(t-1)\phi_i(t)} \right]. \quad (4.8d)$$

Here,  $\xi \in [0, 1]$  is the forgetting factor that assigns a higher weight to the recently collected data points and discounts older measurements, and  $\hat{\gamma}_i(t)$  denotes the estimate of the parameter vector  $\gamma_i$  at time instant  $t$ , which is updated recursively as new data becomes available. In what follows, we introduce the predictive control problem that is needed to be solved.

#### 4.1.2.2 Predictive Control Problem

The main objective of the predictive controller of the CAV is to (a) drive the position tracking state  $e_p(t)$  to a reference  $e_{p,r}(t)$ , (b) drive the speed tracking state  $e_v(t)$  to zero, and (c) minimize CAV-1's control input  $u_1(t)$ . To this end, the receding horizon controller generates the predictive states  $e_p(t+n|t)$ ,  $e_v(t+n|t)$  for  $n = 1, \dots, T_p$  at each time instant  $t$  for a predictive horizon  $T_p$  using the state definitions in (4.3), vehicle dynamics in (4.1) and internal car-following models of the HDVs in (4.5) approximated in the previous section. Then the control input sequence  $U_1(t) := [u_1(t), u_1(t+1), \dots, u_1(t+T_p-1)]^T$  is derived such that the predictive states are driven to their

respective reference states. The predictive control problem thus can be written as

$$\min_{U_1^*(t)} \frac{1}{2} \sum_{n=1}^{T_p} \left[ w_{e_p} (e_p(t+n|t) - e_{p,r}(t+n|t))^2 \right. \quad (4.9)$$

$$\left. + w_{e_v} e_v(t+n|t)^2 + w_u (u_1(t+n-1))^2 \right],$$

subject to :

model: (4.1), (4.2), (4.3),

constraints: (2.4), (4.4),

reference state:  $e_{p,r}(t) := s_1(t)$ ,

where the predictive reference state  $e_{p,r}(t+n|t)$  can be computed using the relation  $e_{p,r}(t) = s_1(t)$  and the dynamics model in (4.1) and (4.3), and  $w_{e_p}, w_{e_v}, w_u \in \mathbb{R}^+$  are the weights on the reference tracking of the position error state  $e_p(t)$ , speed error state  $e_v(t)$  and the CAV-1's control input  $u_1(t)$ , respectively.

The predictive control problem in (4.9) can be transformed into a standard constrained quadratic programming problem and solved using commercially available solvers [199]. At each discrete time instant  $t$ , the optimal control sequence  $U_1^*(t)$  is computed by solving (4.9) and only the first control input  $u_1^*(t)$  is applied. Then the system moves to the next time instant  $t+1$  and the process is repeated until a final time horizon is reached.

**Remark 4.1.2.** While implementing the above control framework, if any of the preceding HDVs leaves the current lane or passes the intersection at any time instant  $t$ , then we simply update the sets  $\mathcal{N}$  and  $\mathcal{N}_{\text{HDV}}$  starting from the next time instant  $t+1$ , where the control problem (4.9) is again solved with the updated information.

### 4.1.3 Numerical Validation

This section validates the performance of the proposed safety-aware data-driven predictive control by numerical simulations at a mixed-traffic signalized intersection.

Table 4.1: Parameters of the controller

Parameters	Value	Parameters	Value
$\tau$	0.1 s	$T_p$	50
$v_{\max}$	15 m/s	$v_{\min}$	0 m/s
$u_{\max}$	3 m/s <sup>2</sup>	$u_{\min}$	-5 m/s <sup>2</sup>
$\rho$	2.0 s	$s_0$	3.0 m
$w_{e_p}$	1	$w_{e_v}$	0.1
$w_u$	1		

In the simulations, we utilize a nonlinear car-following model namely the optimal velocity model (OVM) to generate driving actions of simulated human drivers [200]. The car-following OVM is given as

$$\begin{aligned}
 u_i(t) &= \alpha(V_i(t) - v_i(t)) + \beta\Delta v_i(t), \\
 V_i(t) &= \frac{v_{\max}}{2} (\tanh(\Delta p_i(t) - s_i(t)) + \tanh(s_i(t))).
 \end{aligned}
 \tag{4.10}$$

The parameters of the OVM for each HDV include the driver’s sensitivity coefficients  $\alpha$  and  $\beta$ , and the desired speed  $v_d$ . These parameters for the simulated HDVs are assumed to be different to each other and chosen by random perturbations up to 20% around the following nominal values:  $\alpha = 0.8$ ,  $\beta = 0.6$ ,  $v_d = 15.0$  m/s,  $\rho = 2.0$  s,  $s_0 = 5.0$  m. The parameters and weights in the predictive control framework used for the simulations are given in Table 4.1. The RLS-based estimators are initialized with the following values:  $\gamma_i(0) = [0.67, 0.1, 0.18]^T$  and  $P_i(0) = 0.01 \mathbb{I}_3$  where  $\mathbb{I}_3$  is the  $3 \times 3$  identity matrix, while the forgetting factor is chosen as  $\xi = 1.0$ . Python is used in the simulations in which the constrained optimal control problem is formulated by CasADi framework [201] and solved by a built-in qpOASES solver.

#### 4.1.4 Results and Discussions

The results for a numerical simulation involving a CAV and 2 preceding HDVs are illustrated in Fig. 4.3, in which the speeds and headway of all vehicles are given in Figures 4.3a and 4.3b, respectively. As can be seen from Fig. 4.3b, the simulated HDVs slow down and then stop while approaching the signalized intersection. Given

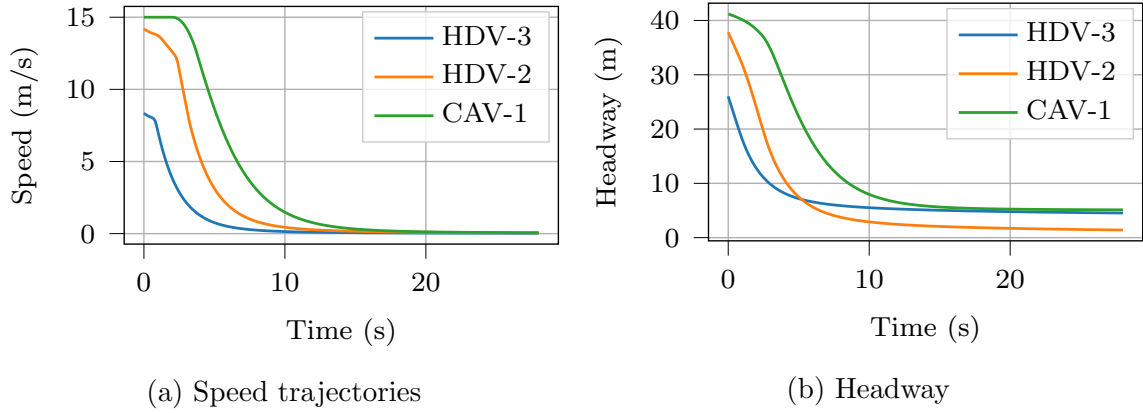


Figure 4.3: Speed and headway of the three vehicles considered in the simulation.

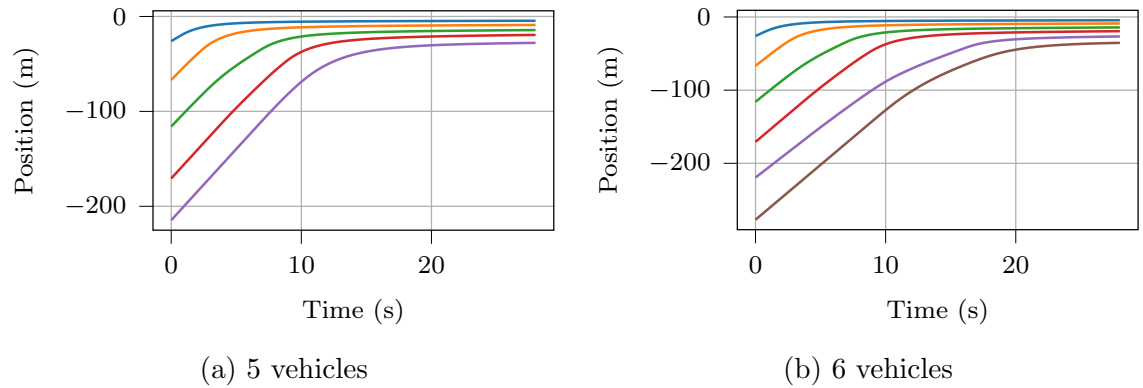


Figure 4.4: Longitudinal trajectories in the simulations with different numbers of vehicles approaching the intersection.

the behavior of the HDVs, the proposed control framework is able to perform safe and comfortable braking for the CAV without violating any of the state, input, and safety constraints.

Moreover, to assess the scalability of the proposed control framework to the number of preceding vehicles, we conduct three other simulations for the scenarios with 5 and 6 vehicles (4 and 5 HDVs, respectively) and demonstrate the vehicle trajectories in Fig. 4.4. These results verify that the proposed control framework works effectively with different numbers of preceding vehicles.

Finally, the estimated parameters in the CTH-RV car-following model for the HDV-2 are depicted in Fig. 4.5. Overall, as more real-time data is added to update

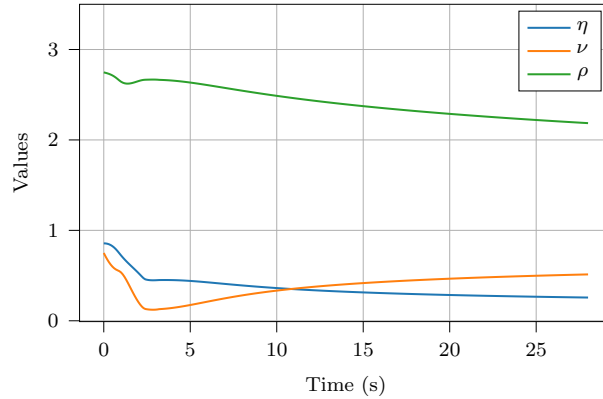


Figure 4.5: Estimates for the car-following parameters of the HDV-2

the estimations, the car-following parameters converge to the set of values that best describe the driving behavior of the HDVs. Therefore, using the linear CTH-RV model and online RLS technique, we can approximate a nonlinear car-following model and use this to predict the future states of the HDVs.

In this section, we addressed the problem of a CAV traveling in a mixed traffic environment and approaching a signalized intersection. A data-driven predictive control framework was developed in which the car-following behavior of HDVs ahead of the CAV is modeled by the CTH-RV model with online estimated parameters through the RLS algorithm. In the proposed framework, by utilizing data-driven car-following models, the CAVs can predict the future behavior of the HDVs and then derive their optimal safety-aware trajectory in a finite horizon. The proposed control framework was validated by numerical simulations with multiple preceding HDVs showing that the generated control actions can ensure safe braking for the CAVs. A direction for future research should focus on extending this framework to consider multi-lane traffic intersections with lane changing behavior of the HDVs.

## 4.2 Coordination at a Mixed Traffic Corridor

One of the research directions towards controlling the CAVs in a mixed traffic environment has been the development of adaptive cruise control [132, 135, 147] where a CAV, preceded by a single or a group of HDVs, applies cruise control to optimize

a given objective, e.g., improvement of fuel economy [136], minimization of backward propagating wave [137, 140], etc. Although these research efforts [97] aim at enhancing our understanding of improving the efficiency through coordination of CAVs in a mixed traffic environment, deriving a tractable solution to the problem of CAV coordination at merging or roundabout scenario remains challenging. Several approaches reported in the literature implemented well-known car-following models, which emulate the human-driving behavior [101, 160], to derive a deterministic quantification of the vehicle trajectory [100, 156]. Other approaches have used car-following models [73] or learning algorithms [105, 106] for CAV coordination in a mixed traffic environment. There have been also some research efforts that have investigated the effects of CAV penetration on a mixed traffic network through microscopic [14] or meso/macroscopic simulation [98, 99] environments.

In this section, we analyze the impact of optimally coordinating CAVs traveling through a mixed traffic corridor including three different scenarios: on-ramp merging, speed reduction zone, and roundabout. In this context, CAVs interact with HDVs at varying penetration rates and different traffic volumes. We study the impact of different penetration rates of CAVs and traffic volumes on the efficiency of the corridor, provide extensive simulation results and report on the benefits in terms of total travel time and fuel economy.

The main features of this section are the (i) development of a simulation environment of an optimal CAV coordination framework at a corridor in a mixed traffic network, and (ii) a detailed analysis of the impact of CAV penetration on the vehicle- and network-level performance, in terms of fuel economy and travel time, under different traffic volumes.

We consider the University of Michigan’s Mcity where CAVs and HDVs are traveling through a particular test route as illustrated by the black trajectory in Fig. 2.7. The route consists of three traffic scenarios, indexed by  $z = 1, 2, 3$ , representing a highway on-ramp, a speed reduction zone, and a roundabout, respectively. Note

that to create traffic congestion in the test route, we consider additional traffic flow at the adjacent roads. Upstream of each traffic scenario, we have the control zone where CAVs coordinate with each other to avoid any rear-end or lateral collision. The length of the control zone is  $L_z \in \mathbb{R}^+$  for each traffic scenario  $z$ . Since the HDVs do not share their state information, we consider the presence of *intelligent coordinators*, which can be loop-detectors, roadside units, or comparable sensory devices, that collect the state information of the HDVs traveling within each control zone. The coordinators transmit the HDVs' state information to each CAV within each control zone using standard vehicle-to-infrastructure communication protocols. We define the area of potential lateral collision to be the *merging zone* of length  $S_z$  specific to traffic scenario  $z$ , as illustrated by the red marked area numbers 1, 2, and 3 in Fig. 2.7. The objective of each CAV is to derive its optimal control input (acceleration/deceleration) to cross the traffic scenarios without any rear-end or lateral collision with the other CAVs and HDVs.

Let  $t_i^{0,z}$  be the time when each vehicle  $i$  enters the control zone towards traffic scenario  $z$ ,  $t_i^{m,z}$  be the time when the each vehicle enters the merging zone of the traffic scenario  $z$ , and  $t_i^{f,z}$  be the time when vehicle  $i$  exits the corresponding merging zone. Let  $\mathcal{N}_z = \{1, \dots, N(t)\}$ ,  $t \in \mathbb{R}^+$ , be a queue of vehicles to be analyzed for traffic scenario  $z$ , where  $N(t)$  is the total number of CAVs within the control zone of the specific traffic scenario  $z$  at time  $t \in \mathbb{R}^+$ . We denote  $\mathcal{N}_{\text{cav}}$  and  $\mathcal{N}_{\text{hdv}}$  to be the set of CAVs and HDVs such that  $\mathcal{N}_{\text{cav}} \cup \mathcal{N}_{\text{hdv}} = \mathcal{N}_z$ . The dynamics of each vehicle  $i \in \mathcal{N}_z$  are modeled as (2.3), where  $p_i(t) \in \mathcal{P}_i$ ,  $v_i(t) \in \mathcal{V}_i$ , and  $u_i(t) \in \mathcal{U}_i$  denote the position, speed, and acceleration/deceleration (control input) of each vehicle  $i$ . Let  $\mathbf{x}_i(t) = [p_i(t) \ v_i(t)]^T$  denote the state of each vehicle  $i$ , with initial value  $\mathbf{x}_i(t_i^{0,z}) = [p_i(t_i^{0,z}) \ v_i(t_i^{0,z})]^T$ . We impose the state, control and safety constraints as in (2.4), (2.7) and (2.5), respectively.

For the CAV  $i \in \mathcal{N}_{\text{cav}}$ , the control input  $u_i(t)$  in (2.3) can be derived within the control zone, the structure of which we discuss in Section 4.2.1. In contrast, we consider a generic car-following model of the following form to derive the control input

of each HDV  $i \in \mathcal{N}_{hdv}$ . In this work, we employ the Wiedemann car-following model proposed in [160]. In the modeling framework described above, we consider perfect communication (Assumption 2.1.2), no lane changes or left/right turns (Assumption 2.1.1), and feasible initial conditions (Assumption 2.1.3).

#### 4.2.1 Hierarchical Control Framework

For each CAV  $i \in \mathcal{N}_{cav}$ , we adopt the optimal control problem presented in Section 2.1, i.e.,

$$\begin{aligned} \min_{u_i} \frac{1}{2} \int_{t_i^{0,z}}^{t_i^{m,z}} u_i^2(t) dt, \quad \forall i \in \mathcal{N}_z, \quad \forall z = 1, 2, 3, \quad (4.11) \\ \text{subject to : (2.3), (2.4),} \\ p_i(t_i^{0,z}) = p_i^{0,z}, \quad v_i(t_i^{0,z}) = v_i^{0,z}, \quad p_i(t_i^{m,z}) = p_z, \\ \text{and given } t_i^{0,z}, t_i^{m,z}, \end{aligned}$$

where  $p_z$  is the location (i.e., entry position) of merging zone  $z$ ;  $p_i^{0,z}, v_i^{0,z}$  are the initial position and speed of vehicle  $i$  when it enters the control zone of traffic scenario  $z$ , respectively. The merging time  $t_i^{m,z}$  can be obtained by solving an upper-level control problem including the safety constraints (2.5), (2.7) in an iterative manner, as detailed in Chapter 3. Suppose that, each CAV  $i \in \mathcal{N}_z$  is aware of the information of the sets  $\mathcal{L}_i^z$  and  $\mathcal{C}_i^z$ , which contain the unique id of the preceding vehicles traveling on the same lane, or on a conflict lane relative to CAV  $i$ , respectively. Then, each CAV  $i$  determines the time  $t_i^{m,z}$  that will be entering the traffic zone  $z = 1, 2, 3$ , upon arrival at the entry of the corridor as follows (see [177]). If vehicle  $(i-1) \in \mathcal{L}_i^z$  and  $(i-1) \in \mathcal{N}_{cav}$ , we have

$$t_i^{m,z} = \max \left\{ \min \left\{ t_{i-1}^{m,z} + \frac{\delta(v_i(t))}{v_{i-1}(t_{i-1}^{m,z})}, t_i^{0,z} + \frac{L_z}{v_{\min}} \right\}, t_i^{0,z} + \frac{L_z}{v_0(t_i^{0,z})}, t_i^{0,z} + \frac{L_z}{v_{\max}} \right\}, \quad (4.12)$$

while, if vehicle  $(i-1) \in \mathcal{C}_i^z$  and  $(i-1) \in \mathcal{N}_{cav}$ , then

$$t_i^{m,z} = \max \left\{ \min \left\{ t_{i-1}^{m,z} + \frac{S_z}{v_{i-1}(t_{i-1}^{m,z})}, t_i^{0,z} + \frac{L_z}{v_{\min}} \right\}, t_i^{0,z} + \frac{L_z}{v_0(t_i^{0,z})}, t_i^{0,z} + \frac{L_z}{v_{\max}} \right\}, \quad (4.13)$$

where  $L_z$  and  $S_z$  are the length of the control zone and the length of the area of potential lateral collision, respectively.

Note that, if the vehicle preceding CAV  $i$  is an HDV, i.e.,  $(i - 1) \in \mathcal{N}_{\text{hdv}}$ , then we apply  $t_{i-1}^{m,z} = t_{i-1}^{0,z} + \frac{L_z}{v_{i-1}(t_{i-1}^{0,z})}$  to estimate the merging time  $t_{i-1}^{m,z}$  of HDV  $i - 1$ . We then use  $t_{i-1}^{m,z}$  in (4.12)-(4.13) to derive the merging time  $t_i^{m,z}$  of CAV  $i$ . The recursion of the above computation is initialized when the first vehicle enters the control zone.

Using Hamiltonian analysis [188], the unconstrained optimal control input  $u_i^*(t)$  of CAV  $i \in \mathcal{N}_z$  and the corresponding state trajectories at time  $t \in [t_i^{0,z}, t_i^{m,z}]$  are [165]

$$u_i^*(t) = a_i \cdot t + b_i, \quad (4.14)$$

where  $a_i, b_i$  are the constants of integration and can be computed using the analysis presented in Section 3.1.2.

For the control of CAVs in a mixed environment, if the physically leading vehicle of a CAV is HDV, the CAV will probe the safety constraint continuously to make an adjustment to its travel behavior. A switching mechanism is applied in the study: the control algorithm for a CAV would always be switched on until the safety constraint (2.5) is activated in terms of the distance between itself and its preceding HDV.

#### 4.2.2 Analysis of the Penetration Impact

To implement the control framework presented in the previous section, we use the microscopic multi-modal commercial traffic simulation software PTV VISSIM [184, 202] by creating a simulation environment replicating Mcity, as shown in Fig. 2.7. The corridor through which the vehicle travels has a length of 1,300 m within the Mcity. The maximum and minimum accelerations considered for each vehicle are 1.5 m/s<sup>2</sup> and -3.0 m/s<sup>2</sup>, respectively. The speed limit on the on-ramp merging, speed reduction zone, and roundabout are 40 m/s, 18.6 m/s, and 25 m/s, respectively. The control zone length is 150 m and the safe headway time considered is 1.2 s. The traffic flow for each volume is 300 [vph/lane], 400 [vph/lane], and 500 [vph/lane]. We employ the desired traffic congestion by modifying the vehicle flow per hour per lane in the considered route and its adjacent roadways.

In this study, we consider the following three different cases:

**Baseline:** We construct the baseline case considering all the vehicles to be HDVs and without any communication capability. The vehicles subscribe to the VISSIM built-in Wiedemann car following model [160] to emulate the driving behavior of real human-driven vehicles. We adopt priority-based (yield/stop) traffic movement at the roundabout and on-ramp merging scenarios.

**Optimal Coordination:** In this case, all the vehicles are CAVs and communicate with each other inside the control zone. Therefore, they can optimize their travel time and fuel efficiency, and plan their optimal trajectories. We consider three isolated coordinators for each traffic scenario. For the uncontrolled paths in-between the control zones, the CAVs revert to the Wiedemann car following model [160] to traverse their respective routes. To apply the optimal control framework, we override VISSIM’s built-in car following module and associated attributes using the DriverModel API.

**Partial Penetration:** To simulate the partial penetration case, we consider both of the above cases as the two extremes and traverse the cases in between with different percentages of CAV inclusion. We adopt a priority-based (yield/stop) traffic movement at the roundabout and on-ramp merging scenarios only for the HDVs, whereas the CAVs are allowed to ignore the traffic signs while exiting a traffic scenario when it is safe to do so.

In our simulation study, we consider high, medium, and low traffic volumes for the test route as 500, 400 and 300 vehicles per hour, and for the adjacent roads as 800, 600 and 400 vehicles per hour, respectively.

We analyzed the impact of 11 different penetration rates of CAVs ranging from 0% to 100% that may have on fuel economy, travel time improvement as well as the mean speed changes, and driving behavior. For the fuel consumption analysis, we used the polynomial metamodel presented in [67]. Using different penetration rates of CAVs, the simulation results allow several observations. First, for all traffic volumes,

fuel economy increases when the penetration rate of CAVs increases, as shown in Fig. 4.6. It is observed that the fuel economy is improved within increasing penetration rate for all traffic volumes. Similarly, the average travel time decreases with the increase in penetration rate, which represents an improvement in the traffic flow of the network (Fig. 4.7). Note that, the average speed of the vehicles increases with decreasing traffic volume, as shown in Fig. 4.7. This is an expected phenomenon, as lower traffic volume results in fewer braking events. On the other hand, the effect of penetration has a significant effect on the average speed of the vehicles, as shown in Fig. 4.8 for a high traffic volume. For 0% penetration rate (top panel of Fig. 4.8), congestion at the traffic scenarios are prevalent. However, with the increase in CAV penetration, the stop-and-go driving behavior decreases (middle panel of Fig. 4.8) and at 100% penetration rate (bottom panel of Fig. 4.8), congestion is completely eliminated. It is also interesting to note that, the low traffic volume case does not have significant variation with different CAV penetration rate, as shown in the travel time and average speed distribution in Fig. 4.7. This is due to the fact that, at low traffic volume, vehicles encounter less congestion events at the conflict points and traverse the traffic corridor in an almost “coordinate” way.

Table 4.2: Fuel economy improvement for HDVs.

CAV penetration rate [%]	Fuel economy improvement [%]		
	High	Medium	Low
10	2.3	-1	0
20	0.3	0.7	5.4
30	-0.3	1.7	2.9
40	1.2	-0.7	3.1
50	2.7	2	4.1
60	2.6	7.4	7.2
70	0.5	5.2	9
80	-1.2	7.5	14.3
90	9.8	18.7	23.4

The fuel economy of the HDVs are summarized in Table 4.2. For all the traffic volume cases, the HDVs exhibit fuel economy improvement as shown in Table 4.2.

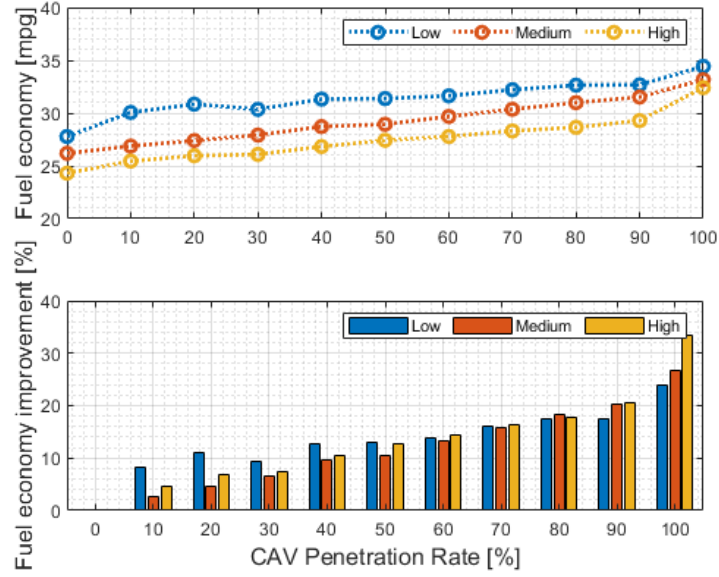


Figure 4.6: Impact of CAV penetration rate on the fuel economy under low, medium, and high traffic volumes.

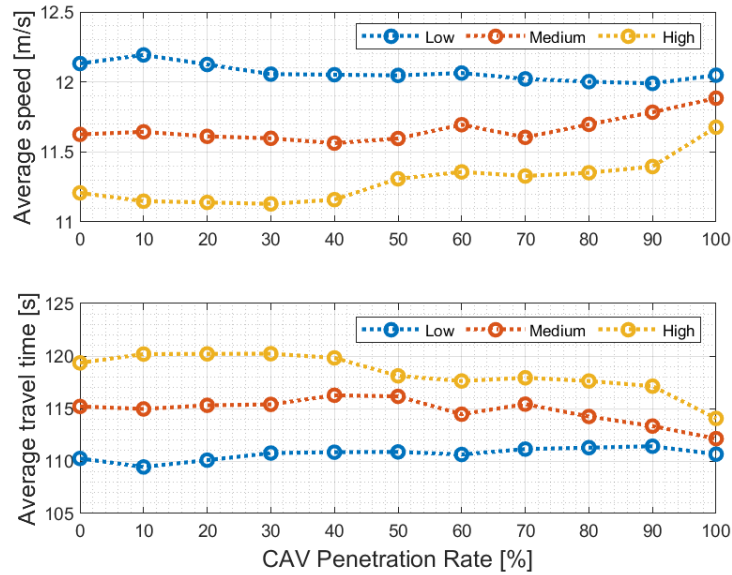


Figure 4.7: Effect of different penetration rates of CAVs on average speed and travel time.

However, the best penetration rate in terms of the HDVs fuel economy is 90%. This

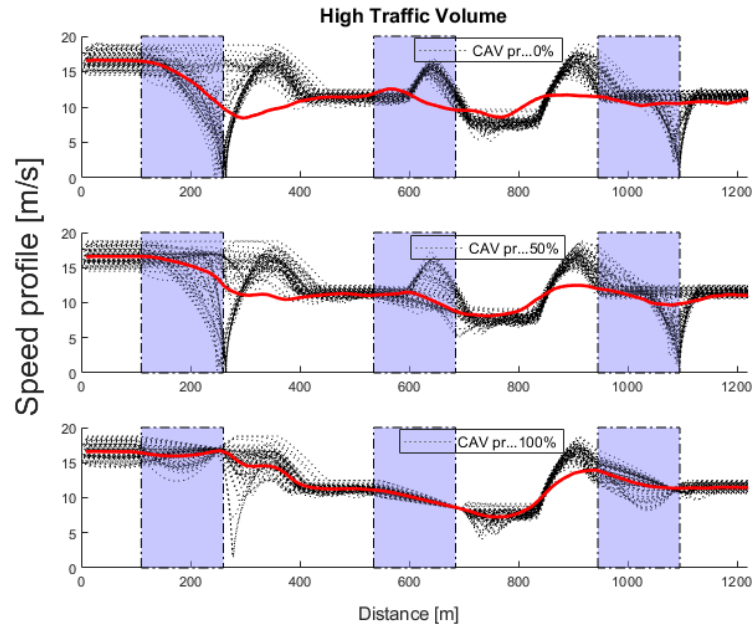


Figure 4.8: High traffic volume speed profile at the baseline, 50% penetration rate and 100% scenario. Stop-and-go driving behavior decreases for 50% and is avoided at 100% penetration case.

significant improvement in HDV fuel economy is due to the fact that, at 90% penetration rate, the CAVs have higher coordination at the traffic junction, which results in a congestion-free environment for the rest of the HDVs.

In this section, the impact of different penetration rates of CAVs and their interaction with HDVs time is analyzed from a network-level perspective. The results indicate that for higher penetration rates, the improvement in fuel economy, travel time and average speed is significant. The analysis also shows similar trend across different traffic volume cases, which indicates that the improvement due to increased CAV penetration scales well with the traffic demand of the network.

## Chapter 5

### PLATOON FORMATION IN A MIXED TRAFFIC ENVIRONMENT

In this chapter, I address the problem of deriving the optimal trajectory of a CAV in a mixed traffic environment that considers the interaction of HDVs. Since HDVs cannot be controlled directly, and any prediction of their future trajectories suffers from stochastic human driving behavior, it is challenging to establish any cooperation between the CAVs and HDVs. The hypothesis is that the motion trajectory of the CAVs can be controlled directly to restrict the motion of its trailing HDVs, thus imparting indirect control on the HDVs. One natural solution to validate the above hypothesis is to leverage the concept of vehicle platooning, where a CAV within the network can be controlled to force the trailing HDVs to form a platoon. In this chapter, I propose a constrained multi-objective receding horizon control framework that considers linear, non-linear, and data-driven prediction models, and enables mixed platoon formation by directly controlling the CAVs with enhanced rear-end collision safety. The optimization objectives of the CAV are (a) to form a platoon with the trailing HDVs, and (b) to minimize its control effort. The proposed platoon formation framework employs a receding horizon controller that uses a *multi-successor safety constraint* to enforce rear-end collision avoidance constraints for multiple trailing HDVs while deriving and implementing the optimal control input of the CAV. I propose two variants of the receding horizon control, namely, a model-dependent and a model-independent framework that employs different prediction models for estimating the HDV trajectories: (a) a naive linear constant speed model, (b) a nonlinear car-following model with nominal parameters and (c) a data-driven model that estimates the driving behavior of the HDVs in real time using recursive least squares algorithm to better predict the

futures trajectories. In short, the approach proposed in this contribution will guarantee the indirect control of the HDVs by forming mixed platoons.

The structure of this chapter is organized as follows. In Section 5.1, I formulate the problem of platoon formation in a mixed traffic environment and derive an analytical solution with feasibility analysis. Then, I present a model-agnostic optimal platoon formation framework in Section 5.2. Continuing further, in Section 5.3 I develop a safety-prioritized framework for creating a mixed platoon of vehicles by proposing a constrained multi-objective receding horizon control approach that considers linear, non-linear, and data-driven prediction models with enhanced safety guarantee.

## 5.1 A Condition-based Control Framework for Platoon Formation

In this section, I address the problem of vehicle platoon formation in a traffic network with partial CAV penetration rates. We investigate the interaction between CAV and human-driven vehicle (HDV) dynamics and provide a rigorous control framework that enables platoon formation with the HDVs by only controlling the CAVs within the network. We present a complete analytical solution of the CAV control input and the conditions under which a platoon formation is feasible. We evaluate the solution and demonstrate the efficacy of the proposed framework using simulation. The specific contributions of this research are: (i) the development of a comprehensive framework that can aim at creating platoon formations of HDVs led by a CAV in a mixed traffic environment, and (ii) an analytical solution for the control input of CAVs (Theorems 5.1.9 and 5.1.14), along with the conditions under which the solution is feasible (Theorems 3.1.7 and 5.1.15). In our exposition, we seek to establish a rigorous control framework that enables the platoon formation in a mixed environment with associated boundary conditions.

### 5.1.1 Problem Formulation

We consider a CAV followed by one or multiple HDVs traveling in a single-lane roadway of length  $L \in \mathbb{R}^+$ . We subdivide the roadway into a *buffer zone* of length  $L_b \in \mathbb{R}^+$ , inside of which the HDVs' state information is estimated (Fig. 5.1) (top), and a *control zone* of length  $L_c \in \mathbb{R}^+$  such that  $L = L_b + L_c$ , where the CAV is controlled to form a platoon with the trailing HDVs, as shown in Fig. 5.1 (bottom). The time that a CAV enters the buffer zone, the control zone, and exits the control zone is  $t^b, t^c, t^f \in \mathbb{R}^+$ , respectively.

Let  $\mathcal{N} = \{1, \dots, N\}$ , where  $N \in \mathbb{N}$  is the total number of vehicles traveling within the buffer zone at time  $t = t^c$ , be the set of vehicles considered to form a platoon. Here, the leading vehicle indexed by 1 is the CAV, and the rest of the trailing vehicles in  $\mathcal{N} \setminus \{1\}$  are HDVs. We denote the set of the HDVs following the CAV to be  $\mathcal{N}_{\text{HDV}} = \{2, \dots, N\}$ . Since the HDVs do not share their local state information with any external agents, we consider the presence of a *coordinator* that gathers the state information of the trailing HDVs traveling within the buffer zone. The coordinator, which can be a group of loop-detectors or comparable sensory devices, then transmits the HDV state information to the CAV at each time instance  $t \in [t^b, t^c]$  using a standard vehicle-to-infrastructure communication protocol.

The objective of the CAV 1 is to derive and implement a control input (acceleration/deceleration) at time  $t^c \in \mathbb{R}^+$  so that the platoon formation with trailing HDVs in  $\mathcal{N}_{\text{HDV}}$  is completed within the control zone at a given time  $t^p \in (t^c, t^f]$ . In our framework, we model the longitudinal dynamics of each vehicle  $i \in \mathcal{N}$  as a double-integrator,

$$\dot{p}_i(t) = v_i(t), \quad \dot{v}_i(t) = u_i(t), \quad t \in \mathbb{R}^+, \quad (5.1)$$

where  $p_i(t) \in \mathcal{P}_i$ ,  $v_i(t) \in \mathcal{V}_i$ , and  $u_i(t) \in \mathcal{U}_i$  are the position of the front bumper, speed, and control input (acceleration/deceleration) of vehicle  $i \in \mathcal{N}$ . The sets  $\mathcal{P}_i$ ,  $\mathcal{V}_i$ , and  $\mathcal{U}_i$ ,  $i \in \mathcal{N}$ , are complete and totally bounded subsets of  $\mathbb{R}$ . Let  $\mathbf{x}_i(t) = [p_i(t) \ v_i(t)]^T$

denote the state vector of each vehicle  $i \in \mathcal{N}$ , taking values in  $\mathcal{X}_i = \mathcal{P}_i \times \mathcal{V}_i$ .

The speed  $v_i(t)$  and control input  $u_i(t)$  of each vehicle  $i \in \mathcal{N}$  are subject to the following constraints,

$$\begin{aligned} 0 < v_{\min} \leq v_i(t) \leq v_{\max}, \quad t \in \mathbb{R}^+, \\ u_{\min} \leq u_i(t) \leq u_{\max}, \quad t \in \mathbb{R}^+, \end{aligned} \quad (5.2)$$

where  $v_{\min}$  and  $v_{\max}$  are the minimum and maximum allowable speed of the considered roadway, respectively, and  $u_{\min}$  and  $u_{\max}$  are the minimum and maximum control input of all vehicles  $i \in \mathcal{N}$ , respectively.

The dynamics (5.1) of each vehicle  $i \in \mathcal{N}$  can take different forms based on the consideration of connectivity and automation. For the CAV  $1 \in \mathcal{N}$ , the control input  $u_1(t)$  can be derived and implemented within the control zone. We introduce and discuss the structure of the control policy in detail in Section 5.1.2. To model the HDV dynamics, we need the following definitions.

**Definition 5.1.1.** The dynamic following spacing  $s_i(t)$  between two consecutive vehicles  $i$  and  $(i - 1) \in \mathcal{N}$  is,

$$s_i(t) = \rho_i \cdot v_i(t) + s_0, \quad (5.3)$$

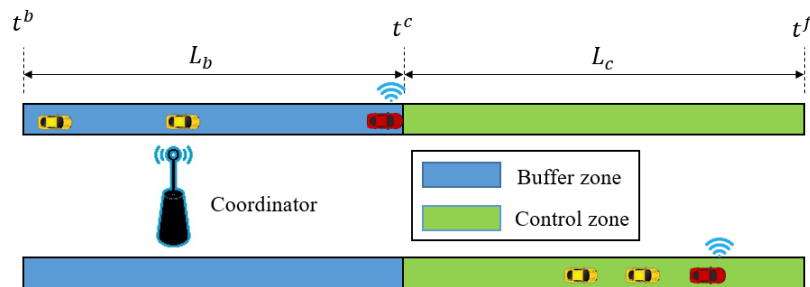


Figure 5.1: A CAV (red) traveling with two trailing HDVs (yellow), where the HDVs' state information is estimated (top scenario) by the coordinator within the buffer zone, and the platoon is formed (bottom scenario) by controlling the CAV inside the control zone.

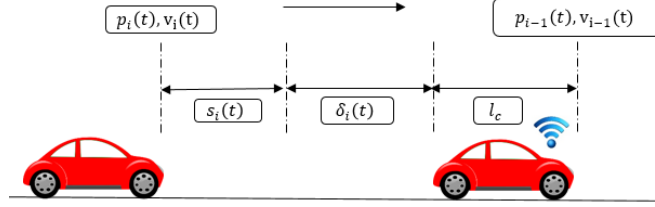


Figure 5.2: Predecessor-follower coupled car-following dynamic.

where  $\rho_i$  denotes a desired time gap that each HDV  $i \in \mathcal{N}_{\text{HDV}}$  maintains while following the preceding vehicle, and  $s_0$  is the standstill distance denoting the minimum bumper-to-bumper gap at stop.

**Definition 5.1.2.** The *headway*  $\Delta p_i(t)$  (see Fig. 5.2) and the *approach rate*  $\Delta v_i(t)$  of vehicle  $i \in \mathcal{N}$  between two consecutive vehicles  $i, (i-1) \in \mathcal{N}$  are  $\Delta p_i(t) = p_{i-1}(t) - p_i(t) - l_c$  and  $\Delta v_i(t) = v_{i-1}(t) - v_i(t)$ , respectively, where  $l_c \in \mathbb{R}^+$  is the length of each vehicle  $i \in \mathcal{N}$ .

**Definition 5.1.3.** The *platoon gap*  $\delta_i(t)$  is the difference between the bumper-to-bumper inter-vehicle spacing and the dynamic following spacing  $s_i(t)$  (see Fig. 5.2) between two consecutive vehicles  $i$  and  $(i-1) \in \mathcal{N}$ , i.e.,

$$\delta_i(t) = p_{i-1}(t) - p_i(t) - s_i(t) - l_c, \quad (5.4)$$

where  $l_c$  is the length of each vehicle  $i \in \mathcal{N}$ .

In our approach, we adopt the optimal velocity car-following model [200], to define the predecessor-follower coupled dynamics (see Fig. 5.2) of each HDV  $i \in \mathcal{N}_{\text{HDV}}$  as follows,

$$u_i(t) = \alpha(V_i(\delta_i(t - \eta_i), s_i(t - \eta_i)) - v_i(t - \eta_i)), \quad (5.5)$$

where  $\alpha$  denotes the control gain representing the driver's sensitivity coefficient,  $\eta_i$  is the driver's perception delay with a known upper bound  $\bar{\eta}$ , and  $V_i(\delta_i(t), s_i(t))$  denotes the equilibrium speed-spacing function,

$$V_i(\delta_i(t), s_i(t)) = \frac{v_{\max}}{2} (\tanh(\delta_i(t)) + \tanh(s_i(t))). \quad (5.6)$$

**Remark 5.1.1.** Based on (5.6), the driving behavior of each HDV  $i \in \mathcal{N}_{\text{HDV}}$  depends on two different modes; (a) *decoupled free-flow mode*: when  $\delta_i(t) > 0$ , each HDV converges to the maximum allowable speed  $v_{\max}$ , and cruises through the roadway decoupled from the state of the preceding vehicle, and (b) *coupled following mode*: when  $\delta_i(t) \leq 0$ , the HDV dynamics becomes coupled with the state of the preceding vehicle  $(i-1) \in \mathcal{N}$ , and  $v_i(t)$  converges to  $v_{i-1}(t)$ . Note that, if there is no preceding vehicle, we set  $\delta_i(t) = \infty$  that activates the decoupled free-flow mode, which results in  $v_i(t)$  converging to  $v_{\max}$ .

**Remark 5.1.2.** The car-following model (5.5) is platoon-stable, i.e., bounded speed fluctuation between two consecutive vehicles in coupled following mode decays exponentially as time progresses [200].

We now provide the following definitions that are necessary for the formulation of our proposed platoon formation framework.

**Definition 5.1.4.** The information set  $\mathcal{I}_1(t)$  of the CAV  $1 \in \mathcal{N}$  has the following structure,

$$\mathcal{I}_1(t) = \{\mathbf{x}_1(t), \mathbf{x}_{2:N}(t)\}, \quad t \in [t^b, t^c], \quad (5.7)$$

where  $\mathbf{x}_{2:N}(t) = [\mathbf{x}_2(t), \dots, \mathbf{x}_N(t)]^T$ .

**Definition 5.1.5.** The steady-state traffic flow between two consecutive vehicles  $i$  and  $(i-1) \in \mathcal{N}$  are established if the platoon gap  $\delta_i(t)$  does not vary with time, and approach rate  $\Delta v_i(t) := v_i(t) - v_{i-1}(t)$  is zero [203], i.e.,

$$\delta_i(t) = c_i, \quad c_i \in \mathbb{R}, \quad \text{and} \quad \Delta v_i(t) = 0. \quad (5.8)$$

We now formalize the problem of platoon formation in a mixed environment addressed in this section as follows.

**Problem 5.1.1.** *Given the information set  $\mathcal{I}_1(t)$  at time  $t = t^c$ , the objective of the CAV  $1 \in \mathcal{N}$  is to derive the control input  $u_1(t)$  so that the HDVs in  $N_{\text{HDV}}$  are forced*

to form a platoon at some time  $t^p \in (t^c, t^f]$  within the control zone while the following conditions hold,

$$v_i(t) = v_{eq}, \quad \delta_i(t) = c_i, \quad c_i \leq 0, \quad \forall t \geq t^p, \quad \forall i \in \mathcal{N},$$

subject to: (5.2),  $p_1(t^p) \leq L_c$ , (5.9)

where,  $v_{eq}$  denotes the equilibrium platoon speed.

**Remark 5.1.3.** In our problem formulation, we impose the restriction that at  $t = t^c$ , there exists at least one HDV  $i \in \mathcal{N}_{\text{HDV}}$  such that  $\delta_i(t^c) > 0$ . To simplify the formulation and without loss of generality, we consider that  $\delta_N(t^c) > 0$ . This ensures that we do not have the trivial case where the group of vehicles in  $\mathcal{N}$  has already formed a platoon at  $t = t^c$ .

In the modeling framework presented above, we impose the following assumption.

**Assumption 5.1.1.** The CAV is on a decoupled free-flow mode (Remark 5.1.1) while all vehicles have reached steady-state traffic flow (Definition 5.1.5) within  $[t^b, t^c]$ .

**Remark 5.1.4.** We restrict the control of the CAV 1 only within the control zone so that we have a finite control horizon  $[t^c, t^f]$ . Outside the control zone, the CAV dynamics follows the car-following model in (5.5).

**Lemma 5.1.6.** For each vehicle  $i \in \mathcal{N}$ ,  $v_i(t^c) = v_{\max}$ .

*Proof.* Since the control input  $u_1(t)$  of the uncontrolled CAV  $1 \in \mathcal{N}$  is determined by (5.5) outside the control zone (Remark 5.1.4), and due to the fact that any vehicle following the dynamics in (5.5) converges to the maximum speed  $v_{\max}$  without the presence of a preceding vehicle (Remark 5.1.1),  $v_1(t)$  converges to  $v_{\max}$ .

For a HDV  $i \in \mathcal{N}_{\text{HDV}}$  traveling under the steady-state traffic flow condition (Assumption 5.1.1),  $\delta_i(t)$  does not vary with time. This implies that each HDV  $i$  either travels with decoupled free-flow mode with  $v_i(t) = v_{\max}$ , or with coupled following mode with  $v_i(t) = v_{i-1}(t) = v_{\max}$ . □

In what follows, first, we address Problem 5.1.1 considering only two vehicles, i.e.,  $N = 2$ , and then generalize the analysis for multiple HDVs, i.e.,  $N > 2$ .

### 5.1.2 Control Framework for Platoon Formation

For  $N = 2$ , CAV  $1 \in \mathcal{N}$  is trailed by HDV  $2 \in \mathcal{N}_{\text{HDV}}$ . The information set  $\mathcal{I}_1(t^c)$  includes  $v_1(t^c) = v_2(t^c) = v_{\max}$  (Lemma 5.1.6), and  $\delta_2(t^c) > 0$  (Remark 5.1.3). The following result characterizes the control structure of CAV  $1 \in \mathcal{N}$  for the platoon formation framework.

**Lemma 5.1.7.** *For a CAV  $1 \in \mathcal{N}$  travelling with a trailing HDV  $2 \in \mathcal{N}_{\text{HDV}}$ , (i) a platoon formation does not occur when  $u_1(t) \geq 0$  for all  $t \in [t^c, t^f]$ , and (ii) a platoon formation occurs with an appropriate control zone of length  $L_c$  when  $u_1(t) < 0$  for all  $t \in [t^c, t^a]$ ,  $t^c < t^a < t^f$ .*

*Proof.* Part (i): For  $u_1(t) \geq 0$  for all  $t \geq t^c$ , we have  $\delta_2(t) > 0$  for all  $t \geq t^c$ , which implies that according to (5.9), no platoon formation will occur.

Part (ii): For  $u_1(t) < 0$  within an arbitrary time horizon  $[t^c, t^a]$ ,  $t^c < t^a < t^f$ , we have  $v_1(t^a) < v_1(t^c)$ . Since  $v_1(t^c) = v_2(t^c) = v_{\max}$  (Lemma 5.1.6), we have  $v_2(t^a) > v_1(t^a)$ . This implies that  $\delta_2(t)$  decreases for all  $t \geq t^a$ . As time  $t$  progresses, given an appropriate control zone of length  $L_c$ , we have  $\delta_2(t) \rightarrow 0$ , which guarantees a platoon formation.  $\square$

When the CAV  $1 \in \mathcal{N}$  applies a control input  $u_1(t)$ ,  $t \in [t^c, t^p]$  based on Lemma 5.1.7 to form a platoon with the HDV  $2 \in \mathcal{N}_{\text{HDV}}$  at time  $t = t^p$ , two sequential steps take place, namely, (i) the *platoon transition* step, where the HDV 2 transitions from the decoupled free-flow mode to the coupled following mode at time  $t = t^s$ ,  $t^c < t^s < t^p$  such that  $\delta_2(t^s) = 0$ , and (ii) the *platoon stabilization* step, where  $v_2(t)$  converges to  $v_1(t)$  at time  $t = t^p$  such that (5.9) is satisfied, and the platoon becomes stable.

**Definition 5.1.8.** The platoon transition duration  $\tau^t$  is the time required for the completion of the platoon transition step, i.e.,  $\tau^t = t^s - t^c$ , and the platoon stabilization

duration  $\tau^s$  is the time required for the completion of the platoon stabilization step, i.e.,  $\tau^s = t^p - t^s$ . Hence, we have  $t^p = t^c + \tau^t + \tau^s$ .

**Remark 5.1.5.** The platoon stabilization duration is  $\tau^s = \eta_i + \tau^r$ , where  $\eta_i$  is the perception delay of HDV  $i \in \mathcal{N}_{\text{HDV}}$ , and  $\tau^r$  is the response time of (5.5) which depends on the driver's sensitivity coefficient  $\alpha$ , maximum allowable speed fluctuation, and the choice of equilibrium speed-spacing function in (5.6), and can be computed using stability analysis presented in [200, 204, 205]. Note that, for  $N \geq 2$ , additional nonlinearities may impact the computation of  $\tau^s$ . In our formulation, we incorporate the upper bound of the perception delay  $\bar{\eta}$  to achieve robustness such that  $\tau^s = \bar{\eta} + \tau^r$ , and consider that  $\tau^r$  is given a priori. Thus we focus only on the analysis of the platoon transition time  $\tau^t$ .

Using Lemma 5.1.7, we construct the structure of the control input  $u_1(t)$  for the CAV  $1 \in \mathcal{N}$  for generating a platoon with the trailing HDV  $2 \in \mathcal{N}$  at time  $t^p \in (t^c, t^f]$ ,

$$u_1(t) = \begin{cases} u_p, & u_p \in [u_{\min}, 0), & t \in [t^c, t^s], \\ 0, & & t \in (t^s, t^f]. \end{cases} \quad (5.10)$$

According to (5.10), the realization of the control input  $u_1(t)$  of the CAV  $1 \in \mathcal{N}$ , which is  $u_p \in (0, u_{\min}]$  in  $t \in [t^c, t^s]$ , yields a linearly decreasing  $v_1(t)$  in  $t \in [t^c, t^s]$ .

The following result provides the unconstrained relation between the platoon transition duration  $\tau^t$  and CAV control input parameter  $u_p$ .

**Theorem 5.1.9.** *For a CAV  $1 \in \mathcal{N}$  and a trailing HDV  $2 \in \mathcal{N}_{\text{HDV}}$ , there exists an unconstrained control input parameter  $u_p$  in (5.10) such that a vehicle platoon can be formed with HDV  $2 \in \mathcal{N}$  at time  $t = t^p$  according to the following condition,*

$$2\delta_2(t^c) + u_p \cdot (\tau^t)^2 = 0. \quad (5.11)$$

*Proof.* At  $t^s = t^c + \tau^t$ , we require  $\delta_2(t^s) = 0$  implying  $p_1(t^s) - p_2(t^s) = s_2(t^s) + l_c$ , which we expand as follows. Using (5.1) at time  $t^s = t^c + \tau^t$ , we have  $p_1(t^c + \tau^t) =$

$p_1(t^c) + v_1(t^c) \cdot \tau^t + \frac{1}{2}u_p \cdot (\tau^t)^2$ . Based on Lemma 5.1.6,  $v_1(t^c) = v_{max}$ . For HDV 2  $\in \mathcal{N}_{HDV}$ ,  $\delta_2(t) > 0$  (Remark 5.1.3) until the platoon transition step at time  $t = t^s$ . This implies, that HDV 2 travels with decoupled free-flow mode as in (5.5), and  $v_2(t) = v_{max}$  for all  $t \in [t^c, t^s]$  (Lemma 5.1.6). Using (5.5) for HDV 2 at time  $t^s = t^c + \tau^t$ , we have,  $v_2(t^c + \tau^t) = v_2(t^c) = v_{max}$  and  $p_2(t^c + \tau^t) = p_2(t^c) + v_2(t^c) \cdot \tau^t$ . Substituting the last equation into (5.3), we have  $s_2(t^s) = s_2(t^c)$ , and hence  $p_1(t^c) + v_1(t^c) \cdot \tau^t + \frac{1}{2}u_p \cdot (\tau^t)^2 - p_2(t^c) - v_2(t^c) \cdot \tau^t = s_2(t^c) + l_c$ . Simplifying using (5.4), the result follows.  $\square$

**Remark 5.1.6.** From (5.11), as  $u_p \rightarrow 0$ , we have  $\tau^t \rightarrow \infty$ , which implies that platoon formation will never occur. If  $u_p > 0$ , then (5.11) yields an infeasible  $\tau^t$ . Therefore,  $u_p$  has to be strictly negative for platoon formation. Note, from (5.11), for  $\delta_2(t) > 0$  and  $t \in \mathbb{R}^+$ , we have  $u_p < 0$ .

### 5.1.2.1 Feasibility of Platoon Formation

In Theorem 5.1.9, we do not explicitly incorporate the state and control constraints in (5.2), and the terminal constraint in (5.9). For a given platoon formation time  $t^p$ , the corresponding control input derived from (5.11) can violate constraints in (5.2). In what follows, we present Lemmas 5.1.10 and 5.1.11 that provide a feasible region of  $\tau^t$  that yields an admissible control input parameter  $u_p$  in (5.11).

**Lemma 5.1.10.** *For CAV 1  $\in \mathcal{N}$ , the platoon transition duration  $\tau^t$  subject to the state and control constraints in (5.2) is feasible if the following condition holds,*

$$\tau^t \geq \max \left\{ \left( \frac{-2\delta_2(t^c)}{u_{\min}} \right)^{\frac{1}{2}}, \frac{2\delta_2(t^c)}{v_1(t^c) - v_{\min}} \right\}. \quad (5.12)$$

*Proof.* Suppose that, for CAV 1  $\in \mathcal{N}$ ,  $u_p = u_{\min}$  yields a corresponding platoon transition duration  $\tau^{t_1}$ . From (5.11), we have  $(\tau^{t_1})^2 = \frac{-2\delta_2(t)}{u_{\min}}$ . Therefore, for any  $\tau^t$  to be feasible such that  $u_p \in [u_{\min}, 0)$ , we require  $\tau^t \geq \tau^{t_1}$ , which yields the inequality with the first term in (5.12).

Now, suppose that for CAV 1  $\in \mathcal{N}$ , a platoon transition duration  $\tau^t$  has associated control input parameter  $u_p$  derived from (5.11). Using (5.1), we have,

$v_1(t^c + \tau^t) = v_1(t^c) + u_p \cdot \tau^t$ . Since  $u_p \in [u_{\min}, 0)$ , we require that  $v_1(t^c + \tau^t) \geq v_{\min}$  to satisfy the state constraint in (5.2). Substituting  $v_1(t^c + \tau^t)$  in the above inequality, we get  $u_p \cdot \tau^t \geq v_{\min} - v_1(t^c)$ . Finally, substituting  $u_p$  from (5.11) in the above equation yields the inequality with the second term in (5.12).

Finally, since both above inequalities yield lower bounds on  $\tau^t$ , we simply take their maximum and get (5.12).  $\square$

**Remark 5.1.7.** The minimum speed value  $v_{\min}$  in (5.12) indicates the allowable speed perturbation during the platoon stabilization step. Hence,  $v_{\min}$  should be selected appropriately to ensure local stability of the platoon [204, 205].

**Lemma 5.1.11.** *For the CAV  $1 \in \mathcal{N}$  subject to the control input (5.10), the following condition must hold in order to complete platoon formation at time  $t = t^p$  within the control zone of length  $L_c$ ,*

$$\tau^t \leq \frac{\phi_1}{2} + \frac{\sqrt{\phi_1^2 + 4\phi_2}}{2}, \quad (5.13)$$

where,  $\phi_1 := \frac{L_c + \delta_2(t^c) - v_1(t^c) \cdot (\tau^r + \bar{\eta})}{v_1(t^c)}$ , and  $\phi_2 := \frac{2\delta_2(t^c) \cdot (\tau^r + \bar{\eta})}{v_1(t^c)}$ .

*Proof.* Suppose that, for CAV  $1 \in \mathcal{N}$ ,  $p_1(t^p) - p_1(t^c) \leq L_c$ . Using (5.10),  $p_1(t^p) = p_1(t^c + \tau^t) + v_1(t^s) \cdot \tau^s$ , which yields

$$p_1(t^c + \tau^t) - p_1(t^c) + v_1(t^s) \cdot \tau^s \leq L_c. \quad (5.14)$$

From (5.1) and (5.10), we have,  $p_1(t^c + \tau^t) = p_1(t^c) + v_1(t^c) \cdot \tau^t + \frac{1}{2}u_p(\tau^t)^2$ , and  $v_1(t^s) = v_1(t^c) + u_p\tau^t$ . Substituting  $p_1(t^c + \tau^t)$ ,  $v_1(t^s)$  into (5.14),  $\tau^s = \tau^r + \bar{\eta}$  from Remark 5.1.5, and using (5.10)-(5.11), we have,  $\tau^t - \frac{2\delta_2(t^c) \cdot \tau^s}{v_1(t^c) \cdot \tau^t} \leq \frac{L_c + \delta_2(t^c) - v_1(t^c) \cdot \tau^s}{v_1(t^c)}$ . Simplifying and letting  $\phi_1 = \frac{L_c + \delta_2(t^c) - v_1(t^c) \cdot (\tau^r + \bar{\eta})}{v_1(t^c)}$ , and  $\phi_2 = \frac{2\delta_2(t^c) \cdot (\tau^r + \bar{\eta})}{v_1(t^c)}$ , the above equation yields a quadratic inequality  $(\tau^t)^2 - \phi_1\tau^t - \phi_2 \leq 0$ , solving which yields (5.13).  $\square$

The following result provides the condition under which for a given platoon formation time  $t^p$  and platoon stabilization duration  $\tau^s$ , the corresponding platoon transition duration  $\tau^t$  is feasible.

**Theorem 5.1.12.** For a CAV  $1 \in \mathcal{N}$  to complete the platoon transition step with its following HDV  $2 \in \mathcal{N}_{HDV}$  with control input  $u_1(t) = u_p$ ,  $t \in [t^c, t^s]$  within the control zone of length  $L_c$ , a platoon transition duration  $\tau^t$  is feasible if

$$\max \left\{ \left( \frac{-2\delta_2(t^c)}{u_{\min}} \right)^{\frac{1}{2}}, \frac{2\delta_2(t^c)}{v_1(t^c) - v_{\min}} \right\} \leq \tau^t \leq \frac{\phi_1 + \sqrt{\phi_1^2 + 4\phi_2}}{2}, \quad (5.15)$$

holds.

*Proof.* The proof follows directly from Lemmas 5.1.10 and 5.1.11.  $\square$

### 5.1.2.2 Scalability of the Control Framework

For  $N > 2$ , the CAV  $1 \in \mathcal{N}$  trailed by multiple HDVs  $j \in \mathcal{N}_{HDV}$  and given  $\mathcal{I}_1(t^c)$ , we have the following conditions,  $v_1(t^c) = v_j(t^c) = v_{\max}$  for all  $j \in \mathcal{N}_{HDV}$  (Lemma 5.1.6), and there exists  $j \in \mathcal{N}_{HDV}$  such that  $\delta_j(t^c) > 0$  (Remark 5.1.3).

**Definition 5.1.13.** For a CAV  $1 \in \mathcal{N}$  followed by  $N \in \mathcal{N}_{HDV}$  HDVs, the cumulative platoon gap  $\Delta(t)$  at time  $t \in [t^c, t^f]$  is,

$$\Delta(t) = p_1(t) - p_N(t) - \sum_{j=2}^N (s_j(t) + l_c). \quad (5.16)$$

In what follows, we extend the analysis presented in Theorems 5.1.9 and 5.1.12, and derive results that enables platoon formation considering multiple trailing HDVs, i.e.,  $N > 2$ . The following theorem provides the unconstrained relation between the platoon transition duration  $\tau^t$  and CAV control input parameter  $u_p$  for  $N > 2$ .

**Theorem 5.1.14.** For a CAV  $1 \in \mathcal{N}$  followed by  $N$  HDVs  $j \in \mathcal{N}_{HDV}$ , there exists an unconstrained control input parameter  $u_p$  in (5.10) such that a vehicle platoon can be formed with HDVs  $j \in \mathcal{N}$  at time  $t = t^p$  according to the following relation,

$$2\Delta(t^c) + u_p \cdot (\tau^t)^2 - 2u_p \tau^t \sum_{j=2}^{N-1} \rho_j = 0. \quad (5.17)$$

*Proof.* At  $t^s = t^c + \tau^t$ , we require  $p_1(t^s) - p_N(t^s) = \sum_{j=2}^{N-1} s_j(t^s) + s_N(t^s) + \sum_{j=2}^N l_c$ . Using (5.1), we have  $p_1(t^c + \tau^t) = p_1(t^c) + v_1(t^c) \cdot \tau^t + \frac{1}{2}u_p \cdot (\tau^t)^2$ , and  $p_N(t^c + \tau^t) = p_N(t^c) + v_N(t^c) \cdot \tau^t$ . Substituting  $p_1(t^c + \tau^t)$  and  $p_N(t^c + \tau^t)$  into the last equation and simplifying, we have,

$$p_1(t^c) - p_N(t^c) - \sum_{j=2}^{N-1} s_j(t^s) - s_N(t^s) - \sum_{j=2}^N l_c = -\frac{1}{2}u_p \cdot (\tau^t)^2. \quad (5.18)$$

At  $t = t^s$ , we have  $s_N(t^s) = s_N(t^c)$ ,  $s_j(t^s) = \rho_j v_1(t^s) + s_0$  and  $s_j(t^c) = \rho_j v_j(t^c) + s_0$  for  $j = 2, \dots, N-1$ . With  $v_1(t^s) = v_1(t^c) + u_p \tau^t$ , we have  $s_j(t^s) = s_j(t^c) + \rho_j u_p \tau^t$ ,  $j = 2, \dots, N-1$ . Using the last equations in (5.18), we have  $p_1(t^c) - p_N(t^c) - \sum_{j=2}^N s_j(t^c) - \sum_{j=2}^{N-1} \rho_j u_p \tau^t - \sum_{j=2}^N l_c = -\frac{1}{2}u_p \cdot (\tau^t)^2$ , and using Definition 5.1.13, the results follows.  $\square$

For  $N > 2$ , the following result provides the condition under which for a given platoon formation time  $t^p$  and platoon stabilization duration  $\tau^s$ , the corresponding platoon transition duration  $\tau^t$  in Theorem 5.1.14 is feasible.

**Theorem 5.1.15.** *For a CAV  $1 \in \mathcal{N}$  to complete the platoon transition step with its following  $N$  HDVs  $j \in \mathcal{N}_{HDV}$  with control input  $u_1(t) = u_p$ ,  $t \in [t^c, t^s]$  within the control zone of length  $L_c$ , a platoon transition duration  $\tau^t$  is feasible if,*

$$\max \left\{ \left( C_1 + \sqrt{C_1^2 - \frac{2\Delta(t^c)}{u_{\min}}} \right), 2C_1 + \frac{2\Delta(t^c)}{v_1(t^c) - v_{\min}} \right\} \leq \tau^t \leq \frac{\phi_3 + \sqrt{\phi_3^2 + 4\phi_4}}{2}, \quad (5.19)$$

holds, where  $C_1 := \sum_{j=2}^{N-1} \rho_j$ ,  $C_2 := L_c - v_1(t^c) \cdot \tau^s$ ,  $\phi_3 := \frac{2C_1 v_1(t^c) + \Delta(t^c) + C_2}{v_1(t^c)}$ , and  $\phi_4 := \frac{2\Delta(t^c) \cdot \tau^s - 2C_1 C_2}{v_1(t^c)}$ .

*Proof.* Suppose that, for CAV  $1 \in \mathcal{N}$ ,  $u_p = u_{\min}$  yields a corresponding platoon transition duration  $\tau^{t_1}$ . From (5.17), we have  $(\tau^{t_1}) = C_1 + \sqrt{C_1^2 - \frac{2\Delta(t^c)}{u_{\min}}}$ , where  $C_1 := \sum_{j=2}^{N-1} \rho_j$ . Therefore, for any  $\tau^t$  to be feasible such that  $u_p \in [u_{\min}, 0)$ , we require  $\tau^t \geq \tau^{t_1}$ , which yields the inequality with the first term in (5.19).

Now for the second inequality term, since  $u_p \in [u_{\min}, 0)$ , we require that  $v_1(t^c + \tau^t) \geq$

$v_{\min}$  to satisfy the state constraint in (5.2). Using (5.1), we have,  $v_1(t^c + \tau^t) = v_1(t^c) + u_p \cdot \tau^t$ . Substituting  $v_1(t^c + \tau^t)$  in the above inequality, we get  $u_p \cdot \tau^t \geq v_{\min} - v_1(t^c)$ . Substituting  $u_p$  from (5.17) and simplifying, we have the inequality with the second term in (5.19). Since both left-hand side inequalities mentioned above give lower bounds on  $\tau^t$ , we simply take their maximum and get the left inequality of (5.19). Finally, using the result of Theorem 5.1.14 and following similar steps to those in the proofs of Lemma 5.1.11, we derive the right inequality of (5.19).  $\square$

### 5.1.3 Numerical Validation: Highway Platooning

To demonstrate the performance of the proposed platoon formation framework, we present the simulation considering  $\mathcal{N} = \{1, 2, 3\}$  consisting of a CAV 1 followed by two HDVs 2 and 3, using numerical simulation in MATLAB R2020b. For a desired platoon formation time  $t^p = 47.2$  s and a given platoon stabilization duration  $\tau^s = 5$  s,  $\tau^t = 42.2$  s is feasible according to Theorem 5.1.15, and we use Theorem 5.1.14 to compute the corresponding control input  $u_p$  for CAV 1. The headway trajectories of HDVs 2 and 3 converge to the equilibrium value and remain time invariant for all  $t > t^p$ , as shown in Fig. 5.3 (bottom). Since the conditions in (5.9) are satisfied for all  $t \geq t^p$ , the platoon formation is completed at time  $t = t^p$  s as indicated by the position trajectories shown in Fig. 5.3 (top).

In Fig. 5.4, we show the robustness of the proposed framework in terms of *platoon formation deviation* representing the percentage deviation of the actual platoon formation time  $t^{ap}$  from the desired platoon formation time  $t^p$ , i.e.,  $\frac{t^{ap} - t^p}{t^p} \times 100[\%]$ , for  $N = 2, 3$  and 4. Here, positive platoon formation deviation indicates delayed platoon formation in actual simulation, and conversely, negative deviation indicates platoon formation before  $t^p$ . Figure 5.4(a) shows that the platoon is formed within 2.5% deviation for all admissible  $\tau^t$ , where the higher  $\tau^t$  values minimizes delayed platoon formation instances. The robustness of the framework under different perception delay  $\eta_i \in [0, 1]$  is showed in Fig. 5.4(b). Since the platoon formation deviations are mostly

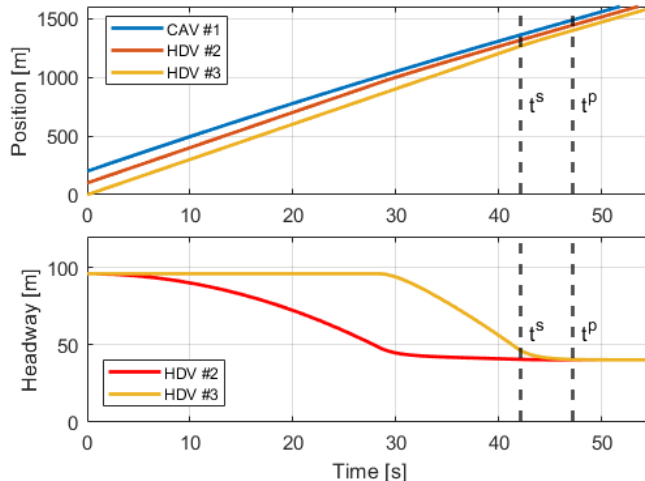


Figure 5.3: Platoon formation for  $N = 3$ , where the position (top) and headway (bottom) of the vehicles are illustrated.

non-positive, the conservative consideration of  $\bar{\eta}$  guarantees platoon formation within the desired platoon formation time  $t^p$ .

Finally, we consider the variation of two car-following parameters, namely the desired time gap  $\rho_i \in [0.5, 1.5]$  and driver's sensitivity coefficient  $\alpha \in [1, 2]$ , to investigate the performance of the proposed framework under random human driving behavior based on (5.5), as shown in Fig. 5.4(c) and (d), respectively. The proposed framework is robust against variation of  $\rho_i$ , and shows delayed platoon formation only near the maximum value of  $\rho_i$ . In contrast, the proposed framework shows delayed platoon formation with  $< 3\%$  deviation for variation of  $\alpha$ . Note that, since  $\tau^s$  is dependent on  $\alpha$ , the appropriate computation of  $\tau^s$  can minimize the platoon formation deviation with varying  $\alpha$ .

Supplementary videos of the simulation and experimental results of the proposed framework as well as the parameters used for the simulation results can be found at: <https://sites.google.com/udel.edu/platoonformation>. To summarize, we presented a framework for platoon formation under a mixed traffic environment, where a leading CAV derives and implements its control input to force the following HDVs to form a

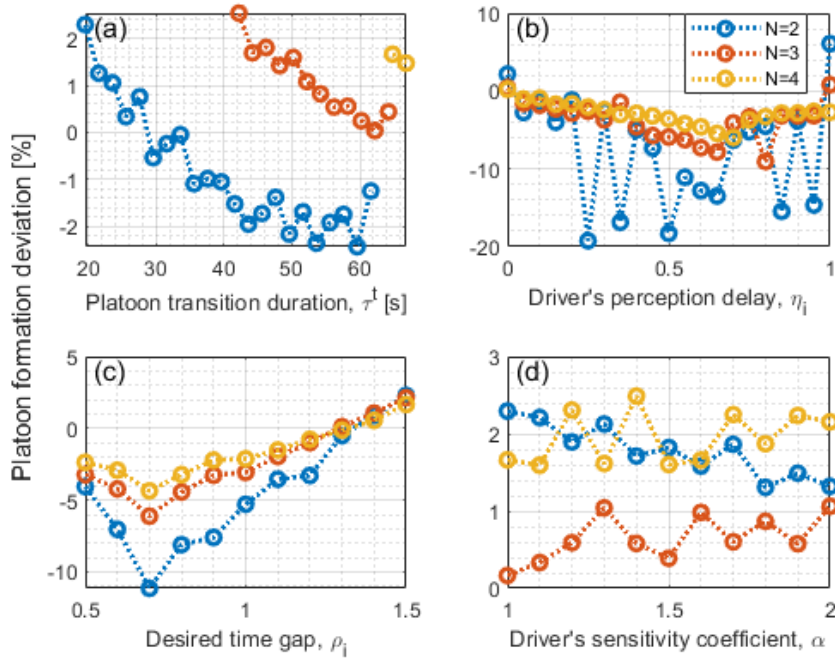


Figure 5.4: Percentage deviation of actual platoon formation time vs. desired platoon formation time for  $N = 2, 3$  and  $4$  under the consideration of different platoon transition duration  $\tau^t$  (subfigure (a)), perception delay  $\eta_i$  (subfigure (b)), and car-following model parameters  $\rho_i$  and  $\alpha$  (subfigure (c)-(d)), respectively.

platoon. Using a predefined car-following model, we provided a complete, analytical solution of the CAV control input intended for the platoon formation. We also provided a detailed analysis of the platoon formation framework and provided conditions under which a feasible platoon formation time exists. Finally, we presented numerical examples to validate the robustness of our proposed framework.

In the following section, we extend the approach by introducing a model-agnostic multi-objective optimal control framework subject to the system constraints.

## 5.2 A Model-Agnostic Optimal Platoon Formation Framework

In this section, we present a multi-objective optimal control framework for each CAV within the traffic network subject to its state and control constraints. The optimization objectives of each CAV are (a) to form a platoon with the trailing HDVs, and

(b) to improve its fuel economy while achieving (a). Our proposed control framework is *model-agnostic*, i.e., it does not require the explicit knowledge of the HDVs' car-following model, and employs a receding horizon controller that uses a *multi-successor communication topology*, i.e., reception of instantaneous motion information from multiple trailing HDVs, to enforce safety while deriving and implementing the optimal control input of the CAV.

We consider the same setup as shown in Fig. 5.1, where a CAV followed by one or multiple HDVs is traveling in a single-lane roadway of length  $L \in \mathbb{R}^+$ , which is subdivided into a buffer zone and a control zone. The CAV enters and leaves the control zone at times  $t^c, t^f \in \mathbb{R}^+$ , respectively. Similar to Section 5.1, we assume the presence of a coordinator, which can be a loop-detector or comparable intelligent device that transmits the HDV state information to the CAV at each time instance  $t \in [t^c, t^f]$  using the standard vehicle-to-infrastructure communication protocol.

Let  $\mathcal{N} = \{1, \dots, N\}$ , where  $N \in \mathbb{N}$  is the total number of vehicles traveling within the buffer zone, be the set of vehicles considered to form a platoon. Here, the leading vehicle indexed by 1 is the CAV, and the rest of the trailing vehicles in  $\mathcal{N}_{\text{HDV}} := \mathcal{N} \setminus \{1\}$  are HDVs. The objective of CAV  $1 \in \mathcal{N}$  is to derive and implement the optimal control input (acceleration/deceleration) such that a platoon formation with the trailing HDVs in  $\mathcal{N}_{\text{HDV}}$  is completed within the control zone of length  $L_c$ .

The dynamics of each vehicle  $i \in \mathcal{N}_z$  are modeled as (5.1), where  $p_i(t) \in \mathcal{P}_i, v_i(t) \in \mathcal{V}_i$ , and  $u_i(t) \in \mathcal{U}_i$  denote the position, speed, and acceleration/deceleration (control input) of each vehicle  $i$ . The sets  $\mathcal{P}_i, \mathcal{V}_i$ , and  $\mathcal{U}_i, i \in \mathcal{N}$ , are complete and totally bounded subsets of  $\mathbb{R}$ . We impose the state and control constraints as in (5.2). Using Definitions 5.1.1 and 5.1.2, we impose the following rear-end collision avoidance constraint

$$\Delta p_i(t) \geq s_i(t), \quad \forall t \in [t^c, t^f]. \quad (5.20)$$

In the modeling framework described above, we consider perfect communication

(Assumption 2.1.2), no lane changes or left/right turns (Assumption 2.1.1), and feasible initial conditions (Assumption 2.1.3).

The control input  $u_i(t)$  of each vehicle  $i \in \mathcal{N}$  in (5.1) can take different forms based on the consideration of connectivity and automation. For CAV  $1 \in \mathcal{N}$ , we derive and implement the control input  $u_1(t)$  using the optimal control framework discussed in Section 5.2.1. For each HDV  $i \in \mathcal{N}_{\text{HDV}}$ , however, we consider a car-following model to represent the predecessor-follower coupled dynamics (see Fig. 5.2), which has the generic structure  $u_i(t) = f(\Delta p_i(t), \Delta v_i(t), v_i(t))$ . Here,  $f(\cdot)$  represents the behavioral function of the car-following model. In this section, we consider that the HDVs' behavioral function  $f$  is unknown to CAV 1.

**Remark 5.2.1.** We restrict the control of the CAV only within the control zone so that we only have a finite optimization horizon  $[t^c, t^f]$  to consider. Outside the control zone, the CAV dynamics follows the car-following model in (5.5).

**Definition 5.2.1.** The information set  $\mathcal{I}_1(t)$  of CAV  $1 \in \mathcal{N}$  at time  $t \in [t^c, t^f]$  is  $\mathcal{I}_1(t) = \{p_{1:N}(t), v_{1:N}(t)\}$ , where  $p_{1:N}(t) = [p_1(t), \dots, p_N(t)]^T$  and  $v_{1:N}(t) = [v_1(t), \dots, v_N(t)]^T$ .

**Definition 5.2.2.** A platoon formation is established at some time  $t^p \in (t^c, t^f)$  if for each vehicle  $i \in \mathcal{N}$ , the headway  $\Delta p_i(t)$  converges to an equilibrium headway  $\Delta p_{eq}$ , and the approach rate  $\Delta v_i(t)$  converges to zero, i.e.,

$$\Delta p_i(t) = \Delta p_{eq}, \quad \Delta p_{eq} \in \mathbb{R}^+, \quad \forall t \geq t^p, \quad (5.21)$$

$$\Delta v_i(t) = 0, \quad \forall t \geq t^p. \quad (5.22)$$

**Remark 5.2.2.** The conditions in (5.21)-(5.22) might be too restrictive to establish a platoon formation in a practical setting. Therefore, we relax these conditions and introduce the following root-mean-squared error based conditions to establish a platoon formation at some time  $t^p \in (t^c, t^f)$ ,

$$\sqrt{\frac{1}{N-1} \sum_{i=2}^N (\Delta p_i(t) - \mu_{\Delta p}(t))^2} \leq \epsilon_{\Delta p}, \quad \forall t \geq t^p, \quad (5.23a)$$

$$\sqrt{\frac{1}{N} \sum_{i=1}^N (v_i(t) - \mu_v(t))^2} \leq \epsilon_v, \quad \forall t \geq t^p, \quad (5.23b)$$

where  $\mu_{\Delta p}(t) := \frac{\sum_{i=2}^N \Delta p_i(t)}{N}$  and  $\mu_v(t) := \frac{\sum_{i=1}^N v_i(t)}{N}$  are the mean headway and mean speed of  $N$  vehicles, respectively, and  $\epsilon_{\Delta p}, \epsilon_v \in \mathbb{R}^+$  are the allowable deviation of  $\Delta p_i(t)$  and  $v_i(t)$  from the equilibrium values  $\Delta p_{eq}$  and  $v_{eq}$ , respectively.

Next, we formally state the platoon formation problem in a mixed environment as follows.

**Problem 5.2.1.** *Given the information set  $\mathcal{I}_1(t)$  for each time  $t \in [t^c, t^f]$ , the objective of the CAV  $1 \in \mathcal{N}$  is to derive its optimal control input  $u_1^*(t)$  so that the each vehicle  $i \in \mathcal{N}$  achieves a platoon formation (Definition 5.2.2) within the control zone.*

**Remark 5.2.3.** In our framework, CAV 1 derives its optimal control input  $u_1^*(t)$  by solving an optimal control problem with the following objectives: (a) formation of platoon with the trailing HDVs (Definition 5.2.2), and (b) improvement of its fuel economy while achieving (a).

In this approach, we adopt a receding horizon control framework with a multi-successor communication topology to address Problem 5.2.1. In what follows, we provide a detailed exposition of the receding horizon control framework that leads to an optimal platoon formation (Remark 5.2.3).

### 5.2.1 Receding Horizon Control Framework

The basic principle of a receding horizon control is that the optimal control input sequence at the current time instance is obtained by solving an optimal control problem online with the prediction horizon  $T_p$ , and only implementing the first element of the solved optimal control input sequence. Then the horizon moves forward one step, and the above process is repeated until the optimization horizon  $T_h$  is reached.

**Remark 5.2.4.** The exit time  $t^f$  of CAV 1 from the control zone depends on the nature of the optimal control input of CAV 1, and thus, it is not known a priori. Let  $t^e$  be the time that the CAV exits the control zone when cruising with a constant speed inside

the control zone. Then,  $t^e = t^c + \frac{L_c}{v_1(t^c)}$ . In our previous work [169], we have shown that a platoon formation with trailing HDVs can be achieved by a non-positive control trajectory of the CAV. Consequently, if we aim at forming the platoon by considering the optimization horizon to be  $T_h = t^e - t^c$ , then we can ensure that the platoon is formed within the control zone.

For CAV 1, we aim to achieve the optimization objectives outlined in Remark 5.2.3 while enforcing rear-end collision avoidance constraint with its trailing HDV. To this end, the adoption of the CAV dynamics in (5.1) is not sufficient; our proposed control framework requires the consideration of an augmented CAV dynamics model.

### 5.2.1.1 Augmented CAV dynamics

To capture the additional characteristics of the platoon formation dynamics from the CAV's control point of view, our proposed control framework uses instantaneous motion information from multiple successive HDVs. Hence, we define two additional states as follows.

**Definition 5.2.3.** The *head-to-tail gap* of the platoon,  $e_{1,1}(t)$  and the *leader-follower gap*,  $e_{1,2}(t)$  are  $e_{1,1}(t) = p_1(t) - p_N(t) - (N - 1)l_c$  and  $e_{1,2}(t) = p_1(t) - p_2(t) - l_c$ , respectively.

The additional states  $e_{1,1}(t)$  and  $e_{1,2}(t)$  enables the augmentation of the CAV dynamics (5.1) with the following set of equations,

$$\dot{e}_{1,1}(t) = v_1(t) - v_N(t), \quad (5.24)$$

$$\dot{e}_{1,2}(t) = v_1(t) - v_2(t). \quad (5.25)$$

**Remark 5.2.5.** The consideration of the head-to-tail gap  $e_{1,1}(t)$  of the platoon enables the formulation of the objective function for the platoon formation problem whereas the leader-follower gap  $e_{1,2}(t)$  enables the enforcement of rear-end collision avoidance constraint in (5.20), leading to a safe platoon formation.

To enable the application of discrete time receding horizon control, we formulate the optimal control problem in discrete time. Suppose, the optimization horizon  $T_h$  is discretized by a sampling time interval  $\tau$  leading to discrete time instance  $k$ . Assuming constant value of control input  $u_1(k)$  during each time step  $[k, (k + 1)]$ , we recast the augmented CAV dynamics (5.1) and (5.24)-(5.25) as linear discrete-time state equations

$$p_1(k + 1) = p_1(k) + v_1(k)\tau + \frac{1}{2}u_1(k)\tau^2, \quad (5.26)$$

$$v_1(k + 1) = v_1(k) + u_1(k)\tau, \quad (5.27)$$

$$e_{1,1}(k + 1) = e_{1,1}(k) + (v_1(k) - v_N(k))\tau + \frac{1}{2}u_1\tau^2, \quad (5.28)$$

$$e_{1,2}(k + 1) = e_{1,2}(k) + (v_1(k) - v_2(k))\tau + \frac{1}{2}u_1\tau^2. \quad (5.29)$$

We define the current state vector  $x_1(k)$ , measured output vector  $y_1(k)$  and the measured disturbance vector  $w_1(k)$  as

$$x_1(k) := \begin{bmatrix} p_1(k) \\ v_1(k) \\ e_{1,1}(k) \\ e_{1,2}(k) \end{bmatrix}, \quad y_1(k) := \begin{bmatrix} v_1(k) \\ e_{1,1}(k) \\ e_{1,2}(k) \end{bmatrix}, \quad w_1(k) := \begin{bmatrix} v_N(k) \\ v_2(k) \end{bmatrix}.$$

The state-space representation of the discrete dynamic in (5.26)-(5.29) is thus

$$x_1(k + 1) = Ax_1(k) + B_u u_1(k) + B_w w_1(k), \quad (5.30)$$

$$y_1(k) = Cx_1(k), \quad (5.31)$$

where, the corresponding state matrix  $A$ , control matrix  $B_u$ , disturbance matrix  $B_w$  and output matrix  $C$  can be computed using (5.26)-(5.31). For the remainder of this section, we drop the subscript 1 denoting the CAV from the discrete state-space model where it does not introduce ambiguity.

### 5.2.1.2 Prediction Model

To solve an online optimization within the prediction horizon  $T_p$ , the receding horizon controller requires a prediction model to take into account the future possible

states. In general, the future system states are predicted based on the model (5.30)-(5.31) and the current state information  $x(k)$ . Let us define the predicted state, predicted output, control and disturbance vector given the prediction horizon  $T_p$  and control horizon  $T_c$  as  $\tilde{X}(k+T_p|k) = [\tilde{x}(k+1|k), \tilde{x}(k+2|k), \dots, \tilde{x}(k+T_p|k)]^T$ ,  $\tilde{Y}(k+T_p|k) = [\tilde{y}(k+1|k), \tilde{y}(k+2|k), \dots, \tilde{y}(k+T_p|k)]^T$ ,  $U(k+T_c) = [u(k), u(k+1), \dots, u(k+T_c-1)]^T$  and  $W(k+T_p) = [w(k), w(k+1), \dots, w(k+T_p-1)]^T$ , respectively. Here  $\tilde{x}(k+n|k)$ ,  $\tilde{y}(k+n|k)$ , and  $w(k+n-1)$ ,  $n = 1, \dots, T_p$ , denote the predicted state, output and disturbance values within the prediction horizon  $T_p$  based on their value at the discrete instance  $k$ , respectively.

The predictive state and associated performance vectors of the receding horizon controller can subsequently be represented as

$$\tilde{X}(k+T_p|k) = \tilde{A}x(k) + \tilde{B}_u U(k+T_c) + \tilde{B}_d W(k+T_p), \quad (5.32)$$

$$\tilde{Y}(k+T_p|k) = \tilde{C}x(k) + \tilde{D}_u U(k+T_c) + \tilde{D}_d W(k+T_p), \quad (5.33)$$

where the predictive system matrices  $\tilde{A}$ ,  $\tilde{B}_u$ ,  $\tilde{B}_d$ ,  $\tilde{C}$  and  $\tilde{D}$  can be computed using the definitions above.

In our formulation, we consider that the measured disturbance  $w(k)$  in (5.32)-(5.33) remains constant within the prediction horizon  $T_p$ . Therefore, we have  $w(k+n|k) = w(k)$ ,  $n = 1, \dots, T_p$ . Consequently, the disturbance vector can be computed as  $W(k+T_p) = [w(k), \dots, w(k)]^T$ . The inaccuracy in modeling the predicted disturbance vector  $W(k+T_p)$  can be compensated by incorporating a feedback scheme into the receding horizon optimization [206].

### 5.2.1.3 Formulation of the Optimal Control Problem

Let us define  $\|z\|_M$  to be the  $M$  weighted norm of an arbitrary vector  $z$  such that  $\|z\|_M := (z^T M z)^{\frac{1}{2}}$ . In order to drive each HDV's state towards the equilibrium platoon state, the primary aim of the CAV controller is to minimize the squared error between

the predicted output  $\tilde{y}(k+n|k)$ ,  $n = 1, 2, \dots, T_p$ , and the corresponding reference output. The first objective function thus takes the form

$$J_1 := \frac{1}{2} \sum_{n=1}^{T_p} \|\tilde{y}(k+n|k) - y_r(k+n)\|_Q^2, \quad (5.34)$$

where the reference output  $y_r(k) := [0, (N-1)(s_0 + \rho [1 \ 0] w(k)), 0]^T$  and the positive semi-definite output weight matrix  $Q := \text{diag}(q_v, q_{e_1}, q_{e_2})$  with the diagonal weight parameters  $q_v$ ,  $q_{e_1}$ ,  $q_{e_2}$  corresponding to the speed  $v_1(k)$ , head-to-tail gap  $e_{1,1}(k)$  and leader-follower gap  $e_{1,2}(k)$ , respectively. Since the measured disturbance  $w(k)$  remains constant within the prediction horizon  $T_p$ , and the reference output  $y_r(k)$  is an explicit function of the measured disturbance  $w(k)$ , the predictive reference output  $y_r(k+n|k)$ ,  $n = 1, \dots, T_p$  remains constant within the prediction horizon  $T_p$  as well. Thus we have  $y_r(k+n|k) = y_r(k)$ ,  $n = 1, \dots, T_p$ .

The second objective of the controller is to improve the fuel economy of the CAV by minimizing the  $L^2$ -norm of the CAV's control input. Hence, we have the second objective function  $J_2 := \frac{1}{2} \sum_{m=1}^{N_c} \|u(k+m-1)\|_R^2$ , where  $R := [w_r]$  is the positive definite weight matrix on the control input with positive weight parameter  $w_r$ .

Finally, combining the above objective functions and using the compact notations from (5.32)-(5.33), we have the final objective function as follows

$$J = \frac{1}{2} \left\| \tilde{Y}(k+T_p|k) - Y_r \right\|_{\bar{Q}}^2 + \frac{1}{2} \|U(k+T_c)\|_{\bar{R}}^2, \quad (5.35)$$

where  $Y_r = [y_r(k), \dots, y_r(k)]^T$ , and  $\bar{Q}$  and  $\bar{R}$  are weight matrices. In our formulation, we consider the constraints on the control input in (5.2), safety in (5.20), and CAV speed in (5.2) associated with the physical limitation of the CAV dynamics, passenger safety, and speed limit of the roadway, respectively. The constraints in the context of

the proposed receding horizon control framework are thus given as

$$u_{\min} \leq u(k+m-1) \leq u_{\max}, \quad m = 1, \dots, T_c, \quad (5.36a)$$

$$e_{1,1}(k+n) \geq (N-1)s_0, \quad n = 1, \dots, T_p, \quad (5.36b)$$

$$e_{1,2}(k+n) \geq s_0, \quad n = 1, \dots, T_p, \quad (5.36c)$$

$$v_{\min} \leq v(k+n) \leq v_{\max}, \quad n = 1, \dots, T_p. \quad (5.36d)$$

With the objective function (5.35), constraints (5.36), dynamics model (5.26)-(5.29), and the information set  $\mathcal{I}_1(k)$ ,  $k = 0, \dots, T_h$  at hand, the optimal control problem can finally be written as

$$\min_{U(k+T_c)} J, \quad (5.37)$$

subject to : (5.26) – (5.29), (5.36) and given  $\mathcal{I}_1(k)$ .

The optimal control problem in (5.37) can be transformed into a standard quadratic programming problem and solved using the active-set algorithm, see [206, 207]. It is possible to soften the state constraints in (5.36) to facilitate the feasibility of the solution of (5.37). However, a significantly large penalty should be incorporated into the objective function in (5.37) using a dimensionless, non-negative slack variable to handle the soft constraint violation, the exposition of which is outside the scope of this section and can be found in [207].

## 5.2.2 Sensitivity, Scalability and Robustness Analysis

To evaluate the performance of the proposed control framework, we adopt the optimal velocity model (OVM) [200] and the intelligent driver model (IDM) [161] to represent the predecessor-follower coupled dynamics of each HDV  $i \in \mathcal{N}_{\text{HDV}}$ . One of the simplest forms of the OVM car-following model [200] is given as

$$u_i(t) = \alpha(V_i(\delta_i(t), s_i(t)) - v_i(t)), \quad (5.38)$$

$$V_i(\delta_i(t), s_i(t)) = \frac{v_d}{2}(\tanh(\delta_i(t)) + \tanh(s_i(t))),$$

where  $\delta_i(t) := \Delta p_i(t) - s_i(t)$ , and  $\alpha$ ,  $V_i(\delta_i(t), s_i(t))$  and  $v_d$  denote the control gain representing the driver's sensitivity coefficient, the equilibrium speed-headway function

and the desired speed of the roadway, respectively. The IDM car-following model [161] for HDV  $i \in \mathcal{N}_{\text{HDV}}$  has the following structure

$$u_i(t) = a \left( 1 - \left( \frac{v_i(t)}{v_d} \right)^\gamma - \left( \frac{\Delta \bar{p}_i(t)}{\Delta p_i(t)} \right)^2 \right), \quad (5.39)$$

$$\Delta \bar{p}_i(t) = s_i(t) + \frac{v_i(t) \Delta v_i(t)}{2ab},$$

where,  $a$ ,  $b$  and  $\gamma$  are the desired acceleration, comfortable braking and acceleration exponent, respectively. The parameters for the car-following models and the receding horizon controller considered in our numerical study can be found in <https://sites.google.com/view/ud-ids-lab/model-agnostic-platoon>.

Table 5.1: Simulation parameters considered.

Parameters	Values
Minimum speed, $v_{\min}$	10.0 [m/s]
Maximum speed, $v_{\max}$	30.0 [m/s]
Maximum deceleration, $u_{\min}$	-3.0 [m/s <sup>2</sup> ]
Maximum acceleration, $u_{\max}$	2.0 [m/s <sup>2</sup> ]
Safe time headway, $\rho$	1.5 [s]
Vehicle length, $l_c$	5 [m]
Buffer zone length, $L_b$	500 [m]
Control zone length, $L_c$	1500 [m]
Optimal velocity model (5.38)	
Driver's sensitivity coefficient, $\alpha$	1.0
Desired speed, $v_d$	30.0 [m/s]
Intelligent driver model (5.39)	
Acceleration exponent, $\gamma$	4.0
Comfortable braking, $b$	3.0 [m/s <sup>2</sup> ]
Desired acceleration, $a$	2.0 [m/s <sup>2</sup> ]

Table 5.2: Receding horizon controller parameters

Parameters	Values
Optimization horizon, $T_h$	65.0 [s]
Prediction horizon, $T_p$	10.0 [s]
Control horizon, $T_c$	2.0 [s]
Sample time, $\tau$	0.1 [s]
Input weight, $w_r$	5.0
Output weight, $Q$	diag(0, 0.2, 0)

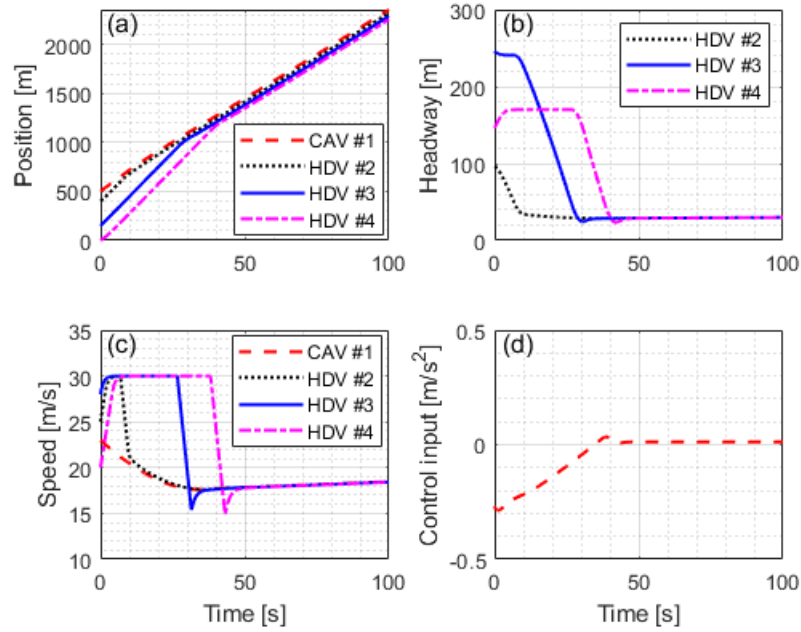


Figure 5.5: Platoon formation with OVM car-following model (5.38) for  $N = 4$ , where the (a) position trajectory, (b) vehicle headway, (c) speed trajectory and (d) the CAV control trajectory are shown.

We conduct the simulation studies using MATLAB R2020b/Simulink with the configuration of Intel Core i7-6700 CPU @ 3.40 GHz. For the first case study, a platoon formation for  $N = 4$  vehicles is shown Fig. 5.5, where the OVM model in (5.38) is considered for the trailing HDVs. The leading CAV and trailing HDVs have randomly selected initial position (Fig. 5.5(a)) and initial speed (Fig. 5.5(c)), respectively. The lead CAV implements the proposed controller to complete the platoon formation operation near 50 s (according to Remark 5.2.2), and the vehicle headway (Fig. 5.5(b)) and speed (Fig. 5.5(c)) converge to some equilibrium value. Additionally, none of the constraints in (5.36) were violated as evident from the headway profile in Fig. 5.5(b), speed profile in Fig. 5.5(c), and CAV's control input trajectory in Fig. 5.5(d), respectively. To validate the model-agnostic nature of the proposed controller, we present a second case study using the IDM model (5.39) (see Fig. 5.6) considering the same initial conditions as in the previous case, which yields similar result without violating any constraints in (5.36), as shown in Figs. 5.6(a)-(d). It is interesting to

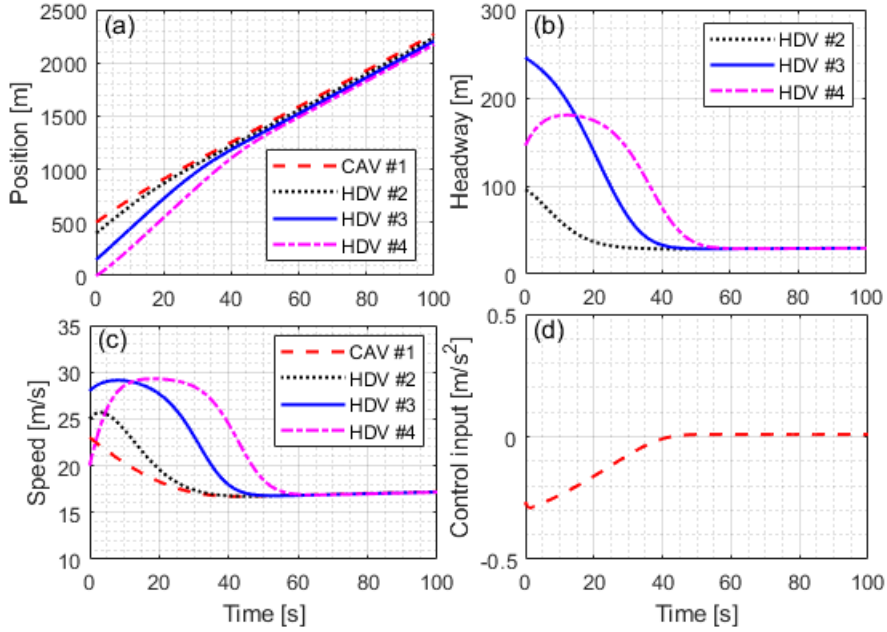


Figure 5.6: Platoon formation with IDM car-following model (5.39) for  $N = 4$ , where the (a) position trajectory and (b) vehicle headway, (c) speed trajectory and (d) the CAV control trajectory are shown.

note that, we have monotonically increasing non-positive linear optimal control input trajectory of the CAV in both of the above cases (see Figs. 5.5(d) and 5.6(d)), which resembles a typical energy-optimal control input trajectory derived using standard Hamiltonian analysis [159, 165]. Note that, we can consider a mixture of OVM and IDM car-following model for the HDVs by appropriately selecting  $\epsilon_{\Delta p}$  and  $\epsilon_v$  in (5.23).

Figure 5.7 shows the sensitivity analysis of the proposed control framework for  $N = 4$  subject to varying controller parameters  $T_p$ ,  $T_c$ , and  $\tau$ , and IDM car-following parameter  $\rho$ . Here, we use (5.23) to compute the platoon formation time. Increasing  $T_p$  and  $\tau$  decrease the platoon formation time, as shown in Figs. 5.7(a) and 5.7(c), respectively, whereas the variation of  $T_c$  does not affect the platoon formation time, as shown in Fig. 5.7(b). However, choosing appropriate  $T_c$  is essential to enforce the constraints in (5.36). Note that, the parameters  $T_p$  and  $\tau$  can be tuned using Figs.

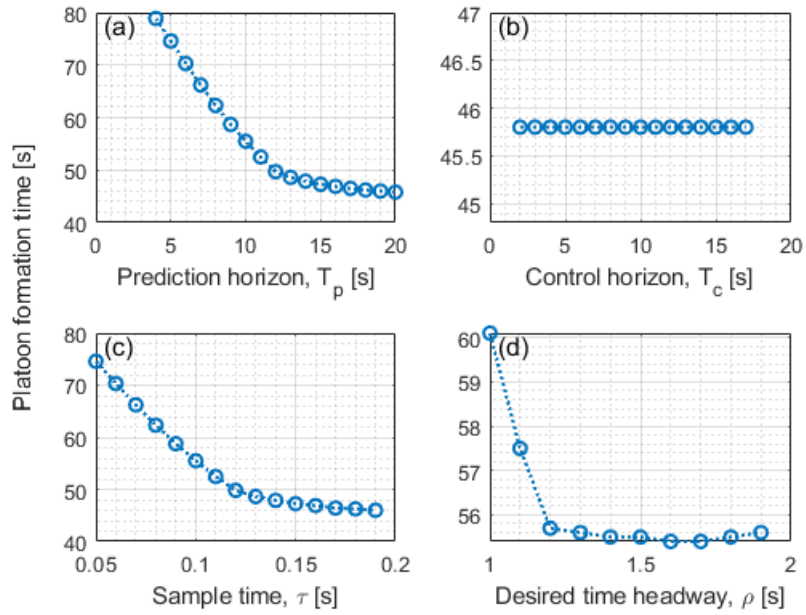


Figure 5.7: Platoon formation with IDM car-following model (5.39) for  $N = 4$ , where the sensitivity of the platoon formation time under varying (a) prediction horizon  $T_p$ , (b) control horizon  $T_c$ , (c) sample time  $\tau$  and (d) desired time headway  $\rho$  are illustrated.

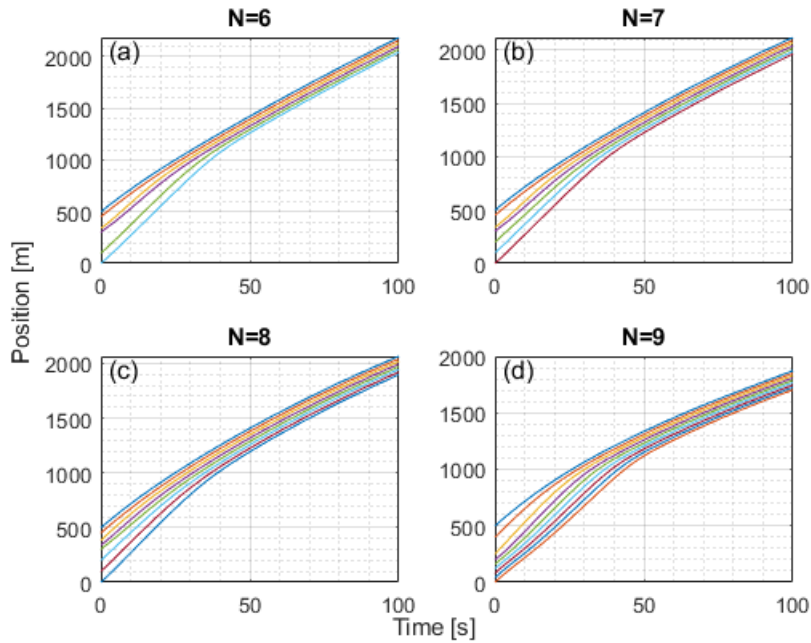


Figure 5.8: Safe platoon formation with IDM car-following model (5.39) for 6, 7, 8 and 9 vehicles.

5.7(a) and 5.7(c) to form a platoon within the desired optimization horizon. The platoon formation time under varying  $\rho$ , which represents different driving behavior of the IDM model, is shown in Fig. 5.7(d). Here, the proposed framework is robust enough to form a platoon within the optimization horizon  $T_h = 65$  s. In all of the cases presented in Figs. 5.7(a)-(d), the proposed controller enables platoon formation without violating any constraints in (5.36). Finally, we investigate the robustness of the proposed framework under different platoon size  $N = 6, 7, 8$  and  $9$  as shown in Fig. 5.8. The position trajectories in Fig. 5.8 indicates that the CAV controller is able to form platoon within the optimization horizon  $T_h = 65$  s without violating any safety constraint in (5.20).

### 5.3 A Safety-Prioritized Predictive Framework for Platoon Formation

Platoon formation with connected and automated vehicles (CAVs) in a mixed traffic environment poses significant challenges due to the presence of human-driven vehicles (HDVs) with unknown dynamics and control action. In this section, we develop a safety-prioritized multi-objective control framework for creating a mixed platoon of vehicles. The optimization objectives of the CAV are (a) to form a platoon with the trailing HDVs, and (b) to minimize its control effort while achieving (a). Our proposed platoon formation framework employs a receding horizon controller that uses a *multi-successor safety constraint* to enforce rear-end collision avoidance constraints for multiple trailing HDVs while deriving and implementing the optimal control input of the CAV. Our proposed control framework ensures indirect control of the trailing HDVs by directly controlling the leading CAV without explicit knowledge of the HDVs' dynamic model, and subject to the system constraints and random initial conditions. We present a model-dependent and a model-independent receding horizon framework that employs different prediction models for estimating the HDV trajectories: (a) a naive constant speed model, (b) a nonlinear car-following model with nominal parameters, and (c) a data-driven model that estimates the driving behavior of the HDVs in real

time using recursive least squares algorithm to better predict the future trajectories. To demonstrate the efficacy of the proposed control framework, we conduct numerical validation and provide the associated sensitivity, robustness, and performance analyses.

The contributions of this section are the induction of: (1) a comprehensive multi-objective platoon formation framework to control the target CAV that aims at forming a platoon with trailing HDVs in a mixed traffic environment given the rear-end safety and system constraints (Section 5.3.2) along with a feasibility analysis (Lemmas 5.3.6 and 5.3.7), (2) a model-independent linear receding horizon control approach (Section 5.3.4) and a model-dependent nonlinear receding horizon control approach (Section 5.3.5.1) to generate the optimal control input for the target CAV to form a platoon, and (3) the development of a data-driven receding horizon control approach (Section 5.3.5.2) for platoon formation, where the driving behavior of the HDVs is estimated with the constant time headway relative velocity (CTH-RV) model and a recursive least squares algorithm. We provide numerical validation of the proposed approaches along with associated sensitivity, robustness, and performance analyses.

### 5.3.1 Comparison with Related Work

The exposition in this section advances the state of the art in the following ways. First, in contrast to the platoon formation and control approaches that have been developed using a distributed MPC framework [123, 132–134], which applies only to a network with 100% CAV penetration, we address the problem of platoon formation considering a mixed traffic environment that includes the interaction of CAVs and HDVs.

Second, compared to the platoon formation approach proposed in [116], where vehicle merging is done by accelerating the trailing vehicles to catch up with the leading ones, we consider a challenging problem of indirectly enforcing the platoon formation since the trailing HDVs cannot be directly controlled. Furthermore, platoon formation in a mixed traffic environment has been discussed in [208], which proposed simple

heuristics to form platoons. In our approach, we optimize the control input of the target CAV subjected to performance objectives and form the platoon with the implementation of receding horizon control with added safety guarantees by imposing multi-successor safety constraints.

Third, cooperative connected cruise control with nonlinear dynamics and communication delays for a mixed connected platoon has been presented in [137, 140], where the CAV controller can only form and maintain a platoon with the preceding vehicle. In contrast, we consider platoon formation with multiple trailing HDVs with unknown vehicle dynamics.

Finally, in contrast to the MPC-based ACC controller that employs predictive model without considering the complex car-following dynamics of the human driver [148, 209], we present a model-dependent approach that considers a nonlinear car-following model with nominal parameters and a linear car-following model with real-time estimated parameters for predicting the HDV behavior during the platoon formation process.

### 5.3.2 Problem Formulation

We consider a scenario where a group of vehicles, consisting of CAVs and HDVs, are traveling on a roadway as shown in Fig. 5.9. We assign unique integer identities to the vehicles considered for the platoon formation problem as follows: (a) the target CAV, which has the objective to form a platoon with its trailing HDVs, is indexed by 1, (b) the preceding vehicle (PV) of CAV-1 is index by 0, and (c) the HDVs trailing CAV-1 are indexed by the order of their distance from the target CAV as  $2, \dots, N$ ,  $N \in \mathbb{N}$  (see Fig. 5.9). The objective of CAV-1 is to derive and implement an optimal control trajectory (acceleration/deceleration) such that a platoon formation with the trailing HDVs is completed satisfying the system constraints and ensuring safety in terms of rear-end collision with the preceding and trailing vehicles.

Next, we define the following sets to represent different groups of vehicles using

the unique identities considered above.

**Definition 5.3.1.** The set of all vehicles considered in our problem formulation is  $\mathcal{N} = \{0, 1, \dots, N\}$ . The set of HDVs trailing CAV-1 is  $\mathcal{N}_{\text{HDV}} = \{2, \dots, N\} \subset \mathcal{N}$ . The set of vehicles to form the platoon is  $\mathcal{N}_p = \{1\} \cup \mathcal{N}_{\text{HDV}}$ .

**Remark 5.3.1.** We generalize our exposition considering the existence of PV-0 which can be either CAV or HDV. In the case where PV-0 does not exist within a user-defined look-ahead distance, we construct the set  $\mathcal{N}$  without the element  $\{0\}$  without loss of generality.

**Remark 5.3.2.** For formulating a valid platoon formation problem for the vehicles in  $\mathcal{N}$ , the set  $\mathcal{N}_{\text{HDV}}$  must be non-empty.

In our formulation, we allow lane changes for HDVs in  $\mathcal{N}_{\text{HDV}}$  during the platoon formation process. If any HDV in  $\mathcal{N}_{\text{HDV}}$  decides to move to a different lane, or an HDV from an adjacent lane moves into the current lane, then we recompute the set  $\mathcal{N}_{\text{HDV}}$  with updated vehicles identities. For example, given  $\mathcal{N}_{\text{HDV}} = \{2, 3, 4\}$ , let us consider two cases: (a) if HDV-3 moves to a different lane, then HDV-4 is updated to become HDV-3, resulting in  $\mathcal{N}_{\text{HDV}} = \{2, 3\}$ , and (b) if an HDV from an adjacent lane moves in between HDV-3 and HDV-4, then the added HDV is assigned an ID of 4, and previously known HDV-4 is updated to become HDV-5 resulting in  $\mathcal{N}_{\text{HDV}} = \{2, 3, 4, 5\}$ . We model the longitudinal dynamics of each vehicle  $i \in \mathcal{N}$  as

$$\dot{p}_i(t) = v_i(t), \tag{5.40a}$$

$$\dot{v}_i(t) = u_i(t), \tag{5.40b}$$

where  $p_i(t) \in \mathcal{P}_i$ ,  $v_i(t) \in \mathcal{V}_i$  and  $u_i(t) \in \mathcal{U}_i$  are the position of the front bumper, speed and control input (acceleration/deceleration command) of each vehicle  $i \in \mathcal{N}$ , respectively. The sets  $\mathcal{P}_i$ ,  $\mathcal{V}_i$ , and  $\mathcal{U}_i$ ,  $i \in \mathcal{N}$ , are complete and totally bounded subsets of  $\mathbb{R}$ .

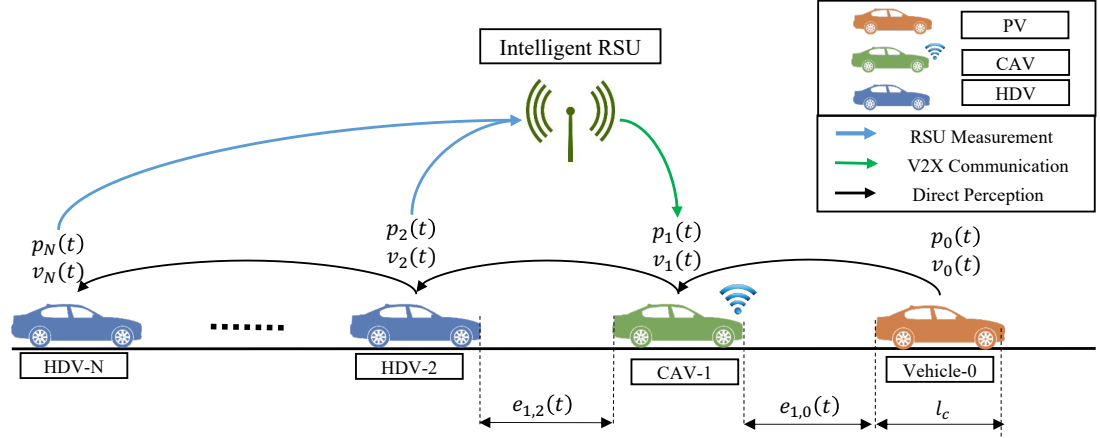


Figure 5.9: The target CAV (green) is traveling with  $N$  trailing HDVs (blue) and a PV (orange). The communication structure is shown according to Section 5.3.2.2.

The speed  $v_i(t)$  and control input  $u_i(t)$  of each vehicle  $i \in \mathcal{N}$  are subjected to the following constraints

$$0 \leq v_{\min} \leq v_i(t) \leq v_{\max}, \quad (5.41a)$$

$$u_{i,\min} \leq u_i(t) \leq u_{i,\max}, \quad (5.41b)$$

where  $v_{\min}$  and  $v_{\max}$  are the minimum and maximum allowable speed of the considered roadway, respectively, and  $u_{i,\min}$  and  $u_{i,\max}$  are the minimum and maximum control input of each vehicle  $i \in \mathcal{N}$ , respectively. To simplify the exposition in the section and without loss of generality, we consider the group of vehicles to be homogeneous, i.e., all the vehicles have the same automotive attributes. Thus, we can consider the same minimum and maximum control input  $u_{\min}$  and  $u_{\max}$  for all the vehicles such that  $u_{i,\min} = u_{\min}$  and  $u_{i,\max} = u_{\max}$  for all  $i \in \mathcal{N}$  in (5.41b).

To formulate the rear-end collision constraint between two consecutive vehicles  $i, (i-1) \in \mathcal{N}$ , we use the following definitions.

**Definition 5.3.2.** The safe following gap  $s_i(t)$  between two consecutive vehicles  $i$  and  $(i-1) \in \mathcal{N}$  is

$$s_i(t) = \rho_i v_i(t) + s_0, \quad (5.42)$$

where  $\rho_i \in \mathbb{R}_{>0}$  denotes a safe time headway that each vehicle  $i \in \mathcal{N}$  maintains while following its immediate preceding vehicle  $i - 1 \in \mathcal{N}$ , and  $s_0 \in \mathbb{R}_{>0}$  is the standstill distance denoting the minimum bumper-to-bumper gap at stop.

**Definition 5.3.3.** The *headway*  $\Delta p_i(t)$  and *approach rate*  $\Delta v_i(t)$  of vehicle  $i \in \mathcal{N}$  denote the bumper-to-bumper inter-vehicle spacing and speed difference, respectively, between the two consecutive vehicles  $i, (i - 1) \in \mathcal{N}$ , i.e.,

$$\Delta p_i(t) = p_{i-1}(t) - p_i(t) - l_c, \quad (5.43a)$$

$$\Delta v_i(t) = v_{i-1}(t) - v_i(t), \quad (5.43b)$$

where  $l_c \in \mathbb{R}_{>0}$  is the length of each vehicle. Since all vehicles under consideration belong to a homogeneous group, they have the same length  $l_c$ .

The rear-end collision avoidance constraint between two consecutive vehicles  $i, i - 1 \in \mathcal{N}$  can thus be written as

$$\Delta p_i(t) \geq s_i(t). \quad (5.44)$$

### 5.3.2.1 Vehicle Control Model

The dynamics (5.40) of each vehicle  $i \in \mathcal{N}$  can take different forms based on the consideration of connectivity and automation. For CAV-1, the control input  $u_1(t)$  is derived by solving a multi-objective optimal control problem, the structure of which we introduce and discuss in detail in Sections 5.3.4 and 5.3.5.

In contrast to the CAV, we consider a generic car-following model based control policy of the following form to define the predecessor-follower coupled dynamics (see Fig. 5.9) of each HDV  $i$  in  $\mathcal{N}_{\text{HDV}}$ ,

$$u_i(t) = f_i(\Delta p_i(t), \Delta v_i(t), v_i(t)), \quad (5.45)$$

where  $f_i(\cdot)$  represents the behavioral model of the car-following dynamics of each HDV  $i$ . There are several car-following models reported in the literature [101, 160, 161, 200]

that can emulate a varied class of human driving behavior. However, to ensure that any car-following model considered in our modeling framework emulates realistic human driving behavior, we impose the following eligibility criteria (see [204] for details). First, a realistic car-following model with behavioral function  $f(\cdot)$  should represent rational driving behavior, i.e., the following inequalities should hold,

$$\frac{\partial f}{\partial \Delta p_i(t)} > 0, \quad \frac{\partial f}{\partial \Delta v_i(t)} > 0, \quad \frac{\partial f}{\partial v_i(t)} < 0, \quad (5.46)$$

The three inequalities in (5.46) essentially mean that a larger headway  $\Delta p_i(t)$  should result in less acceleration (or more braking), a larger approach rate  $\Delta v_i(t)$  should result in more acceleration (or less braking), and the tendency to accelerate (or brake) should be less dependent on the vehicles current speed  $v_i(t)$ . Second, a realistic car-following model should be locally stable, i.e., any initial perturbation of a vehicle's state should decay exponentially as time progresses so that the vehicle can get back to its steady-state driving behavior in finite time. A car-following model is locally stable if roots of the following characteristic equation has both negative real part,

$$\lambda^2 + \left( \frac{\partial f}{\partial \Delta v_i(t)} - \frac{\partial f}{\partial v_i(t)} \right) \lambda + \frac{\partial f}{\partial \Delta p_i(t)} = 0. \quad (5.47)$$

Here, the characteristic equation is parameterized by an arbitrary variable  $\lambda$ . Finally, a suitable car-following model should be string stable such that any perturbation introduced on a vehicle does not grow in magnitude for the rest of the vehicles in a platoon. To ensure that a car-following model is string stable, the following condition should hold

$$\frac{\frac{\partial f}{\partial \Delta p_i(t)}}{\left(\frac{\partial f}{\partial v_i(t)}\right)^3} \left[ \frac{\left(\frac{\partial f}{\partial v_i(t)}\right)^2}{2} - \frac{\partial f}{\partial v_i(t)} \cdot \frac{\partial f}{\partial \Delta v_i(t)} - \frac{\partial f}{\partial \Delta p_i(t)} \right] < 0. \quad (5.48)$$

Note that, since we cannot control the HDV's driving behavior, it is imperative that any choice of car-following model to represent the HDV's behavior abides by the conditions described in (5.46)-(5.48) to ensure rational driving behavior, local stability, and string stability. For the HDVs considered in this section, we adopt a widely used car-following

model, namely, the optimal velocity model (OVM) [200] to define the predecessor-follower coupled dynamics (see Fig. 5.9) of each HDV  $i$  in  $\mathcal{N}_{\text{HDV}}$ . One of the simplest forms of the OVM car-following model [200] is given as

$$u_i(k) = \alpha_i(V_i(\delta_i(k), s_i(k)) - v_i(k)) + \beta_i \Delta v_i(t), \quad (5.49)$$

where  $\alpha_i, \beta_i \in \mathbb{R}_{>0}$ ,  $i \in \mathcal{N}_{\text{HDV}}$  denote the control gain representing the driver's sensitivity coefficient and the speed-dependent coefficient, respectively,  $\delta_i(t) := \Delta p_i(t) - s_i(t)$ , and  $V_i(\delta_i(t), s_i(t))$  denotes the equilibrium speed-spacing function

$$V_i(\delta_i(t), s_i(t)) = \frac{v_d}{2}(\tanh(\delta_i(t)) + \tanh(s_i(t))), \quad (5.50)$$

where  $v_d$  is the desired speed of the roadway. To ensure the eligibility of the OVM model based on (5.46)-(5.48), the car-following parameters  $\alpha_i$ ,  $\beta_i$ , and  $\rho_i$  for each HDV  $i$  have to be selected from feasible sets, as detailed in [204]. Note that, if there is no preceding vehicle, we set  $\Delta p_i(t) = \infty$  that results in  $v_i(t)$  approaching the desired speed  $v_d$  with the progression of time. The car-following model and model predictive controller parameters considered in our numerical study are provided in Section 5.3.6.

Finally, PV-0, if it exists, can be considered to be either a CAV or HDV. CAV-1 does not know the control structure of PV-0 and has to form a platoon without any rear-end safety implication. In this section, we impose an arbitrary control trajectory to PV-0 subjected to the state and control constraints in (5.41) in order to challenge the platoon formation process.

### 5.3.2.2 Communication Structure

CAV-1 is retrofitted with appropriate sensors and communication devices to estimate in real-time the state information of the vehicles in  $\mathcal{N} \setminus \{1\}$ . For example, the state information of PV-0 can be directly measured by the front sensors of CAV-1, whereas the real-time estimation of the state information of the trailing HDVs in  $\mathcal{N}_{\text{HDV}}$  can be done using a vehicle-to-everything communication protocol and/or intelligent

roadside units [193]. Consequently, we can define the structure of the information available to CAV-1 as follows.

**Definition 5.3.4.** The information set  $\mathcal{I}(t)$  available to CAV-1 at time  $t$  is

$$\mathcal{I}(t) = \{\mathbf{p}_{0:N}(t), \mathbf{v}_{0:N}(t)\}, \quad (5.51)$$

where  $\mathbf{p}_{0:N}(t) = [p_0(t), \dots, p_N(t)]^T$  and  $\mathbf{v}_{0:N}(t) = [v_0(t), \dots, v_N(t)]^T$ .

**Remark 5.3.3.** The information set  $\mathcal{I}(t)$  only contains the state information of each vehicle in  $\mathcal{N}$  at time instant  $t$ . The exact structure of the behavioral function  $f_i(\cdot)$  for each vehicle  $i \in \mathcal{N} \setminus \{1\}$  is unknown to CAV-1.

In contrast, the human driver of each HDV  $i$  in  $\mathcal{N}$  can only perceive the state information of the directly preceding vehicle  $i - 1$ . The delay and inaccuracy of such perception and the corresponding driver's action are usually incorporated into the car-following models used for emulating the driving behavior of HDVs.

In our modeling framework, we impose the following assumption about the communication protocol.

**Assumption 5.3.1.** The estimation and transmission of the HDVs' state information to the CAV occur without any delay and error.

Assumption 5.3.1 might be too restrictive. However, it can be relaxed as long as the noise in the measurements and/or delays is bounded. For example, we can determine upper bounds on the state uncertainties as a result of sensing or communication errors and delays, and incorporate these into more conservative safety constraints.

In what follows, we introduce the platoon formation problem.

### 5.3.2.3 Platoon Formation Problem: Mixed Environment

Conventionally, a platoon is defined as a closely-spaced group of vehicles, where each vehicle in the group is traveling with equal headway  $\Delta p_i(t)$  and speed  $v_i(t)$ . This

means that, a platoon is said to be formed for a vehicle group  $\mathcal{N}_p$  at some time  $t = t^p$  if for each vehicle  $i \in \mathcal{N}_p$ ,

$$\Delta p_i(t) = \Delta p_{eq}, \quad t \geq t^p, \quad (5.52a)$$

$$v_i(t) = v_{eq}, \quad t \geq t^p, \quad (5.52b)$$

where,  $\Delta p_{eq}, v_{eq} \in \mathbb{R}_{>0}$  are the equilibrium platoon headway and speed, respectively. However, the conventional definition of platoon formation does not hold for a group of heterogeneous vehicles having different driving behavior as we would expect from a real-world scenario. In the problem we are addressing, each HDV  $i$  in  $\mathcal{N}_{\text{HDV}}$  can have different safe time headway  $\rho_i$  (Definition 5.3.3) and behavioral function  $f_i(\cdot)$ . As a result,  $\Delta p_i(t)$  for each HDV  $i$  in  $\mathcal{N}_{\text{HDV}}$  will converge to different equilibrium values as time  $t$  progresses, violating the conditions of platoon formation in (5.52a). Hence, we need to revise the definition of platoon formation in the context of a heterogeneous vehicle group, as we have in our problem formulation.

**Definition 5.3.5.** For a heterogeneous vehicle group  $\mathcal{N}_p$  with different safe time headway  $\rho_i$  and behavioral function  $f_i(\cdot)$  for each vehicle  $i \in \mathcal{N}_p$ , a platoon is formed at some time  $t = t^p$  if for each vehicle  $i \in \mathcal{N}_p$  the following conditions hold

$$\lim_{t \rightarrow t^p} \|\Delta p_i(t) - s_i(t)\| = 0, \quad (5.53)$$

$$\lim_{t \rightarrow t^p} \|\Delta v_i(t)\| = 0. \quad (5.54)$$

**Remark 5.3.4.** To determine the platoon formation time  $t^p$ , the conditions in Definition 5.3.5 might be too restrictive in practice. Therefore, we introduce the following root-mean-squared-error based conditions to relax the conditions in Definition 5.3.5.

$$\sqrt{\sum_{i=2}^N \left( \Delta p_i(t) - s_i(t) \right)^2} \leq \epsilon_{\Delta p}, \quad \forall t \geq t^p, \quad (5.55)$$

$$\sqrt{\sum_{i=1}^N \left( v_i(t) - \frac{\sum_{i=1}^N v_i(t)}{N} \right)^2} \leq \epsilon_v, \quad \forall t \geq t^p, \quad (5.56)$$

where  $\epsilon_{\Delta p}, \epsilon_v \in \mathbb{R}_{>0}$  are some user-defined small deviation.

Next, we formalize the problem of platoon formation in a mixed traffic environment addressed in the section as follows.

**Problem 5.3.1.** *The objective of CAV-1 in  $\mathcal{N}$  is to derive its control input  $u_1(t)$  given the information set  $\mathcal{I}(t)$  so that the each vehicle  $i \in \mathcal{N}_p$  forms a platoon according to the Definition 5.3.5 satisfying the state, control, and safety constraints in (5.41) and (5.44), respectively.*

**Remark 5.3.5.** In our framework, CAV-1 derives its optimal control input  $u_1^*(t)$  by solving an optimal control problem with the following objectives: (a) formation of a platoon with the trailing HDVs (Definition 5.3.5), and (b) minimization of its control effort while achieving (a).

In this section, we adopt a receding horizon control framework using the communication structure described in Section 5.3.2.2 to address Problem 5.3.1. The basic principle of a receding horizon control framework is that the current control action sequence is obtained by solving an optimization problem (Remark 5.3.5) with a prediction horizon  $T_p$ , and only the first input of the solved control sequence is applied. Then the horizon moves forward a step and the process is repeated until a final horizon  $T_h$  is reached. The choice of the prediction horizon  $T_p$  can influence the performance of the receding horizon framework [206] and consequently, the platoon formation time  $t^p$  [170]. Therefore,  $T_p$  can be considered as a design parameter that needs to be calibrated so that the receding horizon framework can solve Problem 5.3.1 within the given final horizon  $T_h$ .

**Assumption 5.3.2.** For each vehicle  $i \in \mathcal{N}$ , none of the state, control (5.41) and safety constraint in (5.44) are violated at the initial time of the receding horizon control.

Assumption 5.3.2 ensures that the receding horizon control starts with a feasible initial state and control input of each vehicle  $i \in \mathcal{N}$ . Although we have not yet introduced the receding horizon control framework, we can consider the state and

control constraints (5.41) to determine a priori whether Problem 5.3.1 is feasible in the context of the receding horizon control.

### 5.3.3 Feasibility of Platoon Formation

If there exists a roadway of finite length  $L \in \mathbb{R}_{>0}$  to form the platoon, then we need to check whether a feasible choice of final horizon  $T_h$  leads to a feasible Problem 5.3.1.

In our previous work [169, 170], we showed that a platoon formation with trailing HDVs are achieved by non-positive control input of the lead CAV, i.e.,  $u_1(t) \in [u_{\min}, 0]$ . Therefore, we can consider the extremes of  $[u_{\min}, 0]$  to check whether  $T_h$  is feasible. The following result provides the feasibility check of the final horizon  $T_h$ .

**Lemma 5.3.6.** *Let  $t = t^c$  be the initial time when CAV-1 starts deriving and implementing its control input  $u_1(t)$ ,  $t \geq t^c$ , to form a platoon with the trailing HDVs. The final horizon  $T_h$  of the receding horizon control framework that CAV-1 has available to solve Problem 5.3.1 on a given roadway of length  $L \in \mathbb{R}_{>0}$  is bounded by the following relation,*

$$\frac{L}{v_1(t^e)} \leq T_h \leq \mathbb{1}_{L \leq L_s} \tau_1 + (1 - \mathbb{1}_{L \leq L_s}) \tau_2, \quad (5.57)$$

where  $\mathbb{1}_{L \leq L_s}$  is an indicator function,  $L_s := \frac{v_{\min}^2 - v_1^2(t^c)}{2u_{\min}}$ ,  $\tau_1 := \frac{-v_1(t^c) + \sqrt{v_1^2(t^c) + 2u_{\min}L}}{u_{\min}}$  and  $\tau_2 := \frac{v_{\min} - v_1(t^c)}{u_{\min}} - \frac{v_{\min}^2 - v_1^2(t^c)}{2u_{\min}v_{\min}}$ .

*Proof.* Let  $t^e$  be the time that the CAV reaches the end of the available roadway of length  $L$  when cruising with a constant speed  $v_1(t^c)$ . Then,  $t^e = t^c + \frac{L}{v_1(t^c)}$ . Consequently, the minimum time that CAV-1 can take to traverse the distance  $L$  is  $t^e - t^c$ , which is then the lower bound of the horizon  $T_h$  in (5.57).

The maximum time that CAV-1 can take to travel distance  $L$  can be computed by considering the following piecewise control input of CAV-1 constructed using the constraints in (5.41),

$$u_1(t) = \begin{cases} u_{\min}, & \text{if } v_1(t) > v_{\min}, \\ 0, & \text{if } v_1(t) = v_{\min}. \end{cases} \quad (5.58)$$

Let us consider the time  $t = t^s$  where the control input  $u_1(t)$  switches from  $u_1(t) = u_{\min}$  to  $u_1(t) = 0$  in (5.58). Using (5.40), we have  $v_{\min} = v_1(t^c) + u_{\min}(t^s - t^c)$ , which yields  $t^s = t^c + \frac{v_{\min} - v_1(t^c)}{u_{\min}}$ . Furthermore, using (5.40), we can compute that the control switch in (5.58) occurs after traveling the distance  $L_s = \frac{v_{\min}^2 - v_1^2(t^c)}{2u_{\min}}$ . We need to consider the following two cases:

(a) If  $L \leq L_s$ , then the upper bound of  $T_h$  can be computed by solving  $\frac{1}{2}u_{\min}(\tau_1)^2 + v_1(t^c)\tau_1 - L = 0$  for  $\tau_1$ , which yields  $\tau_1 = \frac{-v_1(t^c) + \sqrt{v_1^2(t^c) + 2u_{\min}L}}{u_{\min}}$ . Here,  $\tau_1$  is the upper-bound of  $T_h$ .

(b) If  $L > L_s$ , then CAV-1 travels the distance  $L_s$  with control input  $u_1(t) = u_{\min}$  and time duration  $t^s - t^c$ , and the remaining distance  $L - L_s$  with cruising speed  $v_{\min}$  and time duration  $\frac{L - L_s}{v_{\min}}$ . The maximum time duration  $\tau_2$  to traverse distance  $L$  can be computed using  $\tau_2 = (t^s - t^c) + \frac{L - L_s}{v_{\min}}$ . Using the values of  $t^s, L_s$ , we get,  $\tau_2 = \frac{v_{\min} - v_1(t^c)}{u_{\min}} - \frac{v_{\min}^2 - v_1^2(t^c)}{2u_{\min}v_{\min}}$ .

Combining the above cases, we can derive the upper-bound on the final horizon as  $\mathbb{1}_{L \leq L_s}\tau_1 + (1 - \mathbb{1}_{L \leq L_s})\tau_2$ , which is the right-hand term of the inequality in (5.57).  $\square$

The conditions in (5.57) only provide a formal way to select an appropriate final horizon  $T_h$ . The infeasibility of the final horizon  $T_h$  does not necessarily render Problem 5.3.1 infeasible. Conversely, the feasibility of  $T_h$  does not imply that Problem 5.3.1 will be feasible as well, i.e., a platoon formation is guaranteed. In what follows, given that the final horizon  $T_h$  is feasible according to Lemma 5.3.6, we provide conditions to

investigate whether Problem 5.3.1 is feasible given the constraints (5.41), and a finite roadway of length  $L$  for platoon formation.

Since platoon formation with trailing HDVs is achieved by a non-positive control trajectory of CAV-1, we can check the feasibility of Problem 5.3.1 considering the most aggressively decelerating control structure in (5.58) as discussed in the following Lemma.

**Lemma 5.3.7.** *Suppose that CAV-1 starts deriving and implementing its control input  $u_1(t)$  at time  $t = t^c$  to form a platoon with the trailing HDVs at some time  $t^p \in (t^c, t^c + T_h)$  within a given roadway of length  $L$ , where  $T_h$  is a feasible final horizon bounded by the lower- and upper-values  $\tau_1$  and  $\tau_2$  according to Lemma 5.3.6, respectively. Suppose that CAV-1 has the control structure as in (5.58), and  $L_s$  is the length where control input  $u_1(t)$  switches from  $u_{\min}$  to 0.*

(a) *If  $L_s > L$ , then Problem 5.3.1 is feasible if*

$$0 < \frac{(v_N(t^c) - v_1(t^c)) - \sqrt{(v_N(t^c) - v_1(t^c))^2 - 2u_{\min}\Delta p_s}}{u_{\min}} \leq \tau_1 \quad (5.59)$$

*holds and, (b) if  $L_s \leq L$ , then Problem 5.3.1 is feasible if*

$$0 < \frac{\Delta p_s + v_{\min}\tau_s - L_s}{(v_{\min} - v_N(t^c))} \leq \tau_2 \quad (5.60)$$

*holds, where  $\Delta p_s := \sum_2^N (\Delta p_i(t^c) - s_i(t^c))$ .*

*Proof.* Let us consider that CAV-1 takes the time duration  $\tau_p$  to form a platoon.

Case (a): If  $L_s > L$ , we check whether a platoon can be formed with the control structure (5.58). Suppose that  $\Delta p_s := \sum_2^N (\Delta p_i(t^c) - s_i(t^c))$  is the additional spacing between CAV-1 and HDV- $N$  beyond the dynamic following spacing  $s_i(t^c)$ . Hence, to form a platoon with time duration  $\tau_p$  according to Definition 5.3.5, we require  $v_1(t^c)\tau_p + \frac{1}{2}u_{\min}(\tau_p)^2 - v_N(t^c)\tau_p = \Delta p_s$ . Solving this equation for  $\tau_p$ , we get  $\tau_p = \frac{(v_N(t^c) - v_1(t^c)) - \sqrt{(v_N(t^c) - v_1(t^c))^2 - 2u_{\min}\Delta p_s}}{u_{\min}}$ . The value of  $\tau_p$  is lower-bounded by 0 to ensure positive value and upper-bounded by  $\tau_1$  so that platoon is not formed beyond  $L$ , which yields (5.59).

Case (b): If  $L_s \geq L$ , then to form a platoon with time duration  $\tau_p$ , we require  $L_s + v_{\min}(\tau_p - \tau_s) - v_N(t^c)\tau_p = \Delta p_s$ . Solving for  $\tau_p$ , we get  $\tau_p = \frac{\Delta p_s + v_{\min}\tau_s - L_s}{(v_{\min} - v_N(t^c))}$ , which is lower- and upper-bounded by 0 and  $\tau_2$  to ensure platoon formation within  $L$ .  $\square$

**Remark 5.3.6.** We use the conditions in Lemma 5.3.7 only to investigate the feasibility of Problem 5.3.1 constrained by a limited road space of length  $L$  for the case where platoon formation is not possible even with the most aggressive braking maneuver of CAV-1 (see control structure (5.58)). Satisfaction of the conditions in Lemma 5.3.7, in general, does not guarantee the existence of a solution to Problem 5.3.1 given the optimization criteria discussed in Remark 5.3.5.

In what follows, we provide a detailed exposition of a model-independent receding horizon control framework that aims at solving Problem 5.3.1 with the given objectives (Remark 5.3.5).

#### 5.3.4 Model-Independent Control Framework

Since CAV-1 does not have explicit knowledge of the driving behavior of the HDVs (Remark 5.3.3), CAV-1 employs an internal model to predict the HDV trajectories within the prediction horizon  $T_p$ . We first consider the following model-independent internal model.

**Internal Model 1.** The speed of each HDV in  $\mathcal{N} \setminus \{1\}$  remains constant within the prediction horizon  $T_p$ .

The native state prediction with the assumption of constant speed enables the formulation of a linear receding horizon framework. Before formulating the optimal control problem, we need to consider an augmented CAV dynamics model to incorporate additional features pertaining to a vehicle platoon.

### 5.3.4.1 Augmented CAV Dynamics for Multi-successor Safety

String stability in the context of a vehicular platoon signifies whether the amplitude of any disturbance introduced by the lead vehicle gets amplified downstream, leading to safety implications for the trailing vehicles. In our formulation, the control input  $u_1(t)$  of CAV-1 of a platoon can introduce such instability for the trailing HDVs in  $\mathcal{N}_{\text{HDV}}$ . Since the HDVs cannot be controlled directly, and their driving behavior is unknown, we cannot guarantee string stability. However, to ensure rear-end collision avoidance, we can incorporate safety constraints directly into the optimal control problem, and then solve it using the receding horizon framework which derives the feasible control input sequence for CAV-1 subjected to the added safety constraints within the prediction horizon  $T_p$ .

To capture additional characteristics of the platoon formation dynamics from the CAV's control point of view, we need to define two additional states.

**Definition 5.3.8.** The *leader-follower gap*,  $e_{1,j}(t)$ ,  $j \in \mathcal{N}_{\text{HDV}}$ , is the bumper-to-bumper gap between the CAV and the successive trailing HDVs (see Fig. 5.9),

$$e_{1,2}(t) = p_1(t) - p_2(t) - l_c, \quad (5.61a)$$

$$\vdots$$

$$e_{1,N}(t) = p_1(t) - p_N(t) - (N - 1)l_c. \quad (5.61b)$$

In the case where PV-0 exists immediately preceding CAV-1, then we define an additional state.

**Definition 5.3.9.** The *leader-predecessor gap*,  $e_{1,0}(t)$ , is the bumper-to-bumper gap between the CAV and the immediate predecessor vehicle (see Fig. 5.9),

$$e_{1,0}(t) = p_0(t) - p_1(t) - l_c, \quad (5.62)$$

The definition of the leader-follower gap  $e_{1,j}(t)$ ,  $j \in \mathcal{N}_{\text{HDV}}$  and the leader-predecessor gap,  $e_{1,0}(t)$  can be used to formulate enhanced safety constraints from the

CAV-1's perspective. We refer to these set of constraints as the multi-successor safety constraints that can guarantee a safe platoon formation.

**Lemma 5.3.10.** *Given the leader-follower gap  $e_{1,j}(t)$ ,  $j \in \mathcal{N}_{HDV}$  and the leader-predecessor gap,  $e_{1,0}(t)$ , the rear-end safety constraint in (5.44) is satisfied if the following set of conditions hold*

$$e_{1,0}(t) \geq s_1(t), \quad (5.63a)$$

$$e_{1,2}(t) \geq s_2(t), \quad (5.63b)$$

$$e_{1,3}(t) \geq e_{1,2}(t) + s_3(t), \quad (5.63c)$$

$\vdots$

$$e_{1,N}(t) \geq e_{1,N-1}(t) + s_N(t). \quad (5.63d)$$

*Proof.* We first consider the immediately preceding and following vehicles of CAV-1. According to (5.43a) and (5.62), we have  $\Delta p_1(t) = p_0(t) - p_1(t) - l_c = e_{1,0}(t)$ . Therefore,  $e_{1,0}(t) \geq s_1(t)$  implies  $\Delta p_1(t) \geq s_1(t)$ , which is the safety constraint for CAV-1 in (5.44). Similar steps can be taken to proof that  $e_{1,2}(t) \geq s_2(t)$  satisfies the constraint in (5.44) for HDV-2.

For the state  $e_{1,3}(t)$ , we expand it using (5.61b) as  $e_{1,3}(t) = p_1(t) - p_3(t) - 2l_c = (p_1(t) - p_2(t) - l_c) + (p_2(t) - p_3(t) - l_c) = \Delta p_2(t) + \Delta p_3(t)$ . Since  $\Delta p_2(t) = e_{1,2}(t)$ , we have  $e_{1,3}(t) = e_{1,2}(t) + \Delta p_3(t)$ . This implies that  $e_{1,3}(t) - e_{1,2}(t) \geq s_3(t)$  satisfies the condition  $\Delta p_3(t) \geq s_3(t)$  in (5.44). Following the similar procedure, it can be shown that for a platoon of size  $N$ , the condition  $e_{1,N}(t) - e_{1,N-1}(t) \geq s_N(t)$  satisfies the rear-end safety constraint  $\Delta p_N(t) \geq s_N(t)$  in (5.44). This concludes the proof.  $\square$

**Remark 5.3.7.** While controlling CAV-1, the constraint in (5.44) cannot be employed directly to enforce rear-end safety guarantee. However, the constructed multi-successor safety constraints in (5.63) can guarantee the enforcement of (5.44), thus ensuring a safe platoon formation.

Finally, the definition of the additional states  $e_{1,0}(t)$ ,  $e_{1,2}(t)$ ,  $\dots$ ,  $e_{1,N}(t)$  enables the augmentation of the CAV-1 dynamics (5.40) with the following set of equations

$$\dot{p}_1(t) = v_1(t), \quad (5.64a)$$

$$\dot{v}_1(t) = u_1(t), \quad (5.64b)$$

$$\dot{e}_{1,0}(t) = v_0(t) - v_1(t), \quad (5.64c)$$

$$\dot{e}_{1,2}(t) = v_1(t) - v_2(t), \quad (5.64d)$$

$$\vdots$$

$$\dot{e}_{1,N}(t) = v_1(t) - v_N(t). \quad (5.64e)$$

### 5.3.4.2 Linear Receding Horizon Formulation

To enable the application of a discrete linear receding horizon control framework, we formulate the optimal control problem in discrete time. Let us consider a sampling time interval of  $\tau$  to discretize the optimization horizon into  $k$  discrete instances. The augmented CAV dynamics in (5.64) can be recast into linear discrete time state equations with the following consideration: During each time step  $[k, (k+1)]$ , (a) the control input of the CAV  $u_1(k)$  is constant, and (b) the control input of the vehicles  $u_i(k)$ ,  $i \in \mathcal{N} \setminus \{1\}$  is zero (see Internal Model 1). The linear discrete-time state equations of the augmented CAV dynamics in (5.64) are

$$p_1(k+1) = p_1(k) + v_1(k)\tau + \frac{\tau^2}{2}u_1(k), \quad (5.65a)$$

$$v_1(k+1) = v_1(k) + u_1(k)\tau, \quad (5.65b)$$

$$e_{1,0}(k+1) = e_{1,0}(k) + (v_0(k) - v_1(k))\tau + \frac{\tau^2}{2}u_1(k), \quad (5.65c)$$

$$e_{1,2}(k+1) = e_{1,2}(k) + (v_1(k) - v_2(k))\tau + \frac{\tau^2}{2}u_1(k), \quad (5.65d)$$

$$\vdots$$

$$e_{1,N}(k+1) = e_{1,N}(k) + (v_1(k) - v_N(k))\tau + \frac{\tau^2}{2}u_1(k). \quad (5.65e)$$

We define the current state vector  $\mathbf{x}_1(k) \in \mathbb{R}^{(N+2) \times 1}$ , measured output vector  $\mathbf{y}_1(k) \in \mathbb{R}^{(N+2) \times 1}$  and the measured disturbance vector  $\mathbf{w}_1(k) \in \mathbb{R}^{N \times 1}$  as

$$\mathbf{x}_1(k) := \begin{bmatrix} p_1(k) \\ v_1(k) \\ e_{1,0}(k) \\ e_{1,2}(k) \\ \vdots \\ e_{1,N}(k) \end{bmatrix}, \quad \mathbf{y}_1(k) := \begin{bmatrix} p_1(k) \\ v_1(k) \\ e_{1,0}(k) \\ e_{1,2}(k) \\ \vdots \\ e_{1,N}(k) \end{bmatrix}, \quad \mathbf{w}_1(k) := \begin{bmatrix} v_0(k) \\ v_2(k) \\ \vdots \\ v_N(k) \end{bmatrix}.$$

The state-space representation of the discrete dynamic in (5.65a)-(5.65e) can be written as

$$\mathbf{x}_1(k+1) = \mathbf{A}\mathbf{x}_1(k) + \mathbf{B}_u u_1(k) + \mathbf{B}_w \mathbf{w}_1(k), \quad (5.66)$$

$$\mathbf{y}_1(k) = \mathbf{C}\mathbf{x}_1(k), \quad (5.67)$$

where the corresponding state matrix  $\mathbf{A} \in \mathbb{R}^{(N+2) \times (N+2)}$ , control matrix  $\mathbf{B}_u \in \mathbb{R}^{(N+2) \times 1}$ , disturbance matrix  $\mathbf{B}_w \in \mathbb{R}^{(N+2) \times N}$  and output matrix  $\mathbf{C} \in \mathbb{R}^{(N+2) \times (N+2)}$  can be computed using (5.65). For the remainder of this section, we drop the subscript denoting the CAV from the discrete state-space model where it does not introduce any ambiguity.

In order to solve an online optimization within the prediction horizon  $T_p$ , the receding horizon controller requires a prediction model to take into account the future possible states. Let us denote  $\mathbf{x}(k+n|k)$ ,  $\mathbf{y}(k+n|k)$ , and  $\mathbf{w}(k+n-1)$ ,  $n = 1, \dots, T_p$ , to be the predicted state, output and disturbance vectors within the prediction horizon  $T_p$  based on their value at the discrete instance  $k$ , respectively. In this case, the future system trajectories of  $\mathbf{x}(k+n|k)$ ,  $\mathbf{y}(k+n|k)$ , and  $\mathbf{w}(k+n-1)$  are predicted based on the model (5.65) and the current information  $\mathbf{x}(k)$ ,  $\mathbf{y}(k)$ ,  $\mathbf{w}(k)$ .

In our formulation, we consider that the measured disturbance  $\mathbf{w}(k)$  in (5.66) remains constant within the prediction horizon  $T_p$  (Internal Model 1). Therefore, we have

$$\mathbf{w}(k+n|k) = \mathbf{w}(k), \quad n = 1, \dots, T_p. \quad (5.68)$$

### 5.3.4.3 Optimal Control Problem

Let us define  $\|z\|_M$  to be the  $M$  weighted norm of an arbitrary vector  $z$  such that  $\|z\|_M := (z^T M z)^{\frac{1}{2}}$ . In order to drive each HDV's state towards the equilibrium platoon state, the term  $\Delta p_i(t) - s_i(t)$  for each vehicle  $i \in \mathcal{N}_p$  should converge to zero according to Definition 5.3.5. Therefore, the primary aim of the CAV controller is to minimize the squared error between the leader-follower gap  $e_{1,N}(k)$  and the reference  $e_r(k) = \sum_{i=2}^N s_i(k)$ . To this end, we formulate the first objective function  $J_1$  which represents a reference tracking problem and takes the form

$$J_1 := \frac{1}{2} \sum_{n=1}^{T_p} \|\mathbf{y}(k+n|k) - \mathbf{y}_r(k+n|k)\|_{\mathbf{Q}}^2, \quad (5.69)$$

where the positive semi-definite output weight matrix  $\mathbf{Q}$  is defined as  $\mathbf{Q} = \text{diag}(0, \dots, w_{e_{1,N}})$ , with  $w_{e_{1,N}} \in \mathbb{R}_{>0}$  corresponding to the leader-follower gap  $e_{1,N}(k)$ , and the reference output  $\mathbf{y}_r(k) \in \mathbb{R}^{(N+2) \times 1}$  is considered as

$$\mathbf{y}_r(k) = \left[ 0, \dots, \sum_{i=2}^N s_i(k) \right]^T. \quad (5.70)$$

Note that, only the last element of the reference output  $\mathbf{y}_r(k)$  is non-zero. Using (5.42), this term can be written as

$$\sum_{i=2}^N s_i(k) = (N-1)s_0 + \hat{\boldsymbol{\rho}}^T \hat{\mathbf{w}}(k), \quad (5.71)$$

where  $\hat{\boldsymbol{\rho}} := [\rho_2, \rho_3, \dots, \rho_N]^T$  and  $\hat{\mathbf{w}}(k) := [v_2(k), \dots, v_N(k)]^T$ . Recall that, the measured disturbance  $\mathbf{w}(k)$  remains time-invariant within the prediction horizon  $T_p$ . Therefore,  $\hat{\mathbf{w}}(k)$  also remains constant within the prediction horizon  $T_p$ . Since the reference output  $\mathbf{y}_r(k)$  is an explicit function of  $\hat{\mathbf{w}}(k)$ , the predictive reference output  $\mathbf{y}_r(k+n|k)$ ,  $n = 1, \dots, T_p$  remains constant within the prediction horizon  $T_p$  as well. Thus we have

$$\mathbf{y}_r(k+n|k) = \mathbf{y}_r(k), \quad n = 1, \dots, T_p. \quad (5.72)$$

The second objective of the controller is to minimize the control effort of CAV-1 while forming the platoon. Thus, we have the second objective function as

$$J_2 := \frac{1}{2} \sum_{m=1}^{T_p} \|u_1(k+m-1)\|_{\mathbf{R}}^2, \quad (5.73)$$

where  $\mathbf{R} := [w_u]$  is the positive-definite weight matrix on the control input with a weight parameter  $w_u \in \mathbb{R}_{>0}$ .

Our objective is to derive the control input sequence  $\mathbf{U}_1(k) := [u_1(k), u_1(k+1), \dots, u_1(k+T_p-1)]^T$  such that the predictive states are driven to their respective reference states. The optimal control problem can thus be written as

$$\min_{\mathbf{U}_1(k)} J_1 + J_2, \quad (5.74)$$

subject to :

model: (5.65),

constraints: (5.41a), (5.41b), (5.63), (5.70).

The above optimal control problem can be cast into a standard constrained quadratic programming problem and solved using commercially available mathematical programming solvers [206]. At each sampling time, the CAV measures the current inter-vehicle gap, target HDV's speed, and self speed. Using these measurements, the control sequence  $\mathbf{U}_1(k)$  at time instant  $k$  is computed by solving the optimal control problem (5.74) and only the first control input is applied. Then the system moves to the next time instant  $k+1$ , and the process is repeated.

### 5.3.5 Model-dependent Control Framework

In Section 5.3.4, we have not considered any intrinsic behavioral model of the HDVs in  $\mathcal{N}_{\text{HDV}}$  while formulating the control problem in (5.74). In this section, we present two examples of platoon formation where we consider (a) non-linear HDV models for non-linear receding horizon control and (b) a surrogate linear model for data-driven predictive control.

### 5.3.5.1 Nonlinear Receding Horizon Control

Since we do not consider a behavioral model for the HDVs in Section 5.3.4, we assumed a constant speed prediction model (Internal Model 1) that enables the implementation of linear receding horizon control. However, such assumption can introduce errors in HDVs' state estimation within the prediction horizon  $T_p$ . In this section, we improve the construct of the Internal Model 1 and enable the state trajectory prediction with a non-linear car-following model with fixed nominal parameters.

**Internal Model 2.** The speed of each HDV in  $\mathcal{N}_{\text{HDV}}$  is updated within the prediction horizon  $T_p$  using a nonlinear car-following model with fixed, calibrated parameters. The speed of PV-0 remains constant within the prediction horizon  $T_p$ , as in the Internal Model 1.

For the Internal Model 2, we consider the OVM car-following model (5.49), which is nonlinear in nature. The consideration of the non-linear car-following model makes the discrete dynamics in (5.75) nonlinear, which we solve with a non-linear receding horizon control framework. Note that, we consider the prediction of PV-0 trajectory with the Internal Model 1. This is due to the fact that, the CAV-1 has no knowledge of PV-0's interaction with any of its preceding vehicle. Thus, we cannot implement a car-following model to predict the future trajectory of PV-0 within the prediction horizon, and our only option is to use the Internal Model 1.

The augmented CAV dynamics in (5.64) can be recast into linear discrete time state equations with the following consideration: During each time step  $[k, (k+1)]$ , the control input  $u_1(k)$  of the CAV-1 and  $u_i(k)$  of each HDV  $i$  in  $\mathcal{N}_{\text{HDV}}$  are constant (see Internal Model 2). Then, the set of discretized augmented CAV dynamics in (5.64) are

$$p_1(k+1) = p_1(k) + v_1(k)\tau + \frac{\tau^2}{2}u_1(k), \quad (5.75a)$$

$$v_1(k+1) = v_1(k) + u_1(k)\tau, \quad (5.75b)$$

$$e_{1,0}(k+1) = e_{1,0}(k) + \Delta v_1(k)\tau - \frac{\tau^2}{2}u_1(k), \quad (5.75c)$$

$$e_{1,2}(k+1) = e_{1,2}(k) + \Delta v_2(k)\tau + \frac{\tau^2}{2}(u_1(k) - f_{\text{nom}}(k)), \quad (5.75d)$$

⋮

$$e_{1,N}(k+1) = e_{1,N}(k) + \Delta v_N(k)\tau + \frac{\tau^2}{2}(u_1(k) - f_{\text{nom}}(k)), \quad (5.75e)$$

where  $f_{\text{nom}}(k)$  is the nominal car-following model considered for the Internal Model 2. The nonlinear receding horizon controller generates the predictive states  $e_{1,N}(k+n|k)$  for  $n = 1, \dots, T_p$  at each time instant  $k$  for a prediction horizon  $T_p$  using the state definitions in (5.61), (5.62), vehicle dynamics in (5.75) and internal car-following models of the HDVs in (5.49). The optimal control problem can be written as follows

$$\min_{U_1(k)} J_1 + J_2, \quad (5.76)$$

subject to :

model: (5.75),

constraints: (5.41a), (5.41b), (5.63), (5.70).

### 5.3.5.2 Data-Driven Receding Horizon Control

In this model-dependent approach, we present a data-driven receding horizon control framework to address Problem 5.3.1 with the following internal model.

**Internal Model 3.** The speed trajectory of each HDV  $i$  in  $\mathcal{N}_{\text{HDV}}$  is updated using a linear car-following model within the prediction horizon  $T_p$ , the parameters of which are estimated online. The speed of PV-0 remains constant within the prediction horizon  $T_p$ , as in Internal Model 1.

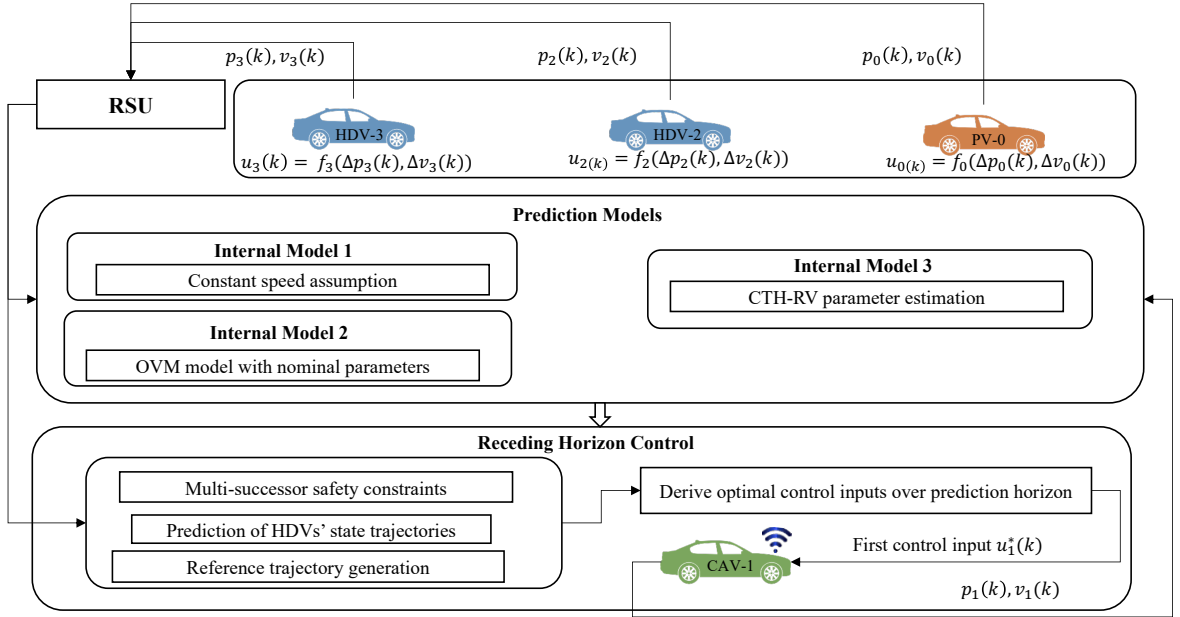


Figure 5.10: The structure of the proposed control framework to address Problem 5.3.1.

We use recursive least squares (RLS) method [196, 197] to estimate the HDVs' car-following parameters for state prediction to address Problem 5.3.1, as shown in Fig. 5.10. The essential steps of the proposed framework are outlined as follows.

1. **Data-driven parameter estimation:** At each time instant  $k$ , the current states  $p_i(k), v_i(k)$  of each following HDV  $i$  in  $\mathcal{N}_{\text{HDV}}$  are communicated to CAV-1. Since the exact car-following model  $f_i$  of each HDV  $i$  in  $\mathcal{N}_{\text{HDV}}$  is unknown to CAV-1, it considers a known linear car-following model to represent the driving behavior of each HDV, and estimates the parameters of the car-following model for each HDV online.
2. **Data-driven control problem:** CAV-1 then uses the estimated car-following model from Step 1 to predict the future state trajectories of the following HDVs, uses a constant speed model to predict the trajectory of PV-0. It then derives its own optimal control input sequence  $\mathbf{U}_1^*(k) := [u_1^*(k), u_1^*(k+1), \dots, u_1^*(k+T_p-1)]^T$  by solving the optimal control problem in (5.76) using the receding horizon control framework. Finally, CAV-1 implements only the first control input  $u_1^*(k)$ .

In what follows, we provide a detailed exposition of the car-following model parameter estimation discussed above.

### 5.3.5.3 Online Car-following Model Parameter Estimation

In this section, we use a recursive least-squared formulation [196] to estimate the parameters of the internal car-following model residing in CAV-1's mainframe to represent the driving behavior of each of the following HDVs. To this end, we consider the constant time headway relative velocity (CTH-RV) model [197, 198]

$$\begin{aligned} v_i(k+1) = & v_i(k) + \eta_i(\Delta p_i(k) - \rho_i v_i(k))\tau + \\ & \nu_i(v_{i-1}(k) - v_i(k))\tau, \end{aligned} \quad (5.77)$$

where the model parameters  $\eta_i$  and  $\nu_i$  are the control gains on the constant time headway and the approach rate, and  $\rho_i$  is the desired safe time headway for each HDV  $i$  in  $\mathcal{N}_{\text{HDV}}$ , respectively. We employ the linear CTH-RV model instead of other complex nonlinear models so that the resulting control problem presented in the next section is thus convex and can be solved efficiently in real-time. Moreover, it is also observed that CTH-RV model is highly comparable to other nonlinear car-following models in terms of data fitting [198].

Suppose that, we measure the speed  $v_i(t)$ , headway  $\Delta p_i(t)$  and approach rate  $\Delta v_i(t)$  data at a frequency corresponding to the sampling time  $\tau$ . Then we can rewrite the CTH-RV model (5.77) for each HDV  $i$  in  $\mathcal{N}_{\text{HDV}}$  in discrete time as  $v_i(k+1) = v_i(k) + \eta_i(\Delta p_i(k) - \rho_i v_i(k))\tau + \nu_i(v_{i-1}(k) - v_i(k))\tau$ , which can be recast as

$$v_i(k+1) = \gamma_{i,1}v_i(k) + \gamma_{i,2}\Delta p_i(k) + \gamma_{i,3}v_{i-1}(k), \quad (5.78)$$

where  $\gamma_1 := (1 - (\eta_i\rho_i + \nu_i)\tau)$ ,  $\gamma_2 := \eta_i\tau$  and  $\gamma_3 := \nu_i\tau$  are the parameters we aim at estimating online. Then we can write the measurements in matrix form as

$$v_i(k+1) = \boldsymbol{\gamma}_i^T \boldsymbol{\phi}_i(k), \quad (5.79)$$

where  $\boldsymbol{\phi}_i(k) := [v_i(k), \Delta p_i(k), v_{i-1}(k)]^T$  is the regressor vector and  $\boldsymbol{\gamma}_i := [\gamma_{i,1}, \gamma_{i,2}, \gamma_{i,3}]^T$  is the parameter vector. If we have  $N_k$  uniformly sampled measurements for  $k = \{1, \dots, T_h\}$ , then we can estimate the  $\gamma$  by solving the following minimization problem

$$\min_{\boldsymbol{\gamma}_i} \frac{1}{2} \sum_{k=1}^{T_h} \xi^{(T_h-k)} [v_i(k) - \hat{v}_i(k|\boldsymbol{\gamma}_i)]^2, \quad (5.80)$$

where,  $\hat{v}_i(k|\boldsymbol{\gamma}_i) := \boldsymbol{\gamma}_i^T \boldsymbol{\phi}_i(k)$  is a prediction of  $v_i(k)$  based on the parameter vector  $\boldsymbol{\gamma}_i$ , and  $\xi \in [0, 1]$  is the forgetting factor that assigns higher weight to the recently collected data points and discounts older measurements. Note that, the objective function in (5.80) is quadratic in  $\boldsymbol{\gamma}_i$ , thus can be minimized analytically that yields

$$\boldsymbol{\gamma}_i = \left[ \sum_{k=1}^{T_h} \boldsymbol{\phi}_i(k) \boldsymbol{\phi}_i^T(k) \right]^{-1} \sum_{k=1}^{T_h} \boldsymbol{\phi}_i(k) v_i(k). \quad (5.81)$$

However, the above estimation procedure requires the storage of  $\boldsymbol{\phi}_i(k)$  and  $v_i(k)$  for all  $k = 0, \dots, T_h$ , and yields the final estimated parameter vector  $\boldsymbol{\gamma}_i$  for time  $T_h$ . Since we are interested in online parameter estimation, it is computationally more efficient to update the intermediate time-dependent parameter vector  $\hat{\boldsymbol{\gamma}}_i$  in (5.81) recursively at each time step  $k = 1, \dots, T_h$  as new data becomes available. Therefore, we employ the following recursive form of (5.81) known as the recursive least squares algorithm [196]

$$\hat{\boldsymbol{\gamma}}_i(k) = \hat{\boldsymbol{\gamma}}_i(k-1) + \mathbf{L}_i(k)[v_i(k) - \hat{v}_i(k)], \quad (5.82a)$$

$$\hat{v}_i(k) = \hat{\boldsymbol{\gamma}}_i^T(k-1) \boldsymbol{\phi}_i(k), \quad (5.82b)$$

$$\mathbf{L}_i(k) = \frac{\mathbf{P}_i(k-1) \boldsymbol{\phi}_i(k)}{\xi + \boldsymbol{\phi}_i^T(k) \mathbf{P}_i(k-1) \boldsymbol{\phi}_i(k)}, \quad (5.82c)$$

$$\mathbf{P}_i(k) = \frac{1}{\xi} \left[ \mathbf{P}_i(k-1) - \frac{\mathbf{P}_i(k-1) \boldsymbol{\phi}_i(k) \boldsymbol{\phi}_i^T(k) \mathbf{P}_i(k-1)}{\xi + \boldsymbol{\phi}_i^T(k) \mathbf{P}_i(k-1) \boldsymbol{\phi}_i(k)} \right]. \quad (5.82d)$$

The recursion of the RLS algorithm in (5.82a) can be initiated at the time instant  $k = 0$  by considering an invertible matrix  $\mathbf{P}_i(0)$  and the vector  $\hat{\boldsymbol{\gamma}}_i(0)$  with some initial values.

### 5.3.6 Simulation Results and Discussion

To validate the effectiveness of the control frameworks presented in the previous sections and evaluate their performance, we conduct extensive numerical simulations. For the sake of concise exposition, we refer to the model-independent linear RHC framework as L-RHC, the model-dependent nonlinear RHC framework as N-RHC, and the data-driven linear RHC framework as DD-RHC. In our analysis, we only consider

Table 5.3: Nominal values of the car-following model

Optimal velocity model	
Driver’s sensitivity coefficient, $\alpha$	0.4
Speed difference coefficient, $\beta$	0.2
Desired speed, $v_d$	30 m/s
Safe time headway, $\rho$	1.8 s

feasible platoon formation problem, i.e., Problem 5.3.1 satisfies the feasibility requirements according to Lemmas 5.3.6 and 5.3.7. Next, we discuss the configuration of the simulation environment and present an in-depth analysis of the simulation results.

### 5.3.6.1 Simulation Setup

We conducted several simulations with different numbers of trailing HDVs, and with or without a preceding vehicle. All three control approaches presented in this section, namely, the L-RHC with constant HDV speed, the N-RHC with nonlinear CFM, and the DD-RHC with recursive least squares estimation of CTH-RV parameters, are evaluated through the simulations. To create a mixed traffic environment with different human driving styles, we employed the non-linear OVM [200] to simulate the driving behavior of the human drivers. The parameters for each human driver’s CFM were considered to be different from each other and chosen during the simulation by random perturbation of up to 30% around nominal values. The nominal values for the OVM car-following model are given in Table 5.3. We imposed a specific speed profile to be followed by the preceding vehicle so that we can analyze the robustness of the platoon formation framework under varying driving behavior. For example, in the simulation, we considered a speed profile of the preceding vehicle that decelerates sharply to the minimum allowable speed and then sharply accelerates back to a higher speed. With the consideration of such an abrupt speed profile of the preceding vehicle, we investigated whether the CAV can avoid rear-end collision with the preceding vehicle.

The parameters and weights in the control framework used for the simulations

Table 5.4: Parameters of the receding horizon control framework

Parameters	Value	Parameters	Value
$\tau$	0.1 s	$T_p$	20
$v_{\max}$	35 m/s	$v_{\min}$	0 m/s
$u_{\max}$	3 m/s <sup>2</sup>	$u_{\min}$	-5 m/s <sup>2</sup>
$\rho$	1.5 s	$s_0$	3.0 m
$w_{e_{1,N}}$	1	$w_u$	1

are given in Table 5.4. We use Python for developing the simulation environment where the receding horizon control problems are formulated by CasADi [199]. We use the qpOASES solver [210] to solve the linear RHC and data-driven RHC, while the nonlinear RHC is solved by the IPOPT solver [211]. In the nonlinear RHC problem, we utilize the nominal values of the OVM as shown in Table 5.3 in the prediction models for all the HDVs. The RLS-based estimators in the data-driven RHC are initialized with the following values:  $\hat{\gamma}_i(0) = [0.67, 0.1, 0.18]^T$  and  $\mathbf{P}_i(0) = 0.01 \mathbb{I}_3$  where  $\mathbb{I}_3$  is the  $3 \times 3$  identity matrix, while the forgetting factor is chosen as  $\xi = 1.0$ . Note that all simulations in this work are performed on a Macbook Pro computer with a 2.7 GHz Quad-Core Intel Core i7 CPU and 16Gb RAM.

Although we conducted extensive numerical simulations using the proposed L-RHC, N-RHC and DD-RHC approaches, we mainly focus on the results of the DD-RHC approach to analyze the platoon formation process, as shown in Figs 5.11 and 5.12. The vehicle trajectories with the L-RHC and N-RHC approaches are relatively similar and can be found in <https://sites.google.com/view/ud-ids-lab/RHC-based-Platoon-Formation>. We provide a detailed comparative analysis of these three approaches later in the analysis.

### 5.3.6.2 Platoon Formation and Safety

We first show the results of the platoon formation process using the proposed DD-RHC framework considering 4 trailing HDVs, i.e.,  $N = 5$ . We consider two different

scenarios: (a) no preceding vehicle and (b) presence of a preceding vehicle with a predefined speed trajectory. The trajectories of all vehicles without and with the preceding vehicle are illustrated in Figs. 5.11 and 5.12, respectively. The trajectories of the vehicles shown in each figure include their positions, speeds, headways, and speed gaps. In the case where no preceding vehicle is considered, Fig. 5.11(c) shows that the headways of the vehicles become time invariant around 20 s, and Fig. 5.11(b) shows that the speeds of the vehicles converge to the same value. This implies that, in both scenarios, the CAV is able to form a platoon with the trailing HDVs. In addition, to challenge the safety guarantee of the CAV during the platoon formation process, we consider the presence of a preceding vehicle with an abrupt decelerating speed profile. As illustrated in Fig. 5.12, even in the presence of a preceding vehicle with aggressive speed profile, the CAV is able to form a platoon with the trailing HDVs while maintaining a safe distance from the preceding vehicle.

Note that, in both of the above scenarios, none of the safety constraints in (5.44) and speed constraint in (5.41a) are violated during the platoon formation process, as evident from Figs. 5.11(c) and 5.12(c), and Figs. 5.11(b) and 5.12(b), respectively. The rear-end safety guarantee can also be visualized by observing the non-intersecting position trajectories of the vehicles in Figs. 5.11(a) and 5.12(a). This indicates the fidelity of the proposed DD-RHC framework in satisfying all the constraints during the platoon formation process.

### 5.3.6.3 Online Parameter Estimation

For the simulation with DD-RHC framework, the estimated parameters in the CTH-RV car-following model for all trailing HDVs are shown in Fig. 5.13. Recall that, CAV-1 characterizes in real time the driving behaviors of the four trailing HDVs with individual set of estimated parameters  $\eta$ ,  $\nu$ , and  $\rho$ . Initially, the estimated values of the car-following parameters show abrupt changes due to the lack of state information transmitted from the HDVs. However, as time progresses, more data points become

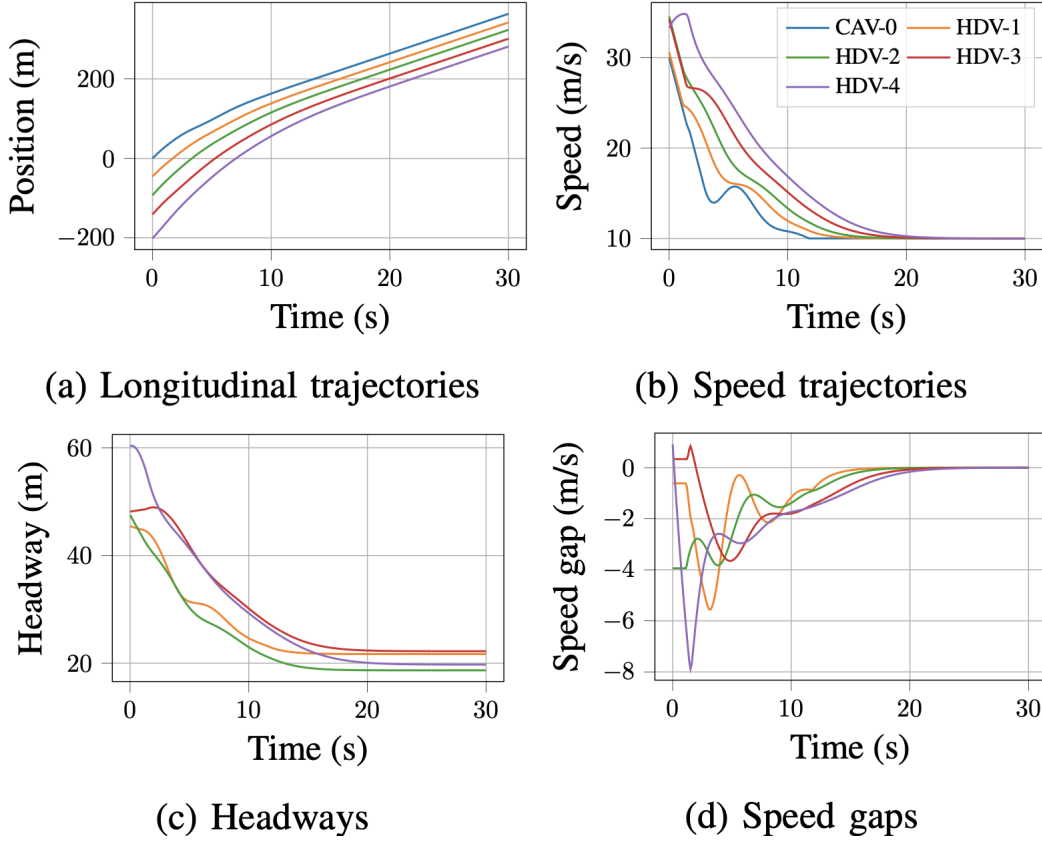


Figure 5.11: Longitudinal trajectories, speed, headways and speed gaps of the vehicles for DD-RHC in the simulation without a preceding vehicle.

available from the HDVs, and the estimation of the car-following parameters stabilizes towards the set of values that best describe the driving behavior of the HDVs. This is consistent with the observation in [197], where parameters estimated using RLS algorithm have been demonstrated to show near-convergence to the actual values. Therefore, we can utilize the linear CTH-RV model and online RLS technique to approximate a nonlinear car-following model such as the OVM so that the resulting RHC problem is convex and thus, can be solved efficiently in real time.

Next, we provide the robustness, scalability, and sensitivity analysis to quantify the performance of the proposed approaches.

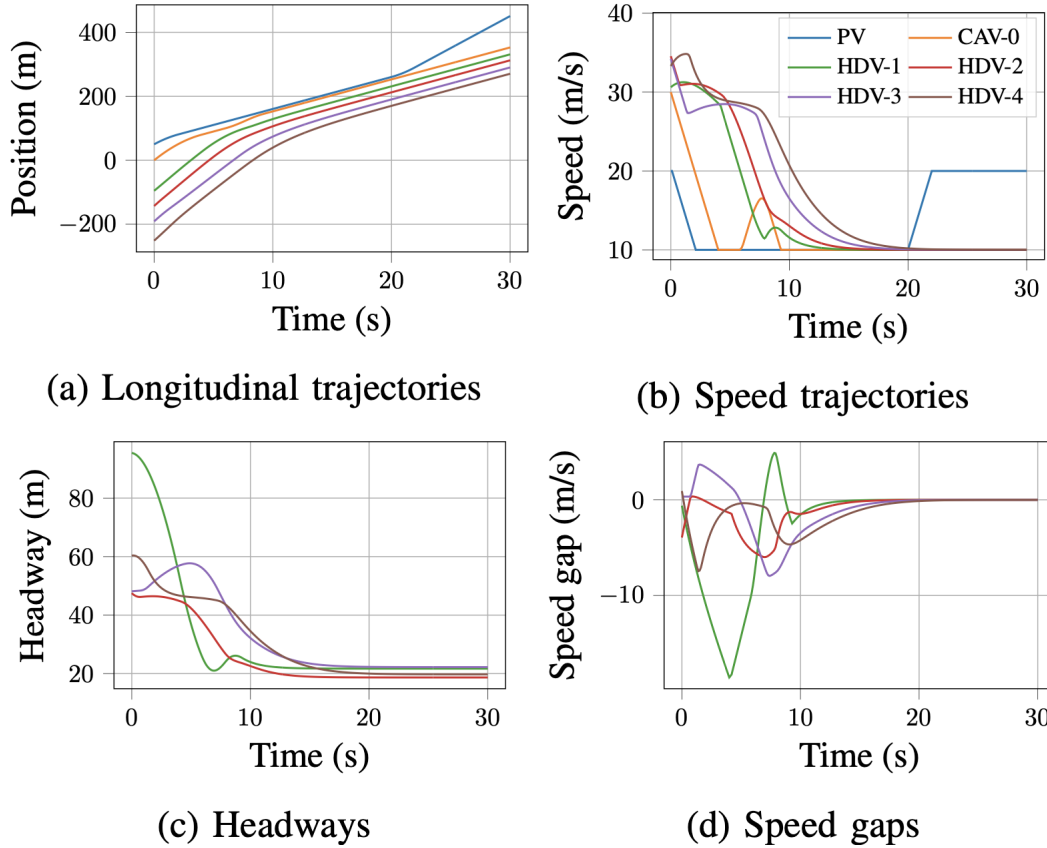


Figure 5.12: Longitudinal trajectories, speed, headways and speed gaps of the vehicles for DD-RHC in the simulation with a preceding vehicle (PV).

#### 5.3.6.4 Scalability

For the scalability analysis, we show the position trajectories for all the vehicles in Fig. 5.14 considering different number of following HDVs. Figure 5.14 verifies that the proposed control framework is able to create and maintain platoons of different sizes. We also analyze the scalability of the proposed RHC approaches from a computational perspective considering platoon sizes from  $N = 3$  to 8, as shown in Table 5.5. The N-RHC framework is less scalable with the platoon length  $N$ , as evident by the higher solving time, compared to the L-RHC and DD-RHC approaches. Therefore, the N-RHC framework might not be suitable for real-time control in dense traffic environments that might require the consideration of higher platoon size.

### 5.3.6.5 Robustness

To investigate the robustness of the proposed RHC approaches, we consider the platoon formation time as a metric, which is computed using Remark 5.3.4. The platoon formation time considering different sizes of platoon ( $N=3$  to  $N=8$ ) is summarized in Table 5.5. Note that we only change the number of trailing HDVs in each simulation while the other setups are identical for a fair comparison. Overall, all three approaches are able to form a platoon with higher platoon lengths, which implies the robustness of the approaches subjected to varying platoon lengths. However, we observe that the N-RHC and DD-RHC approaches can form a platoon with the HDVs faster than the L-RHC approach. We further investigated the robustness of the RHC approaches against human driving behavior. Figure 5.16 shows that the proposed RHC approaches are able to form platoons with the trailing HDVs with different types of human driving behavior represented by a wide range of car-following parameters  $\alpha$ ,  $\beta$ ,  $\rho$  and  $v_d$ .

### 5.3.6.6 Computational Efficiency

For a comprehensive comparison between the proposed RHC approaches, we report the solution time of the three methods in several simulations with different numbers of trailing HDVs in Table 5.5. From the standpoint of computational efficiency, N-RHC takes a significantly longer time for solving the optimization problems compared to the L-RHC and DD-RHC approaches. Therefore, N-RHC might not be suitable for real-time control. Meanwhile, the solving time for the L-RHC and DD-RHC approaches are highly reasonable and are less scaled by increasing the number of trailing HDVs.

### 5.3.6.7 Prediction Accuracy

In Fig. 5.15, we compare the prediction accuracy of three presented internal prediction models. To this end, we consider the trajectory of the last HDV of the platoon. For each model, we collect the root mean square errors of the speed prediction

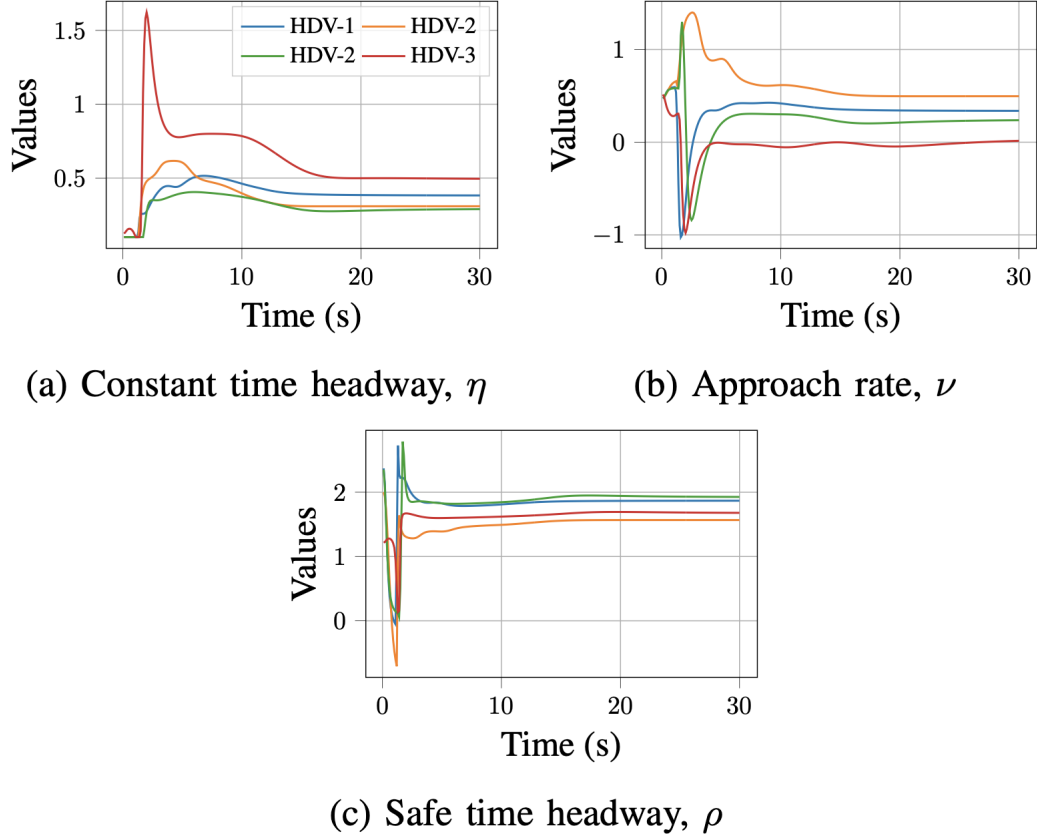


Figure 5.13: Estimates of the car-following parameters for all HDVs.

Table 5.5: Platoon formation time and solving time for L-RHC, N-RHC and DD-RHC in simulations with different number of following HDVs.

$N$	Platoon formation time (s)			Solving time (ms)		
	L-RHC	N-RHC	DD-RHC	L-RHC	N-RHC	DD-RHC
3	16.1	14.4	12.4	5.48	52.32	8.37
4	18.1	17.5	15.3	6.52	48.24	6.19
5	20.3	20.1	18.9	4.51	51.50	7.89
6	23.4	27.1	23.4	4.55	87.45	13.31
7	31.9	25.1	32.5	5.54	107.41	8.42
8	31.6	28.4	31.6	6.02	121.99	10.32

over the current horizon at each time step, which are computed from the differences between predicted speeds using the internal prediction models and the real car-following

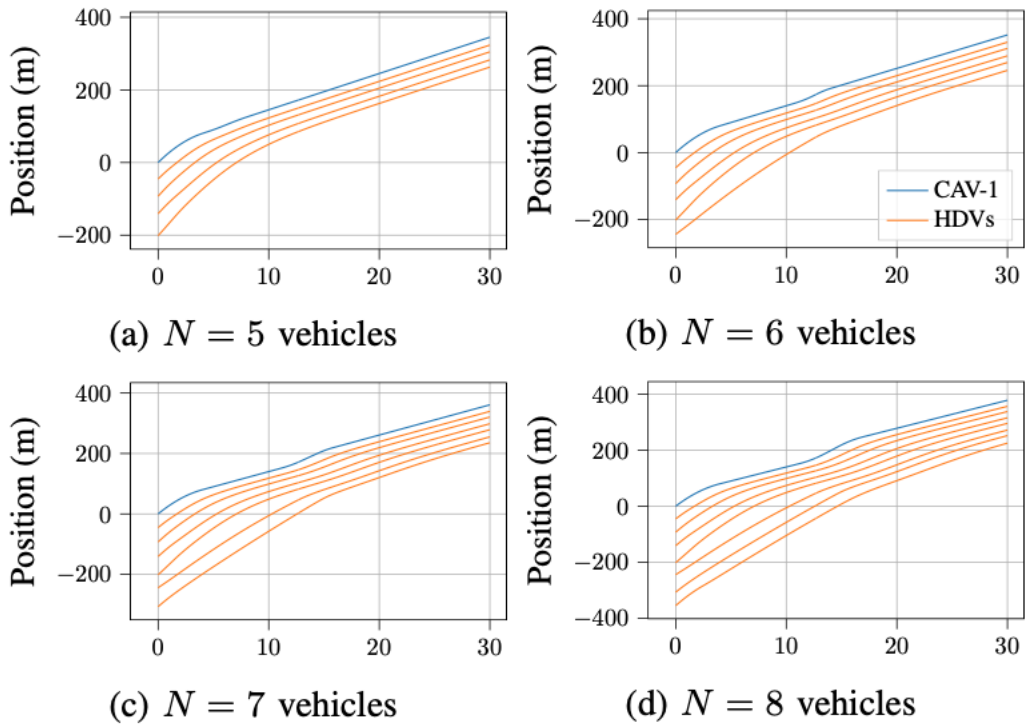


Figure 5.14: Longitudinal trajectories of the vehicles in the simulations with different number of following HDVs.

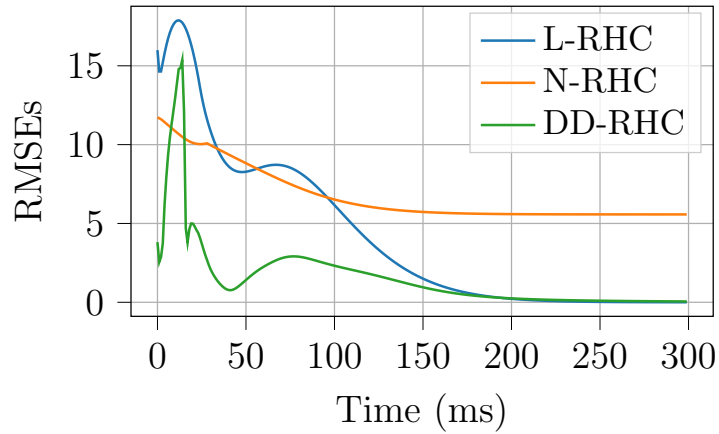


Figure 5.15: Comparison on prediction accuracy of three internal prediction models using root mean square errors (RMSEs).

models of the HDV. The results show that the internal model 1, i.e., the constant-speed model and the internal model 3, i.e., the data-driven model, converges to zero prediction error as time progresses. On the other hand, the internal model 2, which is a nonlinear car-following model with fixed nominal parameters, generally shows very high prediction errors that never converges to zero. This is due to the fact that, the internal model 2 cannot update the nominal values of the car-following parameters to predict the HDV's behavior. Therefore, internal model 2 has the worst performance of all the prediction models considered.

Although, both the errors associated with the internal model 1 and 3 converge to zero, they differ in terms of how quickly they are converging towards accurate prediction. During the platoon formation process, the internal model 1 shows high prediction error, as shown in Fig. 5.15. It can only predict well during the steady-state when the platoon is formed and the vehicles move at constant speeds. This is understandable, since the internal model 1 uses constant speed assumption for prediction, and therefore, cannot capture the transient driving behavior. In contrast, the internal model 3 can update its car-following parameters online from the beginning of the platoon formation process, and predict the HDV's behavior with higher accuracy as time progresses. Overall, the results show that the internal model 3, i.e., the data-driven model, has better accuracy compared to the other two models.

### 5.3.6.8 Sensitivity Analysis

For sensitivity analysis, we consider variations of the HDV's car-following parameters, including the human driver's sensitivity coefficient  $\alpha$ , speed difference coefficient  $\beta$ , desired speed  $v_d$ , and safe time headway  $\rho$ , in the simulations with DD-RHC. Particularly, we conduct several sets of simulations where, in each set, we consider 10 different nominal values for each OVM parameter, while keeping the other parameters constant. Note that, the parameters for each HDV are still randomly perturbed around the nominal values. We collect the platoon formation time for those simulations and

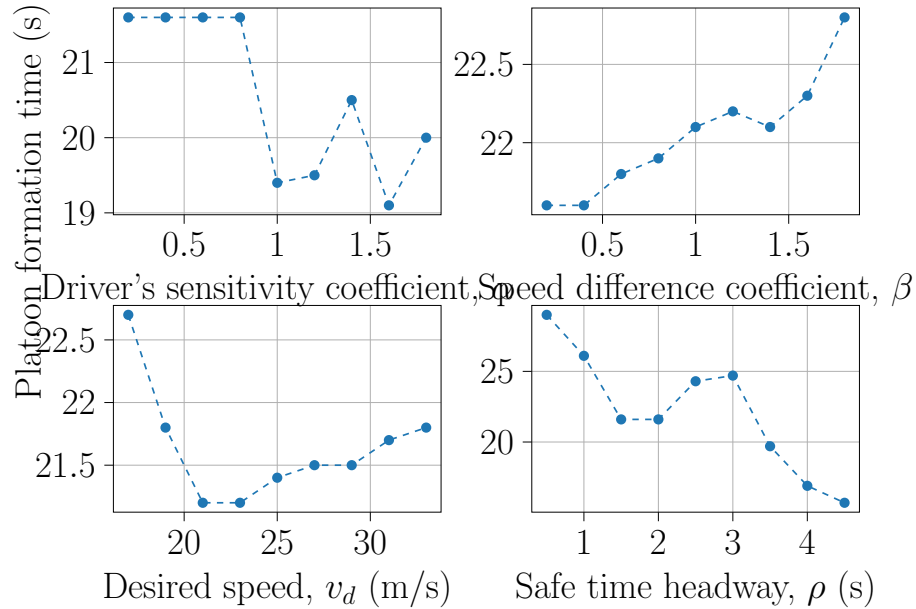


Figure 5.16: Platoon formation time under varying parameters of the OVM car-following models.

show it in Fig. 5.16. The results suggest that with different human driving styles of the following HDVs, the control framework can guarantee the formation of a platoon. However, platoon formation process gets delayed with increasing values  $\beta$  and  $v_d$ , and is expedited with increasing values of  $\alpha$  and  $\rho$ .

In this section, a safety-prioritized multi-objective control framework for creating a mixed platoon of vehicles is proposed, that ensures indirect control of the trailing HDVs by directly controlling the leading CAV, while considering the system constraints and initial conditions. A detailed analysis of the platoon formation framework for a model-dependent and a model-independent receding horizon framework is presented that employs different prediction models for estimating the HDV trajectories: (a) a naive constant speed model, (b) a nonlinear car-following model with nominal parameters and (c) a data-driven model that estimates the driving behavior of the HDVs in real time using recursive least squares algorithm to better predict the future trajectories. Finally, the efficacy of the platoon formation approaches is evaluated by conducting extensive numerical simulations. Under feasible boundary conditions, all

the approaches were able to form a platoon. We provided a comparative analysis of the different prediction models along with the associated sensitivity, scalability, robustness, and performance analyses. We conclude that the proposed DD-RHC framework outperforms the L-RHC and N-RHC approaches in terms of prediction accuracy and computational efficiency.

## Chapter 6

### OPTIMAL PLATOON COORDINATION IN A MIXED TRAFFIC ENVIRONMENT

In this chapter, I address the problem of coordinating CAV platoons at a highway on-ramp merging. The main objective is to leverage the key concepts of CAV coordination and platooning and establish a control framework for platoon coordination aimed at improving network performance while guaranteeing safety. To this end, I present a single-level constrained optimal control framework based on the insight of Section 3.1, and the seminal of Malikopoulos et al. [88], that optimizes the fuel economy and travel time of the platoons while satisfying the state, control, and safety constraints. I also explore the effect of delayed communication among the CAV platoons and propose a robust coordination framework to enforce lateral and rear-end collision avoidance constraints in the presence of bounded delays. The proposed framework provides a closed-form analytical solution to the optimal control problem with safety guarantees that can be implemented in real time. In Section 6.1, I develop the platoon coordination framework for 100% CAV penetration case, and then extend the framework to incorporate a mixed traffic environment in Section 6.2 for an on-ramp merging scenario.

#### 6.1 Cooperative Merging of Platoons with Delayed Communication

The key contributions of this section are (i) the development of a mathematically rigorous optimal control framework for platoon coordination that eliminates stop-and-go driving behavior, and improves fuel economy and traffic throughput of the network, (ii) the derivation and implementation of the optimal control input in real time that

satisfies the state, control, and safety constraints subject to bounded delayed communication, and (iii) the validation of the proposed control framework using a commercial traffic simulator by evaluating its performance compared to a baseline scenario.

To the best of our knowledge, the proposed approach is the first attempt to establish a rigorous constrained optimal control framework for the coordination of vehicular platoons at a highway on-ramp merging in the presence of bounded inter-platoon delays. This research advances the state of the art as follows. First, in contrast to other efforts that neglected state/control constraints [120, 121, 212], our framework guarantees satisfaction of all of the state, control, and safety constraints in the system. Second, our framework unlike the several efforts in the literature at highway on-ramp merging scenario [27, 76, 213, 214] does not impose a strict first-in-first-out queuing policy to ensure lateral safety. Third, in this section, we consider the bounded delay in the inter-platoon communication, which most of the studies in the coordination of vehicular platoons neglect [120, 215, 216]. Finally, our framework yields a closed-form analytical solution while satisfying all of the system constraints, and thus it is appropriate for real-time implementation on board the CAVs [177].

### 6.1.1 Modeling Framework: Platoon Coordination

We consider the problem of coordinating platoons of CAVs in a scenario of highway on-ramp merging (Fig. 6.1). Although our analysis can be applied to any traffic scenario, e.g., signal-free intersections, roundabouts, and speed reduction zones, we use a highway on-ramp as a reference to present the fundamental ideas and results of this section.

The on-ramp merging includes a control zone, inside of which platoons of CAVs communicate with the *coordinator*. The coordinator does not make any decisions for the CAVs and only acts as a database for the CAVs. The paths of the main road and the ramp road intersect at a point called *conflict point*, indexed by  $n \in \mathbb{N}$ , at which lateral collision may occur. We consider that CAVs have formed platoons upstream

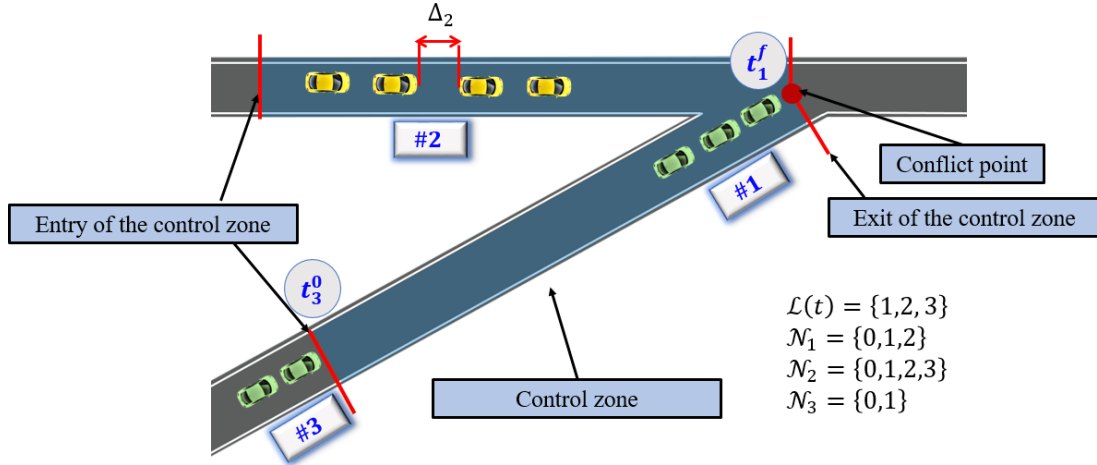


Figure 6.1: On-ramp merging with a single merging point for platoons of CAVs. The control zone is highlighted in light blue color, the entry time and exit time to the control zone are depicted with circles, and example sets of platoon leaders and followers are shown.

of the control zone in a region called *platooning zone*. We refer interested readers to [169, 170, 217] for further details on platoon formation.

### 6.1.1.1 Network Topology and Communication

In our modeling framework, we impose the following communication topology based on the standard V2V and V2I communication protocol as shown in Fig. 6.2.

1. **Bidirectional inter-platoon communication:** The leaders of each platoon can exchange information with each other via the coordinator through a V2I communication protocol. The flow of information is bidirectional.
2. **Unidirectional intra-platoon communication:** The following CAVs of each platoon can subscribe to the platoon leader's state and control information. The flow of information is unidirectional from the platoon leader to the following CAVs within that platoon.

When a platoon leader enters the control zone, it subscribes to the bidirectional inter-platoon communication protocol to connect with the coordinator and access the information of platoons that are already in the control zone. After obtaining this information, the leader derives its optimal control input (acceleration/deceleration) to cross the

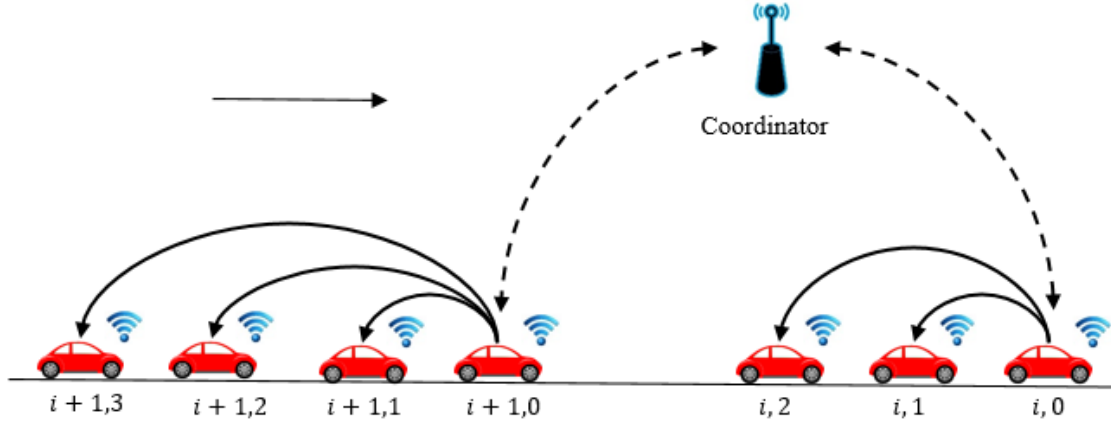


Figure 6.2: Network topology for information flow: (i) bidirectional inter-platoon communication (dashed double-headed arrow) between the platoon leaders via the coordinator, and (ii) unidirectional intra-platoon communication (solid single-headed arrow) from platoon leader to the platoon followers.

control zone without any lateral or rear-end collision with the other CAVs, and without violating any of the state and control constraints. The leader then communicates its derived control input and trajectory information to its followers using the unidirectional intra-platoon communication protocol so that the following CAVs can compute their control input. Finally, the platoon leader transmits its information to the coordinator so that the subsequent platoon leaders can plan their trajectories accordingly. In this section, we enhance our framework to consider delayed transmission during the inter-platoon communication protocol due to the physical distance among the platoons. On the other hand, since the CAVs within each platoon are closely spaced, we consider that there is an instantaneous flow of information within the intra-platoon communication protocol. In our modeling framework, we make the following assumption regarding the nature of delay during the inter-platoon communication protocol.

**Assumption 6.1.1.** The communication delay during the bidirectional inter-platoon communication between each platoon leader and the coordinator is bounded and known a priori.

Assumption 6.1.1 enables the determination of upper bounds on the state uncertainties as a result of sensing or communication errors and delays, and incorporates these into more conservative safety constraints, the exposition of which we provide in Section 6.1.4.

### 6.1.1.2 Dynamics and Constraints

Next, we provide some definitions that are necessary for our exposition.

**Definition 6.1.1.** The queue that designates the order in which each platoon leader entered the control zone is given by  $\mathcal{L}(t) = \{1, \dots, L(t)\}$ , where  $L(t) \in \mathbb{N}$  is the total number of platoons that are inside the control zone at time  $t \in \mathbb{R}_{\geq 0}$ . When a platoon exits the control zone, its index is removed from  $\mathcal{L}(t)$ .

**Definition 6.1.2.** CAVs within platoon  $i \in \mathcal{L}(t)$  are indexed with set  $\mathcal{N}_i = \{0, 1, \dots, m_i\}$ , where 0 and  $m_i \in \mathbb{N}$  denote the leader and last CAV of the platoon  $i$ , respectively. The size of each platoon  $i \in \mathcal{L}(t)$  is thus the cardinality of set  $\mathcal{N}_i$ , and denoted by  $M_i := m_i + 1$ .

In our analysis, we consider that the dynamics of each CAV  $j \in \mathcal{N}_i$  in platoon  $i \in \mathcal{L}(t)$  is governed by a double integrator,

$$\begin{aligned}\dot{p}_{i,j}(t) &= v_{i,j}(t), \\ \dot{v}_{i,j}(t) &= u_{i,j}(t),\end{aligned}\tag{6.1}$$

where  $p_{i,j}(t) \in \mathcal{P}$ ,  $v_{i,j}(t) \in \mathcal{V}$ , and  $u_{i,j}(t) \in \mathcal{U}$  denote position, speed, and control input at  $t \in \mathbb{R}_{\geq 0}$ , respectively. The sets  $\mathcal{P}$ ,  $\mathcal{V}$ , and  $\mathcal{U}$ , are compact subsets of  $\mathbb{R}$ .

**Remark 6.1.1.** In what follows, to simplify notation, we use subscript  $i$  instead of  $i, 0$  to denote the leader of platoon  $i \in \mathcal{L}(t)$ .

Let  $t_{i,0}^0 = t_i^0 \in \mathbb{R}_{\geq 0}$  be the time that leader of platoon  $i \in \mathcal{N}(t)$  enters the control zone, and  $t_{i,0}^f = t_i^f > t_i^0 \in \mathbb{R}_{\geq 0}$  be the time that leader of platoon  $i$  exits the control

zone. Since each CAV  $j \in \mathcal{N}_i$ ,  $i \in \mathcal{L}(t)$ , has already formed a platoon in the platooning zone, when the leader enters the control zone at time  $t_i^0$ , we have  $v_{i,j-1}(t_i^0) - v_{i,j}(t_i^0) = 0$  and  $p_{i,j-1}(t_i^0) - p_{i,j}(t_i^0) - l_c = \Delta_i$ , where  $l_c$  denote the length of each CAV  $j$ , and  $\Delta_i$  is the safe bumper-to-bumper inter-vehicle gap between CAVs  $j, j - 1 \in \mathcal{N}_i$  within each platoon  $i \in \mathcal{L}(t)$ . This bumper-to-bumper inter-vehicle gap is imposed by the platoon forming control in platooning zone upstream of the control zone. After exiting the control zone at  $t_i^f$ , the leader of platoon  $i$  cruises with constant speed  $v_i(t_i^f)$  until the last follower in the platoon exits the control zone. Afterwards, each platoon member  $j \in \mathcal{N}_i, i \in \mathcal{L}(t)$  is controlled by a suitable car-following model [160] which ensures satisfying rear-end safety constraint.

For each CAV  $j \in \mathcal{N}_i$  in platoon  $i \in \mathcal{L}(t)$  the control input and speed are bounded by

$$u_{\min} \leq u_{i,j}(t) \leq u_{\max}, \quad (6.2)$$

$$0 < v_{\min} \leq v_{i,j}(t) \leq v_{\max}, \quad (6.3)$$

where  $u_{\min}, u_{\max}$  are the minimum and maximum control inputs and  $v_{\min}, v_{\max}$  are the minimum and maximum speed limit, respectively.

To ensure rear-end safety between platoon  $i \in \mathcal{L}(t)$  and preceding platoon  $k \in \mathcal{L}(t)$ , we have

$$p_{k,m_k}(t) - p_i(t) \geq \delta_i(t) = \gamma + \varphi \cdot v_i(t), \quad (6.4)$$

where  $m_k$  is the last follower in the platoon  $k$  physically located in front of platoon  $i$  and  $\delta_i(t)$  is the safe speed-dependent distance, while  $\gamma$  and  $\varphi \in \mathbb{R}_{>0}$  are the standstill distance and reaction time, respectively.

Similarly, to guarantee rear-end safety within CAVs inside each platoon  $i \in \mathcal{L}(t)$ , we enforce

$$p_{i,j-1}(t) - p_{i,j}(t) \geq \Delta_i + l_c, \quad \forall j \in \{1, \dots, m_i\}. \quad (6.5)$$

Finally, let  $k \in \mathcal{L}(t)$  correspond to another platoon that has already entered the control zone and may have a lateral collision with platoon  $i \in \mathcal{L}(t)$  at conflict point  $n$ .

For the first case in which platoon  $i$  reaches the conflict point after platoon  $k$ , we have

$$t_i^f - t_{k,m_k}^f \geq t_h, \quad (6.6)$$

where  $t_h \in \mathbb{R}_{>0}$  is the minimum time headway between any two CAVs entering node  $n$  that guarantees safety,  $t_i^f$  is the time that leader of platoon  $i$  exits the control zone (recall that the conflict point  $n$  is at the exit of control zone), and  $t_{k,m_k}^f$  is time that the last CAV in the platoon  $k$  exits the control zone. Likewise, for the second case in which platoon  $i$  reaches the conflict point  $n$  before platoon  $k$ , we have

$$t_k^f - t_{i,m_i}^f \geq t_h. \quad (6.7)$$

**Remark 6.1.2.** Given the time  $t_i^f$  that the platoon leader of platoon  $i \in \mathcal{L}(t)$  exits the control zone, we compute the time  $t_{i,m_i}^f$  that the last platoon member  $m_i \in \mathcal{N}_i$  exits the control zone as

$$t_{i,m_i}^f = t_i^f + \frac{(M_i - 1)(\Delta_i + l_c)}{v_i(t_i^f)}. \quad (6.8)$$

To guarantee lateral safety between platoon  $i$  and platoon  $k$  at a conflict point  $n$ , either (6.6) or (6.7) must be satisfied. Therefore, we impose the following lateral safety constraint on platoon  $i$ ,

$$\min \left\{ t_h - (t_i^f - t_{k,m_k}^f), t_h - (t_k^f - t_{i,m_i}^f) \right\} \leq 0. \quad (6.9)$$

With the state, control and safety constraints defined above, we now impose the following assumption:

**Assumption 6.1.2.** Upon entering the control zone, the initial state of each CAV  $j \in \mathcal{N}_i(t)$ ,  $i \in \mathcal{L}(t)$ , is feasible, that is, none of the speed or safety constraints are violated.

This is a reasonable assumption since CAVs are automated; therefore, there is no compelling reason for them to violate any of the constraints by the time they enter the control zone.

### 6.1.1.3 Information Structure

In this section, we formalize the information structure that is communicated between the CAV leaders and the coordinator inside the control zone.

**Definition 6.1.3.** Let  $\phi_i$  be the vector containing the parameters of the optimal control policy (formally defined in Section 6.1.2) of the leader of platoon  $i \in \mathcal{L}(t_i^0)$ . Then, the *platoon information set*  $\mathcal{I}_i$  that the leader of platoon  $i$  can obtain from the coordinator after entering the control zone at time  $t = t_i^0$  is

$$\mathcal{I}_i = \{\phi_{1:L(t_i^0)-1}, M_{1:L(t_i^0)}, t_{1:L(t_i^0)}^0, t_{1:L(t_i^0)-1}^f\}, \quad (6.10)$$

where  $\phi_{1:L(t_i^0)} := [\phi_1, \dots, \phi_{L(t_i^0)-1}]^T$ ,  $M_{1:L(t_i^0)} := [M_1, \dots, M_{L(t_i^0)}]^T$ ,

$$t_{1:L(t_i^0)}^f := [t_1^0, \dots, t_{L(t_i^0)}^0]^T \text{ and } t_{1:L(t_i^0)-1}^f := [t_1^f, \dots, t_{L(t_i^0)-1}^f]^T.$$

**Remark 6.1.3.** The information structure  $\mathcal{I}_i$  for each platoon  $i \in \mathcal{L}(t_i^0)$  indicates that the control policy, entry time to the control zone  $t_j^0$ , exit time of the control zone  $t_j^f$ , and the platoon size  $M_j$  of each platoon  $j \in \mathcal{L}(t_i^0) \setminus \{i\}$  already existing within the control zone is available to the leader of platoon  $i$  through the coordinator. Note that, although the leader of platoon  $i$  knows the endogenous information  $t_i^0$  and  $M_i$ , it needs to compute the vector of its own optimal control input parameters  $\phi_i$  and the merging time  $t_i^f$ , which we discuss in section 6.2.2.

**Definition 6.1.4.** The *member information set*  $\mathcal{I}_{i,j}(t)$  that each platoon member  $j \in \mathcal{N}_i \setminus \{0\}$  belonging to each platoon  $i \in \mathcal{L}(t)$  at time  $t \in [t_i^0, t_i^f]$  can obtain is

$$\mathcal{I}_{i,j} = \{p_{i,0}(t), v_{i,0}(t), u_{i,0}(t)\}. \quad (6.11)$$

**Remark 6.1.4.** The unidirectional intra-platoon communication protocol allows each platoon member  $j \in \mathcal{N}_i \setminus \{0\}$  belonging to platoon  $i \in \mathcal{L}(t)$  to access the state and

control input information of its platoon leader in the form of  $\mathcal{I}_{i,j}$  at each time  $t \in [t_i^0, t_i^f]$ . The set  $\mathcal{I}_{i,j}$  is subsequently used to derive the optimal control input  $u_{i,j}^*(t)$  of each platoon member  $j$ , which we discuss in detail in Section 6.1.3.

In what follows, we introduce our coordination framework which consists of two optimal control problems. The first problem is to develop an energy-optimal control strategy for the platoon leaders to minimize their travel time while guaranteeing that none of their state, control, and safety constraints becomes active. The second problem is concerned with the optimal control of followers within each platoon in order to maintain the platoon formation while ensuring safety and string stability.

### 6.1.2 Optimal Control of Platoon Leaders

In this section, we extend the single-level optimization framework we developed earlier for coordination of CAVs in [159] to establish a framework for coordinating platoons of CAVs. Upon entrance to the control zone, the leader of platoon  $i \in \mathcal{L}(t)$  must determine the exit time  $t_i^f$  (recall that based on Remark 6.1.1, this is the time that the leader of platoon  $i$  exits the control zone). The exit time  $t_i^f$  corresponds to the unconstrained energy optimal trajectory for the platoon leader ensuring that the resulting trajectory does not activate any of (6.1) - (6.4) and (6.9). The *unconstrained solution* of the leader of platoon  $i$  is given by [159]

$$\begin{aligned} u_i(t) &= 6a_it + 2b_i, \\ v_i(t) &= 3a_it^2 + 2b_it + c_i, \\ p_i(t) &= a_it^3 + b_it^2 + c_it + d_i, \end{aligned} \tag{6.12}$$

where  $a_i, b_i, c_i, d_i$  are constants of integration. The leader of platoon  $i$  must also satisfy the boundary conditions

$$p_i(t_i^0) = p_i^0, \quad v_i(t_i^0) = v_i^0, \quad (6.13)$$

$$p_i(t_i^f) = p_i^f, \quad u_i(t_i^f) = 0, \quad (6.14)$$

where  $p_i$  is known at  $t_i^0$  and  $t_i^f$  by the geometry of the road, and  $v_i^0$  is the speed at which the leaders of platoon  $i$  enters the control zone. The final boundary condition,  $u_i(t_i^f) = 0$ , results from  $v_i(t_i^f)$  being left unspecified [188]. There are five unknown variables that determine the optimal trajectory of the leader of the platoon  $i$ , four constants of integration from (6.12), and the unknown exit time  $t_i^f$ . The value of  $t_i^f$  guarantees that the unconstrained trajectories in (6.12) satisfy all the state, control, and safety constraints in (6.2), (6.3) and (6.4), respectively, and the boundary conditions in (6.14). In practice, for the leader of each platoon  $i \in \mathcal{L}(t)$ , the coordinator stores the optimal exit time  $t_i^f$  and the corresponding coefficients  $a_i, b_i, c_i, d_i$ . We denote the coefficients of the optimal control policy for leader of platoon  $i \in \mathcal{L}(t)$  by vector  $\phi_i = [a_i, b_i, c_i, d_i]^T$ , which is an element of platoon information set for the leader of platoon  $i \in \mathcal{L}(t)$  (Definition 6.1.3). We formally define our single-level optimization framework for platoon leaders as follows.

**Problem 6.1.1.** *Upon entering the control zone, each leader of platoon  $i \in \mathcal{L}(t)$  accesses the information set  $\mathcal{I}_i$  and solves the following optimization problem at  $t_i^0$*

$$\min_{t_i^f \in \mathcal{T}_i(t_i^0)} t_i^f \quad (6.15)$$

subject to:

$$(6.4), (6.9), (6.12),$$

where the compact set  $\mathcal{T}_i(t_i^0) = [\underline{t}_i^f, \bar{t}_i^f]$  is the set of feasible solution of leader of platoon  $i \in \mathcal{N}(t)$  for the exit time that satisfy the boundary conditions without activating the constraints, while  $\underline{t}_i^f$  and  $\bar{t}_i^f$  denote the minimum and maximum feasible exit time computed at  $t_i^0$ .

**Remark 6.1.5.** We can derive the optimal control input of the platoon leaders using the solution of Problem 6.1.1,  $t_i^f$ , the boundary conditions (6.13)-(6.14) and (6.12).

In what follows, we continue our exposition by briefly reviewing the process to compute the compact set  $\mathcal{T}_i(t_i^0)$  at time  $t_i^0$  using the speed and control input constraints (6.2)-(6.3), initial condition (6.13), and final condition (6.14). Details regarding the derivation of the compact set  $\mathcal{T}_i(t_i^0)$  can be found in [218].

The lower-bound  $\underline{t}_i^f$  of  $\mathcal{T}_i(t_i^0)$  can be computed by considering the state and control constraints and boundary conditions as

$$\underline{t}_i^f = \min \left\{ t_{i,u_{\max}}^f, t_{i,v_{\max}}^f \right\}, \quad (6.16)$$

where,

$$\begin{aligned} t_{i,v_{\max}}^f &= \frac{3(p_i(t_i^f) - p_i(t_i^0))}{v_i(t_i^0) + 2v_{\max}}, \\ t_{i,u_{\max}}^f &= \frac{\sqrt{9v_i(t_i^0)^2 + 12(p_i(t_i^f) - p_i(t_i^0))u_{\max}} - 3v_i(t_i^0)}{2u_{\max}}. \end{aligned}$$

Here,  $t_{i,v_{\max}}^f$  and  $t_{i,u_{\max}}^f$  are the times which leader of platoon  $i \in \mathcal{L}(t)$  achieves its maximum speed at the end of control zone and its maximum control input at the entry of the control zone, respectively. Similarly, we derive the upper-bound  $\bar{t}_i^f$  as

$$\bar{t}_i^f = \begin{cases} t_{i,v_{\min}}^f, & \text{if } 9v_i(t_i^0)^2 + 12(p_i(t_i^f) - p_i(t_i^0))u_{\min} < 0, \\ \max\{t_{i,u_{\min}}^f, t_{i,v_{\min}}^f\}, & \text{otherwise,} \end{cases} \quad (6.17)$$

where

$$\begin{aligned} t_{i,v_{\min}}^f &= \frac{3(p_i(t_i^f) - p_i(t_i^0))}{v_i(t_i^0) + 2v_{\min}}, \\ t_{i,u_{\min}}^f &= \frac{\sqrt{9v_i(t_i^0)^2 + 12(p_i(t_i^f) - p_i(t_i^0))u_{\min}} - 3v_i(t_i^0)}{2u_{\min}}. \end{aligned}$$

Similar to the previous case,  $t_{i,v_{\min}}^f$  and  $t_{i,u_{\min}}^f$  are the times at which the leader of the platoon  $i \in \mathcal{L}(t)$  achieves its minimum speed at the end of control zone and its minimum control input at the entry of the control zone, respectively.

Note that, the solution to the optimal control problem 6.1.1 yields the optimal control input  $u_i^*(t)$  for each platoon leader  $i \in \mathcal{L}(t)$  for  $t \in [t_i^0, t_i^f]$ . However, the solution to this problem does not consider the stability criteria of the platoon [219], which is essential to guarantee safety within the platooning CAVs. In the following section, we first introduce the notion of stability during platoon coordination, and then propose a control structure  $u_{i,j}(t)$  for each platoon member  $j \in \mathcal{N}_i \setminus \{0\}$ ,  $i \in \mathcal{L}(t)$  that is optimal subject to constraints, and satisfies the stability properties.

### 6.1.3 Optimal Control of Followers Within Each Platoon

Stability properties of the platoon system are well discussed in the literature [129, 219, 220]. In general, there are two types of stability: (a) local stability, which describes the ability of each platoon member to converge to a given trajectory, and (b) string stability, where any bounded disturbance introduced into the platoon is not amplified while propagating downstream along the vehicle string. In this section, we adopt the following definition of platoon stability that encompasses the above stability notions [220].

**Definition 6.1.5.** A platoon  $i \in \mathcal{L}(t)$  is stable if, for any bounded initial disturbances to all the CAVs  $j \in \mathcal{N}_i$ , the position fluctuations of all the CAVs remain bounded (string stability) and approach zero as time goes to infinity (local stability).

With the stability properties Definition 6.1.5, we introduce the control problem of each platoon member  $j \in \mathcal{N}_i \setminus \{i\}$ ,  $i \in \mathcal{L}(t)$ .

**Problem 6.1.2.** *Each platoon member  $j \in \mathcal{N}_i \setminus \{0\}$ ,  $i \in \mathcal{L}(t)$  needs to derive its control input  $u_{i,j}(t)$  for all  $t \in [t_i^0, t_i^f]$  that*

1. *is energy and time-optimal subject to the state and control constraints in (6.2)-(6.3), and rear-end collision avoidance constraint in (6.5), and*
2. *satisfying the stability properties according to Definition 6.1.5.*

We provide the following proposition that addresses the Problem 6.1.2.

**Proposition 6.1.1.** *For each platoon member  $j \in \mathcal{N}_i \setminus \{0\}$  in the platoon  $i \in \mathcal{L}(t)$ , the optimal control input  $u_{i,j}(t) = u_{i,0}^*(t)$ , where  $u_{i,0}^*(t)$  is the solution to Problem 6.1.1, is an optimal solution to Problem 6.1.2.*

Next, we provide the proof of Proposition 6.1.1 using the following Lemmas.

**Lemma 6.1.6.** *For each platoon member  $j \in \mathcal{N}_i \setminus \{0\}$  in each platoon  $i \in \mathcal{L}(t)$ , the control input  $u_{i,j}(t) = u_{i,0}^*(t)$  for all  $t \in [t_i^0, t_i^f]$  is energy- and time-optimal subject to the control (6.2), state (6.3) and safety constraint (6.5).*

*Proof.* (a) Optimality: We derive the control input  $u_{i,0}^*(t)$  of the leading CAV  $i \in \mathcal{L}(t)$  by solving Problem 6.1.1. The optimal trajectory of the leader of platoon  $i \in \mathcal{L}(t)$  is given by (6.12) for all  $t \in [t_i^0, t_i^f]$ . Thus, for each platoon member  $j \in \mathcal{N}_i \setminus \{0\}$ , the control input  $u_{i,j}(t)$  such that  $u_{i,j}(t) = u_{i,0}^*(t)$  also generates optimal linear control, quadratic speed and cubic position trajectories as in (6.12).

(b) Constraint satisfaction: Since  $u_{i,j}(t) = u_{i,0}^*(t)$ , for each platoon member  $j \in \mathcal{N}_i \setminus \{0\}$ ,  $i \in \mathcal{L}(t)$ , we have  $v_{i,j}(t) = v_{i,0}^*(t)$  for all  $t \in [t_i^0, t_i^f]$ . The trajectories  $v_{i,0}^*(t)$  and  $u_{i,0}^*(t)$  do not violate any constraints in (6.2)-(6.3) since they are derived by solving Problem 6.1.1. Therefore, the trajectories  $v_{i,j}(t)$  and  $u_{i,j}(t)$  of each platoon member  $j$  are ensured to satisfy constraints in (6.2)-(6.3). Additionally, if  $u_{i,j}(t) = u_{i,0}^*(t)$ , the inter-vehicle gap  $p_{i,j-1}(t) - p_{i,j}(t) - l_c$  between two consecutive platoon members  $j, j-1 \in \mathcal{N}_i$ ,  $i \in \mathcal{L}(t)$  is time invariant, and equal to  $\Delta_i$ . Thus, the rear-end safety within CAVs within the platoon  $i$  in (6.5) is guaranteed to be satisfied.  $\square$

**Lemma 6.1.7.** *Each platoon member  $j \in \mathcal{N}_i \setminus \{0\}$  for each platoon  $i \in \mathcal{L}(t)$  with the control input  $u_{i,j}(t) = u_{i,0}^*(t)$  for all  $t \in [t_i^0, t_i^f]$  is locally stable, and the resulting platoon  $i$  is string stable.*

*Proof.* (a) Local stability: Since  $u_{i,j}(t) = u_{i,0}^*(t)$ , for each platoon member  $j \in \mathcal{N}_i \setminus \{0\}$ ,  $i \in \mathcal{L}(t)$ , we have  $v_{i,j}(t) = v_{i,0}^*(t)$  for all  $t \in [t_i^0, t_i^f]$ . Since there is no communication delay within the unidirectional intra-platoon communication protocol, the speed of

each platoon member  $j$  converges instantaneously to the speed of the platoon leader  $v_{i,0}^*(t)$ , which implies local stability.

(b) String stability: A sufficient condition for the string stability of a platoon  $i \in \mathcal{L}(t)$  containing CAVs  $j \in \mathcal{N}_i$  is  $\|\frac{u_{i,j}(s)}{u_{i,j-1}(s)}\|_\infty \leq 1$  [129], where  $u_{i,j}(s)$  is the Laplace transform of the control input  $u_{i,j}(t)$ . Since  $u_{i,j}(t) = u_{i,0}^*(t)$  for all  $t \in [t_i^0, t_i^f]$ , we have  $u_{i,j}(s) = u_{i,0}^*(s)$  for all  $j \in \mathcal{N}_i \setminus \{0\}$ , which yields  $\|\frac{u_{i,j}(s)}{u_{i,j-1}(s)}\|_\infty = 1$ . Thus, each platoon  $i \in \mathcal{L}(t)$  is string stable.  $\square$

#### 6.1.4 Delay in Platoon Communication

In this section, we enhance our framework to include delay in the bi-directional inter-platoon communication. From Assumption 6.1.1, we know that delay is bounded and this bound is known a priori. In particular, suppose the delay in bi-direction communication of platoon leaders takes values in  $[\tau_{\min}, \tau_{\max}]$ , where  $\tau_{\min} \in \mathbb{R}_{\geq 0}$  and  $\tau_{\max} \in \mathbb{R}_{\geq 0}$  correspond to the minimum and maximum communication delay, respectively. To account for the effects of communication delays in our framework, we consider the worst-case scenario. Namely, we consider that it takes  $0.5 \tau_{\max}$  until the coordinator receives the request from the platoon leader, and it takes an extra  $0.5 \tau_{\max}$  for the leader of platoon  $i \in \mathcal{L}(t)$  to receive the platoon information  $\mathcal{I}_i$ . Thus, the leader needs to cruise with the constant speed that it entered the control zone for  $\tau_{\max}$  until it receives the platoon information  $\mathcal{I}_i$  to plan its optimal trajectory. After receiving this information, the platoon leader computes the compact set of the feasible solution  $\mathcal{T}_i$  at time  $t_i^0 + \tau_{\max}$  with initial condition  $v_i(t_i^0 + \tau_{\max})$  and  $p_i(t_i^0 + \tau_{\max})$ . Using the compact set  $\mathcal{T}_i(t_i^0 + \tau_{\max})$  of the feasible solution, the leader derives its optimal control policy by solving Problem 6.1.1. Then, it sends the computed trajectory at time  $t_i^0 + \tau_{\max}$  to the coordinator. In the worst-case scenario, the coordinator receives this information after  $0.5\tau_{\max}$  at  $t_i^0 + 1.5\tau_{\max}$ . To ensure that new arriving platoons have access to this information, we need to have the following constraint on the initial conditions of platoons upon entrance the control zone.

**Proposition 6.1.2.** *Let platoons  $i$  and  $j$ ,  $i, j \in \mathcal{L}(t)$ , enter the control zone at time  $t_i^0$  and  $t_j^0 > t_i^0$ , respectively. In the presence of a bi-directional inter-platoon communication delay, which takes value in  $[\tau_{\min}, \tau_{\max}]$ , the optimal trajectory of platoon  $i$  is accessible to platoon  $j$ , if  $t_j^0 - t_i^0 \geq \tau_{\max}$ .*

*Proof.* Platoon  $i$  computes its optimal trajectory at  $t_i^0 + \tau_{\max}$ , but in the worst-case scenario, due to delay in communication, this information becomes available to the coordinator at  $t_i^0 + 1.5 \tau_{\max}$ . On the other hand, upon entrance the control zone, platoon  $j$  sends a request to the coordinator to receive platoon information  $\mathcal{I}_j$ . However, the coordinator receives this request at  $t_j^0 + 0.5 \tau_{\max}$ . In order to have the optimal trajectory of platoon  $i$  accessible to platoon  $j$  we need to have  $t_j^0 + 0.5 \tau_{\max} \geq t_i^0 + 1.5 \tau_{\max}$ , and the result follows.  $\square$

**Remark 6.1.6.** We can ensure that the condition in Proposition 6.1.2 holds by using an appropriate controller in the platooning zone upstream of the control zone.

### 6.1.5 Implementation of the Optimal Coordination Framework

In Sections 6.1.2, 6.1.3 and 6.1.4, we provided the exposition of the intricacies of our proposed control framework for optimal platoon coordination. In this section, we introduce the approach that can be applied to implement this framework in real time.

While entering the control zone at time  $t_i^0$ , platoon leader  $i \in \mathcal{L}(t)$  obtains the platoon information  $\mathcal{I}_i$  from the coordinator and solves the optimization problem (6.1.1) by constructing the feasible set  $\mathcal{T}_i(t)$  and iteratively checking the safety constraint. The resulting optimal exit time  $t_i^f$  is then used along with the initial (6.13) and boundary (6.14) conditions to derive the vector of control input coefficients  $\phi_i$  using (6.12). Subsequently, each CAV  $j \in \mathcal{N}_i$  in platoon  $i \in \mathcal{L}(t)$  computes its optimal control input  $u_{i,j}(t)$  at each time instance  $t \in [t_i^0, t_i^f]$  using  $\phi_i$ . In what follows, we

provide an algorithm that delineates the step-by-step implementation of the proposed optimal platoon coordination framework.

---

**Algorithm 1** Vehicular Platoons Coordination Algorithm

---

```

1: for  $i \in \mathcal{L}(t)$  do
2:   for  $j \in \mathcal{N}_i$  do
3:     if  $j=0$  then ▷ Platoon leader
4:        $u_{i,j} = 0 \quad \forall t \in [t_i^0, t_i^0 + \tau_{\max})$  ▷ Cruise with constant speed
5:       Compute  $\mathcal{T}_i(t_i^0 + \tau_{\max})$  ▷ Based on (6.16)-(6.17)
6:        $t_i^f, \phi_i \leftarrow \text{Platoon Leader Control}()$  ▷ Algorithm 2
7:        $[a_i, b_i, c_i, d_i] \leftarrow \phi_i$ 
8:        $u_{i,j}(t) \leftarrow 6a_it + 2b_i$  ▷  $\forall t \in [t_i^0 + \tau_{\max}, t_i^f]$ 
9:     else ▷ Platoon followers
10:       $u_{i,j}(t) = u_{i,0}(t)$ 
11:    end if
12:  end for
13: end for

```

---

### 6.1.6 Simulation Example

To evaluate and validate the performance of our proposed optimal platoon coordination framework, we employ the microscopic traffic simulation software VISSIM v11.0 [202]. We create a simulation environment with a highway on-ramp merging, which has a control zone of length 560 m. In our simulation framework, we use VISSIM's *component object model* (COM) interface with Python 2.7 to generate platoons of CAVs on the main road and the on-ramp at different time intervals. The time interval between two consecutive platoon generations is randomized with a uniform probability distribution, and the bounds can be controlled to increase or decrease the traffic volume in each roadway. The length of each platoon is also randomly selected from a set of 2 to 4 vehicles with equal probability. The speed limit of each roadway is set to be 16.67 m/s, and the maximum and minimum acceleration limit is 3 m/s<sup>2</sup> and -3 m/s<sup>2</sup>, respectively. Vehicles enter the main road and the on-ramp with a traffic volume of 700 and 650 vehicle per hour per lane with random initial speed uniformly

---

**Algorithm 2** Platoon Leader Control

---

**Input:** Platoon Information set  $\mathcal{I}_i$ , Compact feasible set  $\mathcal{T}_i(t_i^0 + \tau_i) = [\underline{t}_i^f, \bar{t}_i^f]$

**Output:** Exit time  $t_i^f$ , Coefficients of the optimal control policy  $\phi_i$

```
1:  $t_i^f \leftarrow \underline{t}_i^f$ 
2:  $k \leftarrow$  platoon physically located in front of platoon  $i$ 
3:  $p_{k,m_k}(t) \leftarrow p_k(t) - (M_k - 1)(\Delta_k + l_c)$  ▷ Position of the last follower
4: while  $p_{k,m_k}(t) - p_i(t) < \delta_i(t)$  do ▷ Rear-end safety
5:    $t_i^f \leftarrow t_i^f + dt$ 
6: end while
7:  $lateral \leftarrow$  list of all platoons  $j < i$  from the other road
8: for  $j \in lateral$  do
9:   Compute  $t_{j,m_j}^f$  and  $t_{i,m_i}^f$  from (6.8)
10:  while  $t_i^f - t_{j,m_j}^f < t_h$  AND  $t_j^f - t_{i,m_i}^f < t_h$  do ▷ Lateral safety
11:     $t_i^f \leftarrow t_i^f + dt$ 
12:  end while
13: end for
14: Compute  $\phi_i$  ▷ From (6.12)-(6.14)
```

---

chosen from a set of 13.89 to 16.67 m/s. Videos of the experiment can be found at the supplemental site, <https://sites.google.com/view/ud-ids-lab/CAVPLT>.

To evaluate the performance of the proposed optimal control framework, we simulate the following control cases.

(a) Baseline 1: All vehicles in the network are human-driven vehicles. In this scenario, the Wiedemann car-following model built-in VISSIM [202] is applied. The conflict point of the on-ramp merging scenario has a priority mechanism, where the vehicles on the ramp road are required to yield to the vehicle on the main road within a certain look-ahead distance. Vehicles enter the network individually without forming any platoons.

(b) Baseline 2: Similar to the above case, all the vehicles are human-driven vehicles integrated with the Wiedemann car-following model and follow the priority mechanism set at the conflict point of the on-ramp merging scenario. The difference is that, when vehicles enter the network, they have already formed platoons. Note, we

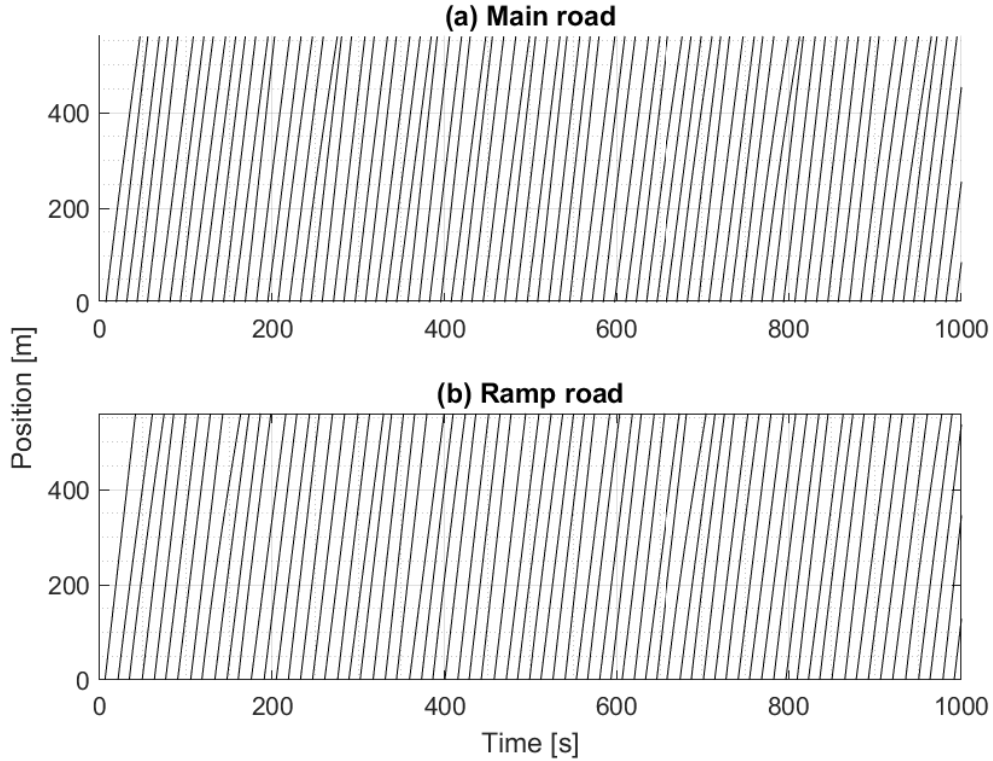


Figure 6.3: The position trajectories of the optimally coordinated CAV platoons at the (a) main road and (b) ramp road are shown.

consider this case to simulate the same initial condition of the optimal coordination case, which we discuss next.

(c) Optimal Coordination: All the vehicles present in the network are connected and automated. They enter the network forming platoons of different sizes and optimize their trajectories based on the optimal coordination framework presented in Section 6.2.2.

We use COM application programming interface to interact with the VISSIM simulator externally and implement the proposed optimal coordination framework. At each simulation time step, we use the VISSIM-COM interface to collect the required vehicle attributes from the simulation environment and pass them to the external python script. The external python script implements the proposed single-level optimal control algorithm (Section 6.1.5) to compute the optimal control input of each CAV

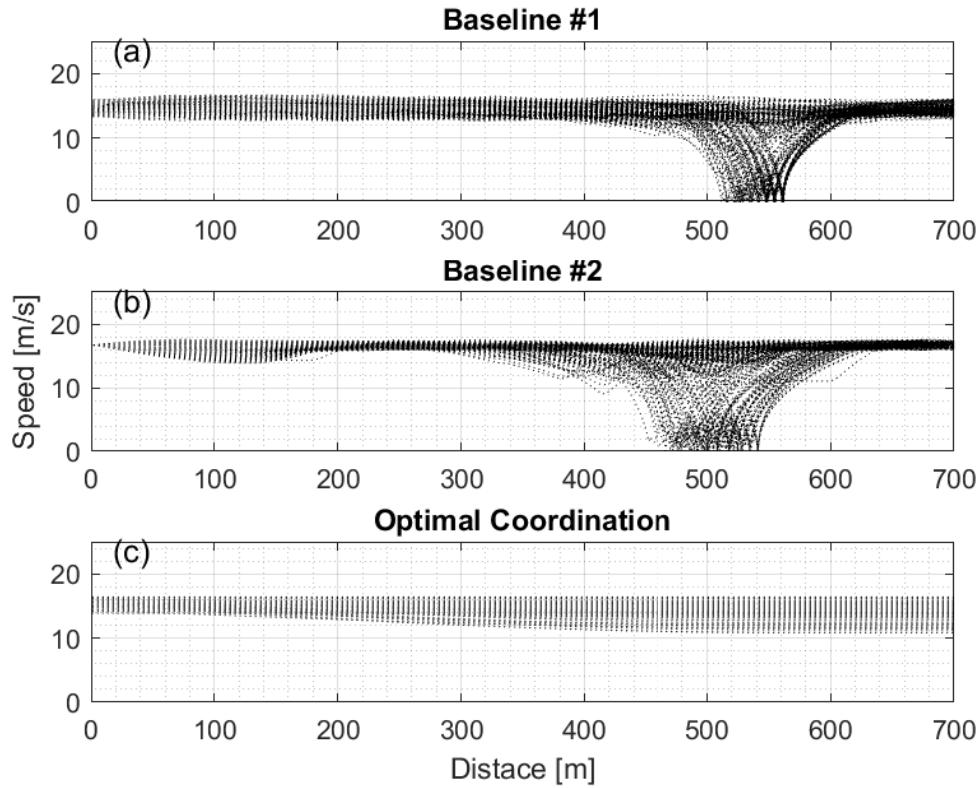


Figure 6.4: Speed profiles of 400 vehicles traveling through the on-ramp merging scenario for three cases: (a) baseline without platooning, (b) baseline with platooning and (c) optimal platoon coordination.

within the control zone. Finally, the speed of each platooning CAV is updated in VISSIM traffic simulator in real-time using the COM interface.

In Fig. 6.4, the position trajectories of the optimal coordinated CAV platoons traveling through the main road and the ramp road of the considered on-ramp merging scenario are shown. The spatial gaps between the trajectory paths indicate that our framework satisfies the rear-end collision avoidance constraint without any violation.

To visualize the performance of the proposed coordination framework in comparison with the baseline cases, we focus on Figs. 6.4 and 6.5. In Fig. 6.4, the speed trajectories of all the vehicles in the network are shown. In Figs. 6.4 (a)-(b), both baseline cases show stop-and-go driving behavior close to the conflict point of the on-ramp

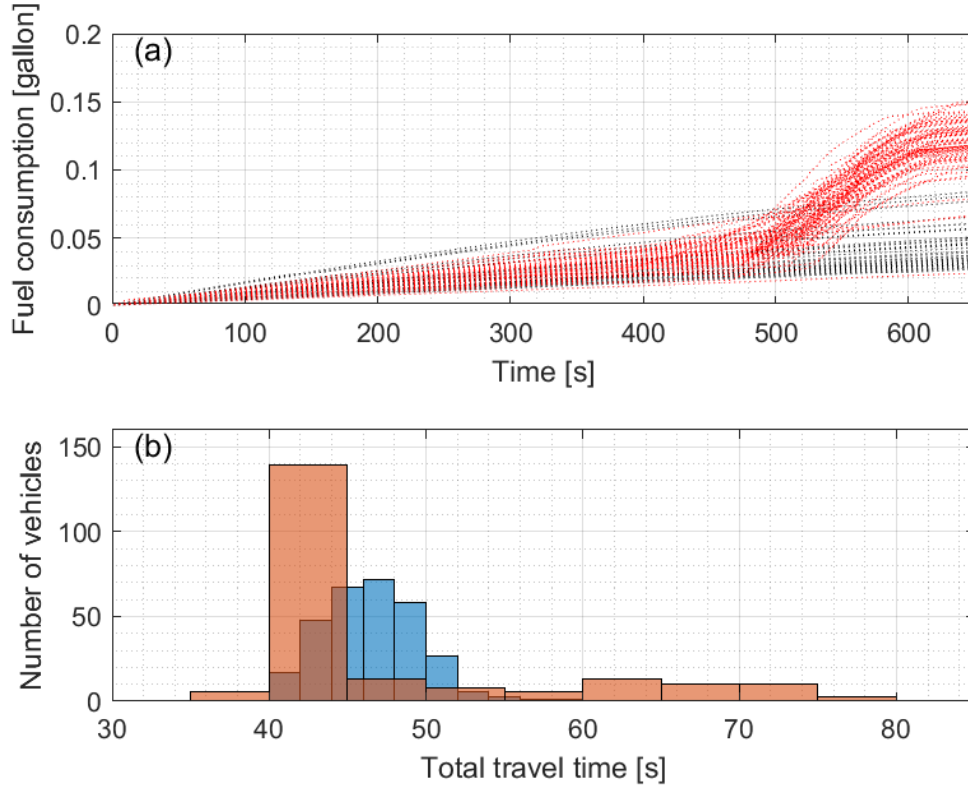


Figure 6.5: Comparison of performance metrics: (a) cumulative fuel consumption of optimal coordination (black) vs. baseline with platooning (red), and (b) total travel time distribution of optimal coordination (blue) vs. baseline with coordination (maroon).

merging scenario. In contrast, with the optimal coordination framework, we are able to eliminate stop-and-go driving behavior, as shown in Fig. 6.4(c). The elimination of the stop-and-go driving behavior has associated benefits, namely, the minimization of transient engine operation and travel time, as shown in Fig. 6.5. In Fig. 6.5 (a), the baseline case with vehicle platoons (red) shows a sudden increase in fuel consumption near the conflict point due to the transient engine operation induced by the stop-and-go driving behavior. In contrast, the cumulative fuel consumption trajectories of the optimally coordinated CAVs (black) remain steady throughout their path. Note that, we use the polynomial metamodel proposed in [67] to compute the fuel consumption of each vehicle. In Fig. 6.5 (b), we illustrate the distribution of total travel time of

the vehicles for the baseline (maroon) and the optimal coordination (blue) framework. The high variance of the travel time for the baseline case compared to the optimal coordination approach indicates increased traffic throughput of the network.

Finally, we provide the summary of the performance metrics in Table 6.1. Based on the simulation, the optimal coordination framework shows significant improvement over the baseline cases in terms of average travel time and fuel consumption.

Table 6.1: Summary of performance metrics

Performance Metrics	Avg. travel time [s]	Avg. fuel consumption [gallon]
Baseline 1	57.33	0.042
Baseline 2	52.79	0.05
Optimal Coordination	46.1	0.022
Improvement (baseline 1) [%]	19.6	46.9
Improvement (baseline 2) [%]	12.7	38.2

## 6.2 Coordination of Mixed Platoons at On-Ramp Merging

In this section, we address the problem of optimal coordination of mixed platoons consisting of CAVs and human-driven vehicles (HDVs) at a highway on-ramp merging. The main objective is to leverage the key concepts of vehicle coordination and platooning and establish a control framework for platoon coordination aimed at improving network performance while guaranteeing safety. To this end, I present a single-level constrained optimal control framework that optimizes the fuel economy and travel time of the mixed platoons while satisfying the state, control, and safety constraints. I also explore the effect of delayed communication among the vehicles within the platoons and propose a robust coordination framework to enforce lateral and rear-end collision avoidance constraints in the presence of bounded delays. I provide a closed-form analytical solution to the optimal control problem with safety guarantees that can be implemented in real time.

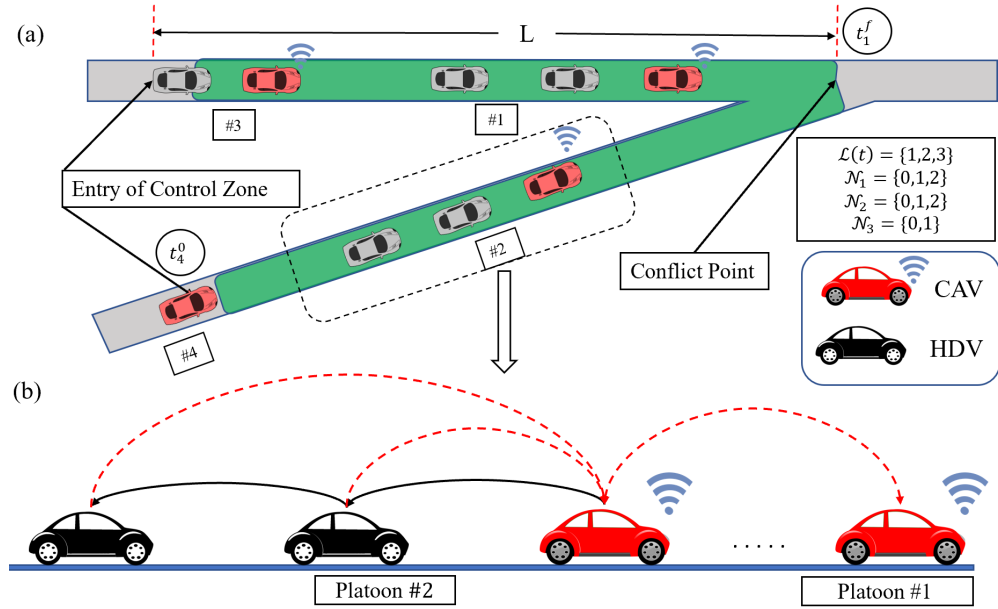


Figure 6.6: (a) On-ramp merging scenario for platoons of mixed vehicles, where the leader of each platoon is the CAV (red vehicles) and the rest of the platoon members are HDVs (gray vehicles). The control zone is highlighted in green color, the entry time  $t_{i,0}^0$  and exit time  $t_{i,0}^f$  to the control zone for each platoon  $i$  are depicted with circles, and example of sets  $\mathcal{L}(t)$  and  $\mathcal{N}_i$  according to the Definitions 6.2.1 and 6.2.2 are shown. (b) Communication structure for information flow: (i) V2V-enabled bidirectional flow of information between the CAVs (double-headed dashed red arrow), (ii) V2V-enabled unidirectional flow of information from the HDVs to the CAVs (single-headed dashed red arrow), and (iii) unidirectional driver perception from preceding vehicle to the following HDVs (single-headed solid black arrow).

### 6.2.1 Modeling Framework: Mixed Platoon

We consider the problem of coordinating mixed platoons at a highway on-ramp merging scenario, where the leaders of each platoon are CAVs and the rest of the platoon members are HDVs, as shown by the red and gray colored vehicles in Fig. 6.6, respectively. Although our proposed framework and analysis for mixed platoon coordination can be extended to any traffic scenario, e.g., signal-free intersections, roundabouts, and speed reduction zones, we use a highway on-ramp as a reference to present the fundamental ideas and results of this work.

The on-ramp merging scenario includes a *control zone* (green road section in

Fig. 6.6), within which the CAVs are controlled to coordinate the platoons. The paths of the main road and the ramp road intersect at a point called *conflict point*, indexed by  $n \in \mathbb{N}$ , at which lateral collision may occur. We consider that CAVs have already formed platoons with the HDVs of the network upstream of the control zone in a region called the *platooning zone*. We refer interested readers to [169, 170, 217] for further details on platoon formation.

We provide the following definitions that are required to formulate the problem.

**Definition 6.2.1.** The queue that designates the order in which each platoon leader enters the control zone is given by  $\mathcal{L}(t) = \{1, \dots, L(t)\}$ , where  $L(t) \in \mathbb{N}$  is the total number of platoons that are inside the control zone at time  $t \in \mathbb{R}_{\geq 0}$ . When a platoon exits the control zone, its index is removed from  $\mathcal{L}(t)$ .

**Definition 6.2.2.** CAVs and HDVs within platoon  $i \in \mathcal{L}(t)$  are indexed with set  $\mathcal{N}_i = \{0, 1, \dots, m_i\}$ , where 0 and  $m_i \in \mathbb{N}$  denote the leader CAV and last HDV of the platoon  $i$ , respectively. The size of each platoon  $i \in \mathcal{L}(t)$  is thus the cardinality of set  $\mathcal{N}_i$ , and denoted by  $M_i := m_i + 1$ .

Let  $t_{i,j}^0 \in \mathbb{R}_{\geq 0}$  and  $t_{i,j}^f > t_{i,0}^0 \in \mathbb{R}_{\geq 0}$  be the times that each vehicle  $j \in \mathcal{N}_i$  of platoon  $i \in \mathcal{L}(t)$  enters and exits the control zone, respectively.

In our modeling framework, we consider the following structure to model the flow of information, as shown in Fig. 6.6.

1. Bidirectional CAV communication: Each CAV is retrofitted with a V2V-enabled receiver and transmitter that enables a bidirectional flow of information. Each CAV can transmit its state information to other CAVs and receive incoming information from other vehicles within the network.
2. Unidirectional HDV communication: Each HDV is retrofitted with V2V-enabled transmission device that it uses to share its state information in real time with the CAVs. It is estimated that 90 % of all cars to be sold in the US within the next couple of years will have connectivity [221].
3. Direct driver perception: The human driver in each HDV can only perceive the immediately preceding vehicle's state information. The flow of information for direct driver perception is unidirectional from the preceding vehicle to the immediately following HDV.

When a platoon leader enters the control zone, it subscribes to the bidirectional CAV communication protocol to connect with other vehicles and access the information of platoons that are already in the control zone. After obtaining this information, the leader CAV derives its optimal control input (acceleration/deceleration) to cross the control zone without any lateral or rear-end collision with the other CAVs, and without violating any of the state and control constraints. For the rest of the platoon members, which are HDVs, the human drivers take control action based on the state information of the directly preceding vehicle received through direct driver perception. Finally, the platoon leader and members transmit their information so that the subsequent platoon leaders can plan their trajectories accordingly. We make the following assumptions regarding the nature of the communication structure.

**Assumption 6.2.1.** No delay and error takes place during the V2V-enabled communication.

**Assumption 6.2.2.** The perception delay for each HDV is bounded, which is known as a priori.

Assumption 6.2.1 may be strong, but it is relatively straightforward to relax as long as the noise in the measurements and/or delays is bounded. For example, we can determine upper bounds on the state uncertainties as a result of sensing or communication errors and delays, and incorporate these into more conservative safety constraints. Assumption 6.2.2 enables the determination of upper bounds on the state uncertainties as a result of sensing or communication errors and delays, and incorporates these into more conservative safety constraints.

### 6.2.1.1 Vehicle Dynamics

In our analysis, we consider that the dynamics of each vehicle  $j \in \mathcal{N}_i$  in platoon  $i \in \mathcal{L}(t)$  is governed by a double integrator,

$$\begin{aligned}\dot{p}_{i,j}(t) &= v_{i,j}(t), \\ \dot{v}_{i,j}(t) &= u_{i,j}(t - \tau_{i,j}),\end{aligned}\tag{6.18}$$

where  $p_{i,j}(t) \in \mathcal{P}$ ,  $v_{i,j}(t) \in \mathcal{V}$ , and  $u_{i,j}(t) \in \mathcal{U}$  denote position, speed, and control input at  $t \in \mathbb{R}_{\geq 0}$ , respectively, and  $\tau_{i,j}$  is the execution delay of the control input  $u_{i,j}(t)$ . The sets  $\mathcal{P}$ ,  $\mathcal{V}$ , and  $\mathcal{U}$  are compact subsets of  $\mathbb{R}$ .

Next, we provide the following definitions that are necessary for our exposition.

**Definition 6.2.3.** The headway  $\Delta p_{i,j}(t)$  and approach rate  $\Delta v_{i,j}(t)$  of vehicle  $j$  with respect to its preceding vehicle  $j - 1$ , where  $j, j - 1 \in \mathcal{N}_i, i \in \mathcal{L}(t)$ , are

$$\Delta p_{i,j}(t) = p_{i,j-1}(t) - p_{i,j}(t) - l_c,\tag{6.19}$$

$$\Delta v_{i,j}(t) = v_{i,j-1}(t) - v_{i,j}(t),\tag{6.20}$$

where  $l_c$  denote the length of each vehicle  $j$ .

**Definition 6.2.4.** For each vehicle  $j \in \mathcal{N}_i$  in platoon  $i \in \mathcal{L}(t)$ ,  $s_{i,j}(t)$  is the safe speed-dependent headway,

$$s_{i,j}(t) := d_{\min} + \rho_{i,j} \cdot v_{i,j}(t),\tag{6.21}$$

where,  $d_{\min}$  and  $\rho_{i,j} \in \mathbb{R}_{>0}$  are the minimum distance at standstill and safe time headway of each vehicle, respectively.

Since each HDV  $j \in \mathcal{N}_i, i \in \mathcal{L}(t)$ , has already formed a platoon in the platooning zone, when the leader CAV enters the control zone at time  $t_{i,0}^0$ , we have  $\Delta v_{i,j}(t_{i,0}^0) = 0$  and  $\Delta p_{i,j}(t_{i,0}^0) = \Delta_i$ , where  $\Delta_i$  is the initial bumper-to-bumper inter-vehicle gap between vehicles  $j, j - 1 \in \mathcal{N}_i$  within each platoon  $i \in \mathcal{L}(t)$ . This bumper-to-bumper inter-vehicle gap is imposed by the platoon forming control in platooning zone upstream

of the control zone. After exiting the control zone at  $t_{i,0}^f$ , the leader of platoon  $i$  cruises with constant speed  $v_i(t_{i,0}^f)$  until the last follower in the platoon exits the control zone.

The control input  $u_{i,j}(t)$  of each vehicle  $j \in \mathcal{N}_i, i \in \mathcal{L}(t)$  in (6.18) can take different forms based on the consideration of connectivity and automation. For each CAV in the platoon  $i \in \mathcal{L}(t)$ , we derive and implement the control input  $u_{i,0}(t)$  using the optimal control framework discussed in Section 6.2.2. Furthermore, due to the assumption of perfect communication (Assumption 6.2.1), we consider  $\tau_{i,0} = 0$  for each CAV in  $i \in \mathcal{L}(t)$ .

On the other hand, the driver perception delay  $\tau_{i,j}$  of each HDV  $j \in \mathcal{N}_i$  of platoon  $i \in \mathcal{L}(t)$  is bounded according to Assumption 6.2.2. Let us consider  $\tau \in \mathbb{R}_{>0}$  to be the upper-bound of  $\tau_{i,j}$ . To ensure the robustness of our proposed framework, we use the upper-bound  $\tau$  of the HDV perception delay, which essentially represents the worst case of perception and reaction delay for a human driver, to model the driving behavior of the HDVs. We consider a car-following model to represent the predecessor-follower coupled dynamics, which has the generic structure  $u_{i,j}(t) = f(\Delta p_{i,j}(t), \Delta v_{i,j}(t), v_{i,j}(t))$ . Here,  $f(\cdot)$  represents the behavioral function of the car-following model.

**Remark 6.2.1.** Although the HDVs share their state information with the CAVs via unidirectional HDV communication, their behavioral function  $f$  is unknown to the CAVs.

In this work, we consider a variation of the optimal velocity model to represent the HDVs' driving behavior as in [137]

$$\dot{u}_{i,j}(t) = \alpha(V(t) - v_{i,j}(t) + \beta(W(t) - v_{i,j}(t))), \quad (6.22)$$

where,

$$V(t) := \begin{cases} 0, & \text{if } \Delta p_{i,j}(t) \leq d_{\min}, \\ \kappa(\Delta p_{i,j}(t) - \Delta p_{st}), & \text{if } d_{\min} \leq \Delta p_{i,j}(t) \leq d_{\max}, \\ v_{\max}, & \text{if } \Delta p_{i,j}(t) \geq d_{\max}, \end{cases}$$

$$W(t) := \begin{cases} v_{i,j-1}(t), & \text{if } v_{i,j-1}(t) < v_{\max}, \\ v_{\max}, & \text{if } v_{i,j-1}(t) \geq v_{\max}. \end{cases}$$

Here,  $\kappa = v_{\max}/(d_{\max} - d_{\min})$ , where  $d_{\max}$  the maximum look-ahead distance for safety consideration. The nominal values of the parameters considered here are  $\alpha = 0.6$ ,  $\beta = 0.5$ ,  $\tau = 0.6$  s,  $\kappa = 0.6$ ,  $v_{\max} = 30$  m/s.

### 6.2.1.2 System Constraints

For each vehicle  $j \in \mathcal{N}_i$  in platoon  $i \in \mathcal{L}(t)$  the control input and speed are bounded by

$$u_{\min} \leq u_{i,j}(t) \leq u_{\max}, \quad (6.23a)$$

$$0 < v_{\min} \leq v_{i,j}(t) \leq v_{\max}, \quad (6.23b)$$

where  $u_{\min}, u_{\max}$  are the minimum and maximum control inputs related to the physical acceleration/deceleration limits of the vehicles, and  $v_{\min}, v_{\max}$  are the minimum and maximum speed limit of the road, respectively. Although the control constraint in (6.23a) applies to all vehicles in the network, we need to take into account the notion of formation control and string stability of the platoons and revisit the control constraint for CAV. To this end, we consider the following cases:

(i) *Formation control during acceleration:* For a strictly positive control input  $u_{i,0} > 0$  for each CAV in  $\mathcal{L}(t)$ , the CAV's information is relayed with a delay of  $(M_i - 1)\tau$  to the last HDV  $j \in \mathcal{N}_i, i \in \mathcal{L}(t)$ . For a positive control input  $u_{i,0} > 0$  of the CAV, this implies that the vehicles within the platoon may break the initial formation, which has serious safety implications for solving the platoon coordination problem. Therefore,

to ensure that the vehicles within the platoon are closely spaced, we only allow non-positive control input for each CAV, i.e.,  $u_{0,i} \leq 0$ .

(ii) *String instability during deceleration:* The delay in information flow towards the trailing HDVs  $j \in \mathcal{N}_i, i \in \mathcal{L}(t)$  also has safety implications due to string stability. During the maximum braking event of the CAV, i.e.,  $u_{i,0} = u_{\min}$ , the headway fluctuation will get amplified for the trailing HDVs, and passenger safety may be compromised. Let us consider  $\hat{u}_{\min}$  to be a minimum deceleration value for which the CAV can avoid string instability. We provide the explicit formulation and derivation of  $\hat{u}_{\min}$  in Section 6.2.2.3. The CAV control input is thus lower-bounded as  $u_{i,j} \geq \max(\hat{u}_{\min}, u_{\min})$ .

With the above information, we can now formulate a control constraint exclusively applicable to the CAVs in the network

$$\max(\tilde{u}_{\min}, u_{\min}) \leq u_{i,j}(t) \leq 0 \quad (6.24)$$

To ensure rear-end safety between platoon  $i \in \mathcal{L}(t)$  and preceding platoon  $k \in \mathcal{L}(t)$ , we have

$$p_{k,m_k}(t) - p_{i,0}(t) \geq s_{i,0}(t), \quad (6.25)$$

where  $m_k$  is the last follower in the platoon  $k$  physically located in front of platoon  $i$  and  $s_i(t)$  is the safe speed-dependent headway of the leader CAV of platoon  $i$ .

Similarly, to guarantee rear-end safety between two consecutive vehicles  $j, j-1$  inside each platoon  $i \in \mathcal{L}(t)$ , we enforce

$$\Delta p_{i,j}(t) \geq d_{\min}, \quad \forall j \in \{1, \dots, m_i\}. \quad (6.26)$$

Finally, let  $k \in \mathcal{L}(t)$  correspond to another platoon that has already entered the control zone, which implies that  $i \in \mathcal{L}(t)$  may have a lateral collision with platoon  $k$  at conflict point  $n$ .

In this work, we enforce a first-in-first-out queuing policy, i.e., platoon  $i$  must cross the conflict point after platoon  $k$ , which is ahead in the queue. For each platoon  $i \in \mathcal{L}(t)$ , lateral collision is possible at the conflict point  $n$  within the set  $\Gamma_i$ ,

$$\Gamma_i := \{t \mid t \in [t_{i,0}^f, t_{i,m_i}^f]\}. \quad (6.27)$$

To guarantee lateral safety between platoon  $i$  and platoon  $k$  at the conflict point  $n$ , the following condition must be satisfied,

$$\Gamma_i \cap \Gamma_k = \emptyset, \quad i, k \in \mathcal{L}(t). \quad (6.28)$$

Therefore, we impose the following lateral safety constraint on platoon  $i$  to satisfy (6.28)

$$t_{i,0}^f - t_{k,m_k}^f \geq t_h, \quad (6.29)$$

where  $t_h \in \mathbb{R}_{>0}$  is the minimum time headway between any two CAVs entering node  $n$  that guarantees safety,  $t_{i,0}^f$  is the time that leader of platoon  $i$  exits the control zone (recall that the conflict point  $n$  is at the exit of control zone), and  $t_{k,m_k}^f$  is time that the last HDV in the platoon  $k$  exits the control zone.

A conservative estimation of  $t_{k,m_k}^f$  can be formulated by assuming a worst-case braking scenario after the platoon leader of the platoon  $k \in \mathcal{L}(t)$  exits the conflict zone. Therefore, one may calculate  $t_{k,m_k}^f$  by considering the behavior limits of the last HDV in the platoon under typical highway driving scenarios, i.e., the last HDV travels to the conflict point with  $u_{k,m_k}(t) \equiv u_{\min}$ .

$$t_{k,m_k}^f = \begin{cases} -\frac{v_{k,m_k} - \sqrt{v_{k,m_k}^2 + 2u_{\min}r_{k,m_k}}}{u_{\min}}, & \text{if } r_{k,m_k} \leq -\frac{v_{k,m_k}^2 - v_{\min}^2}{2u_{\min}}, \\ -\frac{v_{k,m_k} - v_{\min}}{u_{\min}} + \frac{r_{k,m_k} + \frac{v_{k,m_k}^2 - v_{\min}^2}{2u_{\min}}}{v_{\min}}, & \text{otherwise,} \end{cases} \quad (6.30)$$

where  $v_{k,m_k}$  and  $r_{k,m_k}$  represent the current velocity of the last HDV and its current distance from the conflict point. Note that although (6.30) gives a conservative estimation of  $t_{k,m_k}^f$ , this calculation can be done at each time the current status of the HDV is available via V2X. Later in the simulation we will demonstrate that the estimation

becomes less conservative with frequent status update as the HDV approaches conflict zone. However, the conservative approach presented in (6.30) needs to be computed real-time for each time step, which can be computationally taxing. Furthermore, the worst-case scenario considered in this formulation does not incorporate the platoon leader's state information in its formulation. In what follows, we present an alternative formulation based on the platoon leader's state information that can be used to compute the tentative merging time  $t_{k,m_k}^f$  of the last HDV of the platoon.

**Lemma 6.2.5.** *If the leader of the preceding platoon  $k \in \mathcal{L}(t)$  exits the control zone at time  $t_{k,0}^f$  and maintains the exit speed  $v_{k,0}(t_{k,0}^f)$  until the all the platoon members exit the control zone, then the time  $t_{k,m_k}^f$  such that the last platoon member  $m_k \in \mathcal{N}_i$  exits the control zone is*

$$t_{k,m_k}^f = t_{k,0}^f + \frac{(M_k - 1)(\Delta_k + l_c)}{v_{k,0}(t_{k,0}^f)}. \quad (6.31)$$

*Proof.* Suppose that, the leader of the preceding platoon  $k \in \mathcal{L}(t)$  exits the control zone at time  $t_{k,0}^f$  and maintains the exit speed  $v_{k,0}(t_{k,0}^f)$  until the all the platoon members exit the control zone. Since the leader CAV's control input is non-positive according to the constraint in (6.24), the total length of the platoon at time  $t_{k,0}^f$  can be upper-bounded by the initial platoon length of the platoon  $(M_k - 1)\Delta_k$ . Therefore, the last HDV of platoon  $k$  needs to travel the distance  $(M_k - 1)(\Delta_k + l_c)$  with a speed  $v_{k,m_k}(t_{k,0}^f)$  that is also upper-bounded by the leader CAV's speed  $v_{k,0}(t_{k,0}^f)$ . Therefore, considering a conservative estimation of the platoon length and HDV's speed at time  $t_{k,0}^f$ , the time duration that last HDV of the platoon needs to travel to reach the exit of the control zone is  $\frac{(M_k-1)(\Delta_k+l_c)}{v_{k,0}(t_{k,0}^f)}$ , which yields the equation in (6.31).  $\square$

With the state, control and safety constraints defined above, we now impose the following assumption:

**Assumption 6.2.3.** Upon entering the control zone, the initial state of each CAV  $j \in \mathcal{N}_i(t)$ ,  $i \in \mathcal{L}(t)$ , is feasible, that is, none of the speed or safety constraints are violated.

This is a reasonable assumption since CAVs are automated; therefore, there is no compelling reason for them to violate any of the constraints by the time they enter the control zone.

### 6.2.1.3 Information Structure

In this section, we formalize the information structure that is communicated between the CAV leaders and the connected HDVs inside the control zone.

**Definition 6.2.6.** Let  $\phi_i$  be the vector containing the parameters of the optimal control policy (formally defined in Section 6.2.2.1) of the leader of platoon  $i \in \mathcal{L}(t_{i,0}^0)$ . Then, the *platoon information set*  $\mathcal{I}_{i,0}$  that the leader of platoon  $i$  can obtain from other vehicles after entering the control zone at time  $t = t_{i,0}^0$  is

$$\mathcal{I}_{i,0} = \{\phi_{1:L(t_{i,0}^0)}, M_{1:L(t_{i,0}^0)}, t_{1:L(t_{i,0}^0)}^0, t_{1:L(t_{i,0}^0)}^f\}, \quad (6.32)$$

where  $\phi_{1:L(t_{i,0}^0)} := [\phi_1, \dots, \phi_{L(t_{i,0}^0)}]^T$ ,  $M_{1:L(t_{i,0}^0)} := [M_1, \dots, M_{L(t_{i,0}^0)}]^T$ ,

$$t_{1:L(t_{i,0}^0)}^0 := [t_{0,1}^0, \dots, t_{0,L(t_{i,0}^0)}^0]^T, \text{ and } t_{1:L(t_{i,0}^0)}^f := [t_{0,1}^f, \dots, t_{0,L(t_{i,0}^0)}^f]^T.$$

**Remark 6.2.2.** The information structure  $\mathcal{I}_{i,0}$  for the leader CAV of each platoon  $i \in \mathcal{L}(t_{i,0}^0)$  indicates that the control policy, entry time to the control zone  $t_j^0$ , exit time of the control zone  $t_j^f$ , and the platoon size  $M_j$  of each platoon  $j \in \mathcal{L}(t_{i,0}^0) \setminus \{i\}$  already existing within the control zone is available to the leader of platoon  $i$  through V2X communication. Note that, although the leader of platoon  $i$  knows the endogenous information  $t_{i,0}^0$  and  $M_i$ , it needs to compute the vector of its own optimal control input parameters  $\phi_i$  and the merging time  $t_{i,0}^f$ , which we discuss in section 6.2.2.

**Definition 6.2.7.** The *member information set*  $\mathcal{I}_{i,j}(t)$  that each platoon member  $j \in \mathcal{N}_i \setminus \{0\}$  belonging to each platoon  $i \in \mathcal{L}(t)$  at time  $t \in [t_{i,0}^0, t_{i,0}^f]$  can obtain is

$$\mathcal{I}_{i,j} = \{p_{i,j-1}(t), v_{i,j-1}(t)\}. \quad (6.33)$$

**Remark 6.2.3.** The unidirectional driver perception allows each platoon member  $j \in \mathcal{N}_i \setminus \{0\}$  belonging to platoon  $i \in \mathcal{L}(t)$  to access the state and control input information of its immediate preceding vehicle  $j - 1$  in the form of  $\mathcal{I}_{i,j}$  at each time  $t \in [t_{i,0}^0, t_{i,0}^f]$ .

## 6.2.2 Coordination Framework for Mixed Platoons

In what follows, we introduce a single-level optimal coordination framework that consists of two objectives. The first objective is to develop a control strategy for the platoon leaders to minimize their control efforts. The second objective is concerned with minimizing their travel time while guaranteeing that none of their state, control, and safety constraints becomes active.

### 6.2.2.1 Optimal Control of Problem for Platoon Leaders

To establish a framework for coordinating the mixed platoons, we adopt the single-level optimization framework to control the CAVs, which are the platoon leaders, as presented in Section 6.1. We formally define our single-level optimization framework for platoon leaders as follows.

**Problem 6.2.1.** *Upon entering the control zone, each leader of platoon  $i \in \mathcal{L}(t)$  accesses the information set  $\mathcal{I}_i$  and solves the following optimization problem at  $t_{i,0}^0$*

$$\min_{t_{i,0}^f \in \mathcal{T}_i(t_{i,0}^0)} t_{i,0}^f \quad (6.34)$$

subject to:

$$(6.25), (6.29), (6.12),$$

where the compact set  $\mathcal{T}_i(t_{i,0}^0) = [\underline{t}_i^f, \bar{t}_i^f]$  is the set of feasible solution of leader of platoon  $i \in \mathcal{N}(t)$  for the exit time that satisfy the boundary conditions without activating the constraints, while  $\underline{t}_i^f$  and  $\bar{t}_i^f$  denote the minimum and maximum feasible exit time computed at  $t_{i,0}^0$ .

**Remark 6.2.4.** We can derive the optimal control input of the platoon leaders using the solution of Problem 6.2.1,  $t_{i,0}^f$ , the boundary conditions (6.13)-(6.14) and (6.12).

### 6.2.2.2 Feasibility and Existence

We continue our exposition by briefly reviewing the process to compute the compact set  $\mathcal{T}_i(t_{i,0}^0)$  at time  $t_{i,0}^0$  using the speed and control input constraints (6.23a)-(6.23b), initial condition (6.13), and final condition (6.14). Details regarding the derivation of the compact set  $\mathcal{T}_i(t_{i,0}^0)$  can be found in [218].

The lower-bound  $\underline{t}_i^f$  of  $\mathcal{T}_i(t_{i,0}^0)$  can be computed by considering the state and control constraints and boundary conditions as

$$\underline{t}_i^f = \max \left\{ \hat{t}_{i,\text{cruise}}^f, \min \{ t_{i,u_{\max}}^f, t_{i,v_{\max}}^f \} \right\}, \quad (6.35)$$

where,

$$\begin{aligned} t_{i,v_{\max}}^f &= \frac{3(p_i(t_{i,0}^f) - p_i(t_{i,0}^0))}{v_i(t_{i,0}^0) + 2v_{\max}}, \\ t_{i,u_{\max}}^f &= \frac{\sqrt{9v_i(t_{i,0}^0)^2 + 12(p_i(t_{i,0}^f) - p_i(t_{i,0}^0))u_{\max} - 3v_i(t_{i,0}^0)}}{2u_{\max}}, \\ \hat{t}_{i,\text{cruise}}^f &= \frac{(p_i(t_{i,0}^f) - p_i(t_{i,0}^0))}{v_i(t_{i,0}^0)}. \end{aligned}$$

Here,  $\hat{t}_{i,\text{cruise}}^f$  is the time that the CAV requires to cruise the control zone with its initial speed  $v_i(t_{i,0}^0)$ , and  $t_{i,v_{\max}}^f$  and  $t_{i,u_{\max}}^f$  are the times which leader of platoon  $i \in \mathcal{L}(t)$  achieves its maximum speed at the end of control zone and its maximum control input at the entry of the control zone, respectively. Similarly, we derive the upper-bound  $\bar{t}_i^f$  as

$$\bar{t}_i^f = \begin{cases} t_{i,v_{\min}}^f, & \text{if } 9v_i(t_{i,0}^0)^2 + 12(p_i(t_{i,0}^f) - p_i(t_{i,0}^0))u_{\min} < 0, \\ \max \{ t_{i,u_{\min}}^f, t_{i,v_{\min}}^f \}, & \text{otherwise,} \end{cases} \quad (6.36)$$

where

$$\begin{aligned} t_{i,v_{\min}}^f &= \frac{3(p_i(t_{i,0}^f) - p_i(t_{i,0}^0))}{v_i(t_{i,0}^0) + 2v_{\min}}, \\ t_{i,u_{\min}}^f &= \frac{\sqrt{9v_i(t_{i,0}^0)^2 + 12(p_i(t_{i,0}^f) - p_i(t_{i,0}^0))\hat{u}_{\min} - 3v_i(t_{i,0}^0)}}{2\hat{u}_{\min}}, \\ \hat{u}_{\min} &= \max(u_{\min}, \tilde{u}_{\min}). \end{aligned}$$

Similar to the previous case,  $t_{i,v_{min}}^f$  and  $t_{i,u_{min}}^f$  are the times at which the leader of the platoon  $i \in \mathcal{L}(t)$  achieves its minimum speed at the end of control zone and its minimum control input at the entry of the control zone, respectively.

The existence of an optimal solution to Problem 6.2.1 may not be guaranteed given the state, control and safety constraints in (6.24), (6.23b), (6.29) and (6.25). The following lemma provides the condition to check whether Problem 6.2.1 is infeasible and a solution does not exist.

**Lemma 6.2.8.** *Suppose that  $\mathcal{T}_i(t_{i,0}^0)$  is the compact set of a platoon  $i \in \mathcal{L}(t)$  that intends to exit the control with lateral safety constraint (6.29) after the last HDV of the preceding platoon  $k \in \mathcal{L}(t)$  exits the control zone at time  $t_{k,m_k}^f$ . A solution to Problem 6.2.1 does not exist if the compact set  $\mathcal{T}_i(t_{i,0}^0)$  is empty, and  $t_{k,m_k}^f + t_h > \bar{t}_i^f$ .*

*Proof.* It is trivial to show that, if the compact set  $\mathcal{T}_i(t_{i,0}^0)$  is empty, then there does not exist any solution of Problem 6.2.1.

For the second condition, consider the scenario where platoon  $i$  needs to yield to platoon  $k$ . A conservative prediction of the time when the last HDV in platoon  $k$  exits the conflict zone is given by  $t_{k,m_k}^f$  in Lemma (6.2.5), and the leader CAV of platoon  $i$  needs to enter the conflict point after  $t_{k,m_k}^f + t_h$  in the worst case to ensure safety. Thus, the optimal problem needs to be solved on the time domain  $[\max(t_i^f, t_{k,m_k}^f + t_h), \bar{t}_i^f]$ . To ensure the possibility of a solution of Problem 6.2.1, we need

$$t_{k,m_k}^f + t_h \leq \bar{t}_i^f, \quad (6.37)$$

for the  $t_{k,m_k}^f$  given in (6.31). This yields a necessary condition between the states of the last HDV in platoon  $k$  and the leader CAV in platoon  $i$  for a conflict-free coordination of mixed platoons.  $\square$

Note that, the solution to the optimal control problem 6.2.1 yields the optimal control input  $u_i^*(t)$  for each platoon leader  $i \in \mathcal{L}(t)$  for  $t \in [t_{i,0}^0, t_{i,0}^f]$ . However, the solution to this problem does not consider the stability criteria of the platoon [219],

which is essential to guarantee safety within the platooning CAVs. In the following section, we first introduce the notion of stability during platoon coordination, and then propose a control structure  $u_{i,j}(t)$  for each platoon member  $j \in \mathcal{N}_i \setminus \{0\}$ ,  $i \in \mathcal{L}(t)$  that is optimal subject to constraints, and satisfies the stability properties.

### 6.2.2.3 Safety Guaranteed Control Bound Within Each Platoon

To ensure that the HDV followers in each platoon do not have rear-end collisions, we provide a necessary condition regarding the maximal deceleration that the leader CAV in the same platoon may apply. Let us first consider the scenario involving only the leading CAV 0 and the following HDV 1. At time  $t_{i,0}^0$  when CAV 0 enters the control zone, it starts to apply a constant deceleration  $u_{i,0}(t) = \tilde{u}_{\min} (< 0)$ . Considering the human reaction time delay  $\tau$  and deceleration capability  $u_{\min}$  for HDV 1, for the given initial velocities  $v_{i,0} := v_{i,0}(t_{i,0}^0)$  and  $v_{i,1} := v_{i,1}(t_{i,0}^0)$ , and headway  $h_{i,1} := h_{i,1}(t_{i,0}^0)$ , the CAV's deceleration must satisfy the following condition to ensure  $h_{i,1}(t) \geq 0$ ,  $\forall t \geq t_{i,0}^0$ , i.e., a rear-end collision never occurs between CAV 0 and HDV 1.

$$\tilde{u}_{\min} \geq f(v_{i,0}(t_{i,0}^0), v_{i,1}(t_{i,0}^0), h_{i,1}(t_{i,0}^0), \tau, u_{\min}), \quad (6.38)$$

where

$$f(v_{i,0}, v_{i,1}, h_{i,1}, \tau, u_{\min}) = \quad (6.39)$$

$$\begin{cases} \max \left( u_{\min}, \frac{(v_{\min} - v_{i,0})^2}{2h_{i,1} + 2(v_{\min} - v_{i,1})\tau + \frac{(v_{\min} - v_{i,1})^2}{u_{\min}}} \right), & h_{i,1} \in [h_{i,1}^*, \infty) \\ \frac{(v_{i,1} - v_{i,0} - u_{\min}\tau)^2}{2h_{i,1} - u_{\min}\tau^2} + u_{\min}, & \text{otherwise,} \end{cases}$$

$$h_{i,1}^* = -\frac{1}{2}\tau(v_{\min} + v_{i,0} - 2v_{i,1}) + \frac{(v_{i,1} - v_{i,0})(v_{\min} - v_{i,1})}{2u_{\min}}. \quad (6.40)$$

The condition (6.38) is derived by considering that the following HDV 1 applies its maximal deceleration  $u_1(t) = u_{\min}$  on  $t \geq t_{i,0}^0 + \tau$ , i.e.,  $\tau$  time after the leader CAV starts to apply constant input  $\tilde{u}_{\min}$ . Such condition of  $\tilde{u}_{\min}$  guarantees  $h_1(t) \geq 0$ ,  $\forall t \geq t_{i,0}^0$ . Therefore, if (6.38) is violated, a rear-end collision between CAV 0 and

HDV 1 is inevitable under human reaction delay  $\tau$ . We remark that at time  $t_{i,0}^0$ , with the assumption that the platoon is already formed and vehicles are travelling with the same steady-state velocity, i.e.,  $v_{i,0} = v_{i,1}$ , we have  $u_{\min} \leq f(v_{i,0}, v_1, h_1, \tau, u_{\min}) \leq 0$ . That is, the necessary condition (6.38) is always feasible for the CAV to satisfy.

For more general scenario, where there are  $m_i$  HDVs following the CAV 0, the corresponding necessary condition to avoid rear-end collision is given by

$$\tilde{u}_{\min} \geq (f_1 \circ f_2 \circ f_3 \circ \cdots \circ f_{m_i})(u_{\min}), \quad (6.41)$$

where  $\circ$  denotes function composition, and  $f_j := f(v_{j-1}, v_j, h_j, \tau, u_{\min})$  for  $j \in 1, 2, \dots, m_i$ . Note that (6.41) is derived similar to (6.38) by considering the deceleration limit of the last HDV  $m_i$  to satisfy the condition  $h_{i,1}(t) \geq 0 \wedge h_{i,2}(t) \geq 0 \wedge \cdots \wedge h_{i,m_i}(t) \geq 0$ ,  $\forall t \geq t_{i,0}^0$ . This guarantees that rear-end collisions never happen between any following vehicles in the platoon.

So far, we provided the exposition of the intricacies of our proposed control framework for optimal coordination of mixed platoons. The algorithm that can be applied to implement this framework in real time is similar to the one presented in Section 6.1.5 with a slight modification.

---

**Algorithm 3** Vehicular Platoons Coordination Algorithm

---

```

1: for  $i \in \mathcal{L}(t)$  do
2:   for  $j \in \mathcal{N}_i$  do
3:     if  $j=0$  then ▷ Platoon leader
4:        $u_{i,j} = 0 \quad \forall t \in [t_{i,0}^0, t_{i,0}^0)$  ▷ Cruise with constant speed
5:       Compute  $\mathcal{T}_i(t_{i,0}^0)$  ▷ Based on (6.35)-(6.36)
6:        $t_i^f, \phi_i \leftarrow \text{Platoon Leader Control}()$  ▷ Algorithm 2
7:        $[a_i, b_i, c_i, d_i] \leftarrow \phi_i$ 
8:        $u_{i,j}(t) \leftarrow 6a_it + 2b_i$  ▷  $\forall t \in [t_{i,0}^0, t_{i,0}^f]$ 
9:     else ▷ Platoon followers
10:       $u_{i,j}(t) = f_{CFM}$ 
11:    end if
12:  end for
13: end for

```

---

In this section, the key concepts of CAV coordination and platooning were leveraged to establish a rigorous optimal platoon coordination framework for CAVs that improves fuel efficiency and traffic throughput of the network. A single-level optimal control framework is presented that simultaneously optimizes both fuel economy and travel time of the platoons while satisfying the state, control, and safety constraints. The coordination framework was made robust by considering the effect of delayed inter-platoon communication and HDV perception delay to derive a closed-form analytical solution of the optimal control problem using standard Hamiltonian analysis that can be implemented in real time using leader-follower unidirectional communication topology. Finally, the proposed control framework was validated using a commercial simulation environment by evaluating its performance. The proposed optimal coordination framework shows significant benefits in terms of fuel consumption and travel time compared to the baseline cases.

## Chapter 7

### CONCLUSION

#### 7.1 Summary

The contributions in this dissertation provide a rigorous mathematical solution to the problem of optimal control and coordination of CAVs in a mixed traffic environment. First, I have addressed the problem related to the optimal control and coordination of CAVs through traffic scenarios considering state, control, and safety constraints. The key outcomes of this contribution are as follows.

1. The activation cases of different state and control constraint combinations are mathematically characterized and a set of conditions are provided to identify the activation of system constraints as a priori.
2. The interdependence of constraint activation cases can be identified based on the initial boundary conditions.
3. The standard recursive methodology of solving the constrained optimal control problem is improved computationally by the elimination of the intermediate steps of iteration.
4. The junction points between the constrained and unconstrained arcs can be explicitly derived that enable the computation of the constrained optimal control policy with a real-time implementable closed-form analytical solution.

The condition-based framework can increase the computational efficiency of solving a constrained optimal control problem and derive control actions for the CAVs in real time.

Second, I have addressed the problem of deriving the optimal trajectory of a CAV in a mixed traffic environment that considers the interaction of HDVs. The key outcomes of this contribution are as follows.

1. A predictive control approach was developed for deriving safe trajectories for the CAVs in a mixed traffic environment by predicting the future trajectories of the HDVs to ensure collision safety.

2. An indirect approach was developed to control the HDVs by leveraging the concept of vehicle platooning.
3. The platoon formation is formulated as a constrained multi-objective control problem that enables optimal platoon formation by directly controlling the CAVs.
4. The platoon formation framework employs a receding horizon controller that can handle system uncertainties, and enforce enhanced rear-end collision safety.
5. The framework can form platoons by employing different prediction models for estimating the HDV trajectories: (a) a naive linear constant speed model, (b) a nonlinear car-following model with nominal parameters, and (c) a data-driven model that estimates the driving behavior of the HDVs in real time using recursive least squares algorithm to better predict the futures trajectories.

The presented control framework guarantees the indirect control of the HDVs by safely and optimally forming mixed platoons.

Third, I have addressed the problem of vehicle coordination in a mixed traffic environment at traffic scenarios such as signal-free intersections, automated on-ramp merging, etc.

1. The concepts of CAV coordination and platooning were leveraged to establish a rigorous optimal platoon coordination framework in a mixed traffic environment.
2. The vehicle coordination is achieved by employing a single-level optimal control framework that can simultaneously optimize both fuel economy and travel time of the platoons while satisfying the state, control, and safety constraints.
3. The coordination framework is robust against the effect of delayed inter-platoon communication and HDV perception delay.

The presented control framework can establish an automated on-ramp merging scenario in a mixed traffic environment and coordinate the trajectories of the CAVs and HDVs to eliminate congestion.

The research efforts pursued in this dissertation bridge the gap between the two extremes of the mixed traffic environment spectrum, and thus, have a significant impact on the future of mobility. The outcome of the research efforts presented in this dissertation not only provides a vehicle-level performance improvement but also realizes the automated coordination and merging concept, which increases the traffic

performance from a macroscopic viewpoint. Compared to the utopian scenario of 100% CAV penetration, the developed control framework will be implementable online in a real-world mixed traffic network with a variety of scenarios. By adopting the computationally efficient and real-time implementable control framework proposed in this dissertation, CAVs can derive optimal motion primitives that can ensure safe and improved mobility in a mixed traffic environment.

## 7.2 Future Direction

Several avenues can be considered as potential directions for future research. In this dissertation, a double integrator model was considered to model the CAV dynamics. One of the future directions thus can be the inclusion of a more complex form of vehicle dynamics that can accommodate the implications of the optimal control of CAVs. For example, the vehicle dynamics with aerodynamic drag [89], lateral motion [31], road grade [190] or delayed control action [137] can be considered to increase the accuracy in deriving the optimal motion primitives.

The platoon formation and coordination framework presented in this dissertation is developed from a microscopic point of view using vehicle-level control. Investigation of the impact of platoon formation and control in a network-level analysis can yield interesting results, especially considering different platoon characteristics similar to the work of Lioris et al. [16].

Although delay in CAV communication and HDV perception has been considered to some extent in this dissertation, a rigorous mathematical formulation is yet to be developed. Therefore, potential direction for future research can also include the relaxation of the assumption of perfect communication among the CAVs and considering system uncertainty. Several research efforts have explored the effect of system uncertainty by considering dynamic resequencing [91, 92], reinforcement learning [90, 93] and control barrier functions [89, 94].

Finally, different approaches for the estimation and prediction of the HDV state

can be explored to improve the accuracy of the feedback controller. Application of improved recursive least squares algorithm [197], Kalman filter [196], linear-quadratic Gaussian estimator [222] and deep learning approaches [223, 224] can be considered for future development.

## Bibliography

- [1] United Nations. 2018 revision of world urbanization prospects, 2018.
- [2] David Schrank, Bill Eisele, Tim Lomax, et al. Urban mobility report 2019. 2019.
- [3] Traffic congestion. *Economic and environmental of traffic congestion in Europe and the U.S.* (<http://www.inrix.com/economic-environment-cost-congestion/>), 2015.
- [4] Traffic congestion cost the us economy nearly \$87 billion in 2018. *World Economic Forum* ([//www.weforum.org/agenda/2019/03/traffic-congestion-cost-the-us-economy-nearly-87-billion-in-2018/](http://www.weforum.org/agenda/2019/03/traffic-congestion-cost-the-us-economy-nearly-87-billion-in-2018/)), 2018.
- [5] M Desai, RP Harvey, et al. Inventory of us greenhouse gas emissions and sinks: 1990-2015. *Federal Register*, 82(10767):10–1002, 2017.
- [6] Jackeline Rios-Torres and Andreas A Malikopoulos. A survey on the coordination of connected and automated vehicles at intersections and merging at highway on-ramps. *IEEE Transactions on Intelligent Transportation Systems*, 18(5):1066–1077, 2016.
- [7] Traffic safety facts. *National Highway Traffic Safety Administration, DOT HS*, 809:327, 2000.
- [8] Traffic safety facts, 2018. *National Highway Traffic Safety Administration* (<https://crashstats.nhtsa.dot.gov/Api/Public/ViewPublication/812826>, 2019.
- [9] Kevin Spieser, Kyle Treleaven, Rick Zhang, Emilio Frazzoli, Daniel Morton, and Marco Pavone. Toward a systematic approach to the design and evaluation of

- automated mobility-on-demand systems: A case study in singapore. In *Road vehicle automation*, pages 229–245. Springer, 2014.
- [10] Daniel J Fagnant and Kara M Kockelman. The travel and environmental implications of shared autonomous vehicles, using agent-based model scenarios. *Transportation Research Part C: Emerging Technologies*, 40:1–13, 2014.
- [11] Jacopo Guanetti, Yeojun Kim, and Francesco Borrelli. Control of Connected and Automated Vehicles: State of the Art and Future Challenges. *Annual Reviews in Control*, 45:18–40, 2018.
- [12] P Kachroo and Zhijun Li. Vehicle merging control design for an automated highway system. In *Proceedings of Conference on Intelligent Transportation Systems*, pages 224–229, 1997. ISBN 0-7803-4269-0.
- [13] M Antoniotti, A Deshpande, and A Girault. Microsimulation analysis of automated vehicles on multiple merge junction highways. In *IEEE International Conference in Systems, Man, and Cybernetics*, pages 839–844, 1997.
- [14] Bin Ran, Shawn Leight, and Ben Chang. A microscopic simulation model for merging control on a dedicated-lane automated highway system. *Transportation Research Part C: Emerging Technologies*, 7(6):369–388, 1999.
- [15] Remi Tachet, Paolo Santi, Stanislav Sobolevsky, Luis Ignacio Reyes-Castro, Emilio Frazzoli, Dirk Helbing, and Carlo Ratti. Revisiting street intersections using slot-based systems. *PLOS ONE*, 11(3), 2016.
- [16] Jennie Lioris, Ramtin Pedarsani, Fatma Yildiz Tascikaraoglu, and Pravin Varaiya. Platoons of connected vehicles can double throughput in urban roads. *Transportation Research Part C: Emerging Technologies*, 77:292–305, 2017.
- [17] Andreas A Malikopoulos and Liuhui Zhao. Optimal path planning for connected and automated vehicles at urban intersections. In *Proceedings of the 58th IEEE Conference on Decision and Control, 2019*, pages 1261–1266. IEEE, 2019.

- [18] Matthew Hausknecht, Tsz-Chiu Au, and Peter Stone. Autonomous intersection management: Multi-intersection optimization. In *2011 IEEE/RSJ International Conference on Intelligent Robots and Systems*, pages 4581–4586. IEEE, 2011.
- [19] Youssef Bichiou and Hesham A Rakha. Developing an optimal intersection control system for automated connected vehicles. *IEEE Transactions on Intelligent Transportation Systems*, 20(5):1908–1916, 2018.
- [20] J. Rios-Torres, Andreas A Malikopoulos, and Pierluigi Pisu. Online Optimal Control of Connected Vehicles for Efficient Traffic Flow at Merging Roads. In *2015 IEEE 18th International Conference on Intelligent Transportation Systems*, pages 2432–2437, 2015.
- [21] A Mosebach, S Röchner, and J Lunze. Merging control of cooperative vehicles. *IFAC-PapersOnLine*, 49(11):168–174, 2016.
- [22] Xishun Liao, Ziran Wang, Xuanpeng Zhao, Kyungtae Han, Prashant Tiwari, Matthew J Barth, and Guoyuan Wu. Cooperative ramp merging design and field implementation: A digital twin approach based on vehicle-to-cloud communication. *IEEE Transactions on Intelligent Transportation Systems*, 2021.
- [23] Liuhui Zhao, Andreas A Malikopoulos, and Jackeline Rios-Torres. Optimal control of connected and automated vehicles at roundabouts: An investigation in a mixed-traffic environment. In *15th IFAC Symposium on Control in Transportation Systems*, pages 73–78, 2018.
- [24] Ezequiel Debada, Laleh Makarem, and Denis Gillet. Autonomous coordination of heterogeneous vehicles at roundabouts. In *2016 IEEE 19th International Conference on Intelligent Transportation Systems (ITSC)*, pages 1489–1495. Ieee, 2016.
- [25] A A Malikopoulos and J P Aguilar. An Optimization Framework for Driver Feedback Systems. *IEEE Transactions on Intelligent Transportation Systems*, 14(2):955–964, 2013.

- [26] Liuhui Zhao, Andreas A Malikopoulos, and Jackeline Rios-Torres. On the traffic impacts of optimally controlled connected and automated vehicles. In *Proceedings of 2019 IEEE Conference on Control Technology and Applications (CCTA)*, pages 882–887. IEEE, 2019.
- [27] Jackeline Rios-Torres and Andreas A Malikopoulos. Automated and Cooperative Vehicle Merging at Highway On-Ramps. *IEEE Transactions on Intelligent Transportation Systems*, 18(4):780–789, 2017.
- [28] Andreas A. Malikopoulos, Christos G. Cassandras, and Yue J. Zhang. A decentralized energy-optimal control framework for connected automated vehicles at signal-free intersections. *Automatica*, 93:244 – 256, 2018.
- [29] Yue Zhang, Christos G Cassandras, and Andreas A Malikopoulos. Optimal control of connected automated vehicles at urban traffic intersections: A feasibility enforcement analysis. In *2017 American Control Conference (ACC)*, pages 3548–3553. IEEE, 2017.
- [30] Laleh Makarem, Denis Gillet, and Senior Member. Model predictive coordination of autonomous vehicles crossing intersections. In *2013 16th International IEEE Conference on Intelligent Transportation Systems*, number Itsc, pages 1799–1804, 2013.
- [31] Tulga Ersal, Ilya Kolmanovsky, Neda Masoud, Necmiye Ozay, Jeffrey Scruggs, Ram Vasudevan, and Gábor Orosz. Connected and automated road vehicles: state of the art and future challenges. *Vehicle system dynamics*, 58(5):672–704, 2020.
- [32] Taxonomy and definitions for terms related to on-road motor vehicle automated driving systems. *SAE Standard J*, 3016:1–16, 2014.

- [33] Jackeline Rios-Torres and Andreas A Malikopoulos. Impact of partial penetrations of connected and automated vehicles on fuel consumption and traffic flow. *IEEE Transactions on Intelligent Vehicles*, 3(4):453–462, 2018.
- [34] Zijia Zhong, Lee Joyoung, and Liuhui Zhao. Evaluations of Managed Lane Strategies for Arterial Deployment of Cooperative Adaptive Cruise Control . In *TRB Annual Meeting*, Washington DC, USA, 2017.
- [35] Y Zhang and Christos G Cassandras. Decentralized optimal control of connected automated vehicles at signal-free intersections including comfort-constrained turns and safety guarantees. *Automatica*, 109, 2019.
- [36] Jishiyu Ding, Li Li, Hwei Peng, and Yi Zhang. A rule-based cooperative merging strategy for connected and automated vehicles. *IEEE Transactions on Intelligent Transportation Systems*, 21(8):3436–3446, 2019.
- [37] Matthew Barth and Kanok Boriboonsomsin. Energy and emissions impacts of a freeway-based dynamic eco-driving system. *Transportation Research Part D: Transport and Environment*, 14(6):400–410, 2009.
- [38] Irene Michelle Berry. *The effects of driving style and vehicle performance on the real-world fuel consumption of US light-duty vehicles*. PhD thesis, Massachusetts Institute of Technology, 2010.
- [39] Changxu Wu, Guozhen Zhao, and Bo Ou. A fuel economy optimization system with applications in vehicles with human drivers and autonomous vehicles. *Transportation Research Part D: Transport and Environment*, 16(7):515–524, 2011.
- [40] Ioannis A Ntousakis, Ioannis K Nikolos, and Markos Papageorgiou. Optimal vehicle trajectory planning in the context of cooperative merging on highways. *Transportation Research Part C: Emerging Technologies*, 71:464–488, 2016.
- [41] L. Zhao and Andreas A Malikopoulos. Decentralized optimal control of connected and automated vehicles in a corridor. In *2018 21st International Conference on*

- Intelligent Transportation Systems (ITSC)*, pages 1252–1257, Nov 2018. doi: 10.1109/ITSC.2018.8569229.
- [42] Michael Athans. A unified approach to the vehicle-merging problem. *Transportation Research*, 3(1):123–133, 1969. ISSN 00411647. doi: 10.1016/0041-1647(69)90109-9.
- [43] WanKyoo Choi, HongSang Yoon, Kyungsu Kim, Ilyong Chung, and SungJoo Lee. A traffic light controlling flc considering the traffic congestion. In *Advances in Soft Computing—AFSS 2002*, pages 69–75. Springer, 2002.
- [44] Zhiyong Liu. A survey of intelligence methods in urban traffic signal control. *IJCSNS International Journal of Computer Science and Network Security*, 7(7): 105–112, 2007.
- [45] C Dong, Z Liu, and X Liu. Chaos-particle swarm optimization algorithm and its application to urban traffic control. *International Journal of Computer Science and Network Security*, 6(1B):97–101, 2006.
- [46] K. Dresner and P. Stone. Multiagent traffic management: a reservation-based intersection control mechanism. In *Proceedings of the Third International Joint Conference on Autonomous Agents and Multiagents Systems*, pages 530–537, 2004.
- [47] Kurt Dresner and Peter Stone. A multiagent approach to autonomous intersection management. *Journal of artificial intelligence research*, 31:591–656, 2008.
- [48] Arnaud de La Fortelle. Analysis of reservation algorithms for cooperative planning at intersections. *13th International IEEE Conference on Intelligent Transportation Systems*, pages 445–449, September 2010.

- [49] Shan Huang, A.W. Sadek, and Yunjie Zhao. Assessing the Mobility and Environmental Benefits of Reservation-Based Intelligent Intersections Using an Integrated Simulator. *IEEE Transactions on Intelligent Transportation Systems*, 13(3):1201–1214, 2012.
- [50] Ismail H. Zohdy, Raj Kishore Kamalanathsharma, and Hesham Rakha. Intersection management for autonomous vehicles using iCACC. *2012 15th International IEEE Conference on Intelligent Transportation Systems*, pages 1109–1114, 2012.
- [51] Fei Yan, Mahjoub Dridi, and Abdellah El Moudni. Autonomous vehicle sequencing algorithm at isolated intersections. *2009 12th International IEEE Conference on Intelligent Transportation Systems*, pages 1–6, 2009.
- [52] Li Li and Fei-Yue Wang. Cooperative Driving at Blind Crossings Using Intervehicle Communication. *IEEE Transactions in Vehicular Technology*, 55(6):1712,1724, 2006. doi: 10.1109/TVT.2006.878730.
- [53] Feng Zhu and Satish V. Ukkusuri. A linear programming formulation for autonomous intersection control within a dynamic traffic assignment and connected vehicle environment. *Transportation Research Part C: Emerging Technologies*, 2015.
- [54] J Wu, F Perronnet, and A Abbas-Turki. Cooperative vehicle-actuator system: a sequence-based framework of cooperative intersections management. *Intelligent Transport Systems, IET*, 8(4):352–360, 2014.
- [55] Kyoung-Dae Kim and P.R. Kumar. An MPC-Based Approach to Provable System-Wide Safety and Liveness of Autonomous Ground Traffic. *IEEE Transactions on Automatic Control*, 59(12):3341–3356, 2014.

- [56] Joyoung Lee and Byungkyu Park. Development and Evaluation of a Cooperative Vehicle Intersection Control Algorithm Under the Connected Vehicles Environment. *IEEE Transactions on Intelligent Transportation Systems*, 13(1):81–90, 2012. doi: 10.1109/TITS.2011.2178836.
- [57] Hesham Rakha and Raj Kishore Kamalanathsharma. Eco-driving at signalized intersections using V2I communication. In *Intelligent Transportation Systems (ITSC), 2011 14th International IEEE Conference on*, pages 341–346. IEEE, 2011.
- [58] Behdad Chalaki and Andreas A Malikopoulos. An optimal coordination framework for connected and automated vehicles in two interconnected intersections. In *2019 IEEE Conference on Control Technology and Applications (CCTA)*, pages 888–893. IEEE, 2019.
- [59] ASM Bakibillah, MAS Kamal, CP Tan, et al. The optimal coordination of connected and automated vehicles at roundabouts. In *2019 58th Annual Conference of the Society of Instrument and Control Engineers of Japan (SICE)*, pages 1392–1397. IEEE, 2019.
- [60] Kaiyuan Xu, Christos G Cassandras, and Wei Xiao. Decentralized time and energy-optimal control of connected and automated vehicles in a roundabout. *arXiv preprint arXiv:2104.06242*, 2021.
- [61] Andreas A Malikopoulos, Seongah Hong, B Brian Park, Joyoung Lee, and Seung-han Ryu. Optimal control for speed harmonization of automated vehicles. *IEEE Transactions on Intelligent Transportation Systems*, 20(7):2405–2417, 2018.
- [62] Alessandro Colombo and Domitilla Del Vecchio. Least Restrictive Supervisors for Intersection Collision Avoidance: A Scheduling Approach. *IEEE Transactions on Automatic Control*, Provisiona, 2014.

- [63] Qiu Jin, Guoyuan Wu, Kanok Boriboonsomsin, and Matthew Barth. Multi-Agent Intersection Management for Connected Vehicles Using an Optimal Scheduling Approach. *2012 International Conference on Connected Vehicles and Expo (IC-CVE)*, pages 185–190, 2012.
- [64] Behdad Chalaki and Andreas A Malikopoulos. Time-optimal coordination for connected and automated vehicles at adjacent intersections. *IEEE Transactions on Intelligent Transportation Systems*, 2021. doi: 10.1109/TITS.2021.3123479.
- [65] Grant Mahler and Ardalan Vahidi. An optimal velocity-planning scheme for vehicle energy efficiency through probabilistic prediction of traffic-signal timing. *IEEE Transactions on Intelligent Transportation Systems*, 15(6):2516–2523, 2014.
- [66] Laleh Makarem and Denis Gillet. Fluent coordination of autonomous vehicles at intersections. *2012 IEEE International Conference on Systems, Man, and Cybernetics (SMC)*, pages 2557–2562, October 2012.
- [67] M.A.S. Kamal, M. Mukai, J. Murata, and T. Kawabe. Model Predictive Control of Vehicles on Urban Roads for Improved Fuel Economy. *IEEE Transactions on Control Systems Technology*, 21(3):831–841, 2013.
- [68] Xiangjun Qian, Jean Gregoire, Arnaud De La Fortelle, and Fabien Moutarde. Decentralized model predictive control for smooth coordination of automated vehicles at intersection. In *2015 European Control Conference (ECC)*, pages 3452–3458. IEEE, 2015.
- [69] Gurulingesh Raravi, Vipul Shingde, Krithi Ramamritham, and Jatin Bharadia. Merge algorithms for intelligent vehicles. In *Next Generation Design and Verification Methodologies for Distributed Embedded Control Systems*, pages 51–65. 2007. doi: 10.1007/978-1-4020-6254-4\\_5.

- [70] M.a.S. Kamal, J Imura, a. Ohata, T Hayakawa, and K Aihara. Coordination of automated vehicles at a traffic-lightless intersection. *16th International IEEE Conference on Intelligent Transportation Systems (ITSC 2013)*, (Itsc):922–927, October 2013. doi: 10.1109/ITSC.2013.6728350. URL <http://ieeexplore.ieee.org/lpdocs/epic03/wrapper.htm?arnumber=6728350>.
- [71] Engin Ozatay, Umit Ozguner, and Dimitar Filev. Velocity profile optimization of on road vehicles: Pontryagin’s maximum principle based approach. *Control Engineering Practice*, 61:244–254, 2017.
- [72] Antonio Sciarretta, Giovanni De Nunzio, and Luis Leon Ojeda. Optimal eco-driving control: Energy-efficient driving of road vehicles as an optimal control problem. *IEEE Control Systems Magazine*, 35(5):71–90, 2015.
- [73] Nianfeng Wan, Ardalan Vahidi, and Andre Luckow. Optimal speed advisory for connected vehicles in arterial roads and the impact on mixed traffic. *Transportation Research Part C: Emerging Technologies*, 69:548–563, 2016.
- [74] Jackeline Rios-Torres and Andreas A. Malikopoulos. A Survey on Coordination of Connected and Automated Vehicles at Intersections and Merging at Highway On-Ramps. *IEEE Transactions on Intelligent Transportation Systems*, 18(5):1066–1077, 2017.
- [75] Yu Wang, Xiaopeng Li, and Handong Yao. Review of trajectory optimisation for connected automated vehicles. *IET Intelligent Transport Systems*, 13:580–586, 2018.
- [76] Wei Xiao and Christos G Cassandras. Decentralized optimal merging control for connected and automated vehicles with safety constraint guarantees. *Automatica*, 123:109333, 2021.
- [77] Wei Xiao, Christos G Cassandras, and Calin Belta. Decentralized optimal control in multi-lane merging for connected and automated vehicles. In *2020 IEEE 23rd*

- International Conference on Intelligent Transportation Systems (ITSC)*, pages 1–6. IEEE, 2020.
- [78] Y.J Zhang, Andreas A Malikopoulos, and Christos G Cassandras. Optimal control and coordination of connected and automated vehicles at urban traffic intersections. In *Proceedings of the American Control Conference*, pages 6227–6232, 2016.
- [79] Behdad Chalaki and Andreas A Malikopoulos. Optimal control of connected and automated vehicles at multiple adjacent intersections. *IEEE Transactions on Control Systems Technology*, 30(3):972–984, 2022. doi: 10.1109/TCST.2021.3082306.
- [80] Chunhui Yu, Yiheng Feng, Henry X Liu, Wanjing Ma, and Xiaoguang Yang. Corridor level cooperative trajectory optimization with connected and automated vehicles. *Transportation Research Part C: Emerging Technologies*, 105:405–421, 2019.
- [81] Christos G Cassandras. Automating mobility in smart cities. *Annual Reviews in Control*, 44:1–8, 2017.
- [82] Adam Stager, L. Bhan, Andreas A Malikopoulos, and Liuhui Zhao. A scaled smart city for experimental validation of connected and automated vehicles. In *15th IFAC Symposium on Control in Transportation Systems*, pages 120–135, 2018.
- [83] Logan E Beaver, Behdad Chalaki, A M Mahbub, Liuhui Zhao, Ray Zayas, and Andreas A Malikopoulos. Demonstration of a Time-Efficient Mobility System Using a Scaled Smart City. *Vehicle System Dynamics*, 58(5):787–804, 2020.

- [84] Behdad Chalaki, Logan E. Beaver, A M Ishtiaque Mahbub, Heeseung Bang, and Andreas A. Malikopoulos. A research and educational robotic testbed for real-time control of emerging mobility systems: From theory to scaled experiments. *IEEE Control Systems Magazine*, 2022 (in press).
- [85] A. E. Bryson, Jr., W. F. Denham, and S. E. Dreyfus. Optimal programming problems with inequality constraints I: Necessary conditions for extremal solutions. *American Institute of Aeronautics and Astronautics Journal*, 1(11):2544 – 2550, 1963.
- [86] Jihun Han, Antonio Sciarretta, Luis Leon Ojeda, Giovanni De Nunzio, and Laurent Thibault. Safe-and eco-driving control for connected and automated electric vehicles using analytical state-constrained optimal solution. *IEEE Transactions on Intelligent Vehicles*, 3(2):163–172, 2018.
- [87] J. Wang, X. Zhao, and G. Yin. Multi-objective optimal cooperative driving for connected and automated vehicles at non-signalised intersection. *IET Intelligent Transport Systems*, 13(1):79–89, 2019. ISSN 1751-9578. doi: 10.1049/iet-its.2018.5100.
- [88] Andreas A Malikopoulos, Logan E Beaver, and Ioannis Vasileios Chremos. Optimal time trajectory and coordination for connected and automated vehicles. *Automatica*, 125(109469), 2021.
- [89] Behdad Chalaki and Andreas A Malikopoulos. A Barrier-Certified Optimal Coordination Framework for Connected and Automated Vehicles. *arXiv:2203.16418 (in review)*, 2022.
- [90] Behdad Chalaki and Andreas A Malikopoulos. A hysteretic q-learning coordination framework for emerging mobility systems in smart cities. In *2021 European Control Conferences (ECC)*, pages 17–22, 2021.

- [91] Behdad Chalaki and Andreas A. Malikopoulos. A priority-aware replanning and resequencing framework for coordination of connected and automated vehicles. *IEEE Control Systems Letters*, 6:1772–1777, 2022. doi: 10.1109/LCSYS.2021.3133416.
- [92] Yue Zhang and Christos G. Cassandras. A decentralized optimal control framework for connected automated vehicles at urban intersections with dynamic resequencing. In *2018 IEEE Conference on Decision and Control (CDC)*, pages 217–222. IEEE, 2018.
- [93] Behdad Chalaki and Andreas A. Malikopoulos. Robust learning-based trajectory planning for emerging mobility systems. In *2022 American Control Conference (ACC)*, 2022 (accepted) arXiv:2103.03313.
- [94] Aaron D. Ames, Jessy W. Grizzle, and Paulo Tabuada. Control barrier function based quadratic programs with application to adaptive cruise control. In *53rd IEEE Conference on Decision and Control*, pages 6271–6278. IEEE, 2014.
- [95] Adriano Alessandrini, Andrea Campagna, Paolo Delle Site, Francesco Filippi, and Luca Persia. Automated vehicles and the rethinking of mobility and cities. *Transportation Research Procedia*, 5:145–160, 2015.
- [96] Jackeline Rios-Torres and Andreas A. Malikopoulos. Energy impact of different penetrations of connected and automated vehicles: a preliminary assessment. In *Proceedings of the 9th ACM SIGSPATIAL International Workshop on Computational Transportation Science*, pages 1–6, 2016.
- [97] S. Ilgin Guler, Monica Menendez, and Linus Meier. Using connected vehicle technology to improve the efficiency of intersections. *Transportation Research Part C: Emerging Technologies*, 46:121–131, 2014.
- [98] Kun Li and Petros Ioannou. Modeling of traffic flow of automated vehicles. *IEEE Transactions on Intelligent Transportation Systems*, 5(2):99–113, 2004.

- [99] T Taleb, E Sakhaee, A Jamalipour, K Hashimoto, N Kato, and Y Nemoto. A Stable Routing Protocol to Support ITS Services in VANET Networks, 2007.
- [100] Jishiyu Ding, Huei Peng, Yi Zhang, and Li Li. Penetration effect of connected and automated vehicles on cooperative on-ramp merging. *IET Intelligent Transport Systems*, 14(1):56–64, 2020.
- [101] P.G. Gipps. A behavioural car-following model for computer simulation. *Transportation Research Part B: Methodological*, 15(2):105–111, 1981.
- [102] Huifu Jiang, Jia Hu, Shi An, Meng Wang, and Byungkyu Brian Park. Eco approaching at an isolated signalized intersection under partially connected and automated vehicles environment. *Transportation Research Part C: Emerging Technologies*, 79:290–307, 2017.
- [103] Rui Jiang, M-B Hu, Bin Jia, Ruili Wang, and Q-S Wu. Phase transition in a mixture of adaptive cruise control vehicles and manual vehicles. *The European Physical Journal B*, 58(2):197–206, 2007.
- [104] Xi Liu, Ke Ma, and PR Kumar. Towards provably safe mixed transportation systems with human-driven and automated vehicles. In *2015 54th IEEE Conference on Decision and Control (CDC)*, pages 4688–4694. IEEE, 2015.
- [105] Abdul Rahman Kreidieh, Cathy Wu, and Alexandre M Bayen. Dissipating stop-and-go waves in closed and open networks via deep reinforcement learning. In *2018 21st International Conference on Intelligent Transportation Systems (ITSC)*, pages 1475–1480. IEEE, 2018.
- [106] Cathy Wu, Kanaad Parvate, Nishant Kheterpal, Leah Dickstein, Ankur Mehta, Eugene Vinitzky, and Alexandre M Bayen. Framework for control and deep reinforcement learning in traffic. In *2017 IEEE 20th International Conference on Intelligent Transportation Systems (ITSC)*, pages 1–8. IEEE, 2017.

- [107] S. E. Shladover, C. A. Desoer, J. K. Hedrick, M. Tomizuka, J. Walrand, W.-B. Zhang, D. H. McMahon, H. Peng, S. Sheikholeslam, and N. McKeown. Automated vehicle control developments in the PATH program. *IEEE Transactions on Vehicular Technology*, 40(1):114–130, 1991.
- [108] P. Varaiya. Smart cars on smart roads: problems of control. *IEEE Transactions on Automatic Control*, 38(2):195–207, 1993.
- [109] R. Rajamani, H.-S. Tan, B. K. Law, and W.-B. Zhang. Demonstration of integrated longitudinal and lateral control for the operation of automated vehicles in platoons. *IEEE Transactions on Control Systems Technology*, 8(4):695–708, 2000.
- [110] Sadayuki Tsugawa. An overview on an automated truck platoon within the energy its project. *IFAC Proceedings Volumes*, 46(21):41–46, 2013.
- [111] Arturo Dávila and Mario Nombela. Sartre: Safe road trains for the environment. In *Conference on Personal Rapid Transit PRT@ LHR*, volume 3, pages 2–3, 2010.
- [112] Steven E Shladover. PATH at 20—History and major milestones. *IEEE Transactions on intelligent transportation systems*, 8(4):584–592, 2007.
- [113] Santa Maiti, Stephan Winter, and Lars Kulik. A conceptualization of vehicle platoons and platoon operations. *Transportation Research Part C: Emerging Technologies*, 80:1–19, 2017.
- [114] Sogand Karbalaieali, Osama A Osman, and Sherif Ishak. A dynamic adaptive algorithm for merging into platoons in connected automated environments. *IEEE Transactions on Intelligent Transportation Systems*, 21(10):4111–4122, 2019.
- [115] Alexander Johansson, Ehsan Nekouei, Karl Henrik Johansson, and Jonas Mårtensson. Multi-fleet platoon matching: A game-theoretic approach. In *2018 21st International Conference on Intelligent Transportation Systems (ITSC)*, pages 2980–2985. IEEE, 2018.

- [116] Xi Xiong, Erdong Xiao, and Li Jin. Analysis of a stochastic model for coordinated platooning of heavy-duty vehicles. In *2019 IEEE 58th Conference on Decision and Control (CDC)*, pages 3170–3175. IEEE, 2019.
- [117] Logan E. Beaver and Andreas A. Malikopoulos. Constraint-driven optimal control of multi-agent systems: A highway platooning case study. *IEEE Control Systems Letters*, 6:1754–1759, 2022.
- [118] Tyler Ard, Faraz Ashtiani, Ardalan Vahidi, and Hoseinali Borhan. Optimizing gap tracking subject to dynamic losses via connected and anticipative mpc in truck platooning. In *2020 American Control Conference (ACC)*, pages 2300–2305. IEEE, 2020.
- [119] Sebastian Van De Hoef, Karl Henrik Johansson, and Dimos V Dimarogonas. Fuel-efficient en route formation of truck platoons. *IEEE Transactions on Intelligent Transportation Systems*, 19(1):102–112, 2017.
- [120] S.D. Kumaravel, Andreas A Malikopoulos, and R. Ayyagari. Decentralized cooperative merging of platoons of connected and automated vehicles at highway on-ramps. In *2021 American Control Conference (ACC)*, pages 2055–2060, 2021. ISBN 2378-5861. doi: 10.23919/ACC50511.2021.9483390.
- [121] S.D. Kumaravel, Andreas A Malikopoulos, and R. Ayyagari. Optimal coordination of platoons of connected and automated vehicles at signal-free intersections. *IEEE Transactions on Intelligent Vehicles*, pages 1–1, 2021. doi: 10.1109/TIV.2021.3096993.
- [122] Weiming Zhao, Dong Ngoduy, Simon Shepherd, Ronghui Liu, and Markos Papageorgiou. A platoon based cooperative eco-driving model for mixed automated and human-driven vehicles at a signalised intersection. *Transportation Research Part C: Emerging Technologies*, 95:802–821, 2018.

- [123] Dongyao Jia, Kejie Lu, Jianping Wang, Xiang Zhang, and Xuemin Shen. A survey on platoon-based vehicular cyber-physical systems. *IEEE Communications Surveys Tutorials*, 18(1):263–284, 2016. doi: 10.1109/COMST.2015.2410831.
- [124] Anirudh Kishore Bhoopalam, Niels Agatz, and Rob Zuidwijk. Planning of truck platoons: A literature review and directions for future research. *Transportation research part B: methodological*, 107:212–228, 2018.
- [125] Anan Kaku, Masakazu Mukai, and Taketoshi Kawabe. A centralized control system for ecological vehicle platooning using linear quadratic regulator theory. *Artificial Life and Robotics*, 17(1):70–74, 2012.
- [126] William B Dunbar and Derek S Caveney. Distributed receding horizon control of vehicle platoons: Stability and string stability. *IEEE Transactions on Automatic Control*, 57(3):620–633, 2011.
- [127] William Bruce Dunbar. *Distributed receding horizon control of multiagent systems*. PhD thesis, California Institute of Technology, 2004.
- [128] William B Dunbar. Distributed receding horizon control of dynamically coupled nonlinear systems. *IEEE Transactions on Automatic Control*, 52(7):1249–1263, 2007.
- [129] Fabio Morbidi, Patrizio Colaneri, and Thomas Stanger. Decentralized optimal control of a car platoon with guaranteed string stability. In *2013 European Control Conference (ECC)*, pages 3494–3499. IEEE, 2013.
- [130] Yongfu Li and Chuancong Tang. Distributed hierarchical cooperative braking control for connected vehicle platoon. In *2017 Chinese Automation Congress (CAC)*, pages 7612–7617. IEEE, 2017.
- [131] Xianggui Guo, Jianliang Wang, Fang Liao, and Rodney Swee Huat Teo. Distributed adaptive integrated-sliding-mode controller synthesis for string stability

- of vehicle platoons. *IEEE Transactions on Intelligent Transportation Systems*, 17(9):2419–2429, 2016.
- [132] Yang Zheng, Shengbo Eben Li, Keqiang Li, and Wei Ren. Platooning of connected vehicles with undirected topologies: Robustness analysis and distributed h-infinity controller synthesis. *IEEE Transactions on Intelligent Transportation Systems*, 19(5):1353–1364, 2017.
- [133] William B Dunbar and Richard M Murray. Distributed receding horizon control for multi-vehicle formation stabilization. *Automatica*, 42(4):549–558, 2006.
- [134] Yang Zheng, Shengbo Eben Li, Keqiang Li, Francesco Borrelli, and J Karl Hedrick. Distributed model predictive control for heterogeneous vehicle platoons under unidirectional topologies. *IEEE Transactions on Control Systems Technology*, 25(3):899–910, 2016.
- [135] Guni Sharon and Peter Stone. A protocol for mixed autonomous and human-operated vehicles at intersections. In *International Conference on Autonomous Agents and Multiagent Systems*, pages 151–167. Springer, 2017.
- [136] I Ge Jin, Gábor Orosz, Dávid Hajdu, Tamás Insperger, and Jeff Moehlis. To delay or not to delay—stability of connected cruise control. In *Time Delay Systems*, pages 263–282. Springer, 2017.
- [137] Dávid Hajdu, I Ge Jin, Tamás Insperger, and Gábor Orosz. Robust design of connected cruise control among human-driven vehicles. *IEEE Transactions on Intelligent Transportation Systems*, 21(2):749–761, 2019.
- [138] Yao-Ming Yuan, Rui Jiang, Mao-Bin Hu, Qing-Song Wu, and Ruili Wang. Traffic flow characteristics in a mixed traffic system consisting of acc vehicles and manual vehicles: A hybrid modelling approach. *Physica A: Statistical Mechanics and its Applications*, 388(12):2483–2491, 2009.

- [139] Hyuntai Chin, Hiroyuki Okuda, Yuichi Tazaki, and Tatsuya Suzuki. Model predictive cooperative cruise control in mixed traffic. In *IECON 2015 - 41st Annual Conference of the IEEE Industrial Electronics Society*, pages 003199–003205, 2015. doi: 10.1109/IECON.2015.7392593.
- [140] Gábor Orosz. Connected cruise control: modelling, delay effects, and nonlinear behaviour. *Vehicle System Dynamics*, 54(8):1147–1176, 2016.
- [141] Jianglin Lan, Dezong Zhao, and Daxin Tian. Data-driven robust predictive control for mixed vehicle platoons using noisy measurement. *IEEE Transactions on Intelligent Transportation Systems*, pages 1–11, 2021. doi: 10.1109/TITS.2021.3128406.
- [142] Shuo Feng, Ziyu Song, Zhaojian Li, Yi Zhang, and Li Li. Robust platoon control in mixed traffic flow based on tube model predictive control. *IEEE Transactions on Intelligent Vehicles*, 6(4):711–722, 2021.
- [143] Siyuan Gong, Jinglai Shen, and Lili Du. Constrained optimization and distributed computation based car following control of a connected and autonomous vehicle platoon. *Transportation Research Part B: Methodological*, 94:314–334, 2016.
- [144] Yongfu Li, Wenbo Chen, Kaibi Zhang, Taixiong Zheng, and Huizong Feng. Dsrc based vehicular platoon control considering the realistic v2v/v2i communications. In *2017 29th Chinese Control And Decision Conference (CCDC)*, pages 7585–7590. IEEE, 2017.
- [145] Ioannis A Ntousakis, Ioannis K Nikolos, and Markos Papageorgiou. On microscopic modelling of adaptive cruise control systems. *Transportation Research Procedia*, 6:111–127, 2015.

- [146] Chaoru Lu, Jing Dong, Liang Hu, and Chenhui Liu. An ecological adaptive cruise control for mixed traffic and its stabilization effect. *IEEE Access*, 7:81246–81256, 2019.
- [147] Vicente Milanés, Steven E Shladover, John Spring, Christopher Nowakowski, Hiroshi Kawazoe, and Masahide Nakamura. Cooperative adaptive cruise control in real traffic situations. *IEEE Transactions on intelligent transportation systems*, 15(1):296–305, 2013.
- [148] Gerrit JL Naus, Jeroen Ploeg, MJG Van de Molengraft, WPMH Heemels, and Maarten Steinbuch. A model predictive control approach to design a parameterized adaptive cruise control. In *Automotive Model Predictive Control*, pages 273–284. Springer, 2010.
- [149] R Austin Dollar, Tamás G Molnár, Ardalan Vahidi, and Gábor Orosz. Mpc-based connected cruise control with multiple human predecessors. In *2021 American Control Conference (ACC)*, pages 405–411. IEEE, 2021.
- [150] I Ge Jin and Gábor Orosz. Connected cruise control among human-driven vehicles: Experiment-based parameter estimation and optimal control design. *Transportation research part C: emerging technologies*, 95:445–459, 2018.
- [151] Siyuan Gong and Lili Du. Cooperative platoon control for a mixed traffic flow including human drive vehicles and connected and autonomous vehicles. *Transportation research part B: methodological*, 116:25–61, 2018.
- [152] M.A.S. Kamal, J. Imura, T. Hayakawa, A. Ohata, and K. Aihara. A Vehicle-Intersection Coordination Scheme for Smooth Flows of Traffic Without Using Traffic Lights. *IEEE Transactions on Intelligent Transportation Systems*, (99), 2014.
- [153] Gabriel Rodrigues De Campos, Paolo Falcone, and Jonas Sjöberg. Autonomous Cooperative Driving: a Velocity-Based Negotiation Approach for Intersection

- Crossing. In *16th International IEEE Conference on Intelligent Transportation Systems*, number Itsc, pages 1456–1461, 2013. ISBN 9781479929146. doi: 10.1109/ITSC.2013.6728435.
- [154] G. R. Campos, P. Falcone, H. Wymeersch, R. Hult, and J. Sjoberg. Cooperative receding horizon conflict resolution at traffic intersections. In *2014 IEEE 53rd Annual Conference on Decision and Control (CDC)*, pages 2932–2937, 2014.
- [155] Joyoung Lee, Byungkyu (Brian) Park, Kristin Malakorn, and Jaehyun (Jason) So. Sustainability assessments of cooperative vehicle intersection control at an urban corridor. *Transportation Research Part C: Emerging Technologies*, 32: 193–206, 2013.
- [156] Yue Zhang and Christos G Cassandras. The penetration effect of connected automated vehicles in urban traffic: An energy impact study. In *2nd IEEE Conference on Control Technology and Applications*, pages 620–625, 2018.
- [157] Andreas A Malikopoulos and Liuhui Zhao. A closed-form analytical solution for optimal coordination of connected and automated vehicles. In *2019 American Control Conference (ACC)*, pages 3599–3604. IEEE, 2019.
- [158] Tsz-Chiu Au, Shun Zhang, and Peter Stone. Autonomous intersection management for semi-autonomous vehicles. *Handbook of Transportation, Routledge, Taylor & Francis Group*,, 2015.
- [159] Andreas A Malikopoulos, Logan E Beaver, and Ioannis Vasileios Chremos. Optimal time trajectory and coordination for connected and automated vehicles. *Automatica*, 125(109469), 2021.
- [160] Rainer Wiedemann. Simulation des strassenverkehrsflusses. 1974.
- [161] Martin Treiber and Arne Kesting. Traffic flow dynamics. *Traffic Flow Dynamics: Data, Models and Simulation, Springer-Verlag Berlin Heidelberg*, 2013.

- [162] Y Zhang and Christos G Cassandras. An impact study of integrating connected automated vehicles with conventional traffic. *Annual Reviews in Control*, 48: 347–356, 2019.
- [163] Martin Treiber and Arne Kesting. The intelligent driver model with stochasticity—new insights into traffic flow oscillations. *Transportation research procedia*, 23: 174–187, 2017.
- [164] Vicente Milanés and Steven E Shladover. Modeling cooperative and autonomous adaptive cruise control dynamic responses using experimental data. *Transportation Research Part C: Emerging Technologies*, 48:285–300, 2014.
- [165] A M Ishtiaque Mahbub and Andreas A Malikopoulos. Conditions to Provable System-Wide Optimal Coordination of Connected and Automated Vehicles. *Automatica*, 131(109751), 2021. doi: <https://doi.org/10.1016/j.automatica.2021.109751>.
- [166] A M Ishtiaque Mahbub and Andreas A Malikopoulos. Conditions for state and control constraint activation in coordination of connected and automated vehicles. *Proceedings of 2020 American Control Conference*, pages 436–441, 2020.
- [167] AM Ishtiaque Mahbub, Andreas A Malikopoulos, and Liuhui Zhao. Decentralized optimal coordination of connected and automated vehicles for multiple traffic scenarios. *Automatica*, 117(108958), 2020.
- [168] A M Ishtiaque Mahbub, Andreas A Malikopoulos, and L. Zhao. Impact of connected and automated vehicles in a corridor. In *Proceedings of 2020 American Control Conference, 2020*, pages 1185–1190. IEEE, 2020.
- [169] A M Ishtiaque Mahbub and Andreas A Malikopoulos. A Platoon Formation Framework in a Mixed Traffic Environment. *IEEE Control Systems Letters (LCSS)*, 6:1370–1375, 2021.

- [170] A M Ishtiaque Mahbub and Andreas A. Malikopoulos. Platoon Formation in a Mixed Traffic Environment: A Model-Agnostic Optimal Control Approach. *Proceedings of 2022 American Control Conference*, pages 4746–4751, 2022.
- [171] A M Ishtiaque Mahbub, Viet-Anh Le, and Andreas A. Malikopoulos. A Safety-Prioritized Receding Horizon Control Framework for Platoon Formation in a Mixed Traffic Environment. *in review*, 2022.
- [172] A M Ishtiaque Mahbub, Viet-Anh Le, and Andreas A. Malikopoulos. Safety-Aware and Data-Driven Predictive Control for Connected Automated Vehicles at a Mixed Traffic Signalized Intersection. *in review*, 2022.
- [173] A M Ishtiaque Mahbub, Behdad Chalaki, and Andreas A Malikopoulos. A constrained optimal control framework for vehicle platoons with delayed communication. *Network and Heterogeneous Media, Special Issue: Traffic and Autonomy*, 2022 (arXiv:2111.08080).
- [174] A M Ishtiaque Mahbub, Hao Wang, Gabor Orosz, and Andreas A. Malikopoulos. Coordination of Mixed Platoons at On-Ramp Merging: A Constrained Optimal Control Framework. *in review*, 2022.
- [175] A M Ishtiaque Mahbub, Liuhui Zhao, Dimitris Assanis, and Andreas A Malikopoulos. Energy-Optimal Coordination of Connected and Automated Vehicles at Multiple Intersections. In *Proceedings of 2019 American Control Conference*, pages 2664–2669, 2019.
- [176] Liuhui Zhao, A M Ishtiaque Mahbub, and Andreas A Malikopoulos. Optimal vehicle dynamics and powertrain control for connected and automated vehicles. *Proceedings of 2019 IEEE Conference on Control Technology and Applications (CCTA)*, pages 33–38, 2019.

- [177] A M Ishtiaque Mahbub, V. Karri, Darshil Parikh, S. Jade, and Andreas A Malikopoulos. A decentralized time- and energy-optimal control framework for connected automated vehicles: From simulation to field test. In *SAE Technical Paper 2020-01-0579*. SAE International, 2020. doi: 10.4271/2020-01-0579.
- [178] A M Ishtiaque Mahbub and Andreas A Malikopoulos. Concurrent optimization of vehicle dynamics and powertrain operation using connectivity and automation. In *SAE Technical Paper 2020-01-0580*. SAE International, 2020. doi: 10.4271/2020-01-0580.
- [179] A. Valencia, A M Mahbub, and Andreas A Malikopoulos. Performance analysis of optimally coordinated connected automated vehicles in a mixed traffic environment. In *30th Mediterranean Conference on Control and Automation, 2022* (accepted).
- [180] Andreas A. Malikopoulos, Panos Y. Papalambros, and Dennis N. Assanis. Online identification and stochastic control for autonomous internal combustion engines. *Journal of Dynamic Systems, Measurement, and Control*, 132(2):024504–024504, 2010.
- [181] Andreas A. Malikopoulos. A multiobjective optimization framework for online stochastic optimal control in hybrid electric vehicles. *IEEE Transactions on Control Systems Technology*, 24:440–450, 2016.
- [182] Andreas A Malikopoulos. A duality framework for stochastic optimal control of complex systems. *IEEE Transactions on Automatic Control*, 61(10):2756–2765, 2015.
- [183] Chan-Chiao Lin, Zoran Filipi, Yongsheng Wang, Loucas Louca, Huei Peng, Dennis Assanis, and Jeffrey Stein. Integrated, Feed-Forward Hybrid Electric Vehicle

- Simulation in SIMULINK and its Use for Power Management Studies. *SAE International*, 2001. doi: 10.4271/2001-01-1334. URL <http://dx.doi.org/10.4271/2001-01-1334>.
- [184] PTV Group et al. Ptv vissim 7 user manual. *Germany: PTV GROUP*, 2014.
- [185] A. A. Malikopoulos, P.Y. Papalambros, and D.N. Assanis. Optimal engine calibration for individual driving styles. In *SAE Congress*, 2008.
- [186] Andreas A. Malikopoulos, Zoran Filipi, and Dennis N. Assanis. Simulation of an integrated starter alternator (isa) system for the hmwv. In *SAE Technical Papers*, 04 2006. doi: 10.4271/2006-01-0442.
- [187] Dedicated short range communications (dsrc) message set dictionary. *SAE Standard J2735-200911*, Rev. 2009.
- [188] Arthur Earl Bryson and YU Chi Ho. *Applied optimal control: optimization, estimation and control*. CRC Press, 1975.
- [189] D Subbaram Naidu. *Optimal control systems*. CRC press, 2002.
- [190] M a. S Kamal, Masakazu Mukai, Junichi Murata, and Taketoshi Kawabe. Ecological Vehicle Control on Roads With Up-Down Slopes. *IEEE Transactions on Intelligent Transportation Systems*, 12(3):783–794, 2011.
- [191] Martin Treiber, Ansgar Hennecke, and Dirk Helbing. Congested traffic states in empirical observations and microscopic simulations. *Physical review E*, 62(2):1805, 2000.
- [192] Yaping Zhang, Chuanyun Fu, and Liwei Hu. Yellow light dilemma zone researches: a review. *Journal of traffic and transportation engineering (English edition)*, 1(5):338–352, 2014.

- [193] Zhuoxu Duan and Zhengye Yang. Smart city traffic intersection: Impact of video quality and scene complexity on precision and inference. In *in Proc. 19th IEEE Int. Conf. on Smart City, 2021*, 2021.
- [194] Roozbeh Kianfar, Bruno Augusto, Alireza Ebadighajari, Usman Hakeem, Josef Nilsson, Ali Raza, Reza S Tabar, Naga VishnuKanth Irukulapati, Cristofer Englund, Paolo Falcone, et al. Design and experimental validation of a cooperative driving system in the grand cooperative driving challenge. *IEEE transactions on intelligent transportation systems*, 13(3):994–1007, 2012.
- [195] Yanlin Weng and Tiejun Wu. Car-following model of vehicular traffic. In *2001 International Conferences on Info-Tech and Info-Net. Proceedings (Cat. No.01EX479)*, volume 4, pages 101–106 vol.4, 2001. doi: 10.1109/ICII.2001.983768.
- [196] Lennart Ljung and Torsten Söderström. *Theory and practice of recursive identification*. MIT press, 1983.
- [197] Yanbing Wang, George Gunter, Matthew Nice, Maria Laura Delle Monache, and Daniel B Work. Online parameter estimation methods for adaptive cruise control systems. *IEEE Transactions on Intelligent Vehicles*, 6(2):288–298, 2020.
- [198] George Gunter, Raphael Stern, and Daniel B Work. Modeling adaptive cruise control vehicles from experimental data: model comparison. In *2019 IEEE Intelligent Transportation Systems Conference (ITSC)*, pages 3049–3054. IEEE, 2019.
- [199] Joel A E Andersson, Joris Gillis, Greg Horn, James B Rawlings, and Moritz Diehl. CasADi – A software framework for nonlinear optimization and optimal control. *Mathematical Programming Computation*, 11(1):1–36, 2019.
- [200] Masako Bando, Katsuya Hasebe, Akihiro Nakayama, Akihiro Shibata, and Yuki Sugiyama. Dynamical model of traffic congestion and numerical simulation. *Physical review E*, 51(2):1035, 1995.

- [201] Joel AE Andersson, Joris Gillis, Greg Horn, James B Rawlings, and Moritz Diehl. Casadi: a software framework for nonlinear optimization and optimal control. *Mathematical Programming Computation*, 11(1):1–36, 2019.
- [202] Martin Fellendorf and Peter Vortisch. Microscopic traffic flow simulator vissim. In *Fundamentals of traffic simulation*, pages 63–93. Springer, 2010.
- [203] Richard W Rothery. Car following models. *Trac Flow Theory*, 1992.
- [204] R Eddie Wilson and Jonathan A Ward. Car-following models: fifty years of linear stability analysis—a mathematical perspective. *Transportation Planning and Technology*, 34(1):3–18, 2011.
- [205] Lei Zhang, Shengrui Zhang, Bei Zhou, Shuaiyang Jiao, and Yan Huang. An improved car-following model considering desired safety distance and heterogeneity of driver’s sensitivity. *Journal of Advanced Transportation*, 2021, 2021.
- [206] Francesco Borrelli, Alberto Bemporad, and Manfred Morari. *Predictive control for linear and hybrid systems*. Cambridge University Press, 2017.
- [207] Alberto Bemporad, Manfred Morari, and N Lawrence Ricker. Model predictive control toolbox. *User’s Guide, Version, 2*, 2004.
- [208] Shengyue Yao and Bernard Friedrich. Managing connected and automated vehicles in mixed traffic by human-leading platooning strategy: a simulation study. In *2019 IEEE Intelligent Transportation Systems Conference (ITSC)*, pages 3224–3229. IEEE, 2019.
- [209] Bijan Sakhdari, Ebrahim Moradi Shahrivar, and Nasser L Azad. Robust tube-based mpc for automotive adaptive cruise control design. In *2017 IEEE 20th International Conference on Intelligent Transportation Systems (ITSC)*, pages 1–6. IEEE, 2017.

- [210] Hans Joachim Ferreau, Christian Kirches, Andreas Potschka, Hans Georg Bock, and Moritz Diehl. qpOASES: A parametric active-set algorithm for quadratic programming. *Mathematical Programming Computation*, 6(4):327–363, 2014.
- [211] Lorenz T Biegler and Victor M Zavala. Large-scale nonlinear programming using IPOPT: An integrating framework for enterprise-wide dynamic optimization. *Computers & Chemical Engineering*, 33(3):575–582, 2009.
- [212] SRDJAN S Stanković, MILORAD J Stanojević, and DRAGOSLAV D Šiljak. Decentralized suboptimal LQG control of platoon of vehicles. In *Proc. 8th IFAC/IFIP/IFORS Symp. Transp. Syst.*, volume 1, pages 81–86, 1997.
- [213] Huaxin Pei, Shuo Feng, Yi Zhang, and Danya Yao. A cooperative driving strategy for merging at on-ramps based on dynamic programming. *IEEE Transactions on Vehicular Technology*, 68(12):11646–11656, 2019.
- [214] Fuguo Xu and Tielong Shen. Decentralized optimal merging control with optimization of energy consumption for connected hybrid electric vehicles. *IEEE Transactions on Intelligent Transportation Systems*, 2021.
- [215] Sebastian Van De Hoef, Jonas Mårtensson, Dimos V Dimarogonas, and Karl Henrik Johansson. A predictive framework for dynamic heavy-duty vehicle platoon coordination. *ACM Transactions on Cyber-Physical Systems*, 4(1):1–25, 2019.
- [216] Xin Chang, Haijian Li, Jian Rong, Xiaohua Zhao, et al. Analysis on traffic stability and capacity for mixed traffic flow with platoons of intelligent connected vehicles. *Physica A: Statistical Mechanics and its Applications*, 557:124829, 2020.
- [217] Alon Tuchner and Jack Haddad. Vehicle platoon formation using interpolating control. *IFAC-PapersOnLine*, 48(14):414–419, 2015.
- [218] Behdad Chalaki, Logan E Beaver, and Andreas A Malikopoulos. Experimental validation of a real-time optimal controller for coordination of cars in a multi-lane

- roundabout. In *31st IEEE Intelligent Vehicles Symposium (IV)*, pages 504–509, 2020.
- [219] Gerrit JL Naus, Rene PA Vugts, Jeroen Ploeg, Marinus JG van De Molengraft, and Maarten Steinbuch. String-stable cacc design and experimental validation: A frequency-domain approach. *IEEE Transactions on vehicular technology*, 59(9):4268–4279, 2010.
- [220] Shuo Feng, Yi Zhang, Shengbo Eben Li, Zhong Cao, Henry X Liu, and Li Li. String stability for vehicular platoon control: Definitions and analysis methods. *Annual Reviews in Control*, 47:81–97, 2019.
- [221] Forbes.com. Meeting the growing demand for connected car data. URL <https://www.forbes.com/sites/tmobile/2021/08/28/meeting-the-growing-demand-for-connected-car-data/>.
- [222] Guo Xie, Dan Zhang, Xinhong Hei, and Fucui Qian. A feasible control strategy for lqg control problem with parameter and structure uncertainties. In *2014 Tenth International Conference on Computational Intelligence and Security*, pages 548–552. IEEE, 2014.
- [223] Meixin Zhu, Xuesong Wang, and Yinhai Wang. Human-like autonomous car-following model with deep reinforcement learning. *Transportation research part C: emerging technologies*, 97:348–368, 2018.
- [224] Zhaobin Mo, Rongye Shi, and Xuan Di. A physics-informed deep learning paradigm for car-following models. *Transportation research part C: emerging technologies*, 130:103240, 2021.

## Appendix A

Table A.1: Traffic volume at different routes within Mcity network.

	<b>High</b>	<b>Medium</b>	<b>Low</b>
<b>Main Route</b> [vph/lane]	500	400	300
<b>Highway</b> [vph/lane]	800	600	400
<b>SRZ</b> [vph/lane]	1400	1100	800
<b>Roundabout</b> [vph/lane]	700	550	400

Table A.2: Simulation Parameters

<b>Vehicle Parameters</b>	
Maximum Acceleration [ $m/s^2$ ]	1.5
Maximum Deceleration [ $m/s^2$ ]	3.0
Safe Time Headway [s]	1.2
<b>Traffic Network</b>	
Corridor Length [m]	1500
Control Zone Length [m]	100
SRZ Length [m]	125
<b>Speed Limit</b>	
On-Ramp Merging [mph]	40
Speed Reduction Zone [mph]	18.6
Roundabout [mph]	25

Table A.3: VESIM parameters calibrated with Audi A3 specification.

<b>Vehicle Parameters</b>	
Tire Model	Michelline 225/60 r16
Weight (No driver) [ <i>lb</i> ]	3616
Rolling Resistance Coeff.	0.010
Frontal Area [ <i>in</i> x <i>in</i> ]	56.1 x 60
Traction Torque Loss [%]	0.95
Aerodynamic Drag Coeff.	0.32
Tire Traction Efficiency	0.96
Maximum Braking Force [ <i>N</i> ]	12000
<b>Transmission</b>	
Gear Ratio [1-6]	3.50, 2.77, 1.85, 1.02, 1.02, 0.84
Gear Efficiency [1-6]	0.98, 0.98, 0.98, 0.98, 0.98, 0.98
Gear Inertia [1-6]	0.0023, 0.0009, 0.0023, 0.0009, 0.0023, 0.0009
Forward Drive Ratio	3.75
Forward Drive Efficiency	0.966
<b>Engine (TFSI) Parameters</b>	
Cylinder Volume [ <i>cc</i> ]	1395
Maximum Engine Power [ <i>kW</i> ]	110
Maximum Engine Torque [ <i>Nm</i> ]	250
Engine Speed at Peak Torque [ <i>rpm</i> ]	1750 4000
Engine Inertia [ <i>kg/m<sup>2</sup></i> ]	0.15
<b>Battery Pack</b>	
Capacity [ <i>kWh</i> ]	8.8
Number of Cell/Module	12
Number of Modules	8
Maximum Voltage/Cell [ <i>volt</i> ]	4.2
Minimum Voltage/Cell [ <i>volt</i> ]	2.1
Maximum Battery Power [ <i>kW</i> ]	75
<b>IMG Unit</b>	
Maximum Motor Power [ <i>kW</i> ]	100
Maximum Motor Torque [ <i>Nm</i> ]	300
Maximum Generator Torque [ <i>Nm</i> ]	-300
Motor Speed at Peak Torque [ <i>rpm</i> ]	2000
Rotor's Rotational Inertia [ <i>kg/m<sup>2</sup></i> ]	0.1
<b>Energy Conversion (MPGe)</b>	
Gallon to Equivalent <i>CO</i> <sub>2</sub>	8.887e-3
kWh to Equivalent <i>CO</i> <sub>2</sub>	7.44e-4